HYBRID HIE
DEVELOPMENT
EXPERIMENTATIO

in pa

I

HYBRID HIERARCHICAL BIO-BASED MATERIALS: DEVELOPMENT AND CHARACTERIZATION THROUGH EXPERIMENTATION AND COMPUTATIONAL SIMULATIONS

By

Mahmoodul Haq

A DISSERTATION

Submitted to
Michigan State University
in partial fulfillment of the requirements
for the degree of

DOCTOR OF PHILOSOPHY

CIVIL ENGINEERING

2009

HYBRID H
DEVELOPME
EXPERIMENTA

Environmentally fri

tained by harnessing the s

and micro- scale) reinforcem

resins. Bio-based co

environmental appeal a

advantage of multiscale rein

when combined with bio-

thermal and barrier proper

composites. Moreover, the

environmental impact. While

been studied for synthetic c

for developing new types of s

dissertation focused on devel

effort to understand and e

characterization and computa

Bio-based composites

natural or bio-resin (epoxidize

and nanosilicate (nanoclay) in

ABSTRACT

HYBRID HIERARCHICAL BIO-BASED MATERIALS: DEVELOPMENT AND CHARACTERIZATION THROUGH EXPERIMENTATION AND COMPUTATIONAL SIMULATIONS

By
Mahmoodul Haq

Environmentally friendly bio-based composites with improved properties can be obtained by harnessing the synergy offered by hybrid constituents such as multiscale (nano- and micro- scale) reinforcement in bio-based resins composed of blends of synthetic and natural resins. Bio-based composites have recently gained much attention due to their low cost, environmental appeal and their potential to compete with synthetic composites. The advantage of multiscale reinforcement is that it offers synergy at various length scales, and when combined with bio-based resins provide stiffness-toughness balance, improved thermal and barrier properties, and increased environmental appeal to the resulting composites. Moreover, these hybrid materials are tailorable in performance and in environmental impact. While the use of different concepts of multiscale reinforcement has been studied for synthetic composites, the study of multiphase/multiscale reinforcements for developing new types of sustainable materials is limited. The research summarized in this dissertation focused on development of multiscale reinforced bio-based composites and the effort to understand and exploit the synergy of its constituents through experimental characterization and computational simulations.

Bio-based composites consisting of petroleum-based resin (unsaturated polyester), natural or bio-resin (epoxidized soybean and linseed oils), natural fibers (industrial hemp), and nanosilicate (nanoclay) inclusions were developed. The work followed the "materials by

' philosophy by

explore

of bio-resin

counter-balance

impact strength an

toughness. T

can be brou

A multiscale

to the de

into nano-scale

design o

phase material w

problem to dete

in greater

Overall, eco-frie

were succes

sustainable bio-b

and hou

of understandi

in this work,

types of hierarchica

design" philosophy by incorporating an integrated experimental and computational approach to strategically explore the design possibilities and limits. Experiments demonstrated that the drawbacks of bio-resin addition, which lowers stiffness, strength and increases permeability, can be counter-balanced through nanoclay reinforcement. Bio-resin addition yields benefits in impact strength and ductility. Conversely, nanoclay enhances stiffness but seems to decrease toughness. Thus, the traditionally seen opposite measures of stiffness and toughness can be brought to an efficient balance through the combination of bio-resin and nanoclay. A multiscale computational approach, namely a multi-FE based approach, was implemented to the developed materials to extrapolate the experimental matrix, to provide insight into nano-scale behavior beyond measurements and to hopefully serve as a tool for computational design of hybrid materials. Additionally, an enhanced RVE for modeling the three-phase material was determined by solving a topology optimization based material layout problem to determine the distribution of bio-resin, thereby allowing modeling the nanostructure in greater detail and closer to reality.

Overall, eco-friendly, tailorable, cost-effective and multiscale reinforced bio-based composites were successfully developed. The improved multifaceted features possible for these sustainable bio-based materials are likely to increase their appeal for use in transportation and housing structural applications. Additionally, it is believed that the approach of understanding complex materials by integrating simulations and experiments, as attempted in this work, holds great promise, and a similar methodology can be applied for other types of hierarchical materials, thereby providing guidance in designing those materials.

To my parents and my wife,

for their continuous prayers, sacrifices,

guidance and support.

AC

Praise be to the L

It is difficult to oversta

enthusiasm, inspiration, and his

research great fun for me. Th

and great vision helped me na

would have been lost without h

I wish to thank the me

Misra, Dr. Ronald Harichand

constructive comments. Additio

Dr. Manjusri Misra for sharing

their guidance, encouragement a

I would like to thank M

Structures Center for their help

thank Mr. Siavosh Ravanbaksh

laboratories. I would also like t

for their help in electron micros

I would like to thank D

understanding of materials. I

Engelmann for their help in m

this research. I would also lik

throughout my stay at MSU.

Lastly, and most impor

and my wife Sarah, for their pa

ACKNOWLEDGEMENTS

Praise be to the LORD, The Most Beneficent, The Most Merciful

It is difficult to overstate my gratitude to my advisor, Dr. Rigoberto Burgueño. His enthusiasm, inspiration, and his efforts to explain things clearly and simply, helped to make research great fun for me. Throughout my dissertation, his encouragement, sound advice and great vision helped me navigate through the difficult times during my PhD studies. I would have been lost without him.

I wish to thank the members of PhD committee, Dr. Amar Mohanty, Dr. Manjusri Misra, Dr. Ronald Harichandran, and Dr. Alejandro Diaz for their valuable time and constructive comments. Additionally, very special thanks are due to Dr. Amar Mohanty and Dr. Manjusri Misra for sharing with me their expertise in biocomposite materials, and ofr their guidance, encouragement and support throughout this research.

I would like to thank Mr. Michael Rich and the staff of Composite Materials and Structures Center for their help in manufacturing and material testing. Also, I would like to thank Mr. Siavosh Ravanbaksh and Mr. Joseph Nguyen for their help at Civil Engineering Laboratories. I would also like to thank the staff at MSU's Center of Advanced Microscopy for their help in electron microscopy imaging.

I would like to thank Dr. Hiroaki Miyagawa for his initial help in processing and understanding of materials. I thank Janelle Musch, Richard McClary and Lindsey Diggelmann for their help in manufacturing of biocomposite materials at different stages of this research. I would also like to thank my colleagues for their friendship and support throughout my stay at MSU.

Lastly, and most importantly, I would like to thank my family, specially my parents and my wife Sarah, for their patience, sacrifices and support. To them, I dedicate this thesis.

am grateful to my b

[illegible] the most to

This study wa

25-459666. Additio

work were obtained

the Graduate School

acknowledged.

I am grateful to my brother Zia for having confidence in me and supporting me when it mattered the most: to chase my dream.

This study was mainly funded by the National Science Foundation under grant CMS-0409666. Additionally, financial support in the form of assistanships and fellowship awards were obtained from the Department of Civil and Environmental Engineering, and the Graduate School at Michigan State University. All contributions are gratefully acknowledged.

TABLE OF CONTENTS

CHAPTER 1.

CHAPTER 2.

CHAPTER 3.

BIO-BASED POLYMER NA

CHAPTER 4.

BIO-BASED POLYMER NA

CHAPTER 5.

CHAPTER 6.

CHAPTER 7.

CHAPTER 8.
FE-BASED MULTISCAL

CHAPTER 9.
MODELING OF THREE-
DETERMINING BIO-RES
BASED MATERIAL DESIG

CHAPTER 10.

SUMMARY AND CONCLU

CHAPTER 10.

LIST OF TABLES

Images i

LIST OF FIGURES

Images in this dissertation are presented in color.

Figure 9-11. Comparison of te
three-phase RVEs with exp

Chapter 1. Introduction

1.1 Motivation

Environmentally friend
by harnessing the sync
micro- scale) reinforcemen
resins. Bio-based comp
environmental appeal and
of multiscale reinfor
combined with bio-ba
and barrier properti
composites. Moreover, these
environmental impact. While t
studied for synthetic con
developing new types of su
focused on develo
to understand and exp
characterization and computati

Environmental concern
composites has propell
renewable sources [1-1][1-2
polymer matrices ha
environmental friendliness, an
Nonetheless, the use of

Chapter 1. Introduction

1.1 Motivation

Environmentally friendly bio-based composites with improved properties can be obtained by harnessing the synergy offered by hybrid constituents such as multiscale (nano- and micro- scale) reinforcement in bio-based resins composed of blends of synthetic and natural resins. Bio-based composites have recently gained much attention due to their low cost, environmental appeal and their potential to compete with synthetic composites. The advantage of multiscale reinforcement is that it offers synergy at various length scales, and when combined with bio-based resins provide stiffness-toughness balance, improved thermal and barrier properties, and increased environmental appeal to the resulting composites. Moreover, these hybrid materials are tailorable in performance and in environmental impact. While the use of different concepts of multiscale reinforcement has been studied for synthetic composites, the study of multiphase/multiscale reinforcements for developing new types of sustainable materials is limited. The research summarized in this dissertation focused on development of multiscale reinforced bio-based composites and the effort to understand and exploit the synergy of its constituents through experimental characterization and computational simulations.

Environmental concerns related to the use of synthetic, or petroleum-based, polymer matrix composites has propelled the development of composite materials based on natural or renewable sources [1-1][1-2]. Biocomposites, composed of natural fibers in synthetic or natural polymer matrices have recently gained much attention due to their low cost, environmental friendliness, and their potential to compete with synthetic composites [1-3][1-4]. Nonetheless, the use of bio-based composites has been limited due to their lower

mechanical and thermo-physi
conventional structural materia
friendliness and performance ar
of petroleum-based resin with
based resins improve toughne
increase in toughness compro
stiffness and toughness are c
required for an efficient compo
fibers, or nanoclays.

The biocomposite use
heterogeneities in different re
petro- resin, bio resin, natural
classified into three length sca
blends + nanoclay inclusions)
and c) macroscale (structura
shape, properties and spatial c
fibers and bio-resin). From a
experimental measurements v
properties, for each scale. Her
incorporating an integrated ex
the design possibilities and lin

Figure 1-1 provides a
this work. Apart from exper
focused on developing comp

mechanical and thermo-physical properties compared to synthetic composites and conventional structural materials [1-5]. A promising compromise between environmental friendliness and performance are bio-based resins, or bio-blends, obtained by replacing part of a petroleum-based resin with natural bio-resin. In addition to higher natural content, bio-based resins improve toughness of the resulting resin blend [1-6]-[1-8]. However, this increase in toughness compromises stiffness, barrier and thermal properties [1-6]-[1-8]. Stiffness and toughness are opposing performance parameters and a proper balance is required for an efficient composite. One way to attain this balance is the addition of layered silicates, or nanoclays.

The biocomposite used in this study is a hybrid heterogeneous material with heterogeneities in different relative dimension scales containing four major components: petro- resin, bio resin, natural fibers, and nano-clay inclusions. This biocomposite can be classified into three length scales (see Figure 1-1), namely: a) nanoscale (resin system: resin blends + nanoclay inclusions), b) microscale (resin system + natural fiber reinforcement), and, c) macroscale (structural component). The effective properties depend on the size, shape, properties and spatial distribution of the heterogeneities (in our case, nanoclay, short fibers and bio-resin). From a time and cost point of view, it is an infeasible task to perform experimental measurements with all possible combinations of volume fractions and phase properties, for each scale. Hence, the work followed the "materials by design" philosophy by incorporating an integrated experimental and computational approach to strategically explore the design possibilities and limits.

Figure 1-1 provides a schematic of the overall multiscale methodology carried out in this work. Apart from experimental characterization at nano and micro-scales, the work focused on developing computational (finite element) models at each scale. The models were

developed such that they resem
simulation of material behavior
at respective scales and the res
transmission and scanning elec
respective scales. Representativ
structure at each scale. The res
with theoretical models and ex
models and experimental resu
and experimental inaccuracie
computational tool to obtain
validate and verify the model
the next level is possible.

The bio-based resin
unsaturated polyester) and b
with nanoclay. The distributi
electron microscopy, but sir
observed. In order to model
model the three-phase ma
material layout problem wa
develop an enhanced three
optimization in an attempt t
order to accurately solve the
simplified into idealized mo
micro-macro finite element

developed such that they resemble the microstructure at their respective scales. This enables simulation of material behavior close to reality and understanding the phenomena occurring at respective scales and the resulting material behavior. Electron microscopy tools such as transmission and scanning electron microscopy were used to model clay and fibers at their respective scales. Representative volume elements (RVEs) were modeled or obtained from literature at each scale. The results of the computational models at each scale were compared with theoretical models and experimental results. Discrepancies between the computational models and experimental results may occur due to various assumptions made in the model and experimental inaccuracies. Nonetheless, in order to use the respective models as a computational tool to obtain the next hierarchical level properties, it becomes essential to validate and verify the model with experiments, such that accurate transfer of information to the next level is possible.

The bio-based resin system used in this study has blends of petro-polymer (UPE, unsaturated polyester) and bio-polymer (derivatives of soybean and linseed oil) reinforced with nanoclay. The distribution of nanoclay in the polymer matrix could be observed using electron microscopy, but similar distribution of bio-resin in primary petro-resin cannot be observed. In order to model the hybrid composite to great detail, it is essential to realistically model the three-phase material, and hence the distribution of bio-resin was sought. A material layout problem was designed and implemented in this work. This was aimed to develop an enhanced three phase RVE by using experimental data along with topology optimization in an attempt to provide insight to the distribution of bio-resin in the RVE, and not to accurately solve the material design problem. The resulting material layouts were simplified into idealized models and used in multiscale simulations. In this work, a direct micro-macro finite element based approach, also referred as multi-level FE approach was

sed [1-9][1-10]. The tensi
nocomposites was simulated
ia.

The experimental part
-based nanocomposites a
echanical and barrier proper
dditionally, optimal material
lance in multiple properties w
of experiments such that
computational models to pr
nstituents and any macro
proach, namely a multi-FE
to extrapolate the experiment
asurements and to hopefull
dditionally, an enhanced R
sing a topology optimizati
of bio-resin, thereby allowin
ality. Overall, eco-friendly,
mposites were successfull
hese sustainable bio-based
ansportation and housing
proach of understanding
dopted in this work, hol
other types of hierarchical m

used [1-9][1-10]. The tensile response of hybrid biocomposites and bio-based nanocomposites was simulated using multi-FE scheme and compared with experimental data.

The experimental part of this research resulted in novel processing techniques of bio-based nanocomposites and comprehensive characterization of thermo-physical, mechanical and barrier properties of bio-based clay nanocomposites and biocomposites. Additionally, optimal material concentrations that provided ease of processing with good balance in multiple properties were obtained. The objective was to perform a limited amount of experiments such that the experimental information can be used to develop computational models to predict the behavior of materials for any combination of constituents and any macroscale structural component. A multiscale computational approach, namely a multi-FE based approach, was implemented to the developed materials to extrapolate the experimental matrix, to provide insight into nano-scale behavior beyond measurements and to hopefully serve as a tool for computational design of hybrid materials. Additionally, an enhanced RVE for modeling the three-phase material was determined by solving a topology optimization based material layout problem to determine the distribution of bio-resin, thereby allowing modeling the nanostructure in greater detail and closer to reality. Overall, eco-friendly, tailorable, cost-effective and multiscale reinforced bio-based composites were successfully developed. The improved multifaceted features possible for these sustainable bio-based materials are likely to increase their appeal for use in transportation and housing structural applications. Additionally, it is believed that the approach of understanding complex materials by integrating simulations and experiments, as attempted in this work, holds great promise, and a similar methodology can be applied for other types of hierarchical materials, thereby providing guidance in designing those materials.

[illegible] Objectives

The goal of this work w

incorporating an integrated expe

the design possibilities and limi

exploited to the maximum. Mo

and methods to manufactur

Experimental data will provide

overall objectives of the work c

- Global objective: To

  effective, environment

- To use synergy of mate

  has balanced or super

  materials and multisca

  bio-based materials.

- To develop and use re

  clay nanocomposites

  techniques for produc

- To perform key expe

  characterizing the resu

  processing and effects

  experiments will prov

- To develop and use

  experiments and to el

1.2 Objectives

The goal of this work was to develop eco-friendly, hybrid bio-based composites by incorporating an integrated experimental and computational approach to strategically explore the design possibilities and limits, such that the synergy offered by these materials could be exploited to the maximum. Moreover, as a part of the study efficient processing techniques and methods to manufacture nanocomposites and biocomposites were investigated. Experimental data will provide input to validate models and the development of RVEs. The overall objectives of the work can be summarized as follows:

- **Global objective:** To obtain / use a rational approach in development of cost-effective, environment friendly, multifunctional hybrid hierarchical biocomposites.
- To use synergy of materials at various length scales, such that the resulting composite has balanced or superior properties than the virgin base material. The synergy of materials and multiscale reinforcement provides multifunctionality to the resulting bio-based materials.
- To develop and use relatively efficient processing techniques to synthesize bio-based clay nanocomposites and biocomposites. Also, to study the feasibility of these techniques for producing large structural components
- To perform key experiments at each scale. The experiments will not only help in characterizing the resulting material properties but will provide the limits / bounds in processing and effects of constituents on resulting parameter(s). Most importantly experiments will provide vital information for developing computational models.
- To develop and use validated computational models at each scale through key experiments and to eliminate the costly trial and error approach.

- To link the computatio
  and accurately transferr
  multi-level finite elemen

1.3 *Background*

1.3.1 Bio based composite

Classical fiber reinfor
aerospace applications, but ha
and stiffness at low weights a
fibers such as carbon, or glas
polyesters. However, environ
dependability on non-renew
synthetic FRP composites a
natural fiber composites or b

Biocomposites are co
cotton, coir, bamboo etc.) a
urethane, phenolics, etc.) or
triglycerides, animal fats, et
performance concerns such
14, Bio-based resins, or bi
based resin with natural bio
that they can increase the t
toughness due to the inc
stiffness [1-6][1-15]-[1-17],

- To link the computational models at each scale, such that information is adequately and accurately transferred through computational models at various length scales. A multi-level finite element technique has been used.

1.3 Background

1.3.1 Bio based composite materials and Biocomposites

Classical fiber reinforced polymer (FRP) composites were initially targeted for aerospace applications, but have transitioned into numerous other fields where high strength and stiffness at low weights are required. In general, high strength and modulus synthetic fibers, such as carbon, or glass, are mixed with petroleum based resins, such as epoxies and polyesters. However, environmental concerns, such as biodegradability, recycling issues and dependability on non-renewable petroleum reserves, have limited the wide spread use of synthetic FRP composites and have propelled the development of alternatives such as natural fiber composites or biocomposites [1-1][1-2][1-5][1-11]-[1-13]

Biocomposites are comprised of natural fibers (e.g., flax, hemp, jute, cellulose, kenaf, cotton, coir, bamboo etc.) and petroleum based resins (unsaturated polyester, epoxy, poly urethane, phenolics, etc.) or natural bioresins (epoxidized vegetable oils, polyoles, maleinated triglycerides, animal fats, etc.)[1-2]-[1-4]. The use of only bio-resins has been limited due to performance concerns such as low mechanical and thermo-physical properties [1-6][1-7][1-14]. Bio-based resins, or bio-blends, obtained by replacing/blending part of the petroleum based resin with natural bio-resin have been developed by our group and it has been found that they can increase the toughness of the composites [1-6][1-7]. However, the increase in toughness due to the increase in bio-resin content is generally achieved by sacrificing stiffness [1-6][1-15]-[1-17], barrier [1-16] and thermal [1-16][1-17] properties. Stiffness and

ghness are opposing perfor
efficient biocomposite. One
ered silicates or nanoclays for

As discussed earlier, en
ural fiber composites (bioc
ture and automotive i
composites for load bearing
ength, non-uniform fiber s
perature. Work in our grou
University of Delaware [1-3]
uld be overcome with efficie
ocomposite panels was fou
ventional materials as well a
nd moisture susceptibility
ementioned studies did
ocomposites. The incorpor
ovide reinforcements to
nforcement has been studie
1-22]. Conversely, the
ends of petroleum and bio-r

132 Enhancement throug

Nanocomposites: An O

toughness are opposing performance parameters and a proper balance is required to develop an efficient biocomposite. One of the methods of attaining this balance with the addition of layered silicates or nanoclays for nano-reinforcement.

As discussed earlier, environmental concerns have relatively increased the demand of natural fiber composites (biocomposites). Initial use has been in flooring, siding, roofing, furniture and automotive interiors [1-1][1-3][1-18]. Nonetheless, consideration of biocomposites for load bearing applications has been limited due to their lower stiffness and strength, non-uniform fiber sizes, high moisture absorption and low stability at high temperature. Work in our group [1-5][1-11][1-12][1-13][1-19] and similar work by researchers at university of Delaware [1-3][1-4] has shown that stiffness shortcomings of biocomposites could be overcome with efficient hybrid and cellular designs, and the performance of cellular biocomposite panels was found to be as efficient as building flooring systems from conventional materials as well as E-glass/polyester panels. Nonetheless, the issues of thermal and moisture susceptibility of biocomposites are still a concern. Moreover, the aforementioned studies did not include bio-resin or nanoclays in the manufacture of biocomposites. The incorporation of nanoclays and natural fibers in the resin systems provide reinforcements to resin systems at two different scales. Similar multiscale reinforcement has been studied for synthetic fibers for mechanical and electrical properties [1-20]-[1-22]. Conversely, the use of nanoclays and natural fiber reinforcement in resin blends of petroleum and bio-resins is very limited.

1.3.2 Enhancement through Nano-reinforcement & Nanocomposite processing

Polymer Nanocomposites: An Overview

Polymers reinforced w

enhancements in modulus, the

silicates or nanoclays consist o

extremely large surface areas

exchange capacities of clay

functionalizations with a host

performance gaps of moistur

composites.

Depending on the func

the host polymer, the platelets

penetrate between the platele

chains, exfoliated or separat

obtained. While the exfoliate

barrier properties, it has been

toughness for the resulting n

properties in polymers with

established. Le Baron et al

nanocomposites. Apart from

introduces multifunctionality

barrier properties, flammabili

characterization of bio-based

[illegible]) was used as the prima

methyl soyate (EMS) and epo

Polymers reinforced with layered silicates or nanoclays have shown to exhibit enhancements in modulus, thermal and barrier properties at low concentrations. Layered silicates or nanoclays consist of stacks of sheet like platelets with thickness of ~ 1 nm and extremely large surface areas and aspect ratios. The large surface areas and high cation exchange capacities of clay platelets enable the use of nanoclay with proper functionalizations with a host of polymers enabling the opportunity to circumvent the performance gaps of moisture and thermal dimensional instability of bio-fiber polymer composites.

Depending on the functionalization of the clay and the compatibility of the clay with the host polymer, the platelets in the stacks are separated to enable the polymer chains to penetrate between the platelets. Depending on the degree of penetration of the polymer chains, exfoliated or separated, and intercalated or stacked b) clay morphologies are obtained. While the exfoliated morphology may produce enhancement in modulus and barrier properties, it has been found that intercalated composites produce better gains in toughness for the resulting nanocomposites. The enhancement of mechanical and barrier properties in polymers with the addition of small concentrations of nanoclays is well established. Le Baron et al [1-23] provide a good review on polymer clay hybrid nanocomposites. Apart from the increase in stiffness, the inclusion of nanoclay particles introduces multifunctionality to the resulting nanocomposite resin system by enhancing barrier properties, flammability and ablation resistance. As a part of this study, experimental characterization of bio-based clay nanocomposites was performed. Unsaturated polyester (UPE) was used as the primary petroleum based resin. Two bio-resins, namely epoxidized methyl soyate (EMS) and epoxidized methyl linseedate (EML) were blended with UPE. The

tails and results of the
nanocomposites are provide

mer Nanocomposites: Process

Polymer clay nano
polymerization, melt compo
been widely used in the ind
degradation of polymers. Sol
the literature to produce na
utilized SBPT generally in
of the solvent and the nanocl
by removal of the solvent to
this process is that it is ener
solvent removal. Moreover
properties of the resulting nan
in bio based resins may lead to
of the resulting nanocomposit
bio based clay nanocomposite

As a part of this stu
solvent based processing tec
effective approach. Polymer c
styrene-based unsaturated po
with acetone as the solvent.
and clay as it led to issues
studied and the effects of

details and results of the experimental characterization for EMS and EML based nanocomposites are provided in Chapter 3 and Chapter 4 respectively.

Polymer Nanocomposites: Processing

Polymer clay nanocomposites have been synthesized commonly by in-situ polymerization, melt compounding and solvent based techniques. Melt compounding has been widely used in the industry but has been questioned as it raises issues of thermal degradation of polymers. Solvent based processing techniques (SBPT) have been reported in the literature to produce nanocomposites with clay platelets that are well dispersed and exfoliated. SBPT generally involves sonication (mechanical stirring and ultrasonic agitation) of the solvent and the nanoclay, mixing of the polymer with the sonicated solution, followed by removal of the solvent to obtain the desired nanocomposites. One of the drawbacks of this process is that it is energy inefficient, as large amounts of energy is required in the solvent removal. Moreover solvent residues in the polymer may adversely affect the properties of the resulting nanocomposites. Also, excessive energy spent in solvent removal in bio based resins may lead to phase separation of the resin blend and affect the properties of the resulting nanocomposite. Thus, efficient processing techniques are required to obtain bio based clay nanocomposites in an energy-efficient and robust manner.

As a part of this study, an investigation was performed to evaluate the various solvent based processing techniques for CPNCs so as to identify a time, energy and cost effective approach. Polymer clay nanocomposites were processed using SBPT with blends of styrene-based unsaturated polyester (UPE) and bio-resin (EMS, epoxidized methyl soyate) with acetone as the solvent. The SBPT became infeasible at higher concentrations of EMS and clay as it led to issues in solvent (acetone) removal. Four different techniques were studied and the effects of energy spent on sonnication, styrene content in UPE and

processing technique on
nanocomposites were stud
by modifying the process
processes were found to p
UPE clay nanocomposit
multifunctional composites
are provided in Chapter 2 a

1.3.3 Hybrid Biocompo

The bio-based nan
above were combined wi
multiscale biocomposites.
Section 1.1. As discussed
these systems provide rei
multiscale reinforcement h
properties [1-20]-[1-22]. M
multiscale reinforcement su
petroleum and bio-resins i
work is not reported else
UPE/EMS and UPE/EM
for various material prope
thermal expansion, moisture
The details and results of
Chapter 6.

processing technique on tensile, impact and barrier properties of the resulting nanocomposites were studied. Acetone (solvent) removal and related issues were overcome by modifying the processing techniques and eliminating the use of acetone. Two novel processes were found to produce balanced mechanical and barrier properties for bio-based UPE/clay nanocomposites and hold promise for the development of bio-based multifunctional composites. A detailed explanation of the processing study and its outcomes are provided in Chapter 2 and reference [1-24].

1.3.3 Hybrid Biocomposites from Bio-based Resins & Nanoclays

The bio-based nanocomposite resins synthesized and characterized as discussed above were combined with natural hemp fiber reinforcement to develop novel hybrid multiscale biocomposites. A brief introduction of generic biocomposites was provided in Section 1.1. As discussed earlier, the incorporation of nanoclays and natural fibers in the resin systems provide reinforcements to resin systems at two different scales. Similar multiscale reinforcement has been studied for synthetic fibers for mechanical and electrical properties [1-20]-[1-22]. Meanwhile, the development of biocomposites with the use of multiscale reinforcement such as nanoclays and natural fiber reinforcement in resin blends of petroleum and bio-resins is very unique to this work, and to the author's knowledge such work is not reported elsewhere. The bio-based nanocomposite resins synthesized from UPE/EMS and UPE/EML combinations with nanoclay were experimentally characterized for various material properties such as tensile properties, impact strength, coefficient of thermal expansion, moisture absorption/diffusivity, and tensile failure surface characteristics. The details and results of such characterization studies are provided in Chapter 5 and Chapter 6.

1.4 Modeling and simula

The enhancement gai

fillers, etc.) is experimentall

able to predict the overa

polymer-filler systems. It is cor

properties of a polymer-filler

modulus of the filler, modu

prediction of the homogenized

the literature. Various theorie

advantages and limitations. Ov

mean field approaches, variatio

methods, embedded cell appr

empirical formulae such as Ha

The simplest method

properties are calculated as a

weighted by their volume fr

microstructural property, the

linear material properties [1-2

effective-medium theories d

developed by various researc

1-9], and others [1-9]. Effe

boundary value problem for

take into account for the p

1.3.4 Modeling and simulation of micro/nano reinforced polymers

The enhancement gained from nanoscale fillers (e.g. nanotubes, silica, layered silicates, etc.) is experimentally well established. Many analytical and numerical models are available to predict the overall effective/homogenized properties of these heterogeneous polymer-filler systems. It is commonly accepted that the overall effective physico-mechanical properties of a polymer-filler material depends on the type of the filler, its aspect ratio, modulus of the filler, modulus of the matrix, concentration of the filler, etc. Hence, prediction of the homogenized properties of heterogeneous materials is widely documented in literature. Various theories and models have been proposed, each with their own advantages and limitations. Overall, homogenization techniques can be classified into [1-25]: mean field approaches, variational bound methods, periodic microfield approaches /unit cell methods, embedded cell approaches, windowing approaches, rules of mixtures and semi-empirical formulae such as Halpin-Tsai methods, etc.

The simplest method of homogenization is the rule of mixtures wherein the overall properties are calculated as an average over the respective properties of the constituents weighed by their volume fractions. Clearly, this method takes into account only one microstructural property, the volume fraction, and is applicable for simple geometries and linear material properties [1-23][1-25]. A more sophisticated method is the self-consistent or effective-medium theories developed by Eshelby [1-26]. Eshelby's theory was further developed by various researchers including Hashin [1-27], Hashin and Shtrikman [1-28], Hill [1-29], and others [1-9]. Effective overall properties are obtained as an analytical solution of a boundary value problem for a spherical/ellipsoidal particle in an infinite matrix. In order to take into account for the particle-particle interactions, Mori-Tanaka [1-25] modified the

inclusion theory. M
perties of particulate comp
Extended, or modified
variations in fiber c
[1-25][1-30].

Another mathematical
Bensoussan et al. [1-31] an
is the ratio of characteri
used in an asymptotic ex
ciples are then used to
computational methods, unit
methods depends on the sele
RVE). The RVE should b
microstructure and small
corresponding RVE's are the
analytical or numerical me
geometries in great detail (sp
investigation of the influen
interactions, etc., on the c
simulate the macroscopic
subjected to a given loading
[1-25].

Unlike most convent
and unique modeling is

Eshelby inclusion theory. Mori-Tanaka estimates are commonly used to estimate elastic properties of particulate composites and are found to agree reasonably with experimental results. Extended, or modified, Mori-Tanaka schemes have been proposed that also take into account variations in fiber orientations and fiber lengths using probability distribution functions [1-25][1-30].

Another mathematical approach is the asymptotic homogenization method reported by Bensoussan et al. [1-31] and Sanchez [1-32]. In this method "natural length parameter," which is the ratio of characteristic size of the heterogeneities to a measure of macrostructure, is used in an asymptotic expansion of the displacement and stress fields. Variational principles are then used to create a link between the scales [1-9][1-25]. Among the computational methods, unit cell methods have become widely used. The success of these methods depends on the selection of the unit cell or the representative volume element (RVE). The RVE should be selected such that it is large enough to represent the microstructure and small enough to allow efficient computational modeling. The corresponding RVE's are then analyzed with proper loading and boundary conditions via analytical or numerical methods. Unit cell methods allow modeling of micro-scale geometries in great detail (specifically in finite element based unit cell methods) and enable investigation of the influence of different geometrical features, interfaces, interparticle interactions, etc., on the overall material response. However, since these approaches formulate the macroscopic constitutive relations based on the behavior of a single RVE subjected to a given loading history, they are in fact successful only for small deformations [1-9][1-25].

Unlike most conventional fillers, the modeling of nanoclays, or layered silicates, pose new and unique modeling issues such as: a) particle size, b) hierarchical modeling, and c) interface and gallery propertie

successful in predicting homo

length scale is in the order

composites, depending on

Exfoliated clays may be in ra

may be in the order of micr

nanocomposites exhibit both

ms. micromechanical mode

shows the limitation in mod

magnitudes. The concepts

micromechanical models can

Researchers have tried to add

inclusion." Sheng et al. [1-33

finite element) micromechan

pseudo inclusion model using

pseudo inclusion size. Miyaga

The aforementioned studies

the hierarchical nature of poly

agreement with experimenta

modeling of polymer/clay na

the chemical compatibility, c

interfacial properties will

morphologies, wherein the c

material in the galleries is not

interface and gallery properties [1-33]. Analytical micromechanical models have proved to be successful in predicting homogenized properties of conventional composites where the filler length scale is in the order of tens of microns or larger [1-33]. In nanoclay reinforced composites, depending on the processing, the clay morphology varies significantly. Exfoliated clays may be in range of nanometers and highly intercalated clay agglomerations may be in the order of micrometers. Moreover, it is commonly agreed that polymer/clay nanocomposites exhibit both exfoliated and intercalated (hierarchical) morphologies. Clearly, most micromechanical models cannot handle this complexity [1-33]. More importantly, it shows the limitation in modeling hierarchical morphologies that can vary by orders of magnitudes. The concepts of "matrix" and "particle" that are well-defined in micromechanical models can no longer be directly applied to polymer-clay nanocomposites. Researchers have tried to address this issue by defining an "effective particle" or a "pseudo inclusion." Sheng et al. [1-33] employ an "effective particle" in analytical and numerical (finite element) micromechanical models. Similarly, Brune and Bicerano [1-34] developed a pseudo inclusion model using the Halpin-Tsai empirical model by substituting the effective pseudo inclusion size. Miyagawa et al. [1-6] used the same concept in Mori-Tanaka models. The aforementioned studies with the concept of "effective particle" have shown to model the hierarchical nature of polymer/clay nanocomposites successfully and have reported good agreement with experimental data [1-6][1-33][1-34]. The final and most important issue in modeling of polymer/clay nanocomposites is the particle-polymer interface. Depending on the chemical compatibility, or functionalization, of the nanoclay and polymer the resulting interfacial properties will vary considerably [1-35]. Additionally in intercalated clay morphologies, wherein the clay platelets are in stacks (called galleries), the properties of the material in the galleries is not fully understood [1-33].

The above menti

modeling of such comp

simulation address these is

morphologies, non-linear

complex hierarchical nat

considered in this work. N

micro-macro methoc

materials [1-9][1-10][1-36]

methods [1-10][1-36][1-37

multi-level methods [1-38]

1.3.3 Multiscale metho

Multiscale modelin

Specifically, multiscale mo

length and time scales asso

The multiscale, co

hierarchical modeling of

properties and behavior fr

information. Ideally, a mul

from nano to macro. In ot

the bulk continuous struct

modeling scheme that link

take into account the

modeling scheme that i

The above mentioned issues specific to polymer/clay nanocomposites make modeling of such composites challenging. Finite element (FE) based modeling and simulation address these issues and enable modeling of interfaces, different particle sizes and morphologies, non-linear material properties and complex loading [1-25]. Due to the complex hierarchical nature of polymer/clay nanocomposites multiscale models are considered in this work. Not limited to polymer/clay nanocomposites, multiscale models or direct micro-macro methods have been used for homogenization of different heterogeneous materials [1-9][1-10][1-36]-[1-39]. These models have also been termed as "multiscale methods [1-10][1-36][1-37]," "FE^2 methods [1-38]," "integrated methods [1-39]," and "multi-level methods [1-38]", and are briefly described in the following section.

1.3.5 Multiscale methodology

Multiscale modeling covers a wide range of simulations and modeling techniques. Specifically, multiscale modeling can be coined as any modeling scheme spanning both length and time scales associated with analyses that describe material behavior (Figure 1-2,[1-40]). The multiscale, computational modeling of materials has a primary challenge: hierarchical modeling of materials; namely, the accurate prediction of physical/chemical properties and behavior from nanoscale to macroscale without loss of intrinsic structural information. Ideally, a multiscale modeling scheme would be the one that links all the scales from nano to macro. In other words, it should connect the discrete molecular structure with the bulk continuous structure. Nevertheless, it has been found that the literature terms any modeling scheme that links any two scales a multiscale modeling scheme; although it may not take into account the quantum or atomistic behavior of the material. For instance, a modeling scheme that integrates a micromechanics (microstructure) and structural

mechanics (macro/global) mo
be referred as a multiscale
atomistic scale.

In this study, the che
with bio-resin and that of c
interactions. These aspects ar
as molecular dynamics. This
this work and hence a multi-
regime is studied. Neverthel
simulation behavior from at
modeling scheme to study all

FE - based homogenization

Various homogenizat
process of homogenization i
the macroscopic homogene
constants and stress-strain
generalized continua, const
materials, it is difficult to fit
to establish a stress-strain re
does not require any constr
properties are obtained from
[1-10] [1-25][1-36]. Henc
literature prescribes that FI
constituents [1-9][1-36]: (1)

mechanics (macro/global) model to obtain the behavior of a material or structure would still be referred as a multiscale method, although it failed to propagate properties from the atomistic scale.

In this study, the chemical compatibility or functionalization between the petro-resin with bio-resin and that of clay with resin system is governed by atomistic and molecular interactions. These aspects are generally studied using tools in computational modeling such as molecular dynamics. This aspect of atomistic/molecular modeling is beyond the scope of this work and hence a multi-level modeling that links different scales within the continuum regime is studied. Nevertheless, it has been shown that it is possible to integrate material simulation behavior from atomistic scale. It is clear that this would be the ideal multiscale modeling scheme to study all material parameters.

FE — based homogenization:

Various homogenization techniques exist and have been used widely in the past. The process of homogenization involves finding the average properties at a lower scale due to the macroscopic homogeneous deformations. In other words, it involves finding elastic constants and stress-strain (constitutive) relations that relate the two scales. For any generalized continua, constitutive equations are very difficult to write, and in complex materials, it is difficult to fit experimental data. Instead of trying to build differential systems to establish a stress-strain relation at a macroscale, a multi-level finite element computation does not require any constitutive equations to be written at the macroscopic scale; all non-linearites are obtained from separate FE analyses at lower hierarchical (micro/nano) scale [1-9][1-10] [1-25][1-36]. Hence, FE-based homogenization would be used in this research. Literature prescribes that FE based models are constructed using the following three main constituents [1-9][1-36]: (1) modeling of the mechanical behavior at the lower scale (the

RVE; (2) localization rule

given overall strain), and (

solving the micromechanic

Multiscale FE mo

behavior at the macroscale a

material behavior. In this st

later used by Kouznetsova

integration point of the

computation is performed.

boundary conditions are d

integration point is derived

the RVE volume. The con

point is derived from the R

is no need to specify ma

macroscopic integration p

provides a good explanation

schematic representation o

work multi-level FE meth

nanocomposites and hybrid

behavior. The details and re

14 *Method / Approac*

The goal of this wo

incorporating an integrated e

RVE), (2) localization rule which determines the local solutions inside the unit cell (for any given overall strain), and (3) homogenization rule giving the macroscopic stress tensor, knowing the micromechanical stress state.

Multiscale FE modeling is an iterative procedure that assumes homogenized behavior at the macroscale and enables the incorporation of large deformations and arbitrary material behavior. In this study, the multi-level FE approach as developed by Smit [1-10] and later used by Kouznetsova [1-9] and Breuls [1-36] is proposed. In this approach, to each integration point of the macroscopic mesh an RVE is assigned and a separate FE computation is performed. From a macroscopic deformation tensor (F_{macro}), appropriate boundary conditions are derived to be imposed on the RVE. The macroscopic stress at integration point is derived from the RVE by averaging the resulting RVE stress field over the RVE volume. The consistent macroscopic stiffness matrix at macroscopic integration point is derived from the RVE stiffness matrix. When using this multi-level approach there is no need to specify macroscopic constitutive behavior, instead the behavior at the macroscopic integration point it is derived from associated microstructure. Breuls [1-36] provides a good explanation and derivation of the complete multi-level modeling scheme. A schematic representation of the multi-level FE scheme is provided in Figure 1-3. In this work multi-level FE methodology was used to predict the tensile behavior of bio-based nanocomposites and hybrid biocomposites and the results were compared with experimental behavior. The details and results are provided in Chapter 8.

1.4 Method / Approach

The goal of this work was to develop eco-friendly, hybrid bio-based composites by incorporating an integrated experimental and computational approach to strategically explore the design possibilities and l

computation, material mode

Since experiments are a key

classified into two major ta

Simulations - Computationa

Each of these tasks was acco

1.4.1 Experimentation -

a) Development of cost

of bio-based polymer

b) Use of CPNCs for bi

c) Characterization of C

1.4.2 Simulations - Comp

Nanoscale Modeling:

a) RVEs/unit cells that

without bio-resins su

within acceptable tole

b) The degree of inte

experimental results (

performed.

c) The distribution of b

problem and validati

Micro/Mesoscale Modeling:

the design possibilities and limits. As discussed earlier, the approach will integrate multiscale computation, material modeling and optimization and is schematically shown in Figure 1-4. Since experiments are a key part of modeling at each scale, the overall research study can be classified into two major tasks: Experimentation - Processing and characterization, and Simulations - Computational Models, material layout optimization and multiscale modeling. Each of these tasks was accomplished with subdivision of tasks as follows:

1.4.1 Experimentation – Processing & Characterization:

a) Development of cost and time efficient processing techniques for the development of bio-based polymer clay nanocomposites (Chapter 2).

b) Use of CPNCs for biocomposite plates using hand layup and VARTM.

c) Characterization of CPNCs and biocomposites(Chapter 3 - Chapter 6).

1.4.2 Simulations - Computational Models & Multiscale Modeling

Nanoscale Modeling:

a) RVEs/unit cells that can accurately represent the nano-reinforced polymers with or without bio-resins such that the RVE can accurately provide material parameters within acceptable tolerance to experimental results were developed.

b) The degree of intercalation of nanoclay by validating virgin UPE results with experimental results (Number of layers in intercalated gallery obtained by TEM) was performed.

c) The distribution of bio-resin was determined through a material layout optimization problem and validation by comparing to experimental results

Micro/ Mesoscale Modeling:

d) A simplified computa

properties are obta

polymer/clay RVEs

hybrid biocomposites

Hybrid / Macroscale Modeling

A multi-level finite e

tion, through proper RVE

Chapter 8). A schematic d

work is provided in Figure 1-

is shown in Figure 1-5(c) v

removed due to time and co

tensile response of hybrid b

extended to model mechanic

1.5 Scope

The study aimed at c

hybrid hierarchical biocomp

minor experiments, by incorp

to strategically explore the

biocomposites is a result of

The work aimed at utilizin

parameters, phenomena and

biocomposite, such that only

the detrimental effects a

a) A simplified computational model (RVE) similar to that of nanoscale, wherein resin properties are obtained from lower-scale analyses of appropriate bio-blend polymer/clay RVEs was developed and implemented in multiscale analyses for hybrid biocomposites.

Multi-level / Macroscale Modeling:

A multi-level finite element approach that integrated the three scales, from nano to macro, through proper RVEs and phenomenological models at each scale was impelemented (Chapter 8). A schematic description of the overall computational approach used in this work is provided in Figure 1-5 . The large scale biocomposites manufacturing and simulation as shown in Figure 1-5(c) was initially proposed to be a part of the work, but was later removed due to time and cost point of view. Nevertheless, the approach presented up to the tensile response of hybrid biocomposites validates the approach and is believed that it can extended to model mechanical behavior of large scale structural components.

1.5 Scope

The study aimed at developing cost-effective environmental friendly, multifunctional hybrid hierarchical biocomposites using a rational approach that eliminates costly trial and error experiments, by incorporating an integrated experimental and computational approach to strategically explore the design possibilities and limits. The efficiency of the hybrid biocomposites is a result of the synergy of the different constituents at various length scales. The work aimed at utilizing this synergistic effect to its full extent by identifying key parameters, phenomena and behavior of the various constituents that make the resultant biocomposite, such that only the beneficial effect of each of the constituent is revealed and the detrimental effects are suppressed, thereby leading to a superior/balanced

multifunctional hybrid bioco
various length scales provided
n effects of constituents on r
development of efficient comp

The study aimed a
homogenized macroscopic be
dimensional scales. At the m
defined; instead the constituti
averaging results of detailed n
heterogeneities at the nano/m

The proposed study cu
be extended to thermal and d
of micro/nanoscale mechani
macroscopic properties by p
Overall, a successful mode
development of novel, effici
development of bio-based m
lead to sustainable, environm
benefiting the agricultural in
prediction of macroscopic
shapes. Similar methodolo
hierarchical materials there
materials.

multifunctional hybrid biocomposite. Experimental characterization these materials at various length scales provided vital information on bounds/limits of processing and limits on effects of constituents on resultant properties. Most importantly, the experiments aid the development of efficient computational models.

The study aimed at implementing a computational scheme that models a homogenized macroscopic behavior taking into considerations the heterogeneities at lower dimensional scales. At the macroscopic scale, no constitutive/phenomenological model is defined; instead the constitutive behavior at macroscopic integration points is determined by averaging results of detailed modeling of the lower-scale material structure. The influence of heterogeneities at the nano/micro scale was studied.

The proposed study currently focused on mechanical behavior. A similar approach can be extended to thermal and diffusion analyses. The approach will increase the understanding of micro/nanoscale mechanisms governing various parameters, thereby enabling tailoring of macroscopic properties by proper synergy and distribution of materials at respective scales. Overall, a successful modeling scheme, as the one used in this research could enable development of novel, efficient, cost effective multifunctional materials. On the other hand, development of bio-based materials and their applications for structural applications would lead to sustainable, environmental friendly, bio-degradable and cost effective materials, while benefiting the agricultural industry. The success of this computational scheme will enable prediction of macroscopic responses for various material compositions and macroscopic shapes. Similar methodology could be applied for other types of nanoparticles and hierarchical materials thereby providing guidance in designing such hybrid hierarchical materials.

1.6 Organization

- The dissertation has b
  introduction to the wo
- Chapter 2 reports th
  techniques for develop
- Chapter 3 and Chap
  nanocomposites with
- Chapter 5 and Cha
  biocomposites produ
  and Chapter 4, respe
- Chapter 7 provides a
  mechanical and barri
- Chapter 8 reports th
  and hybrid biocompo
- Chapter 9 provides
  problem that aimed
  of bio-resin in a nan
  parameters and expe
- Finally, Chapter
  recommendations.

1.6 Organization

- The dissertation has been organized into <u>ten</u> chapters. The first chapter provides an introduction to the work with a brief background, scope and objectives of this work.
- Chapter 2 reports the study on development of novel solvent based processing techniques for development of bio-based nanocomposites.
- Chapter 3 and Chapter 4 report the experimental characterization of bio-based nanocomposites with EMS and EML bio-resins, respectively.
- Chapter 5 and Chapter 6 provide the experimental characterization of hybrid biocomposites produced from the nanocomposite resins as reported in Chapter 3 and Chapter 4, respectively.
- Chapter 7 provides an overview of numerical and analytical models to predict the mechanical and barrier properties of bio-based nanocomposites.
- Chapter 8 reports the multiscale simulations of tensile response of nanocomposites and hybrid biocomposites using a multi-level FE technique.
- Chapter 9 provides an overview and results of a material layout optimization problem that aimed at determining an enhanced RVE, that obtains the distribution of bio-resin in a nanocomposite RVE by minimizing the error between homogenized parameters and experimental target properties.
- Finally, Chapter 10 provides concluding remarks, research needs and recommendations.

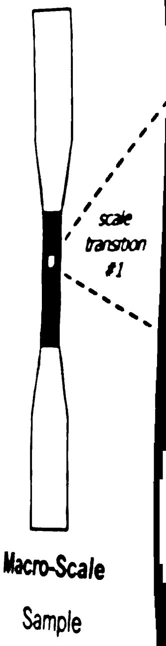

Figure 1-1. Schemati

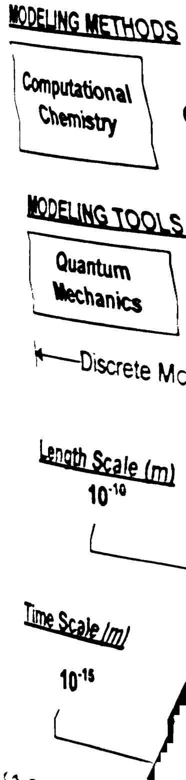

Figure 1-2. Computation

1.7 Tables and Figures

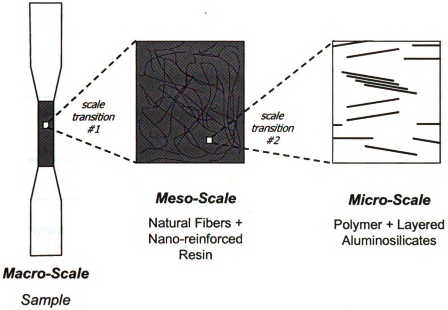

Figure 1-1. Schematic showing multiscale components and phase transitions

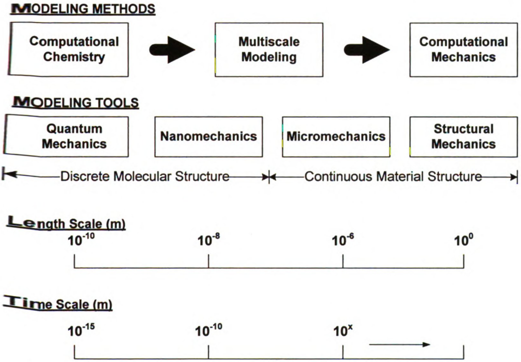

Figure 1-2. Computation materials – Length, time scales, modeling methods and associated tools [1-40].

Figure 1

Fig

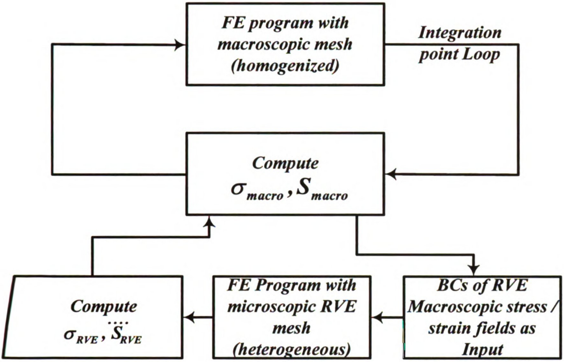

Figure 1-3. Schematic of multiscale FE approach (Adapted from [1-10]).

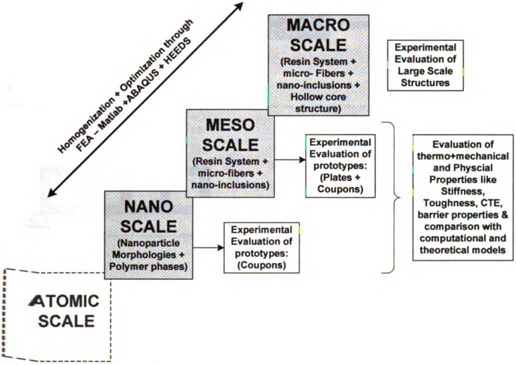

Figure 1-4. Hierarchical Modeling and Evaluation Techniques

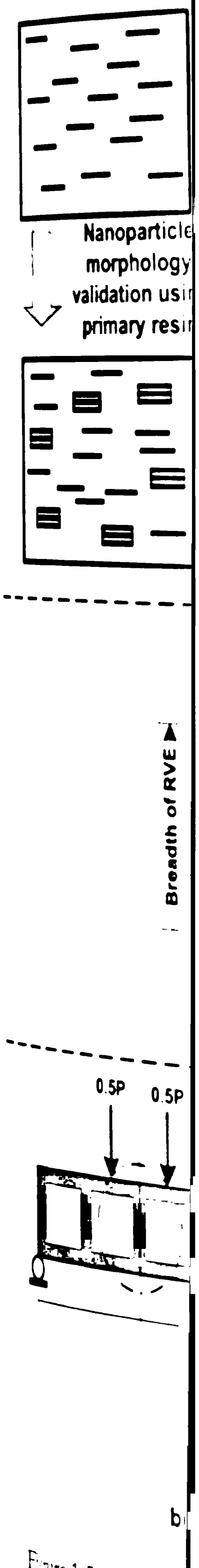

Figure 1-5. Overall a

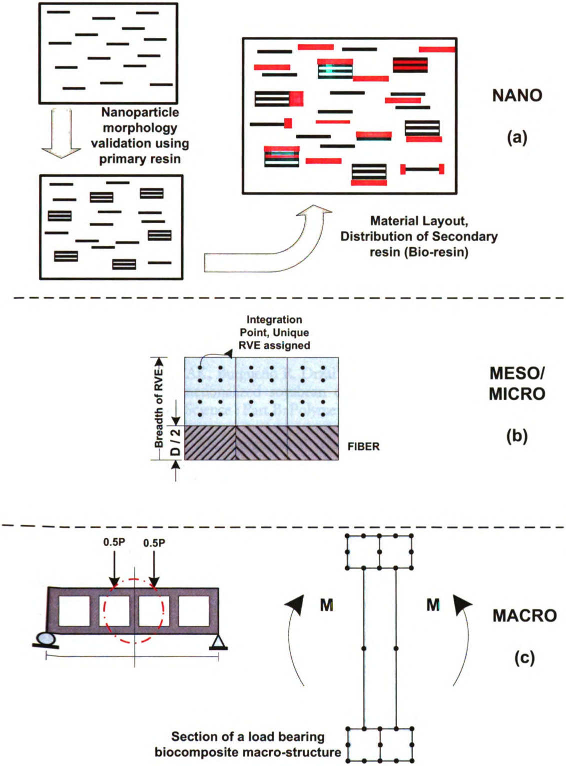

Figure 1-5. Overall approach of multiscale modeling for load bearing biocomposites

References

[1] Mohanty AK, Misra
Biocomposites: A
276/277:1-24.

[2] Nickel J, Riedel U. Ac

[3] Donnell AO, Dweib
resin. Composites

[4] Morye SS, Wool RP.
a novel modified
407-146.

[5] Burgueño R, Quag
Sustainable cellu
resin for housin
2005, 13:139-149

[6] Miyagawa H, Mohan
from blends of
Journal of Polym

[7] Miyagawa H, Moha
biobased unsat
Industrial and En

[8] Miyagawa H, Mohan
thermophysical
nanocomposites.

[9] Kouznetsova V, Br
modeling of hete

[10] Smit RJM, Brekelma
of nonlinear he
Computational

[11] Burgueño R, Quag
biofiber-based
Applied Science

[12] Burgueño R, Qua
Hierarchical ce
Material Science

1.8 References

[1-1]. Mohanty AK, Misra M, Hinrichsen G. Biofibers, Biodegradable Polymers and Biocomposites: An Overview. Macromolecular Materials and Engineering. 2000; 276/277:1-24.

[1-2]. Nickel J, Riedel U. Activities in biocomposites. Materials Today. 2003, 6:44-48.

[1-3]. Donnell AO, Dweib MA, Wool RP. Natural fiber composites with plant oil based resin. Composites Science and Technology. 2004, 64: 1135-1145.

[1-4]. Morye SS, Wool RP. Mechanical properties of glass/flax hybrid composites based on a novel modified soyabean oil matrix material. Polymer Composites. 2005, 26: 407-146.

[1-5]. Burgueño R., Quagliata MJ, Mehta GM, Mohanty AK, Misra M, Drzal LT. Sustainable cellular biocomposites from natural fibers and unsaturated polyester resin for housing panel applications. Journal of Polymers and Environment. 2005, 13:139-149.

[1-6]. Miyagawa H, Mohanty AK, Burgueño R, Drzal LT, Misra M. Novel biobased resins from blends of functionalized soyabean oil and unsaturated polyester resin. Journal of Polymer Science : Part B: Polymer Physics. 2007, 45:698-704.

[1-7]. Miyagawa H, Mohanty AK, Burgueño R, Drzal LT, Misra M. Development of biobased unsaturated polyester containing functionalized vegetable oils. Industrial and Engineering Chemistry Research. 2006, 45:1014-1018.

[1-8]. Miyagawa H, Mohanty AK, Burgueño R, Drzal LT, Misra M. Characterization and thermophysical properties of unsaturated polyester-layered silicate nanocomposites. Journal of Nanoscience and Nanotechnology. 2006, 6:464-471.

[1-9]. Kouznetsova V, Brekelmans WAM, Baaijens FPT. An approach to micro-macro modeling of heterogeneous materials. Computation Mechanics. 2001, 27:37-48.

[1-10]. Smit RJM, Brekelmans WAM, Meijer HEH. Prediction of the mechanical behavior of nonlinear heterogeneous systems by multi-level finite element modeling. Computational methods in Applied Mechanical Engineering. 1998, 155: 181-192.

[1-11]. Burgueño R, Quagliata MJ, Mohanty AK, Mehta GM, Drzal LT, Misra M. Hybrid biofiber-based composites for structural cellular plates. Composites Part A: Applied Science and Manufacturing. 2005, 36:581-593.

[1-12]. Burgueño R, Quagliata MJ, Mohanty AK, Mehta GM, Drzal LT, Misra M. Hierarchical cellular designs for load bearing biocomposite beams and plates. Material Science and Engineering A. 2005, 390: 178-187.

[1-13] Burgueño R, Quaglia
bearing natural fi
Applied Science a

[1-14] Mohanty AK, Miyaga
organoclay and bi
ANTEC, Confere

[1-15] Mishra S, Misra M,
Performance of
Composites Scien

[1-16] Haq M, Burgueño
polyester/layered
properties. Comp

[1-17] Ratna D. Mechanic
modified epoxy r

[1-18] Shengton III HW, W
Hong C. An
Construction. Pr
Technolgoy, Hon

[1-19] Quagliata MJ. Devel
and Plates for
University, East

[1-20] Kinloch AJ, Moham
toughness of car
matrices. Journa

[1-21] Hsiao TK, Alms J.
adhesives to join
2003, 14:791-79

[1-22] Gojny FH, Wichma
modification on
reinforced poly

[1-23] Le Baron PC, Wan
overview. Appli

[1-24] Haq M, Burgueño
Unsaturated-Po
Limits. Compos

[1-25] Bohm, HJ. A Short
FMD Report, 3

[1-13]. Burgueño R, Quagliata MJ, Mohanty AK, Mehta GM, Drzal LT, Misra M. Load bearing natural fiber composite cellular beams and panels. Composites part A: Applied Science and Manufacturing. 2004, 35:645-656.

[1-14]. Mohanty AK, Miyagawa H, Burgueño R, Misra M. Biobased nanocomposites from organoclay and blends of unsaturated polyester and functionalized vegetable oil. ANTEC, Conference Proceedings. 2005, 4:52-56.

[1-15]. Mishra S, Misra M, Tripathy SS, Nayak SK, Mohanty AK. Studies on Mechanical Performance of Bio fiber / Glass reinforced polyester hybrid composites. Composites Science and Technology. 2003, 63:1377-1385.

[1-16]. Haq M, Burgueño R, Mohanty AK, Misra M. Bio-based unsaturated polyester/layered silicate nanocomposites: characterization and thermo-physical properties. Composites Part A. 2009; 40:540-547.

[1-17]. Ratna D. Mechanical properties and morphology of epoxidized soyabean oil-modified epoxy resin. Polymer International. 2001; 50:179-184.

[1-18]. Shengton III HW, Wool RP, Hu B, Donnell AO, Bonnaille L, Can E, Chapas R, Hong C. An All-Natural composite Material Roof System for Residetial Construction. Proceedings of International Conference on Advances of Building Technolgoy, Hong Kong, China, December 2002.

[1-19]. Quagliata MJ. Development and Characterization of Biocomposite Cellular Beams and Plates for Load-Bearing Components. Masters Thesis, Michigan State University, East Lansing, MI; 2003.

[1-20]. Kinloch AJ, Mohammed RD, Taylor AC, Sprenger S, Egan D. The interlaminar toughness of carbon fibre reinforced plastic composites using 'hybrid-toughened' matrices. Journal of Material Science. 2006, 41:5043-5046.

[1-21]. Hsiao TK, Alms J, Advani SG. Use of epoxy/multiwalled carbon nanotubes as adhesives to join graphite fiber reinforced polymer composites. Nanotechnology. 2003, 14:791-793.

[1-22]. Gojny FH, Wichmann MHG, Fiedler B, Bauhofer W, Schulte K. Influence of nano-modification on the mechanical and electrical properties of conventional fiber-reinforced polymers. Composites Part A. 2005, 36:1525-1535.

[1-23]. Le Baron PC, Wang Z, Pinnavaia TJ. Polymer – layered silicate nanocmposites: an overview. Applied Clay Science. 1999, 15:11-29

[1-24]. Haq M, Burgueño R, Mohanty AK, Misra M. Processing Techniques for Bio-based Unsaturated-Polyester/Clay Nanocomposites: Tensile Properties, Efficiency, and Limits. Composites – Part A 2009; 40:394-403.

[1-25]. Bohm, HJ. A Short Introduction to Basic Aspects of Continuum Mechanics." CDL-FMD Report, 3 (1998). Vienna Institute of Technology.

[26] Eshelby JD. The
Proceedings

[27] Hashin Z. The
Mechanics. 1

[28] Hashin Z, Shrik
multiphase
11:127-140,

[29] Hill R. A self-co
and Physics

[30] Duschlbauer D
Composites
Localization
Materials 20

[31] Bensoussan A,
Structures, 1

[32] Sanchez-Palenci
in Physics, 1

[33] Sheng N, Boyc
micromecha
clay particle.

[34] Brune DD, Bice
and compre
exfoliation a

[35] Drown EK, Mo
The surface
poly(trimeth
Technology,

[36] Breuls RGM, Se
local cell d
element app

[37] Van der Sluis O,
heterogeneo
Mechanics o

[38] Feyel F, Chaboc
behvior of
Applied Mec

[1-26]. Eshelby JD. The determination of the field of an ellipsoidal inclusion and related. Proceedings of the Royal Soceity of London, Part A. 1957, 241:376-296.

[1-27]. Hashin Z. The elastic modulii of heterogenous materials. Journal of Applied Mechanics. 1962, 29:143-150.

[1-28]. Hashin Z, Shrikman S. A variational approach to the theory of elastic behavior of multiphase materials. Journal of the Mechanics and Physics of Solids. 1963, 11:127-140,

[1-29]. Hill R. A self-consistent mechanics of composite materials. Journal of the Mechanics and Physics of Solids. 1965, 13: 213-222.

[1-30]. Duschlbauer D, Bohm HJ, Petermann HE. Computational Simulation of Composites Reinforced by planar random fibers: Homogenization and Localization by Unit Cell and Mean Field Approaches. Journal of Composite Materials 2006, 40:2217-2234.

[1-31]. Bensoussan A, Lionis JL, Papanicolau G. Asymptotic Analysis for Periodic Structures, 1978. North Holland, Amsterdam.

[1-32]. Sanchez-Palencia E. Non-homogeneous Media and Vibration Theory. Lecture Notes in Physics, 1980. Springer-Verlag, Berlin.

[1-33]. Sheng N, Boyce MC, Parks DM, Rutledge GC, Abes JI, Cohen RE. Multiscale micromechanical modeling of polymer/clay nanocomposites and the effective clay particle. Polymer 2004, 45:487-506.

[1-34]. Brune DD, Bicerano J. Micromechanics of nanocomposites: Comparison of tensile and compressive elastic modulii, and prediction of effects of incomplete exfoliation and imperfect alignment on modulus. Polymer 2002, 43:369-387.

[1-35]. Drown EK, Mohanty AK, Parulekar Y, Hasija D, Harte BR, Misra, M, Kurian JV. The surface characteristics of organoclays and their effect on the properties of poly(trimethylene terephtahalate) nanocomposites. Composites Science and Technology, 2007, 67:3168-3175.

[1-36]. Breuls RGM, Sengers BG, Oomens CWJ, Bouten CVC, Baaijens FPT. Predicting local cell deformations in engineered tissue constructs: A multi-level finite element approach. Transactions of the ASME 2002; 124:198-207.

[1-37]. Van der Sluis O, Schreurs PJG, Brekelmans WAM, Meijer HEH. Overall behavior of heterogeneous elastoviscoplastic materials: effect of microstructural modeling. Mechanics of Materials 2000, 32:449-462.

[1-38]. Feyel F, Chaboche JL. FE2 multiscale approach for modeling the elastoviscoplastic behvior of long fiber SiC/Ti composite materials. Computational Methods in Applied Mechanical engineering. 2000, 183:309-330.

[illegible] Matsui K, Tera
solids with
606.

[illegible] Gates, T.S., C
materials:
Composite

[1-39]. Matsui K, Terada K, Yuge K. Two-scale finite element analysis of heterogeneous solids with periodic microstructures. Computers and Structures 2004, 82:593-606.

[1-40]. Gates, T.S., Odegard, G.M., Frankland, S.J.V., and Clancy, T.C., "Computational materials: Multiscale modeling and simulation of nanostructured materials" Composites Science and Technology. 65 (2005) 2416-2434.

Chapter 2. Develo

2.1 Abstract

Bio-based clay/polymer

and epoxidized methyl

Four methods were

incorporation of high

performed using electr

sequence, and sonicatio

and composite quality.

the incorporation of hig

bio-resin added after so

and exfoliation, and hi

sequence led to enhanced

2.2 Introduction

Bio-based resin

petroleum based resins

to obtain novel, value

alternatives for petrole

propelled from an envi

overview on bio-polym

Haq, M. Burgueño, R., M
Polymer/Clay Nanocompo
4394-453.

Chapter 2. Development of Bio-based Clay Nanocomposites [1]

2.1 Abstract

Bio-based clay/polymer nanocomposites using blends of styrene-based unsaturated polyester and epoxidized methyl soyate were manufactured using solvent-based processing techniques. Four methods were evaluated to assess limitations related to solvent removal and incorporation of high clay and bio-resin content. Nanocomposite characterization was performed using electron microscopy and tensile tests. Solvent type, bio-resin addition sequence, and sonication energy were the key parameters governing processing efficiency and composite quality. Processes with bio-resin added after solvent removal show promise in incorporation of high bio-resin and nanoclay contents. Use of acetone as a solvent with bio-resin added after solvent removal led to nanocomposites with good nanoclay dispersion and exfoliation, and high tensile modulus. Direct sonication in the base resin diluted with styrene led to enhanced and balanced gains in stiffness and toughness.

2.2 Introduction

Bio-based resin systems obtained as blends of functionalized vegetable oils and petroleum based resins or vegetable oil based resin systems can be reinforced with nanoclays to obtain novel, value added applications for natural polymers [2-1]. The development of alternatives for petroleum derived materials with plant-based renewable materials has been propelled from an environmental viewpoint [2-1]-[2-4]. Mohanty et al. [2-2] provide a good overview on bio-polymers, bio-fibers and bio-based composites, biocomposites. Bio-based

---

[1] Haq, M., Burgueño, R., Mohanty, A.K., and Misra, M., "Processing Techniques for Bio-based Unsaturated-Polyester/Clay Nanocomposites: Tensile Properties, Efficiency, and Limits," Composites - Part A. 2009; 40:394-403.

rms defined as a co
ers as secondary co
ystem [2-5][2-6]. This
the system, leading
ughness seriously a
properties of the res
parameters and a prop
research has shown th
properties of rigidity a
modification [2-1]. On
from the addition of b
processing of nanoclay
of nanoclay reinforced
separation and thermal
these processing issu
processing techniques f

Petroleum-base
shown to impart multif
stiffness but improve
properties [2-8]. The re
with nanoclays has yiel
improvement due to a
polymers [2-6]. Moreove
which are commonly us

resins defined as a combination of *petroleum based resins* as primary constituent and *natural bio-resins* as secondary constituent, have shown to improve the toughness of the resulting resin system [2-5][2-6]. This increase in toughness is due to the reduction in cross-link density in the system, leading to increased plastic deformations [2-7]. However, this increase in toughness seriously affects the modulus [2-5]-[2-7], thermal [2-6][2-7] and barrier [2-6] properties of the resulting polymer. Stiffness and toughness are opposing performance parameters and a proper balance is required to develop an efficient biocomposite. Moreover, research has shown that use of plant-oil based polymeric materials do not show adequate properties of rigidity and strength for load-bearing applications by themselves and require modification [2-1]. One approach pursued by the authors is to recover the property losses from the addition of bio-resin by the addition of layered silicates or nanoclays. Although the processing of nanoclay reinforced polymers is well established, the solvent-based processing of nanoclay reinforced bio-based resin systems brings about new issues, such as phase separation and thermal degradation of the polymer constituents [2-6]. This work addresses these processing issues and summarizes the development of suitable solvent-based processing techniques for efficient production of nanoclay reinforced bio-based polymers.

Petroleum-based polymers reinforced with layered silicates, or nanoclays, have been shown to impart multifunctionality to the resulting polymers with enhancements not only on stiffness but improvements in thermal, barrier, flammability and ablation resistance properties [2-8]. The reinforcement of soy [2-1][2-9][2-10] and corn [2-11] based bio-resins with nanoclays has yielded similar results. In spite of the noted enhancements, stiffness improvement due to addition of nanoclay also increases the brittleness of the resulting polymers [2-6]. Moreover, petroleum-based resins such as unsaturated polyesters (UPEs), which are commonly used due to their low cost, ease of handling and good balance of mechanical, electrical, ch

[2-12][2-13]. As far as bi

required for structural a

soybean oil with petro

thermoset [2-2][2-5][2-6

renewable resins has

thermophysical characte

and UPE with nanocla

varying bio-resin and n

increasing bio-resin co

stiffness. Partial recov

properties were achi

nanocomposites thus

toughness) [2-1][2-5][2

base polymer with incre

It is commonly

of nanoclay reinforced

nanoclay in the matrix

morphologies are expec

morphologies is typicall

nanoclay depends on

nanoclay with the host

preparation of nanocla

polymerization, melt i

mechanical, electrical, chemical and fire resistance properties, are inherently brittle in nature [2-12][2-13]. As far as bio-resins, their mechanical and thermal properties are far lower than required for structural applications. Research has shown that the blending of functionalized soybean oil with petro-based resins (UPE) can increase toughness of the petro-based thermoset [2-2][2-5][2-6][2-13]. The substitution of non-renewable synthetic resins with renewable resins has been proposed and studied considerably [2-5][2-13]-[2-17]. The thermophysical characterization of bio-based resin systems using functionalized soybean oil and UPE with nanoclay has been performed by our group [2-6] by studying the effect of varying bio-resin and nanoclay content on tensile, impact, moisture and tensile properties. Increasing bio-resin content was shown to improve ductility and toughness but reduces stiffness. Partial recovery of lost stiffness and improvements in thermal and barrier properties were achieved with nanoclay reinforcement. The resulting bio-based nanocomposites thus showed multifunctional properties with improved mechanical (toughness) [2-1][2-5][2-6][2-15][2-16], thermal [2-1] and barrier properties [2-6] than the base polymer with increased environmental appeal.

It is commonly agreed that the enhancement of physical and mechanical properties of nanoclay reinforced polymers is dependent on the distribution and morphology of nanoclay in the matrix. In order to obtain maximum benefits from nanoclays, exfoliated morphologies are expected. However, in reality, a combination of intercalated and exfoliated morphologies is typically obtained [2-18][2-19]. The degree of exfoliation and intercalation of nanoclay depends on the processing technique and compatibility (functionalization) of nanoclay with the host polymer system. The four main processes currently used for the preparation of nanoclay reinforced polymer systems are exfoliation-adsorption, in-situ polymerization, melt intercalation, and template synthesis [2-8][2-20]. The exfoliation-

adsorption process is
nanoclay and polymer
method or solution b
and is reported to c
functionalization, sol
nanoclay is exfoliate
polymer is soluble. W
the solvent. This pro
The polymer is then a
The nanocomposite n

Considerable
with a variety of solv
[2-17][2-18][2-19][2-2
Alexandre and Dubo
and resulting proper
acetone as a solv
nanocomposites. Th
were partially exfoli
nanocomposites synt
a solvent. Nanocon
prepared by simple n
dispersion of organo
between nanoclays a
were studied by inter

adsorption process is a solvent-based process in which a solvent compatible with both nanoclay and polymer is used. Hence, this process is also referred to as the common solvent method or solution based processing technique (SBPT). SBPT is a widely used technique and is reported to consistently give exfoliated morphologies provided that proper clay functionalization, solvent and blending conditions are met [2-21]. In this process, the nanoclay is exfoliated or separated into individual sheets using a solvent in which the polymer is soluble. When using an adequate solvent, the nanoclay can be easily dispersed in the solvent. This process is facilitated by stirring and the application of ultrasonic energy. The polymer is then added to the mixture for adsorption to the delaminated nanoclay sheets. The nanocomposite resin system is obtained upon solvent removal [2-20].

Considerable work on nanocomposites from solvent based processing techniques with a variety of solvents has been reported in the literature for both conventional polymers [2-12][2-18][2-19][2-21][2-23]-[2-26] and bio-based polymers [2-1][2-6][2-9][2-10][2-11][2-27]. Alexandre and Dubois [2-20] and Le Baron et al. [2-22] provide a good review on synthesis and resulting properties of a wide range of polymers. Miyagawa et al. [2-12][2-25] used acetone as a solvent in synthesizing epoxy/clay [2-25] and polyester/clay [2-12] nanocomposites. The resulting nanocomposites were well dispersed and clay morphologies were partially exfoliated and intercalated. Hutchinson et al. [2-24] compared epoxy/clay nanocomposites synthesized by simple direct mixing in virgin resin, and by using acetone as a solvent. Nanocomposites processed with acetone had better dispersion than those prepared by simple mixing. Burgentzle et al. [2-23] evaluated the parameters controlling the dispersion of organophillic nanoclays in various organic solvents by studying the interaction between nanoclays and solvent molecules at various scales. The interactions at nanoscale were studied by interlayer spacing, at microscale by studying the rheological behavior of clay

suspensions, and
observed that high
the proper balanc
was essential for dis
solvent blending
polystyrene using c
was obtained when
bio-based clay nanc
nano-whiskers on t
nanoclay or alumin
epoxy/vegetable o
homogeneous disp
bio-based clay nan
divinyl-benzene.
morphologies. Liu
epoxidized soybean

Research
unsaturated polyest
has been achieved,
clay and bio-resin
for solvent remova
about problems of
clay content requ
exfoliation. This re

suspensions, and at macroscale by analyzing swelling of nanoclay in solvents. It was observed that high surface energy solvents were effective for gelation at the microscale, and that proper balance between the hydrophilic and hydrophobic parts of solvent molecules was essential for dispersion of organophilic clays. Morgan and Harris [2-21] investigated how solvent blending with and without high energy mixing dispersed two types of clay in polystyrene using chlorobenzene as a solvent. They found that a high degree of exfoliation was obtained when organo-montmorillonite clay and high energy sonication were used. For bio-based clay nanocomposites, Miyagawa et al. [2-27] studied the effect of clay and alumina nano-whiskers on the mechanical properties of epoxy/vegetable oil blends. In each case, the nanoclay or alumina whiskers were sonicated in acetone for 2 hours and then mixed with the epoxy/vegetable oil blend. The resulting nanoclay composites were reported to have homogeneous dispersion and exfoliated morphologies. Lu and Larock [2-11] synthesized bio-based clay nanocomposites by cationic polymerization of corn-oil with styrene and divinyl-benzene. The resulting nanocomposites were reported to have intercalated morphologies. Liu et al. [2-9], Uyama et al. [2-1], and Song et al. [2-10] synthesized epoxidized soybean oil/clay nanocomposites by direct sonication in soybean oil.

Research in our group [2-6] synthesized clay nanocomposites on blends of unsaturated polyester and soybean oil. While good dispersion and exfoliation of the nanoclay has been achieved, the standard SBPT restricts the incorporation of higher concentrations of clay and bio-resin content. One of the drawbacks of SBPT is the amount of energy required for solvent removal. The use of solvent based processing for bio-based resin systems brings about problems of phase separation and thermal degradation of polymers [2-6]. Increase of clay content requires an increase of the solvent solution for proper dispersion and exfoliation. This requires a large amount of energy to remove the solvent, which can cause

thermal degradation
nanoclay-reinforced
structural compone
there is a need for e

The choice
the aim was to deve
manufacturing large-
vacuum assisted res
developments and in
]. Hence, the aim w
of other techniques

In this work,
development of nano
processing methods
based polymer/clay n
unsaturated polyester
solvent. Four differen
developed by our grou
elongations at failure
characterization of nan
and similar work with
communication. The e
Transmission electron
of the nanoclay. Scanni

thermal degradation of the polymers. Moreover, the research in our group aims in using nanoclay-reinforced bio-based resin systems for manufacturing large scale load-bearing structural components, and therefore large quantities of resin systems are required. Hence, there is a need for efficient processing that can also handle large quantities.

The choice of using SBPT to develop bio-based nanocomposites is two fold. First, the aim was to develop nanoclay reinforced thermoset resin systems that could be used in manufacturing large-scale bio-based structural components (such as sandwich panels) using vacuum assisted resin transfer molding (VARTM). And secondly, this work presents new developments and improvements to the recommendations from an earlier study using SBPT [6]. Hence, the aim was to develop improvements on the SBPT and a study on the feasibility of other techniques was not performed as it was beyond the scope of the research aim.

In this work, solvent based processing techniques were studied for efficient development of nanoclay-reinforced bio-based resin systems, by evaluating different processing methods that can maximize the amount of bio-resin and nanoclay content. Bio-based polymer/clay nanocomposites were processed using SBPT for blends of styrene based unsaturated polyester (UPE) and epoxidized methyl soyate (EMS) with acetone as the solvent. Four different processing techniques were studied by modifying the baseline SBPT developed by our group [2-6][2-12]. Only tensile properties, namely: modulus, strength and elongations at failure were studied. Comprehensive thermophysical, mechanical and barrier characterization of nanocomposite resins with soy-based resins are reported elsewhere [2-6] and similar work with linseed oil based resins is in progress and will be forthcoming in future communication. The effects of sonication energy and styrene content were also studied. Transmission electron microscopy was used to study the degree of dispersion and exfoliation of the nanoclay. Scanning electron microscopy was used to study the features of the tensile fracture surfaces. A co

feasible amount of bio-

provided.

2.3 Experimental

Four different

reinforced with nano

nanocomposites. In th

nomenclature used, tes

2.3.1 Materials

The main comp

Reichhold Inc., N

epoxidized methyl soya

The nanoclay used in t

resin system (mixture o

Sigma Aldrich, MO) as

A constant ratio by wei

for all samples. The m

promoter and 1.50 parts

°C for 2 hours. For all p

Branson 750 W ultra-soni

fracture surfaces. A comparison of the four processes with respect to processing time, feasible amount of bio-resin and clay content, drawbacks and overall efficiency is also provided.

2.3 Experimental Methods

Four different processes were studied for the development of bio-based resin blends reinforced with nanoclay inclusions. Tensile properties were studied for the resulting nanocomposites. In the following sections, details on materials, description of processes, nomenclature used, testing and characterization details are provided.

2.3.1 Materials

The main component was ortho unsaturated polyester resin (UPE, Polylite® 32570-00, Reichhold Inc., NC), which contains 33.5 wt.% styrene. A bio-based modifier, epoxidized methyl soyate (EMS, Vikoflex® 7010, Arkema Inc, PA) replaced parts of UPE. The nanoclay used in this work was Cloisite 30B® (Southern Clay Products, Inc. TX). The resin system (mixture of UPE, EMS and organoclay) was processed with cobalt naphthenate (Sigma Aldrich, MO) as a promoter and 2-butanone peroxide (Sigma Aldrich) as an initiator. A constant ratio by weight of the resin system to the promoter and initiator was utilized to cure all samples. The mixing ratio was 100 parts by weight of the resin system to 0.03 parts promoter and 1.50 parts initiator. Samples were cured at 100 °C for 2 hours, followed by 160 °C for 2 hours. For all processes in this study, the sonication energy was applied using Cole - Parmer 750 W ultra-sonicator with a 25 mm diameter solid probe.

3.3.2 Testing & Ch

Tensile tests

loading was 5 mm/n

The dispersion and n

with transmission ele

carried using a diamo

nm thick. A JEOL 1

obtain bright field ima

emission scanning elec

coated with a thin gold

3.4 *Processing Te*

Research in ou

structural application

resin transfer moldi

the processing tech

that would be requ

single batch proc

content was 5 wt.

25 g of bio-resin *(*

herein is based on

our group to develop

d was modified with th

while also increasing the

2.3.2 Testing & Characterization

Tensile tests were performed according to ASTM D638 standards. The rate of loading was 5 mm/min. Six tensile specimens were tested for each nanocomposite system. The dispersion and morphology of nanoclay inclusions in the nanocomposite were observed with transmission electron microscopy (TEM). Ultramicrotomy at room temperature was carried using a diamond knife with an included angle of 4° to produce sections around 70 nm thick. A JEOL 100CX TEM with LaB_6 filament with 120 kV acceleration was used to obtain bright field images. The tensile failure surfaces were observed with a JEOL 6400 field emission scanning electron microscope (SEM) at 10 kV acceleration voltage. Specimens were coated with a thin gold film prior to SEM observations.

2.4 Processing Techniques

Research in our group has been aimed at manufacturing of bio-based composites for structural applications using these nano-reinforced bio-based resins through vacuum assisted resin transfer molding (VARTM). As a result, in order to estimate the overall efficiency of the processing technique(s), the quantities of the resins used in this study were the same as that would be required during the manufacturing of large-scale biocomposite components. A single batch processed 500 g of resin (UPE+EMS). As discussed earlier, the bio-resin content was 5 wt.% and clay content was 3 wt.%. Hence, for a single batch, 475 g of UPE, 25 g of bio-resin (EMS) and 15.464 g of nanoclay were used. The processing study reported herein is based on modifications to a baseline solvent based processing technique used by our group to develop polymer-clay nanocomposites [6][12]. The baseline technique (Process A) was modified with the aim of increasing the feasible amounts of bio-resin and nanoclay while also increasing the overall efficiency of the process, thereby leading to four novel approaches. A det

following. For all

provided:

Process A: T

with a magnetic st

studies, the quantity

The acetone + nan

sonication probe fo

removed and both

mixture (UPE + EM

plate at 55 °C until a

acetone was remove

method is that durin

removed. The amou

acetone removal pr

blended with the ini

promoter, and the cu

Process A is shown i

At higher con

Process A: 1) the res

phase separation betw

pressures during the

nanoclay loading less t

approaches. A detailed description of the baseline process (Process A) is explained in the following. For all other processing techniques the modifications made to Process A are provided:

Process A: This is the baseline processing technique. To a 2000 ml beaker equipped with a magnetic stir bar, nanoclay (3 wt.%) and acetone (750 ml) were added. From trial studies, the quantity of acetone was determined to be 50 ml acetone per gram of nanoclay. The acetone + nanoclay solution was continuously stirred, while it was sonicated using a sonication probe for the desired time or energy. After sonication, the ultrasonic probe was removed and both the UPE (475 g) and EMS (25 g) resins were added. The resulting mixture (UPE + EMS + acetone + nanoclay) was continuously stirred while placed on a hot plate at 55 °C until approximately 75% of the acetone was removed (3 hours). The remaining acetone was removed by vacuum extraction at 55 °C for 24 hours. A drawback of this method is that during the acetone removal process, the styrene present in the UPE is also removed. The amount of lost styrene was re-introduced to the blend after completing the acetone removal process. The processed solution was cooled to room temperature and blended with the initiator and promoter followed by curing. The amounts of initiator and promoter, and the curing temperature are provided in Section 2.3.1. A flow chart explaining Process A is shown in Figure 2-1.

At higher concentrations of EMS and nanoclay two problems were encountered in Process A: 1) the resin seemed to cross-link during the acetone removal process, and 2) phase separation between EMS and UPE was observed, leading to instability at high vacuum pressures during the acetone extraction process. These problems were not observed at nanoclay loading less than 1.5 wt.% and EMS contents of less than 10%. Hence, Process B

solved by making
EMS) content.

Process B: I
acetone is removed
Process B solved th
enabled incorporati
during the acetone
UPE present is rela
the amount of bio-

The proble
the solvent extracti
to issues of excess
hampers the prop
developed to elimin

Process C: P
UPE resin and bio
system, the tempe
energies. Thus, son
to cool down to ro
and applying energ
process. Additiona
damage the sonica
reduce the resin sys

evolved by making slight modifications to Process A to increase the nanoclay and bio-resin (EMS) content.

Process B: In this process (Figure 2-1) the bio-resin is not added until all of the acetone is removed. After acetone removal, the EMS is added along with the lost styrene. Process B solved the problems of phase separation and gelling during acetone removal and enabled incorporation of higher clay contents. Nonetheless, since only neat UPE is present during the acetone removal process, at high bio-resin and nanoclay contents, the amount of UPE present is relatively small, thereby making the resin system highly viscous and limiting the amount of bio-resin content that can be added.

The problems associated with in bio-nanocomposite processing are mainly due to the solvent extraction step. The common solvent used in this work was acetone. In addition to issues of excessive energy and time required for solvent removal, any residual acetone hampers the properties of the resulting resin system. Processes C and D were thus developed to eliminate the use of acetone.

Process C: Process C (Figure 2-1) consists of sonicating the nanoclay directly in the UPE resin and bio-resin is added after sonication. Due to the viscosity of the UPE resin system, the temperature of the solution increases rapidly even at very low sonication energies. Thus, sonication energy is applied in steps of 20 kJ and the resin system is allowed to cool down to room temperature before the next step is applied. The process of cooling and applying energy in steps does not allow high sonication energies to be achieved by this process. Additionally, at high clay contents, the increased viscosity of resin system can damage the sonication equipment. As a result, Process D (Figure 2-1) was developed to reduce the resin system viscosity.

Process D: In this p

additional styrene solution

thereby issues of residual

excess styrene is removed

for approximately 6 hours

foreign solvent (i.e., aceto

processes A and B. Noneth

the nanocomposites synth

exfoliation, but the use c

efficiency of such processe

Process E: Process E

vacuum use for removal of

except that acetone is re

stirring - i.e., not using a

the sonicated nanoclay

indicating total removal

at the end.

In this work, a

maintain same proces

for all *processes*, there

Hence, *the* properties *o*

various processes *can be*

Process D: In this process the resin system viscosity is reduced by adding 50 wt.% additional styrene solution to the system. Styrene is an inherent component of neat UPE and thereby issues of residual solvent in the resin system are eliminated. After sonication, the excess styrene is removed by mechanical stirring and application of constant heat (~55 °C) for approximately 6 hours. Processes C and D eliminate the use of vacuum to remove the foreign solvent (i.e., acetone), thereby improving the time and energy efficiency relative to processes A and B. Nonetheless, as shown later, it was found in microscopic observations that nanocomposites synthesized with acetone as solvent produced better dispersion and exfoliation, but the use of vacuum and heat in acetone removal was limiting overall efficiency of such processes. As a result, Process E was developed.

Process E: Process E (Figure 2-1) was developed with the goal of eliminating the vacuum use for removal of acetone in processes A and B. Process E is similar to process B, except that acetone is removed only through heating on a hot plate while mechanically stirring - i.e., not using a vacuum. Acetone removal is monitored by measuring the weight of the sonicated nanoclay/resin solution until no further decrease in weight is observed, indicating total removal of solvent. Any lost styrene and the target bio-resin content is added at the end.

In this work, after solvent removal, irrespective of the solvent, care was taken to maintain same processing conditions (amounts of promoter and initiator, curing time etc.,) for all processes, thereby minimizing the effects introduced due to varying cure conditions. Hence, the properties of the resulting nanocomposites and the nanoclay morphology from various processes can be directly compared.

2.5 *Processing Varia*

2.5.1 Styrene Content i

The UPE used in t
of UPE with EMS reduce
expected that premature c
overall styrene content. H
the overall styrene content
styrene level to the level or

2.5.2 Sonication Energy

It is commonly agre
and exfoliation of the resu
the nanoclay particles and
efficiency. Moreover, using
properties while also achie
sonication energy, levels of
processing techniques stu
showed that 60 kJ of en
particles. Hence processes
energy of 300 kJ was late
increased viscosity of the r
step.

2.5 Processing Variables

2.5.1 Styrene Content in Resin System

The UPE used in this study had a styrene content of 33.5 wt.%. Partial replacement of UPE with EMS reduces the overall styrene content of the resulting resin system. It is suspected that premature curing during the acetone removal step was due to the reduction in overall styrene content. Hence, the effect of styrene content was studied by: a) maintaining the overall styrene content at 33.5 wt.% for the blended resin system, and, b) keeping the styrene level to the level originally present in the UPE part of the blended system.

2.5.2 Sonication Energy

It is commonly agreed that increased sonication time, or energy, improves dispersion and exfoliation of the resulting nanocomposites. Nevertheless, excessive energy may break the nanoclay particles and reduce their aspect ratio, which reduces the reinforcement efficiency. Moreover, using optimum sonication energy would be essential to obtain desired properties while also achieving cost, time and energy efficiency. To assess the influence of sonication energy, levels of 60 kJ and 300 kJ were studied. Processes B and C were initial processing techniques studied with 60 kJ of energy. Electron microscopy observations showed that 60 kJ of energy was insufficient for adequate dispersion of the nanoclay particles. Hence processes D and E were sonicated only with 300 kJ of energy. A sonication energy of 300 kJ was later used for process B, but was infeasible for process C due to increased viscosity of the resin system, application of energy in steps and cooling after each step.

253 Material Content

In order to comp

processes must have simil

effects of variations in

communication. Neverthe

various nanoclay and bio-

[2-6]. A moderate amount

study and it is believed

concentrations. Similarly,

was chosen to avoid the p

and initiate at EMS conter

the various parameters in

ID.² The styrene weight I

wt.% styrene content in t

Weight ID is denoted by

system obtained from Pr

sonication energy, and co

total resin system at 33.5

energy of 60 kJ was appli

60 kJ. An asterisk (*) is m

sonication energy. Since

baseline neat resins with

For neat resins, the follo

2.5.3 Material Content and Nomenclature

In order to compare the various processing techniques in this study, each of the processes must have similar amounts of nanoclay and bio-resin. Detailed presentation of the effects of variations in clay and bio-resin content is beyond the scope of this communication. Nevertheless, work by our group on characterizing nanocomposites with various nanoclay and bio-resin contents obtained from Process A have already been reported [2-6]. A moderate amount of clay content (3 wt.%) was selected for all resin systems in this study and it is believed that conclusions of the study can be extended to other clay concentrations. Similarly, all processes were done with 5 wt.% bio-resin content. This level was chosen to avoid the problem of phase separation, as it was suspected that this problem can initiate at EMS contents beyond 10 wt.%. The following nomenclature is used to define the various parameters in this study: *"Process ID/Clay Content/Sonication Energy/Styrene Weight ID."* The styrene weight ID indicates whether additional styrene was added to maintain 33.5 wt.% styrene content in the total resin system. If additional styrene was added, the Styrene Weight ID is denoted by "A", else by "B." For example, "B/3/300/A" denotes a resin system obtained from Process B containing 3 wt.% of nanoclay processed with 300kJ of sonication energy, and containing additional styrene to maintain styrene concentration in the total resin system at 33.5 wt.%. In Process C, due to high viscosity issues, the sonication energy of 60 kJ was applied in two ways: a) steps of 20 kJ and b) continuous application of 60 kJ. An asterisk (*) is marked next to 60 kJ to indicate continuous application of 60 kJ of sonication energy. Since the nanoclay resin systems contain 5% EMS, corresponding baseline neat resins with no nanoclay were processed with and without additional styrene. For neat resins, the following nomenclature is used: "NEAT-95/5-A". The term NEAT indicates no nanoclay is p

The last term indicates the

2.6 *Results*

A comparison of

microscopic characterizati

process, the results are clas

the resin system. Since th

results indicate the effec

obtained from them. Resu

2.6.1 Overall Processin

Table 2-1 provide

study. The overall efficienc

the following factors: proc

viscosity and cooling iss

properties). The factors

processing technique (Sec

energy required in proces

applied (heat + stirring) d

qualitative and is intend

properties of the resulting

was observed that process

indicates no nanoclay is present and the resin system contains 95%UPE and 5% bio-resin. The last term indicates the styrene weight ID as explained earlier.

2.6 Results

A comparison of the various processing techniques, tensile test results and microscopic characterization of the nanocomposites are provided in this section. For each process, the results are classified with respect to the amount of sonication energy supplied to the resin system. Since the nanoclay and EMS content was the same for all processes, the results indicate the effect of the processing technique and the nanoclay morphologies obtained from them. Results are also compared with the properties of neat resin systems.

2.6.1 Overall Processing Efficiency

Table 2-1 provides a comparison of the processing techniques evaluated in this study. The overall efficiency of the processing system was determined by taking into account the following factors: processing time, relative energy demand, phase separation problems, viscosity and cooling issues, and most importantly the resulting material (i.e., tensile properties). The factors influencing the time and relative energy demand depend on processing technique (Section 3). The "relative energy demand" qualitatively compares the energy required in processing and includes the applied sonication energy and the energy applied (heat + stirring) during solvent removal. The relative energy demand parameter is qualitative and is intended for relative comparison of the various processes. Tensile properties of the resulting bio-nanocomposites are provided in following section. Overall, it was observed that processes B and D had good efficiency relative to other processes.

2.6.2 Tensile Propert

The summary o
sonication energies of
styrene content on tensi
the processing techniqu
compared separately fro
properties are compare

a Tensile Modulus

Tensile modulu
Figure 2-3 for sonicatio
KJ of applied energy
indicates that the son
observed that on ave
provided higher tensile
with similar bio-resin
increased cross-linking
With respect to neat re
the tensile modulus by
maintained and by 13 %

Nanocomposit
33 % and 50 % highe
Similarly, Process D le
neat UPE resin for 3
increase of 15 % whe

2.6.2 Tensile Properties

The summary of tensile test results is provided in Table 2-2 and Table 2-3 for sonication energies of 60 kJ and 300 kJ, respectively. Effects of sonication energy and styrene content on tensile properties are provided in this section. For relative comparison of the processing techniques, the resin systems in which styrene weight was maintained are compared separately from those in which styrene content was not maintained. The tensile properties are compared to those of neat UPE.

a) Tensile Modulus

Tensile modulus results for the various processes are provided in Figure 2-2 and Figure 2-3 for sonication energies of 60 kJ and 300 kJ, respectively. Process C used only 60 KJ of applied energy due to viscosity issues. The asterisk (*) in process C in Figure 2-2 indicates that the sonication energy was applied continuously and not in steps. It was observed that on average, nanocomposites from resin systems with additional styrene provided higher tensile modulus by about 20 % relative to their counterpart resin systems with similar bio-resin and clay contents but no additional styrene. This is attributed to increased cross-linking provided by styrene and reduction of the overall bio-resin content. With respect to neat resins, it was observed that the addition of bio-resin (5 wt.%) reduced the tensile modulus by an average of 4 % for resin systems in which styrene weight was maintained and by 13 % for resin systems with no additional styrene.

Nanocomposites from process B had tensile modulus values that were, on average 38 % and 50 % higher than neat UPE resin for sonication energies of 60 kJ and 300 kJ. Similarly, Process D led to nanocomposites with average tensile modulus 16 % higher than neat UPE resin for 300 kJ of sonication energy. Process C showed an average modulus increase of 15 % when 60 kJ of sonication energy was applied continuously, but showed

ick change in modulus
process which showed
:: kJ of sonication er
system.

: Ultimate Tensile S

Ultimate tensile
and Figure 2-3 for son
synthesized from all pro
The authors attribute th
to the relatively brittle p
ductility. While there is
a parallel effort to this
content increases, the s
reducing the ultimate te
also reduces the ultima
showed a decrease of in
which styrene weight w
or additional styrene.
strengths, approximately
the thermal degradation
acetone removal proces
and D had tensile stre
approximately 40 % and

little change in modulus when the same energy was applied in steps. Process E was the only process which showed a decrease in tensile modulus of about 50 % relative to neat UPE at 300 kJ of sonication energy. This is mainly attributed to the residual acetone in the resin system.

b) Ultimate Tensile Stress

Ultimate tensile stress results for the various processes are provided in Figure 2-2 and Figure 2-3 for sonication energies of 60 kJ and 300 kJ, respectively. Nanocomposites synthesized from all processes had lower ultimate tensile stresses than the neat resin systems. The authors attribute this to the stress concentrations created by the nanoclay reinforcement in the relatively brittle polymer matrix which in turn lead to lower tensile strength and lower ductility. While there is no general consensus on this point of view, computational studies by a parallel effort to this work [2-29] have shown evidence to this mechanism.. As nanoclay content increases, the stiffness and brittleness of the resulting resin systems increases thus reducing the ultimate tensile strength and ductility [2-6]. Moreover, the addition of bio-resin also reduces the ultimate tensile strength. For example, neat bio-based resins (no nanoclay) showed a decrease of in ultimate tensile strengths by approximately 5 % for resin systems in which styrene weight was maintained and a reduction of about 14 % for resin systems with no additional styrene. Nanocomposites from processes B and E had the lowest tensile strengths, approximately 54 % and 70 % lower than the neat UPE resin. This is attributed to the thermal degradation of the resin system due to prolonged exposure to heat during the acetone removal process. Nanocomposites synthesized with direct sonication processes C and D had tensile strengths greater than those made with processes B and E, yet with approximately 40 % and 44 % lower strength than neat UPE, respectively.

Elongation at Failure

The elongations at
Figure 2-4 and Figure 2
neat resins, the addition of
seems to make the system
process B had the lowest d
and 44 %, in ultimate tens
from process C, the resin s
approximately 8 % highe
applied in steps. Thus, th
energy in steps seems to a
from process E, which ca
increased ductility relative

In summary, the
processes, except process
largest improvement. Pro
strengths. Processes C and
sonication energy lead to
exfoliation of clay partic
resulting nanocomposites
techniques could be select

c) Elongation at Failure

The elongations at failure for nanocomposites from various processes are provided in Figure 2-4 and Figure 2-5 for sonication energies of 60 kJ and 300 kJ respectively. For neat resins, the addition of EMS increases the ductility. Nevertheless, the additional styrene seems to make the system more brittle and reduces the ductility. Nanocomposites from process B had the lowest ductility, followed by process C, with an average reduction of 47 % and 44 %, in ultimate tensile strain respectively relative to neat UPE. For nanocomposites from process C, the resin systems in which sonication energy was applied continuously, had approximately 8 % higher failure strains than the resin systems processed with energy applied in steps. Thus, the alternating cooling and heating required to apply sonication energy in steps seems to affect the behavior of the resulting resin system. Nanocomposites from process E, which can lead to residual acetone showed poor stiffness properties but increased ductility relative to nanocomposites from other processes.

In summary, the tensile modulus due to addition of nanoclay increased for all processes, except process E (attributed to residual acetone), with Process B showing the largest improvement. Processes that led to high tensile modulus had lower ductility and strengths. Processes C and D had a balance of stiffness and toughness properties. Increased sonication energy lead to higher tensile modulus, which is attributed to better dispersion and exfoliation of clay particles. While various processes lead to different properties for the resulting nanocomposites, they are all considered viable and stable. Thus, the processing techniques could be selected depending on the application and desired tensile properties.

2.3 Morphology of Na

Figure 2-6 and
nanocomposites from vari
degree of dispersion and ex
Process B (Figure 2-6a a
exfoliation relative to othe
processing. Process B is sir
result, the degree of exfo
assumed to be similar
Nanocomposites from pro
resin showed relatively p
Figure 2-6b). This was
process C, nanocompos
showed relatively bette
sonication energy appli
viscosity with increase
When applying sonica
temperature before the
the drop in temperatur
a direct sonication me
the viscosity. Nanoco
Process C (Figure 2-
nanocomposites resu
seems that agglomer

2.6.3 Morphology of Nanoclay Inclusions

Figure 2-6 and Figure 2-7 show transmission electron micrographs for nanocomposites from various processes at 60 kJ and 300 kJ of energy, respectively. The degree of dispersion and exfoliation was found to increase with increasing sonication energy. Process B (Figure 2-6a and Figure 2-7a) led to the highest degree of dispersion and exfoliation relative to other processes. This is due to the use of solvent for dispersion during processing. Process B is similar to process E, except for the solvent removal technique. As a result, the degree of exfoliation and dispersion of nanocomposites from process E are assumed to be similar to that obtained from process B, and thus not provided. Nanocomposites from process C, in which nanoclay was directly sonicated in the neat UPE resin showed relatively poor dispersion and agglomeration of clay particles (encircled in Figure 2-6b). This was due to the high viscosity of the resin system. Nevertheless, for process C, nanocomposites obtained from continuous application of sonication energy showed relatively better dispersion than nanocomposites from similar process with sonication energy applied in steps (Figure 2-6c). This could be due to the decrease in viscosity with increase in temperature during sonication, thus enabling better dispersion. When applying sonication energy in steps the resin system is cooled back to room temperature before the next energy step is applied. This increases the system viscosity due to the drop in temperature and affects the dispersion of nanoclay particles. Process D was also a direct sonication method, but the resin system was diluted with styrene, thereby reducing the viscosity. Nanocomposites from process D showed better dispersion than those from process C (Figure 2-7b). Also, the degree of exfoliation was considerably improved in nanocomposites resulting from process D relative to those obtained from process C. It seems that agglomerated clay particles resulting from process C (encircled in Figure 2-6) improve into partiall

TEM micrographs re

process B followed

consistent with the

obtained from proce

dispersion and exfo

intercalated nanoclay

2.6.4 Fractograph

The roughne

properties and critica

is attributed to bri

nanocomposites [2-

determine the degr

nanocomposites fro

tensile fracture surf

observations, sampl

consistent with rela

2-8e for 60 kJ and 3

dispersion, it follo

nanocomposites. T

nanocomposites fro

smoother than thos

fracture surface roug

improve into partially intercalated particles (Figure 2-7c) when using process D. Overall, TEM micrographs revealed better dispersion and exfoliation for the nanocomposites from process B followed by those from Process D. The enhanced nanoclay morphology is consistent with the relatively superior tensile modulus results of the nanocomposites obtained from processes B and D. The micrographs confirm a well known fact that good dispersion and exfoliation are beneficial for stiffness improvement (seen in B) while intercalated nanoclays are better for toughness improvement (seen in D).

2.6.4 Fractographic Observations

The roughness of the fracture surface has generally been associated to fracture properties and critical strain energy release rates [2-28]. A smooth featureless fracture surface is attributed to brittle failures and rougher fracture surfaces are attributed to tougher nanocomposites [2-27][2-28]. Tensile fracture surfaces were evaluated to qualitatively determine the degree of dispersion and the improved fracture properties of resulting nanocomposites from different processing methods. Figure 2-8a shows the relatively smooth tensile fracture surface of a neat resin with 5% EMS content. As discussed for the TEM observations, samples from process B had the best dispersion of clay particles. This is consistent with relatively rougher fracture surfaces as observed in Figure 2-8b and Figure 2-8e for 60 kJ and 300 kJ respectively. If higher sonication energy produces better nanoclay dispersion, it follows that it should also lead to rougher surfaces in the resulting nanocomposites. This is supported by images in (Figure 2-8c and Figure 2-8d) for nanocomposites from process C that show rougher fracture surfaces than neat UPE but smoother than those obtained from Process B. There was no significant difference in fracture surface roughness due to variations in the way that sonication energy was applied:

continuous (Figure 2-8d
rougher surfaces than all

2.7 *Discussion*

Processing plays
processing technique sh
but should also be effic
observed that the solven
the system. The use of a
clay particles. Neverthele
time, cost and energy. M
properties of resulting n
from process E, which h
part of the primary resin
styrene and hence, styren
into the resin system. Th
balance of stiffness and d

The elimination
sonication of nanoclay in
amount of time and ene
application of sonication
the feasibility of this p
obtained due to the hi

continuous (Figure 2-8d) and in steps (Figure 2-8c). Nanocomposites from process D had rougher surfaces than all other samples except those from process B.

2.7 Discussion

Processing plays a vital role in the resulting properties of nanocomposites. The processing technique should not only produce nanocomposites with enhanced properties, but should also be efficient with respect to energy, cost and time. In this study, it was observed that the solvent played an important role in determining the overall efficiency of the system. The use of acetone as a solvent produced better dispersion and exfoliation of clay particles. Nevertheless, extraction of solvent foreign to the resin system is inefficient in time, cost and energy. Moreover, the residual foreign solvent produces adverse effects on properties of resulting nanocomposites. This was observed in nanocomposites obtained from process E, which had poor tensile properties. Therefore, a solvent that is an inherent part of the primary resin is preferred. In this study, the UPE resin contained 33.5 wt.% styrene and hence, styrene monomer was used to dilute the solution and sonicate directly into the resin system. The nanocomposites produced by such process (D) showed a good balance of stiffness and ductility.

The elimination of solvent was achieved in process C, which involved direct sonication of nanoclay in the resin system and no solvent extraction. It required the least amount of time and energy. Nevertheless, viscosity related issues, such as system cooling, application of sonication energy in steps, and excess load on the sonication probes hamper the feasibility of this process. Moreover, the desired degree of exfoliation may not be obtained due to the high viscosity and insufficient sonication energy. Overall, viscosity issues, poor dispersion and exfoliation and moderate improvements in the resulting properties limit the efficiency of Process C.

Tensile testing revealed superior tensile modulus, relative to neat UPE, for nanocomposites from process B, followed by those from process D. Samples obtained from processes C had only a moderate increase in tensile properties relative to neat UPE. Process E samples had a reduction in tensile modulus and this was attributed to the residual acetone. Regarding ductility or elongations at failure, of the resulting nanocomposites, those from process B had the least ductility, while those from processes C, D and E had moderate levels of ductility. Similarly, samples from process B had the lowest tensile strength, while those from process D had the highest. Overall, the effects of bio-resin and nanoclay complement each other, producing composites with a good stiffness-toughness balance [2-6]. Yet, in order to take the benefits of the hybridization of nanoclay and bio-resin blends, the processing technique must enable incorporation of high contents of nanoclay and bio-resin.

The TEM micrographs showed that the nanocomposites from process B had better degrees of dispersion and exfoliation followed by those from process D. The nanocomposites obtained from direct sonication (process C), had poor dispersion and agglomerated clay particles. The samples from process E were similar to those from process B, but had poor tensile properties due to the effects of residual acetone. Similarly, the fractographic observations of tensile failure surfaces using SEM showed rougher surfaces in samples with well dispersed nanoclay. The increased surface area from the rough surface can be associated with the higher energy necessary for crack propagation. Since the tougher clay particles deviate the crack propagation front around them, thus creating new surfaces. Thus, proper dispersion of clay particles would lead to rougher surfaces. Consequently, if fracture

surface roughness
obtained through p

Overall, the
fabricating nanoclay
enhancements whil
tensile properties. P
and D used acetone
limiting the use of p
if any, affects the
laboratory scale qua
Process D is ideal fo
components with a
and applications ei
nanocomposites.

28 *Conclusions*

Bio-based resi
with natural polymers
improved toughness.
have been shown to
processing of nanoclay
as phase separation, t
maximum feasible bio-
efficient solvent-based

surface roughness is indicative of better nanoclay dispersion, the best dispersion was obtained through process B followed by process D.

Overall, the study indicated that processes B and D are desirable methods for fabricating nanoclay reinforced bio-based resins. Process B leads to the best tensile modulus enhancements while process D allows obtaining nanocomposites with a good balance of tensile properties. Process D was more time and energy efficient than process B. Processes B and D used acetone and styrene as solvents, respectively. Solvent extraction is the major step limiting the use of process B as it is time and energy inefficient. Moreover, residual acetone, if any, affects the properties of the resulting nanocomposites. Process B is ideal for laboratory scale quantities and in applications wherein high modulus is the principal criteria. Process D is ideal for producing larger quantities of resin systems such as for large structural components with a reasonable balance of properties. Depending on the desired properties and applications either of the processes could be used to develop bio-based clay nanocomposites.

2.8 Conclusions

Bio-based resin systems from partial substitution of petroleum-based resins (primary) with natural polymers (secondary) provide environmental friendliness, cost-effectiveness and improved toughness. The drawbacks from the addition of bio-resins to the base polymer have been shown to be recoverable through nanoclay reinforcement. Solvent-based processing of nanoclay reinforced bio-based resin systems brings about new challenges, such as phase separation, thermal degradation of the resin system and limitations on the maximum feasible bio-resin and nanoclay content. This study was aimed at finding an efficient solvent-based processing technique for the synthesis of nanoclay reinforced bio-

based resin system
sonication energy, p
of the techniques
properties of the re
resin after solvent r
base polymer and th
of primary resin) as
and reduced the tim
relatively large amou
lower processing tim
efficiency. Two proc
efficiency. Process B
dispersion and exfo
consists of direct sc
process eliminates th
resulting nanocompo
improvement of stiffn
either of these proc
nanocomposites. This
and evaluated tensile
physical characterizati
develop and/or identi
nanocomposites can of

based resin systems by assessing and comparing four evolving methods. The effects of sonication energy, processing time, solvent type and the associated processing issues for each of the techniques were assessed by evaluating the nanoclay morphology and the tensile properties of the resulting polymer nanocomposites. It was found that the addition of bio-resin after solvent removal avoids problems associated with phase separation between the base polymer and the bio-resin additive. Direct sonication and use of styrene (inherent part of primary resin) as a solvent resolved the drawbacks of foreign solvent (acetone) residue and reduced the time required for solvent removal. Processes that enable incorporation of relatively large amount of bio-resin and nanoclay content with minimal processing problems, lower processing time and desirable tensile properties were considered to have good overall efficiency. Two processes, namely processes B and D, were found to have good overall efficiency. Process B consists of using acetone as a solvent and led to the best nanoclay dispersion and exfoliation, resulting in samples with high tensile modulus. Process D consists of direct sonication of nanoclay in the resin system diluted with styrene. This process eliminates the use of a foreign solvent, thereby reducing processing time, and the resulting nanocomposites showed a good balance of tensile properties, namely a balanced improvement of stiffness and toughness. Depending on desired properties and applications, either of these processes is deemed suitable for effective production of bio-based nanocomposites. This study used electron microscopy for characterizing qualitative features and evaluated tensile properties only. A more comprehensive thermo-mechanical and physical characterization, along with processing constraints, would clearly be needed to develop and/or identify a processing technique that maximizes the benefits that bio-based nanocomposites can offer.

Processing Parameters
Relative Energy Demand
Time
Problems [a]
Max. nanoclay [b]
Max. bio-resin [b]
Cooling need [c]
Vacuum use
Probe issues
Tensile properties
Efficiency

[a] Problems of phase
requires application

2.9 Tables and Figures

Table 2-1. Comparison of processing techniques.

Processing Parameters	Process ID				
	A	B	C	D	E
Relative Energy Demand	high	high	moderate/low	moderate	High
Time	high	high	low	moderate	moderate/high
Problems [a]	yes	no	no	no	no
Max. nanoclay [b]	1.5	5	3	5	5
Max. bio-resin [b]	10	20	30	30	20
Cooling need [c]	no	no	yes	none/moderate	no
Vacuum use	yes	yes	no	no	no
Probe issues	none	none	high	moderate/none	none
Tensile properties	N/A	high modulus, low strength	low modulus	modulus & strength balance	low modulus
Efficiency	poor	moderate/good	moderate	good	poor/moderate

[a] Problems of phase separation and curing during processing; [b] In wt.%; [c] High viscosity requires application of energy in steps and cooling to room temp.

Table 2-2. Experin

Process ID
B/3/60/A
B/3/60/B
C/3/60/B
C/3/60*/B
NEAT UPE
NEAT-95/5-A
NEAT-95/5-B

E: Tensile Modulu
$\bar{x}$: Average, σ: St

Table 2-3. Exp

Process ID
B/3/300/A
B/3/300/B
D/3/300/A
D/3/300/B
E/3/300/A
E/3/300/B

E: Tensile Modulus,
$\bar{x}$: Average, σ: Stan

Table 2-2. Experimental results for various processes at sonication energy of 60 kJ

Process ID	E, GPa		UTS, MPa		EF, %	
	$\bar{x}$	σ	$\bar{x}$	σ	$\bar{x}$	σ
B/3/60/A	4.88	1.06	20.17	3.12	0.74	0.25
B/3/60/B	4.02	1.04	17.61	5.78	0.74	0.03
C/3/60/B	3.50	0.26	22.70	3.33	0.73	0.16
C/3/60*/B	4.05	0.51	26.93	2.80	0.79	0.06
NEAT UPE	3.53	0.43	43.86	1.03	1.41	0.01
NEAT-95/5-A	3.40	0.25	41.87	7.83	1.41	0.32
NEAT-95/5-B	3.08	0.81	37.52	7.91	1.59	0.39

E: Tensile Modulus, UTS: Ultimate Tensile Strength, EF: Elongation at Failure
$\bar{x}$: Average, σ : Standard Deviation

Table 2-3. Experimental results for various processes at sonication energy of 300 kJ.

Process ID	E, GPa		UTS, MPa		EF, %	
	$\bar{x}$	σ	$\bar{x}$	σ	$\bar{x}$	σ
B/3/300/A	5.32	2.08	11.54	3.30	0.44	0.07
B/3/300/B	4.95	1.32	9.94	3.21	0.64	0.22
D/3/300/A	4.10	0.67	24.41	2.10	0.84	0.14
D/3/300/B	3.42	0.14	26.82	5.62	1.14	0.11
E/3/300/A	1.75	0.51	12.51	1.76	1.06	0.33
E/3/300/B	1.16	0.23	9.05	2.89	1.29	0.36

E: Tensile Modulus, UTS: Ultimate Tensile Strength, EF: Elongation at Failure
$\bar{x}$: Average, σ : Standard deviation

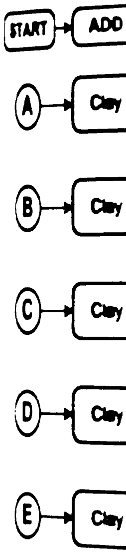

Fi

Figu

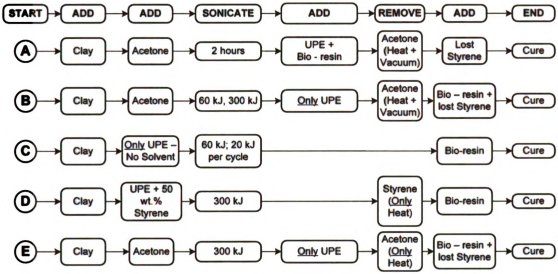

Figure 2-1. Schematic description of various processing techniques.

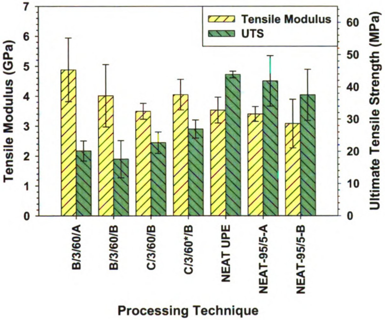

Figure 2-2. Tensile modulus and strength at sonication energy of 60 kJ.

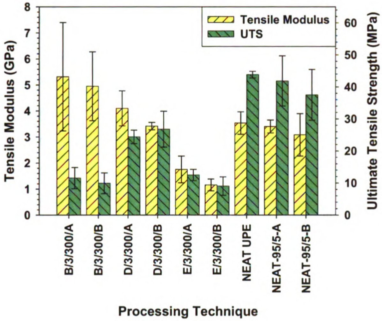

Figure 2-3. Tensile modulus and strength at sonication energy of 300 kJ.

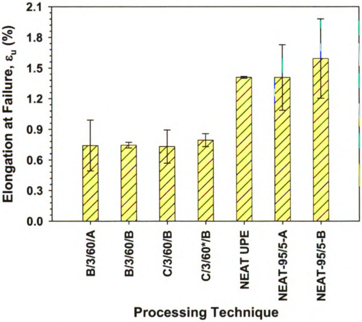

Figure 2-4. Tensile failure strains at sonication energy of 60 kJ.

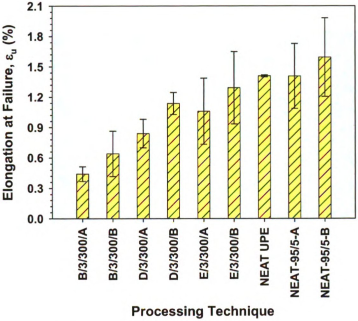

Figure 2-5. Tensile failure strains at sonication energy of 300 kJ.

Figure 2-6.
processed
process C

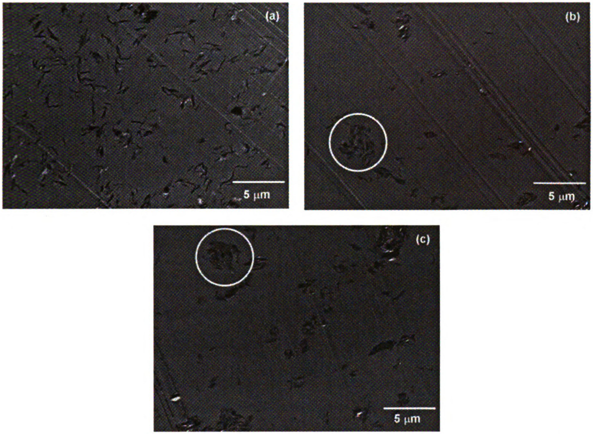

Figure 2-6. TEM micrographs showing clay dispersion and exfoliation for nanocomposites processed at 60 kJ, a) process B, b) process C with sonication energy applied in 3 steps, c) process C with 60 kJ applied continuously. Encircled regions reveal agglomerated stacks of clay particles.

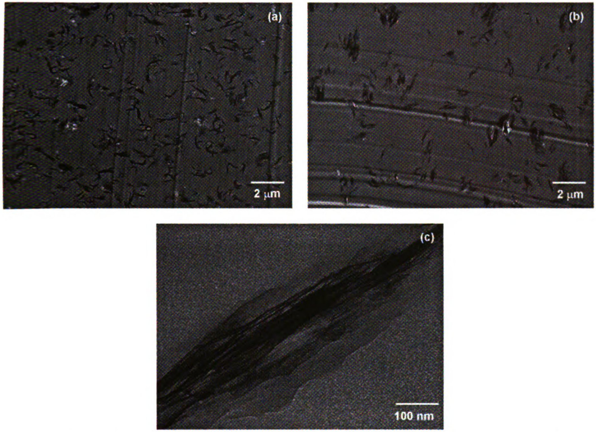

Figure 2-7. TEM micrographs showing clay dispersion and exfoliation for nanocomposites processed at 300 kJ, a) process B, b) process D, c) High magnification of an intercalated particle from process D nanocomposite.

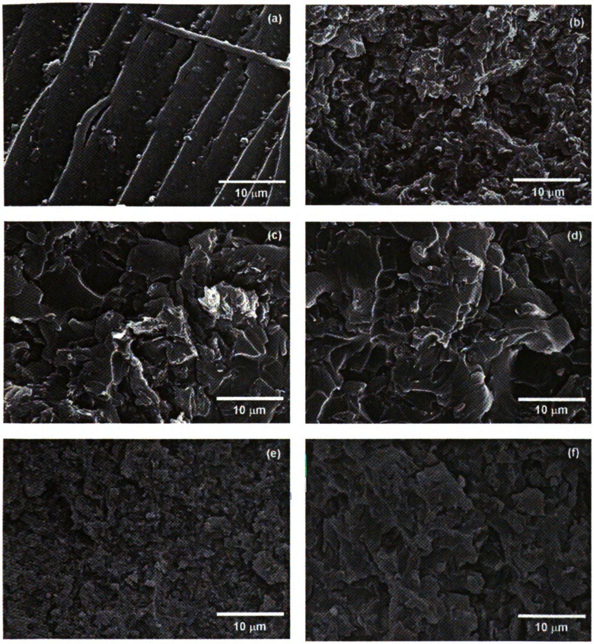

Figure 2-8. SEM images showing tensile fracture surface morphologies for the nanocomposites from various processes: a) neat UPE, b) process B at 60 kJ, c) process C with sonication energy applied in 3 steps, 60 kJ, d) process C at 60 kJ (continuous), e) process B at 300 kJ, and, f) process D at 300 kJ

2.10 References

[2-1]. Uyama H,
nanocom
Mater 2

[2-2]. Mohanty A
biocomp

[2-3]. Burgueño R
bearing
2004; 35

[2-4]. Nickel J, Rie

[2-5]. Miyagawa H,
from ble
Polym Sc

[2-6]. Haq M, B
polyester/
properties

[2-7]. Ratna D. M
modified e

[2-8]. Pinnavaia TJ,
2001.

[2-9]. Liu Z, Erhan
epoxidized

[2-10]. Song B, Chen
oil/clay nan

[2-11]. Lu B, Larock
organoclay
292:863-872

[2-12]. Miyagawa H, M
thermophys
nanocompo

[2-13]. Bakar M, Djaid
unsaturated

[2-14]. Ratna D, Ban
Sci Techno

2.10 References

[2-1]. Uyama H, Kuwabara M, Tsujimoto T, Nakano M, Usuki A, Kobayashi S. Green nanocomposites from renewable resources: Plant oil-clay hybrid materials. Chem Mater 2003; 15:2492-2494.

[2-2]. Mohanty AK, Misra M, Hinrichsen G. Biofibers, Biodegradable polymers and biocomposites: an overview. Macromol Mater Eng 2000; 276/277:1-24.

[2-3]. Burgueño R, Quagliata MJ, Mohanty AK, Mehta GM, Drzal LT, Misra M. Load bearing natural fiber composite cellular beams and panels. Composites Part A 2004; 35:645-656.

[2-4]. Nickel J, Riedel U. Activities in biocomposites. Mater Today 2003; 6:44-48.

[2-5]. Miyagawa H, Mohanty AK, Burgueño R, Drzal LT, Misra M. Novel bio-based resins from blends of functionalized soyabean oil and unsaturated polyester resin. J Polym Sci, Part B: Polym Phys 2007; 45: 698-704.

[2-6]. Haq M, Burgueño R, Mohanty AK, Misra M. Bio-based unsaturated polyester/layered silicate nanocomposites: characterization and thermo-physical properties. Composites Part A, Communicated.

[2-7]. Ratna D. Mechanical properties and morphology of epoxidized soyabean oil-modified epoxy resin. Polym Int 2001; 50:179-184.

[2-8]. Pinnavaia TJ, Beall GW. Polymer-Clay Nanocomposites, John Wiley & Sons, Ltd., 2001.

[2-9]. Liu Z, Erhan SZ, Xu J. Preparation, characterization and mechanical properties of epoxidized soybean oil/clay nanocomposites. Polymer 2005; 46:10119-10127.

[2-10]. Song B, Chen W, Liu Z, Erhan S. Compressive properties of epoxidized soybean oil/clay nanocomposites. Int J Plast 2006; 22:1549-1568.

[2-11]. Lu B, Larock RC. Bio-Based nanocomposites from corn oil and functionalized organoclay prepared by cationic polymerization. Macromol Mater Eng 2007; 292:863-872.

[2-12]. Miyagawa H, Mohanty AK, Burgueño R, Drzal LT, Misra M. Characterization and thermophysical properties of unsaturated polyester-layered silicate nanocomposites. J Nanosci Nanotechnol 2006; 6:464-471.

[2-13]. Bakar M, Djaider F. Effect of plasticizers content on the mechanical properties of unsaturated polyester resin. J Thermoplast Compos Mater 2007; 20:53-64.

[2-14]. Ratna D, Banthia AK. Epoxidized soybean oil toughened epoxy adhesive. J Adhes Sci Technol 2000; 14:15-25.

[2-15]. Miyagawa H,
properties
Macromol

[2-16]. Miyagawa H,
properties
Macromol

[2-17]. Haq M, Burgu
blends of
natural fib

[2-18]. Pourabas B, Ra
solvent / n

[2-19]. Ludueña LN, A
nanocomp

[2-20]. Alexandre M,
properties a

[2-21]. Morgan AB, H
solvent blen

[2-22]. Le Baron PC,
overview. A

[2-23]. Burgentzle D, D
coatings I.
Colloid Inte

[2-24]. Hutchinson JM,
resin in orga
3763.

[2-25]. Miyagawa H,
processing a

[2-26]. Tran NH, Den
RN. Disper
Sci 2006; 29

[2-27]. Miyagawa H,
nanowhiske
from bio-b
7009.

[2-15]. Miyagawa H, Mohanty A, Misra M, Drzal LT. Thermo-physical and impact properties of epoxy containing epoxidized linseed oil, 1: Anhydride cured epoxy. Macromol Mater Eng 2004; 289:629-635.

[2-16]. Miyagawa H, Mohanty A, Misra M, Drzal LT. Thermo-physical and impact properties of epoxy containing epoxidized linseed oil, 2: Amine cured epoxy. Macromol Mater Eng 2004; 289:636-641.

[2-17]. Haq M, Burgueño R, Mohanty AK, Misra M. Hybrid bio-based composites from blends of unsaturated polyester and soybean oil reinforced with nanoclay and natural fibers. Compos Sci Technol, Communicated.

[2-18]. Pourabas B, Raeesi V. Preparation of ABS/montmorillonite nanocomposite using a solvent / non solvent method. Polymer 2005; 46: 5533-5540.

[2-19]. Ludueña LN, Alvarez VA, Vazques A. Processing and microstructure of PCL/clay nanocomposites. Mater Sci Eng A 2007; 460-461:121-129.

[2-20]. Alexandre M, Dubois P. Polymer-layered silicate nancomposites: preparation, properties and uses of a new class of materials. Mater Sci Eng R 2000; 28:1-63.

[2-21]. Morgan AB, Harris JD. Exfoliated polystyrene–clay nanocomposites synthesized by solvent blending with sonication. Polymer 2004; 45:8695-8703.

[2-22]. Le Baron PC, Wang Z, Pinnavaia, TJ. Polymer – layered silicate nanocomposites: an overview. Appl Clay Sci 1999; 15:11-29.

[2-23]. Burgentzle D, Duchet J, Gerard JF, Jupin A, Fillon B. Solvent based nanocomposite coatings I. Dispersion of organophilic montmorillonite in organic solvents. J Colloid Interface Sci 2004; 278:26-39.

[2-24]. Hutchinson JM, Montserrat S, Roman F, Cortes P, Campos L. Intercalation of epoxy resin in organically modified montmorrillonite. J Appl Polym Sci 2006; 102:3751-3763.

[2-25]. Miyagawa H, Rich MJ, Drzal LT. Amine cured epoxy/clay nanocomposites. I processing and chemical characterization. J Polym Sci B 2004; 42:4384-4390.

[2-26]. Tran NH, Dennis GR, Milev AS, Kannaraga GSK, Williams P, Wilson MA, Lamb RN. Dispersion of organically modified clays with n-alcohols. J Colloid Interface Sci 2006; 297:541-545.

[2-27]. Miyagawa H, Mohanty A, Drzal LT, Misra M. Effect of clay and alumina-nanowhisker reinforcements on the mechanical properties of nanocomposites from bio-based epoxy: a comparative study. Ind Eng Chem Res 2004; 43:7001-7009.

[2-28]. Wang L, Wang K, Chen L, Zhang Y, He C. Preparation, morphology and thermal/mechanical properties of epoxy/clay nanoclay composite. Composites Part A. 2006; 37:1890-1896.

[2-29]. Haq M, Burgueño R. Modeling and simulation of bio-based polymer/clay nanocomposites through a multi-level FE approach. In:Proceedings of Sixth International conference on Computation of Shell & Spatial Structures. New York, May, 2008. p.1-4.

Chapter 3. Bio

3.1 Abstract

Proper stiffn
properties can be ob
defined as blends o
polymer nanocompo
soy bean oil) conten
properties such as te
absorption, toughnes
morphologies and c
microscopy. The resu
structural applications.

3.2 Introduction

Fiber reinforce
having high strength a
low density synthetic/
phenolic resins. Howe
and dependability on
spread use of syntheti

---

[1] Hac, M, Burgueño, R,
Nanocomposites: Characte

Chapter 3. Bio-based Polymer Nanocomposites: I – UPE / EMS [1]

3.1 Abstract

Proper stiffness-toughness balance along with enhancement in other thermo-physical properties can be obtained by incorporating layered silicates (nanoclay) in bio-based resins, defined as blends of functionalized vegetable oils and petroleum-based resins. Bio-based polymer nanocomposites with varying clay concentration and varying bio-resin (epoxidized soy bean oil) content in unsaturated polyester resins were manufactured. Thermo-physical properties such as tensile modulus and strength, coefficient of thermal expansion, moisture absorption, toughness, and glass-transition temperatures were studied. Fracture surface morphologies and characterization of nanocomposites were performed using electron microscopy. The resulting bio-blend nanocomposites exhibit promising results for use in structural applications.

3.2 Introduction

Fiber reinforced polymer (FRP) composites are generally made of synthetic fibers having high strength and modulus such as carbon, glass, or aramid and are combined with low density synthetic/petroleum based resins made of unsaturated polyesters, epoxy or phenolic resins. However, environmental concerns such as biodegradability, recycling issues and dependability on non-renewable petroleum reserves are creating concerns on the wide spread use of synthetic FRP composites and propelled the development of alternatives for

---

[1] Haq, M., Burgueño, R., Mohanty, A.K., and Misra, M., "Bio-based Unsaturated Polyester/Layered Silicate Nanocomposites: Characterization and Thermo-Physical Properties," Composites – Part A. 2009; 40:540-547.

both synthetic fibers and petroleum resins for the development of bio-based composites, or biocomposites [3-1]-[3-4].

Natural fiber composites or biocomposites are comprised of natural fibers (e.g. flax, hemp, jute, cellulose, kenaf, cotton, coir, bamboo etc.) and *petroleum based resins* (unsaturated polyester, epoxy, poly urethane, phenolics, etc.) or *natural bio-resins* (epoxidized vegetable oils, polyoles, maleinated triglycerides, animal fats, etc.) [3-4]-[3-6]. The use of all-natural bio-resins has been limited due to performance based concerns such as low mechanical and thermo-physical properties [3-7]-[3-9]. Bio-based resins obtained from partial replacement of non-renewable synthetic resins (in this case, petroleum based unsaturated polyester, UPE) with renewable resins, or bio-resins, such as functionalized vegetable oils (in this case, epoxidized methyl soyate, EMS) have been shown to improve the toughness of resulting resin system [3-1][3-7][3-8]. This increase in toughness is generally achieved by sacrificing stiffness [3-10], barrier and thermal properties of the resulting resin systems. However, these concerns caused by blending of EMS, can be overcome by introduction of layered silicates (nanoclay). Moreover, stiffness and toughness are opposing performance parameters and a proper balance is required to develop an efficient bio-based resin system.

Polymers reinforced with layered silicates or nanoclays have been shown to exhibit enhancements in modulus, thermal and barrier properties at low concentrations. Layered silicates or nanoclays consist of stacks of sheet like platelets with thickness of ~1 nm and extremely large surface areas and aspect ratios. The platelets in the stacks are separated as the polymer/resin penetrates into these platelets. Depending on the degree of penetration of the polymer, intercalated and exfoliated clay morphologies are obtained. The intercalated morphologies allow penetration of the polymer in between clay platelets to an extent that the stacks/galleries of clay platelets expand but do not separate. The polymer penetration is observed by an increase in d-spacing (clay platelet interlayer spacing). Exfoliated clay morphology is obtained when the individual platelets in the stack are completely separated. Clays are generally treated or functionalized to be compatible with the host polymer. Depending on the functionalization and processing technique, different clay morphologies are obtained. The efficiency of the resulting polymer-clay resin system depends on the clay morphology. The enhancement of mechanical and barrier properties in polymers with addition of small concentrations of nanoclays is well established in literature. Le Baron et al. [3-11] provide a good review on polymer clay hybrid nanocomposites. Apart from the increase in stiffness, the inclusion of nanoclay particles introduces multifunctionality to the resulting nanocomposite resin system by enhancement in barrier properties, flammability and ablation resistance.

Among thermoset resins, petroleum-based unsaturated polyesters (UPE) are commonly used due to their low cost, ease of handling, and good balance of mechanical, electrical, chemical properties and fire resistance properties [3-7][3-12][3-13]. However, UPE resins are inherently brittle in nature. Research has shown the increase in modulus both below and above glass transition temperature of UPE resins reinforced with nanoclays. Nair et al. [3-10] show that the increase in stiffness is generally obtained by compromising toughness. They also report that the toughness of layered silicate composites is dependent on the morphology and concentration of clay content. At low concentrations, proper dispersion and exfoliation improves the toughness whereas at higher clay concentrations, mixtures of exfoliated and intercalated morphologies perform better [3-10].

The substitution of non-renewable synthetic resins (in this case petroleum-based UPE) with renewable resins such as functionalized vegetable oils (in this case EMS) has been proposed and studied [3-7][3-9][3-13]. Soybean oil is available abundantly across the United sizes, and varieti

functionalized ve

However, more

return to agricultu

The incre

the stiffness of

toughness but co

have a better sti

moisture absorpt

with the enhanc

combination of n

multifunctional

incorporating the

The impac

wt.% nanoclay (

on thermo-physi

Cloisite 30B® n

thereby showing

study uses Cloisi

clay and bio-resi

Experimental eva

temperature (T_g),

absorption prope

States, and varieties of epoxidized soybean oils are already commercially available [3-9]. Such functionalized vegetable oils (FVO) have been found for coatings and plasticizer additives. However, more value-added applications of such epoxidized vegetable oils will give much return to agriculture, thereby reducing the burden of petroleum-based products [3-9].

The increase in stiffness due to the addition of nanoclay inclusions will thus increase the stiffness of the resin system and decrease toughness. Addition of EMS enhances toughness but compromises stiffness. It follows that the result of blended resin system could have a better stiffness-toughness balance than the original UPE. Similarly, the increase in moisture absorption in the bio-based resin due to addition of EMS can be circumvented with the enhanced barrier properties obtained from nanoclay reinforcement. Hence, the combination of nanoclay platelets with blends of EMS and UPE resins would result in novel multifunctional composites with superior properties to that of virgin resin systems incorporating the beneficial properties of both clay reinforcement and EMS blends.

The impact properties and dynamic mechanical analysis of EMS-UPE blend with 2.5 wt.% nanoclay (Nanomer® I.44PA) has been reported by our group [3-9]. Moreover, study on thermo-physical properties of UPE reinforced with various organo-clays had shown that Cloisite 30B® nanoclays produced higher degree of exfoliation than Nanomer® I.44PA, thereby showing better improvements in the thermo-physical properties [3-12]. Hence, this study uses Cloisite 30B® and reports on further efforts to evaluate the effect of varying the clay and bio-resin contents and expanding the set of measured thermo-physical properties. Experimental evaluation of tensile properties, toughness, storage modulus, glass transition temperature (T_g), linear coefficient of thermal expansion above and below T_g and moisture absorption properties were studied. The degree of dispersion and exfoliation of nanoclay in

the resins systems was
surfaces were characteri

3.3 Experimental

Experimental
characterization were
inclusions. In the follo
and testing details are p

3.3.1 Materials

The main con
unsaturated polyester re
33.5 wt.% styrene. A b
Inc, PA) replaced up to
(Southern Clay Product
organoclay) was process
2-butanone peroxide (S
resin system to the pro
was 100 parts by weig
Samples were cured at

3.3.2 Experimental

The amount of
resin component UPE
resin (no clay) systems
nanoclay inclusions v

the resins systems was characterized using transmission electron microscopy. The fracture surfaces were characterized using scanning electron microscopy.

3.3 Experimental Methods

Experimental determination of thermo-physical properties and material characterization were performed on bio-based resin blends reinforced with nanoclay inclusions. In the following sections, details on materials, processing, parameters studied, and testing details are provided.

3.3.1 Materials

The main component of the engineered bio-based resin system was ortho unsaturated polyester resin (UPE, Polylite® 32570-00, Reichhold Inc., NC), which contains 33.5 wt.% styrene. A bio-resin, epoxidized methyl soyate (EMS, Vikoflex® 7010, Arkema Inc, PA) replaced up to 20 wt.% of UPE. The nanoclay used in this work was Cloisite 30B® (Southern Clay Products, Inc. TX). The bio-based resin system (blend of UPE, EMS and organoclay) was processed with cobalt naphthenate (Sigma Aldrich, MO) as a promoter and 2-butanone peroxide (Sigma Aldrich) as an initiator. The constant ratio by weight of the resin system to the promoter and initiator was utilized to cure all samples. The mixing ratio was 100 parts by weight of the resin system to 0.03 part promoter and 1.50 part initiator. Samples were cured at 100°C for 2 hours, followed by 160°C for 2 hours.

3.3.2 Experimental Matrix and Nomenclature

The amount of bio-resin (epoxidized methyl soyate, EMS) that replaced the primary resin component UPE, was varied from 0% to 20%, in increments of 5%. A total of 5 neat resin (no clay) systems were obtained. Each of these resin systems were then reinforced with nanoclay inclusions varying from 0 wt.% to 1.5 wt.% in increments of 0.5 wt.%. For nanoclay reinforced re

possible, as higher amo

resin systems were obt

clay and EMS content

is used to describe the

"B" represents the am

weight fraction of nan

ID" in Table 1 is refe

and is reinforced wit

"X" in Table 3-1 indi

3.3.3 Polymer Na

The bio-base

UPE. For nanoclay

only 5% and 10% E

100/0/0, 95/5/0 a

1.0 wt. % and 1.5

systems were proc

nanocomposites. F

to 20%. The proce

previously reporte

The nanoclay was

of acetone to 1 ki

amount of energy

nanoclay reinforced resin systems, substitution of only 5% and 10% EMS in UPE was possible, as higher amounts caused processing problems. A total of 9 nanoclay reinforced resin systems were obtained. A summary of the experimental matrix describing the varying clay and EMS contents is provided in Table 3-1. In this report, the following nomenclature is used to describe the resin system: *"A/B/C"*, where *"A"* refers to the amount of UPE and *"B"* represents the amount of EMS as percentage of the resin system, and *"C"* refers to the weight fraction of nanoclay inclusions in the polymer resin system. For example, Specimen ID 7 in Table 1 is referred as 95/5/0.5, indicating it has 95 parts of UPE and 5 parts of EMS and is reinforced with 0.5 wt.% of nanoclay platelets. The specimen identifications labeled "X" in Table 3-1 indicate processing problems and are described in the following section.

3.3.3 Polymer Nanocomposite Processing

The bio-based resin system (UPE +EMS) had varying amounts of EMS that replaced UPE. For nanoclay reinforced resin systems, due to processing problems, substitution of only 5% and 10% EMS in UPE was possible resulting in three main polymer resin systems (100/0/0, 95/5/0 and 90/10/0). For every resin system, clay contents of 0 wt.%, 0.5wt. %, 1.0 wt. % and 1.5 wt.% were processed. A total of 9 sets of nanoclay reinforced resin systems were processed and thermo-physical properties were studied for the resulting nanocomposites. For neat resin systems (no clay), the amount of EMS was varied from 0% to 20%. The processing technique for nanoclay reinforced resin systems is similar to that previously reported by our group [3-9][3-12] and is described schematically in Figure 3-1. The nanoclay was sonicated in acetone using a solution concentration of more than 50 liters of acetone to 1 kilogram of clay, while it was constantly stirred by a magnetic stirrer. The amount of energy spent on sonication was maintained to be around 30 kJ for all resin

systems. After so
mixed with a ma
remaining aceton
hours. At higher
the resin seemed
phase separation
acetone removal
contents of up t
process, the styre
lost styrene was
content in the UP
bio-resin reduces
that the prematur
styrene content.
maintain the over
and addition of t
After proper mix
hours followed by
provided in Figure

The comb
was the maximu
aforementioned p
process was also
was overcome by a

systems. After sonication, the UPE and EMS were added to the acetone-clay solution and mixed with a magnetic stirrer on a hot plate to remove a majority of the acetone. The remaining acetone was removed by vacuum extraction at approximately 55°C for 12-24 hours. At higher concentrations of both EMS and clay, two problems were encountered: (1) the resin seemed to cross-link (harden / gel) during the acetone removal process, and (2) phase separation between EMS and UPE was observed leading to problems during the acetone removal vacuum extraction process. These problems were not observed at clay contents of up to 1.5 wt.% and EMS blends of up to 10%. During the acetone removal process, the styrene present in UPE was also removed along with the acetone. Hence the lost styrene was added after the acetone removal process was completed. The styrene content in the UPE used in this study was 33.5 wt.%. Replacement of part of the UPE with bio-resin reduces the overall styrene content of the resulting resin system. It was suspected that the premature curing of resin blends during acetone removal was due to the reduction in styrene content. Hence, for bio-based resin systems, additional styrene was added to maintain the overall styrene content at 33.5 wt.% for the resin system. After acetone removal and addition of the lost styrene, the promoter and initiator were blended in the solution. After proper mixing of all components, the nanocomposites were cured at 100 °C for 2 hours followed by 160 °C for 2 hours. A flow chart explaining the processing technique is provided in Figure 3-1.

The combination of 10% EMS and 1.5 wt.% clay in UPE (resin system 90/10/1.5) was the maximum that could be achieved with the current processing technique. The aforementioned phase separation issue of EMS and UPE during acetone vacuum extraction process was also observed for this (90/10/1.5) resin system. The phase separation problem was overcome by adding EMS resin after the acetone removal process was completed. It will

be shown in later
the actual proce
modification in t
contents. Althoug
scope of this co
techniques on th
forthcoming in a

3.3.4 Testing &

Tensile tes
was measured usi
modulus and P
measurements, wh
were obtained fron
case of resin syste
determined with a
at an oscillation fre
respectively. DMA
of 22 mm x 15 mm
of 2°C/min. The gl
the loss factor was
performed only on k
numbers: 1, 3, 5, 12
above and below th

be shown in later sections that this modification provides better barrier properties relative to the actual process, but has little or no influence on other parameters studied. This modification in the processing technique enables incorporation of higher clay and EMS contents. Although a detailed discussion on the effect of processing techniques is beyond the scope of this communication, a study that evaluated the effect of various processing techniques on thermo-physical properties of bio-based polymer nanocomposites will be forthcoming in a future communication.

3.3.4 Testing & Characterization

Tensile tests were performed according to the ASTM D638 standard. Poisson's ratio was measured using a biaxial extensometer. The rate of loading was 5 mm/min. Tensile modulus and Poisson's ratio measurements were made from the extensometer measurements, whereas the ultimate tensile strength and elongation at break measurements were obtained from the machine grip movement. Six tensile specimens were tested for each case of resin system in the study (see Table 3-1). Dynamic mechanical properties were determined with a TA Instruments DMA Q800 operating in the three-point bending mode at an oscillation frequency of 1.0 Hz. The amplitude and static force were 75 μm and 1.0 N, respectively. DMA specimens were in the form of rectangular bars with nominal dimensions of 2.2 mm x 15 mm x 50 mm. Data was collected from ambient to 150 °C at a scanning rate of 2°C/min. The glass transition temperature, T_g was determined as the temperature where the loss factor was maximum. Two specimens were tested per case studied. Tests were performed only on key specimens in the experimental matrix, namely specimen identification numbers: 1, 3, 5, 12 and 14 (see Table 3-1). The linear coefficient of thermal expansions above and below the glass transition temperature was obtained by thermo-mechanical

analysis using a TA
temperature to 14
throughout the tes
coefficient of therm
only on key specim
1,3,5, 12 and 14
samples in an envir
in weight of the sa
in an environment
of approximate di
nanocomposite. T
eliminate edge effe
for first 4 days, fol
was confirmed (~
at steady state.
numerically integ
tests. The dispers
transmission elec
using a diamond
thick. A JEOL 1
bright field im
nanocomposites
microscope (SE
film prior to SE

analysis using a TA instruments TMA 2940 apparatus. The samples were heated from room temperature to 140 °C at a rate of 3 °C/min. Strain and temperature was measured throughout the test. The linear slope of strain-temperature curve is reported as the coefficient of thermal expansion. Two specimens were tested per case. Tests were performed only on key specimens in the experimental matrix, namely specimen identification numbers: 1, 3, 5, 12 and 14 (see Table 3-1). Moisture absorption testing was performed by storing samples in an environmental chamber at 30°C and 90% humidity and measuring the increase in weight of the samples. Moisture absorption testing was performed by storing the samples in an environmental chamber at 30 °C and 90% relative humidity. Two rectangular samples of approximate dimensions: 63.5 mm x 12.7 mm x 3.2 mm were used for each bio-based nanocomposite. The edges of samples were coated with a two-part impervious epoxy to eliminate edge effects. The weight increase of the samples was measured for every 24 hours for first 4 days, followed by once every week until steady state (no further increase in weight) was confirmed (~50 days). Moisture absorption was evaluated as the percent weight gained at steady state. The energy absorbed per unit volume (toughness) was obtained by numerically integrating the experimental stress-strain curves obtained from direct tensile tests. The dispersion and morphology of clay inclusions in resin systems was observed with transmission electron microscopy (TEM). Ultramicrotomy at room temperature was carried using a diamond knife with an included angle of 4° to produce sections approximately 70nm thick. A JEOL 100CX TEM with LaB_6 filament with 120kV acceleration was used to obtain bright field images. The failure surfaces from direct tensile testing of polymer nanocomposites were observed with a JEOL 6400 field emission scanning electron microscope (SEM) at 10 kV acceleration voltage. Specimens were coated with a thin gold film prior to SEM observations.

3.4 *Results*

3.4.1 Tensile T

Tensile m
clay contents are p
(no clay) are prov
considered as the
composites in this
trend suggests th
reduction in avera
20% EMS blends
increase the averag
considering only t
resulting composit

The failu
nanocomposites a
strains and ultima
3-6. Considering o
contents, the tens
similar note, the
strengths and failu
variation. This va
effect of residual a
a statistical analy

3.4 Results

3.4.1 Tensile Tests & Properties

Tensile modulus results for unmodified and bio-based resin systems with varying clay contents are provided in Figure 3-2. Tensile Modulus and Poisson's ratio of neat resins (no clay) are provided in Figure 3-3. The virgin UPE composite (0% EMS, 0% nanoclay) is considered as the baseline composite and will be used to compare the performance of other composites in this study. Considering only the average values of tensile modulus, the overall trend suggests that the tensile modulus decreased with addition of bio-resin (EMS). The reduction in average tensile modulus values was approximately 25% and 40%, for 10% and 20% EMS blends, respectively. Similarly, the addition of nanoclay (1.5 wt.%) seems to increase the average tensile modulus by approximately 15%, relative to neat UPE. Similarly, considering only the average values, the overall trend suggests increase in Poisson's ratio of resulting composites with increasing EMS content (Figure 3-3).

The failure strains and ultimate tensile strengths of nanoclay reinforced nanocomposites are provided in Figure 3-4 and Figure 3-5, respectively. Also, the failure strains and ultimate tensile strengths of neat (no clay) resin systems are provided in Figure 3-6. Considering only the average values, the overall trend suggests that with increasing EMS contents, the tensile failure strains increased while the tensile strengths decreased. On a similar note, the nanoclay addition revealed increase in stiffness and reduction in tensile strengths and failure strains. The results of tensile strengths and failure strains showed a large variation. This variation may be due to many factors including processing issues, such as effect of residual acetone, EMS-UPE phase interactions, clay-matrix interaction, etc. Ideally, a statistical analysis considering these variations should be performed to ascertain quantitatively t

considered bey

cannot be con

constituents or

stiffness due to

(toughness) due

3.4.2 Dynam

The sto

resin systems (n

provided in Fig

storage modulus

was recovered b

with increasing

for the 90/10/1.

the contrary was

the 90/0/1.5 res

(see section on na

3.4.3 Thermal

The linear

resin systems (nar

provided in Figur

increased the coeff

quantitatively the effects of EMS and nanoclay on resulting parameters. Such a study was considered beyond the scope of this work, and hence precise effects of EMS and nanoclay cannot be concluded. Only an overall trend and approximate range of the effects of the constituents on resulting properties is provided. Overall, it seems that the increase in stiffness due to the addition of nanoclay inclusions was balanced by the increase in ductility (toughness) due to the addition of the EMS bio-resin.

3.4.2 Dynamic Mechanical Analysis

The storage modulus and glass transition temperatures (T_g) of key resin bio-based resin systems (namely specimen identification numbers: 1, 3, 5, 12 and 14, see Table 3-1) are provided in Figure 3-7. Similar to the tensile modulus, the average values suggests that the storage modulus of the resin systems decreased with increasing bio-content and this decrease was recovered by nanoclay inclusions. The glass transition temperatures seem to increase with increasing EMS and clay content. It was expected that the glass transition temperature for the 90/10/1.5 resin system to be higher than its neat resin counterpart 100/0/1.5, but the contrary was found. This is attributed to the modification in the processing technique of the 90/0/1.5 resin system, wherein the bio-resin was added after the acetone was removed (see section on nanocomposite processing).

3.4.3 Thermal Mechanical Analysis

The linear coefficient of thermal expansion (CTE) above and below T_g for the key resin systems (namely specimen identification numbers: 1, 3, 5, 12 and 14, see Table 3-1) is provided in Figure 3-8. The overall trend suggests that the addition of bio-resin (EMS) increased the coefficient of linear thermal expansion. Considering only the average values, it

seems that the valu
approximate increas
resins. The addition
was observed that th
than neat UPE, nev
relative to the neat
wherein the 20% EN
system, the values o
values of CTE with
CTE value below T_g
1.5 wt.% nanoclay
slightly higher than
represented by an
addition of nanoc
improvements in th
of thermal properti

3.4.4 Moisture A

The moistu
50 days and is sho
moisture absorptio
hours) in an envir
resin system was o

seems that the values of CTE below T_g increased with increasing EMS content, with an approximate increase of around 20% for 10% EMS blends (no clay) relative to neat UPE resins. The addition of nanoclay seems to recover the lost CTE due to addition of EMS. It was observed that the 90/10/1.5 resin system had an average CTE value around 10% higher than neat UPE, nevertheless an approximate reduction in average value of around 10%, relative to the neat (no clay) 10% EMS resin system. Unlike the values of CTE below T_g wherein the 20% EMS resin system had average CTE values lower than the 10% EMS resin system, the values of CTE above T_g showed a more consistent trend of increase in average values of CTE with increasing EMS content. The addition of 20% EMS revealed that the CTE value below T_g was higher on average by around 5 %, relative to virgin UPE. By adding 1.5 wt.% nanoclay to the 10% EMS resin system, the average value of CTE below T_g was slightly higher than the virgin UPE composite. In both cases, the thermal properties lost (represented by an increasing CTE) due to addition of EMS were partially recovered by addition of nanoclay. At the same time, increasing the amount of clay content and improvements in the processing technique would enable larger recoveries and enhancement of thermal properties of the resulting composite.

3.4.4 Moisture Absorption Tests

The moisture absorbed by the polymer resin systems was measured over a period of 50 days and is shown as a plot of percent weight absorbed versus time in Figure 3-9. The moisture absorption of all nanocomposites stabilized after approximately 35 days (800 hours) in an environmental chamber. The representative moisture absorption value for a resin system was obtained after the steady state was achieved. It was observed that moisture

absorption increase
res. matrix bio resi
(no EMS blends),
diffusion barrier p
A similar trend wa
in increasing moist
due to the addition
technique. As disc
than other resin sy
processing techniq
(no clay), the incr
system relative to
showed a decrease
system. Thus the
recovered by nano
seems to indicate

3.4.5 Energy A

The relati
systems used in th
tensile tests. The
calculated and is
values of energy a
increasing EMS co

absorption increased with increasing EMS content. The moisture absorption results for the test matrix bio resin systems in this study are provided inFigure 3-10. For UPE resin systems (no EMS blends), it was observed that an increase in clay content enhanced the moisture diffusion barrier properties, i.e. moisture absorption decreased with increasing clay content. A similar trend was not observed for EMS blend resin system. The effect of the EMS blend in increasing moisture absorption seems to overpower the enhancement of barrier properties due to the addition of clay. However this effect was observed to be dependent on processing technique. As discussed earlier, the 90/10/1.5 had a processing technique slightly different than other resin systems, in which the EMS bio-resin was added after acetone removal. This processing technique seems to give better moisture barrier properties. For neat resin systems (no clay), the increase in average moisture absorption values for a 10% EMS blend resin system relative to neat UPE was around 5%. The addition of 1.5 wt.% clay to the 10% EMS showed a decrease of around 5% in average moisture absorption, relative to the neat UPE system. Thus the loss in barrier properties due to addition of EMS content seems to be recovered by nanoclay inclusions. In this case, the 10% EMS resin system with 1.5 wt.% clay seems to indicate better barrier properties than the virgin UPE composite.

3.4.5 Energy Absorbed per Unit Volume (Toughness)

The relative comparison of the toughness of various bio-blend nanocomposite resin systems used in this study was performed by integrating the stress-strain curves from direct tensile tests. The amount of energy absorbed per unit volume of the nanocomposite was calculated and is provided in Figure 3-11. The overall trend considering only the average values of energy absorbed suggests that that the toughness of the composites increased with increasing EMS content and decreased with increasing clay content. Research has shown that

the addition of
dependent on th
exfoliated clay m
partially exfoliate

A large v
earlier, detailed
precisely obtain t
considered and h
obtained. As the
energy absorbed
considering only
absorbed (toughn
blend. The decre
brittleness by add
the EMS bio-resi
systems, for the s
had approximatel
systems (no EMS)

3.4.6 Transmis

Figure 3-
nanocomposites.
matrix. It was o
intercalated and w

the addition of nanoclay inclusions can enhance the toughness of the composite, but is dependent on the morphology of the clay platelets [3-10]. At low concentrations, the well-exfoliated clay morphology produces better toughness properties and at higher clay contents partially exfoliated and intercalated morphologies perform better in toughness [3-10].

A large variation was observed in the amount of energy absorbed. As mentioned earlier, detailed statistical analyses considering the variations should be performed to precisely obtain the effects of EMS and nanoclay. In this work, only the average values are considered and hence a qualitative effect and overall trends based on average values could be obtained. As the amount of energy absorbed was obtained from tensile tests, the variation in energy absorbed is due to the large variations in the tensile failure strains. Nevertheless, considering only the average values of energy absorbed the average values of energy absorbed (toughness) seems to be improved by around 40% for neat resins with a 10% EMS blend. The decrease in average energy absorbed values (toughness) due to the increase of brittleness by addition of nanoclay inclusions seems to be partially recovered by addition of the EMS bio-resin. The comparison of resin systems with 10% EMS and virgin UPE resin systems, for the same amount of clay revealed that, on average, the 10% EMS resin systems had approximately 75% better energy absorption than similar nanoclay reinforced UPE resin systems (no EMS).

3.4.6 Transmission Electron Microscopy

Figure 3-12 (a and b) shows the bright field TEM micrographs of clay/UPE nanocomposites. Figure 3-12 (a) shows a general view of clay platelets distributed in UPE matrix. It was observed that the clay platelets were partially exfoliated and partially intercalated and were well distributed in the resin matrix. Similar micrographs were observed

for EMS blends as th
Figure 3-12 (b) show
morphology of the c
element. In order t
sonication process c
exfoliation of the cl
to breaking of the
composite properti
procedure should
thermo-physical pr
outcomes will be p

3.4.7 Fractograp

Figure 3-1
surfaces of neat
inclusions, respect
to fracture prope
surface is attribut
nanocomposites
The SEM mi
Figure 3-13 (a))
wt.% clay inclus
blends and incre
clay leads to

for EMS blends as the same amount of energy was spent on all resin systems in processing. Figure 3-12 (b) shows a high magnification micrograph focusing on the stacked intercalated morphology of the clay particle. Three to four particles were observed in each intercalated element. In order to obtain better exfoliation, additional energy must be spent in the sonication process of clay. It is expected that higher sonication energies will provide better exfoliation of the clay platelets, at the same time; excessive sonication energy/time may lead to breaking of the clay platelets, thus reducing the aspect ratios and leading to inferior composite properties. Processing techniques with varying sonication energies and mixing procedure should be studied to better understand the resulting morphology and their thermo-physical properties of composites. Such a study is in progress by the authors and outcomes will be provided in future communications.

3.4.7 Fractographic Observations (Scanning Electron Microscopy)

Figure 3-13(a) and Figure 3-13 (b) show the SEM micrographs of tensile fracture surfaces of neat UPE composite and 10% EMS blend composite with 1.5wt.% clay inclusions, respectively. The roughness of the fracture surface has generally been associated to fracture properties and critical strain energy release rates. A smooth featureless fracture surface is attributed to brittle failures, and rougher fracture surfaces are attributed to tougher nanocomposites [3-14].

The SEM micrograph for neat UPE was found to be relatively smooth and featureless (Figure 3-13 (a)). Figure 3-13 (b) shows the SEM micrograph for 10% EMS blend with 1.5 wt.% clay inclusion. The roughness of the fracture surfaces increased with increasing EMS blends and increasing clay content. This suggests that the combination of EMS blend and clay leads to tougher composites. Research has shown that the change in fracture

morphology suggests
At low concentratio
properties and at hig
perform better in tou
to toughness of the
structural parameters
the fracture and toug

3.5 *Discussion*

The results
composites show
polymer nanocomp
resins) in UPE res
original virgin U
scatter/variations
failure-dependent
strengths. Detail
performed to qua
nanoclay. In this
and overall tren
(bio-resin) seem
the addition of
system, i.e., a re
toughness bala

morphology suggests different toughening mechanism at low and high clay loading [3-10]. At low concentrations, the well-exfoliated clay morphology produces better toughness properties and at higher clay contents partially exfoliated and intercalated morphologies perform better in toughness [3-10]. It is difficult to quantitatively relate the fracture surface to toughness of the composites [3-14] as this requires better understanding of micro-structural parameters, such as crack propagation mechanisms and interface studies to relate the fracture and toughness to the surface morphologies.

3.5 Discussion

The results of the thermo-physical characterization of bio-blend layered silicate composites show a wide variety of multifunctional properties of the resulting bio-based polymer nanocomposites. It was observed that the combination of nanoclays and EMS (bio-resins) in UPE resin systems lead to composites with similar or better properties than the original virgin UPE resin system. As expected, the experimental data revealed scatter/variations in measured parameters. These variations were specifically larger for failure-dependent parameters, such as tensile failure strains, tensile strengths and impact strengths. Detailed statistical analyses taking into account these variations should be performed to quantitatively and precisely obtain the effects of constituents, namely EMS and nanoclay. In this work, only the average values were considered and hence a qualitative effect and overall trends based on average values could be obtained. Overall, the addition of EMS (bio-resin) seems to increase toughness but reduces stiffness of the resin systems. Similarly, the addition of nanoclay seems to increase the stiffness along with brittleness of the resin system, i.e., a reduction in toughness and ductility. The study shows that a proper stiffness-toughness balance can be obtained by controlling the amount of bio-resin and nanoclay

contents. Moreov
properties, like imp

Direct tens
around 25% and 4
time, the average
1.5 wt.% nano-cla
and nano-clay inc
10% lower than th
due to addition
experimental mat
contents and bett
90/10/1.5 resin sy
30% reduction in
system with no cla

The redu
improvement in t
of energy absorb
decreased with ad
was found to hav
neat UPE. The 1
75% better toughn
UPE resin system
UPE resin syste

contents. Moreover, the resulting nanocomposites show value added multifunctional properties, like improvements in barrier and thermal properties.

Direct tensile tests revealed a decrease of in the average values of tensile modulus by around 25% and 40% with blends of 10% and 20% EMS in neat UPE (no clay). At the same time, the average tensile modulus values increased by approximately 15% with addition of 1.5 wt.% nano-clay inclusions. The resin system that had the largest amount of EMS (10%) and nano-clay inclusion (1.5 wt.%) was found to have an average tensile modulus around 10% lower than the virgin UPE (no nanoclay, no EMS). Although, the average stiffness lost due to addition of EMS was not completely recovered by addition of nanoclay in this experimental matrix, the authors have confidence that this is possible with higher clay contents and better processing. Nevertheless, the lower average tensile modulus value for 90/10/1.5 resin system is not surprising, since it is an improvement from the approximate 30% reduction in average tensile modulus value observed for the 10% EMS neat resin system with no clay.

The reduction in stiffness due to addition of EMS was accompanied by an improvement in toughness of the resulting bio-based resin. Overall trend of averafge values of energy absorbed suggests that toughness increased with increasing EMS content and decreased with addition of nanoclay. The neat (no clay) 10% EMS bio-based resin system was found to have around 40% higher toughness (average energy absorbed value) relative to neat UPE. The 10% EMS bio-blend systems with varying clay contents had approximately 75% better toughness (average energy absorbed value) relative to similar nanoclay reinforced UPE resin systems. It was observed that the incorporation of EMS and nanoclay in to the UPE resin systems provided improved stiffness-toughness balance. At the same time,

processing techniques
enable incorporation

The thermal
similar to the tensile
CTE and moisture
absorption of the
effects of EMS b
mechanisms (tortu
properties with the
CTE and a decreas
[illegible]% with addition
average CTE belo
this case, the ther
EMS were partia
clay content an
enhancement of
properties which
complete recove
increased the av
resin system. T
moisture absor
increase in mo
nanoclay platel

processing techniques and the functionalization of clays and resins need to be improved to enable incorporation of higher amounts of EMS and clay contents.

The thermal and barrier properties of the resin systems in the study showed trends similar to the tensile modulus values obtained from tensile tests. The overall trend of average CTE and moisture absorption values suggests that addition of EMS increased the moisture absorption of the resulting bio-based resin. Additionally, results indicate that the adverse effects of EMS blends on moisture absorption can be recovered through the barrier mechanisms (tortuous path) provided by the nanoclay particles. A reduction in thermal properties with the addition of EMS in bio-based resins was characterized by an increase in CTE and a decrease in T_g. The average CTE below T_g value was found to increase by around 20% with addition of 10% EMS, relative to neat UPE. By adding 1.5 wt.% nanoclay, the average CTE below T_g value was approximatley 10% higher than that of the virgin UPE. In this case, the thermal properties lost (represented by an increase in CTE) due to addition of EMS were partially recovered by addition of nanoclay. As before, increasing the amount of clay content and improvement of the processing methods would enable recovery and enhancement of thermal properties of resulting composite. Unlike the case of thermal properties which were only partially recovered, average moisture barrier properties suggest complete recovery at 1.5 wt.% nanoclay content. The addition of 10% EMS to neat UPE increased the average moisture absorption value by approximately 5% relative to virgin UPE resin system. The 10% EMS blend with 1.5 wt.% clay had around 5% lower average moisture absorption value relative to the virgin UPE resin system. Thus, it seems that the increase in moisture absorption due to addition of EMS was compensated by addition of nanoclay platelets.

Tensile fracture su
reinforcements were ev
had the most smooth a
similar scaled images
associated the roughne
energy rates. This is su
larger strain energy rec
surface is indicative of
of both EMS and nar
provide a tougher mat
of UPE/EMS clay nar
some material propert
recovered by the syner

3.6 *Conclusions*

The development
polymers has many
improved toughness
characterization of na
blends, or bio-based
was observed that
stiffness/modulus of
EMS was partially r
reinforced UPE/EM

Tensile fracture surfaces of the bio-based resin systems with and without nanoclay reinforcements were evaluated through a scanning electron microscope. Neat virgin UPE had the most smooth and featureless fracture surface. It was observed that the roughness of similar scaled images increased with increasing EMS and clay content. Research has associated the roughness of the fracture surface with fracture properties and critical strain energy rates. This is supported by the concept that the larger the fracture surface area, the larger strain energy required for the cracks to propagate [3-14]. Hence, a rougher fracture surface is indicative of a tougher material. The increase in surface roughness due to addition of both EMS and nanoclay suggests that the combination of EMS and clay composites provide a tougher material. Overall, the results of thermo-physical property characterization of UPE/EMS clay nanocomposites show multifunctional behavior wherein the decrease in some material properties due to the addition of EMS or clay was completely or partially recovered by the synergistic effect of the hybrid material system.

3.6 Conclusions

The development of bio-based resin systems from the blends of synthetic and natural polymers has many benefits including environmental friendliness, cost effectiveness and improved toughness of the resulting composites. Thermo-physical properties and characterization of nanoclay reinforced bio-based composites was performed on UPE/EMS blends, or bio-based resins, with varying contents of EMS and nanoclay reinforcements. It was observed that the addition of EMS increased the toughness and decreased the stiffness/modulus of the resulting composites. The decrease in modulus due to addition of EMS was partially recovered through nanoclay reinforcement. As a result, the nanoclay reinforced UPE/EMS composites showed improved stiffness-toughness balance. Similarly,

the reduction in therm
with nanoclay reinfor
EMS/UPE blends pr
similar properties than
At the same time, mor
that higher amounts of
maximize the multifun

3.7 Acknowledge

The presented
Foundation under Gr
authors are also than
Ashland Specialty Ch
findings and conclusio
necessarily reflect the

the reduction in thermal and barrier properties due to the addition of EMS were recovered with nanoclay reinforcement. Thus, the synergistic combination of nanoclay reinforced EMS/UPE blends produces hybrid multifunctional nanocomposites with enhanced or similar properties than the virgin resin and holds great promise for use in wide applications. At the same time, more work needs to be done in improving the processing techniques such that higher amounts of bio-resin content and nanoclay reinforcement can be incorporated to maximize the multifunctionality these bio-based hybrid nanocomposites can offer.

3.7 Acknowledgements

The presented material is based upon work supported by the National Science Foundation under Grant No. CMS-0409666, which the authors gratefully acknowledge. The authors are also thankful to Kemlite Inc., Joliet, IL, Arkema Inc., Philadelphia, PA and Ashland Specialty Chemical Co., Columbus OH, for supplying samples. Any opinions, findings and conclusions expressed in this material are those of the authors alone and do not necessarily reflect the views of the National Science Foundation.

3.8 *Tables and Fi*

Table 3-1. Experimen

Clay Content (wt.%)
0.0
0.5
1.0
1.5

Nomenclatur
it has 95 parts
of nanoclay. X
current proces

3.8 Tables and Figures

Table 3-1. Experimental matrix showing specimen identification numbers and variation in clay and EMS contents

Clay Content (wt.%)	Amount of EMS substituting UPE in UPE-EMS blend. (as % of UPE)				
	0%	5%	10%	15%	20%
0.0	1	2	3	4	5
0.5	6	7	8	X	X
1.0	9	10	11	X	X
1.5	12	13	14	X	X

Nomenclature Example: Specimen ID 7 is referred as 95/5/0.5, indicating it has 95 parts of UPE and 5 parts of EMS and is reinforced with 0.5 wt.% of nanoclay. X – indicates resin systems that could not be achieved with current processing technique

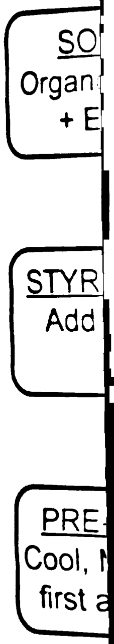

Figure 3-1

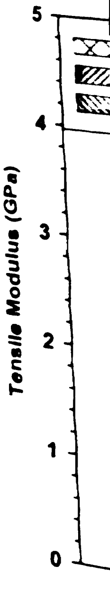

Figure 3-2. E

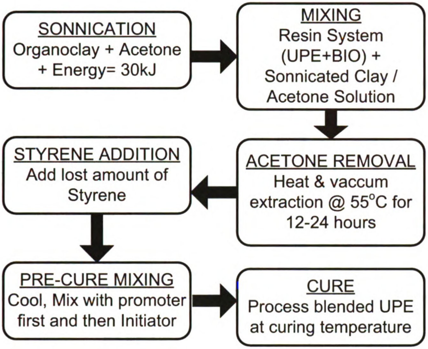

Figure 3-1. Processing technique of nanoclay reinforced EMS-UPE blends

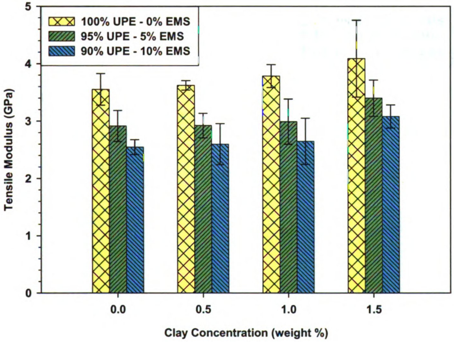

Figure 3-2. Experimental tensile modulus of bio-blend resin systems with varying clay contents

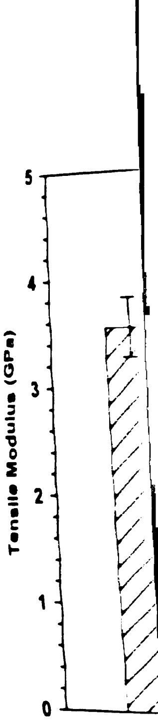

Figure 3-3. Exper

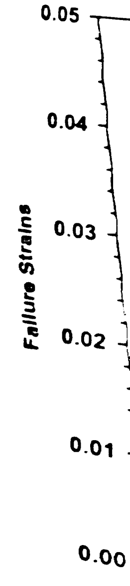

Figure 3-4

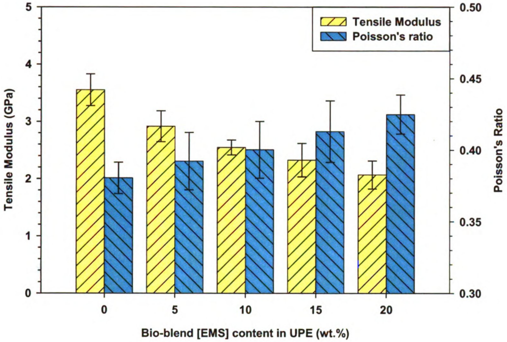

Figure 3-3. Experimental tensile modulus and Poisson's ratio of neat resin (no clay) systems

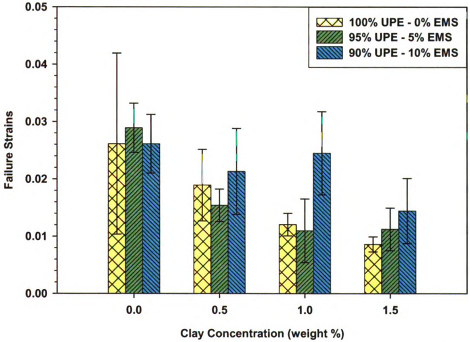

Figure 3-4. Tensile strains at failure of bio-blend resin systems with varying clay contents

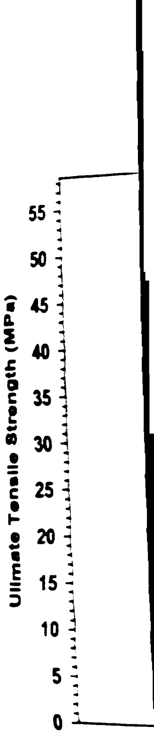

Figure 3-5. Ultim

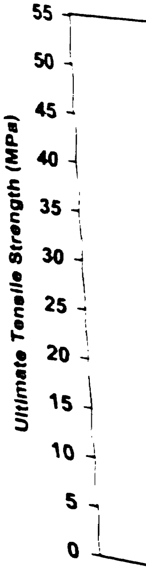

Figure 3-6

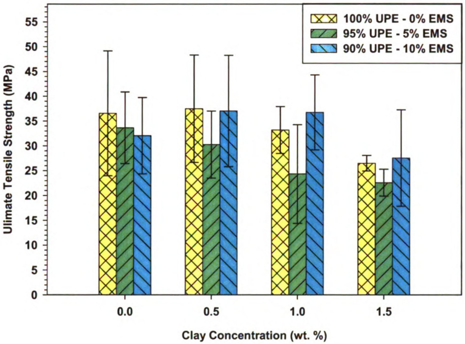

Figure 3-5. Ultimate tensile strengths of bio-blend resin systems with varying clay contents

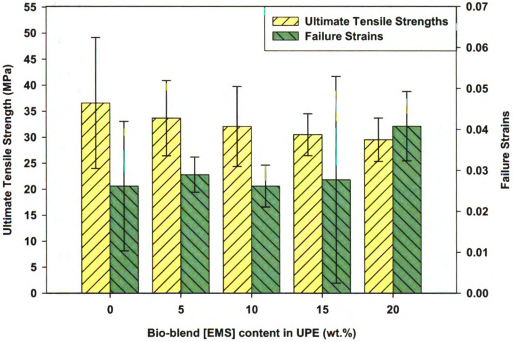

Figure 3-6. Ultimate tensile strengths and failure strains of neat resin (no clay) systems

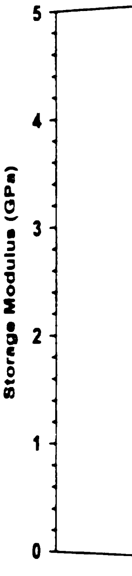

Figure 3.

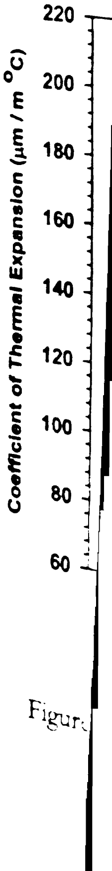

Figur

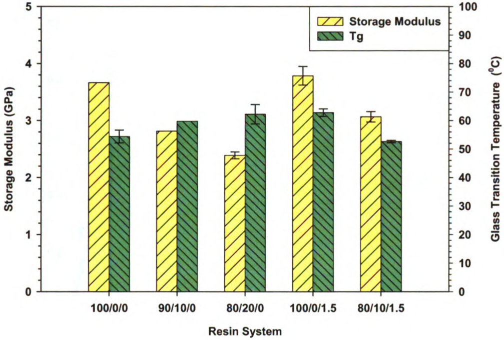

Figure 3-7. Storage Modulus and Glass Transition Temperature of Bio-blend Nanocomposites

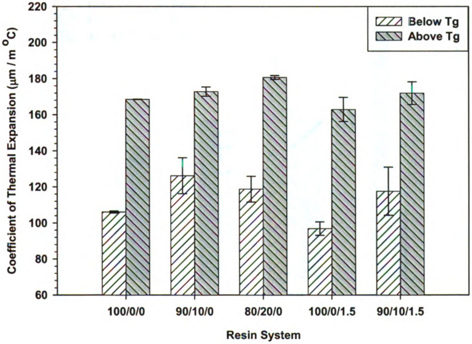

Figure 3-8. Linear coefficient of thermal expansion above and below T_g

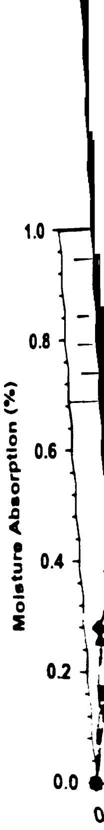

Figure 3-9.

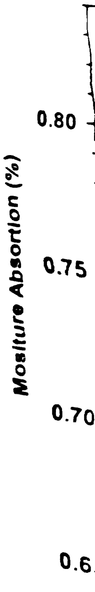

Figure 3.

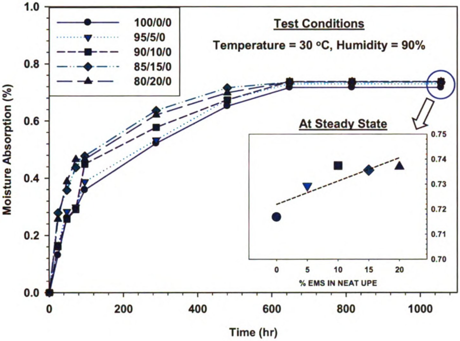

Figure 3-9. Moisture absorption of neat resins (no clay). The inset plot compares the moisture absorption after steady state has been achieved

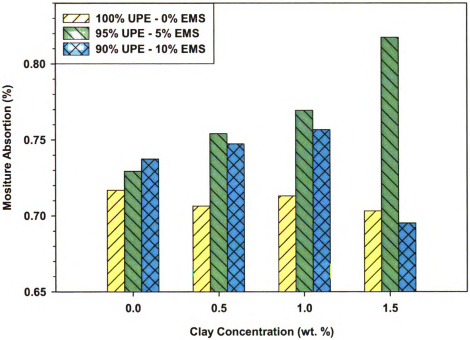

Figure 3-10. Moisture absorption of bio-blend resin systems with varying clay contents

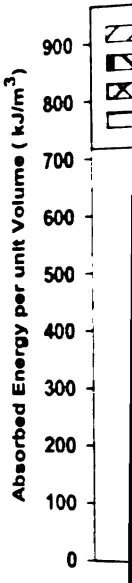

Figure 3-11. Abs

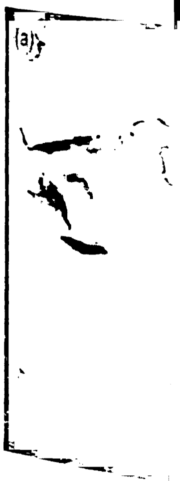

Figure 3-12. Bri
exfoliated and in
μm, b) High ma
intercalated part

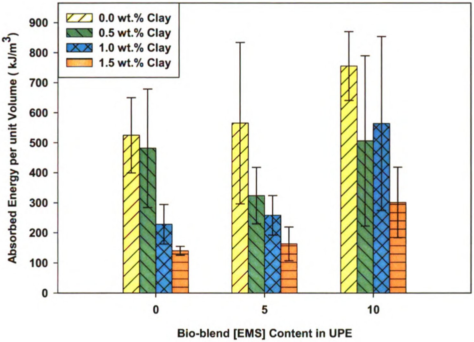

Figure 3-11. Absorbed energy per unit volume (toughness) of bio-blend resin systems with varying clay contents

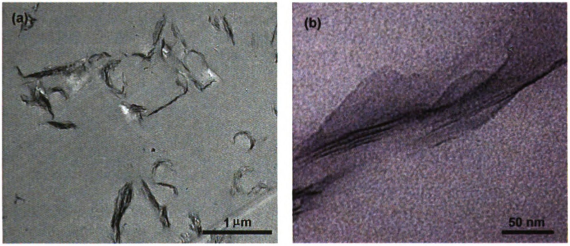

Figure 3-12. Bright-field TEM micrographs revealing homogenous dispersion with partially exfoliated and intercalated clay particles in UPE matrix. a) Low magnification, scale bar = 1 μm, b) High magnification, scale bar = 50 nm, approximately 3 to 4 particles per gallery of intercalated particle.

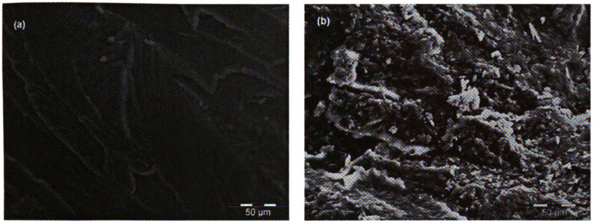

Figure 3-13. SEM micrographs of tensile failure surfaces, a) Neat UPE without inclusions, scale bar = 50 μm, b) 10% bio-blend [EMS] in UPE with 1.5 wt.%. clay inclusions, scale bar = 50 μm.

3.9 References

[3-1]. Mohanty AK
Biocompo

[3-2]. Burgueño R
Sustainab
resin for h

[3-3]. Burgueño R,
bearing n
2004; 35:6

[3-4]. Nickel J, Ried

[3-5]. Donnell AO,
resin. Co

[3-6]. Morye SS, W
on a nov
146.

[3-7]. Miyagawa H
biobased
Chem Re

[3-8]. Miyagawa H
from ble
Polym Sc

[3-9]. Mohanty AK
organocl
ANTEC

[3-10]. Nair SV, Go
-6,6 com

[3-11]. Le Baron P
overview

[3-12]. Miyagawa H
thermop
nanocon

[3-13]. Bakar M, D
unsatura

3.9 References

[3-1]. Mohanty AK, Misra M, Hinrichsen G, Biofibers, Biodegradable Polymers and Biocomposites: An Overview. Macromol Mater and Eng. 2000; 276/277:1-24.

[3-2]. Burgueño R, Quagliata MJ, Mehta GM, Mohanty AK, Misra M, Drzal LT. Sustainable cellular biocomposites from natural fibers and unsaturated polyester resin for housing panel applications" J Polym Environ 2005; 13:139-149.

[3-3]. Burgueño R, Quagliata MJ, Mohanty AK, Mehta GM, Drzal LT, Misra M. Load bearing natural fiber composite cellular beams and panels." Composites Part A. 2004; 35:645-656.

[3-4]. Nickel J, Riedel U. Activities in biocomposites. Mater Today 2003; 6:44-48

[3-5]. Donnell AO, Dweib MA, Wool R.P. Natural fiber composites with plant oil based resin. Compos Sci Tech 2004, 64:1135-1145.

[3-6]. Morye SS, Wool RP. Mechanical properties of glass /flax hybrid composites based on a novel modified soyabean oil matrix material. Polym Compos 2005, 26:407-146.

[3-7]. Miyagawa H, Mohanty AK, Burgueño R, Drzal LT, Misra M. Development of biobased unsaturated polyester containing functionalized vegetable oils. Ind Eng Chem Res. 2006; 45:1014-1018.

[3-8]. Miyagawa H, Mohanty AK, Burgueño R, Drzal LT, Misra M. Novel biobased resins from blends of functionalized soya bean oil and unsaturated polyester resin. J Polym Sci Part B: Polym Phys 2007; 45: 698-704

[3-9]. Mohanty AK, Miyagawa H, Burgueño R, Misra M. Biobased nanocomposites from organoclay and blends of unsaturated polyester and functionalized vegetable oil. ANTEC, Conference Proceedings. 2005; 4: 52-56

[3-10]. Nair SV, Goettler LA, Lysek, B.A. Toughness of nanoscale and multiscale polyamide -6,6 composites. Polym Eng Sci. 2002; 42:1872-1882.

[3-11]. Le Baron PC., Wang Z, Pinnavaia TJ. Polymer – layered silicate nanocomposites: an overview. Appl Clay Sci. 1999; 15:11-29

[3-12]. Miyagawa H, Mohanty AK, Burgueño R, Drzal LT, Misra M. Characterization and thermophysical properties of unsaturated polyester-layered silicate nanocomposites. J Nanoscience and Nanotech. 2006; 6:464-471.

[3-13]. Bakar M, Djaider F. Effect of plasticizers content on the mechanical properties of unsaturated polyester resin. J Thermoplast Compos Mater. 2007; 20:53-64.

[14] Wang L, Wa
thermal/m
Part A. 20

[3-14]. Wang L, Wang K, Chen L, Zhang Y, He C. Preparation, morphology and thermal/mechanical properties of epoxy/clay nanoclay composite. Composites Part A. 2006; 37:1890-1896

Chapter 4. Bio-b

4.1 Abstract

Bio-based nan
reinforced with nan
evaluation of their p
twelve nanocomposit
to 5 wt.% nanoclay
technique and exper
nanoclay reinforcem
EML content show
nanoclay show prom
based nanocomposit

4.2 Introductio

Environmen
conventional polym
petroleum and veg
produce composite
properties that are s

Bio-based p
the primary const

---

[1] Haq, M., Burgueño
UPE/EML blends an
performance," Commu

Chapter 4. Bio-based Polymer Nanocomposites: II - UPE / EML [1]

4.1 Abstract

Bio-based nanocomposites, defined as blends of petroleum and vegetable oil resins reinforced with nanoclay, can lead to synergistic material property enhancement; and evaluation of their performance and limits can allow for their optimal design. An array of twelve nanocomposite designs with up to 30% epoxidized methyl linseedate (EML) and up to 5 wt.% nanoclay in unsaturated polyester were manufactured using a solvent-based technique and experimentally characterized. Recovery of most properties was possible with nanoclay reinforcement for EML contents up to 20%, whereas polymer blends with 30% EML content showed little improvement. Systems with up to 20% EML and 2.5 wt.% nanoclay show promise due to processing ease and balanced properties. The developed bio-based nanocomposites have potential as sustainable multifunctional materials.

4.2 Introduction

Environmentally friendly composites with material properties that can compete with conventional polymers can be obtained by reinforcing nanoclay in polymer blends of petroleum and vegetable oil based resins. Such hybrid combinations have been found to produce composites that exhibit synergistic behavior with improvements to multiple properties that are superior or similar to the base petroleum polymer.

Bio-based polymer systems, defined as a combination of petroleum-based resins as the primary constituent and natural bio-resins as the secondary constituent, can be

---

[1] Haq, M., Burgueño, R., Mohanty, A.K., and Misra, M., "Bio-based polymer nanocomposites from UPE/EML blends and nanoclay: Development, experimental characterization and limits to synergistic performance," Communicated – Composites: Part A

reinforced with nano
1]. The developmen
renewable materials
Mohanty et al. [4-2]
composites, or bioco
been shown to impro
This increase in toug
to increased plastic d
the modulus [4-5][4-
polymer. Stiffness a
balance is required to
use of plant-oil base
strength for load-be
approach pursued by
resin by the addition

The reinforc
has been shown to
enhancements not c
ablation resistance p
bio-resins like soy-
Polymer/clay nano
articles exist on thi
improvement due
polymers [4-6]. Mo

reinforced with nanoclay to obtain novel, value added applications for natural polymers [4-1]. The development of alternatives for petroleum-derived materials with plant-based renewable materials has been propelled from an environmental viewpoint [4-1]-[4-4]. Mohanty et al. [4-2] provide a good overview on bio-polymers, bio-fibers and bio-based composites, or biocomposites. The blending of bio-resin with petroleum-based resin has been shown to improve the toughness of the resulting polymer system [4-2][4-5][4-6][4-7]. This increase in toughness is due to the reduction in cross-link density in the system, leading to increased plastic deformations [4-7]. However, this increase in toughness seriously affects the modulus [4-5][4-6][4-7], thermal [4-6][4-7] and barrier [4-6] properties of the resulting polymer. Stiffness and toughness are opposing performance parameters and a proper balance is required to develop an efficient biocomposite. Moreover, research has shown that use of plant-oil based polymeric materials do not show adequate properties of rigidity and strength for load-bearing applications by themselves and require modification [4-1]. One approach pursued by the authors is to recover the property losses from the addition of bio-resin by the addition of layered silicates, or nanoclays.

The reinforcement of petroleum-based polymers with layered silicates, or nanoclays, has been shown to impart multifunctionality to the resulting polymer nanocomposite with enhancements not only on stiffness but improvements in thermal, barrier, flammability and ablation resistance properties [4-8]. Nanoclay reinforcement has also been used with natural bio-resins like soy- [4-1][4-9][4-10] and corn-based [4-11] resins with similar enhancements. Polymer/clay nanocomposites are well understood and considerable literature and review articles exist on this topic [4-8][4-12]-[4-14]. In spite of the noted enhancements, stiffness improvement due to addition of nanoclay also increases the brittleness of the resulting polymers [4-6]. Moreover, petroleum-based polymers such as unsaturated polyesters (UPEs),

which are commonl
mechanical, electrical
16]. The use of all-na
such as low mechanic
non-renewable synth
studied considerably
hybrid combinations
synergistic behavior
multifunctional prop
bio-based nanocom
be recovered by add

The initial a
unsaturated polyest
epoxidized methyl s
nanoclay (Cloisite
incorporation of b
nanoclay and bio-r
materials with impr
stiffness, thermal a
addition resulted i
recovery of stiffn
recommendations:
higher amounts of
a detailed characte

which are commonly used due to their low cost, ease of handling and good balance of mechanical, electrical, chemical and fire resistance properties, are inherently brittle[4-15][4-16]. The use of all-natural bio-polymers has been limited due to performance based concerns such as low mechanical and thermo-physical properties [4-5][4-17][4-18]. The substitution of non-renewable synthetic polymers with renewable polymers has been thus proposed and studied considerably [4-5][4-16]-[4-24]. As discussed earlier, composites obtained from the hybrid combinations of petro-based resin, bio-resin and nanoclay have been found to exhibit synergistic behavior with balanced stiffness-toughness properties along with other multifunctional properties. Hence, the hypothesis of the work presented here was to obtain bio-based nanocomposites wherein the reduction in properties due to bio-resin addition can be recovered by addition of nanoclay.

The initial attempt at this hypothesis was performed by blending petroleum based unsaturated polyester (UPE) with functionalized vegetable oil as the bio-resin, namely epoxidized methyl soyate (EMS) [4-6]. The resulting bio-based resins were processed with nanoclay (Cloisite 30B®). The processing technique used allowed only a limited incorporation of bio-resin (10%) and nanoclay (1.5 wt.%). In spite of low amounts of nanoclay and bio-resin, the results showed promise in the synergistic behavior of these materials with improvements in toughness due to addition of bio-resin and enhancements in stiffness, thermal and moisture barrier properties due to nanoclay addition. The nanoclay addition resulted in complete recovery of moisture barrier properties but only partial recovery of stiffness and other properties. This study [4-6] led to the following recommendations: a) improve the processing technique such that incorporation of relatively higher amounts of bio-resin (>10%) and nanoclay (>1.5 wt.%) were possible, b) to perform a detailed characterization of an array of nano-reinforced bio-based polymer systems to

study the effects of
material combinatior
behavior. Moreover,
using UPE with E
linseedate) [4-17] fou
higher in EMS-base
blends should perfor

In this work
UPE/EMS nanocor
were made. First, an
identified from a de
30 wt.% EML and
amounts of nanocla
limits on the effec
allowing the identifi
of properties along
modulus, strengths
linear coefficient o
The degree of r
nanocomposites w
resin and nanoclay
scanning electron
purposes not prov

study the effects of constituents on the synergistic behavior, and c) to find optimized material combinations that have ease of processing along with enhanced synergistic behavior. Moreover, studies by Miyagawa et. al [4-5][4-17] on neat resin (no clay) blends, using UPE with EMS (epoxidized methyl soyate) [4-5] and EML (epoxidized methyl linseedate) [4-17] found that stiffness loss due to addition of functionalized vegetable oil was higher in EMS-based resin systems. This suggests that nanocomposites from UPE/EML blends should perform better than those from UPE/EMS blends.

In this work, the shortcomings and recommendations from the above-mentioned UPE/EMS nanocomposites study [4-6] were taken into consideration and improvements were made. First, an EML bio-resin was used. Secondly, an improved manufacturing method identified from a detailed processing study [4-25], and which allowed incorporation of up to 30 wt.% EML and 5.0 wt.% was used. Since it was possible to incorporate relatively large amounts of nanoclay and EML contents, this study was also aimed at finding performance limits on the effects of EML and nanoclay on the resulting nanocomposites, thereby allowing the identification of optimized material combinations that would result in a balance of properties along with ease of processing. Experimental evaluation of tensile properties (modulus, strengths and failure strains), impact strengths, glass transition temperature (T_g), linear coefficient of thermal expansion and moisture diffusivity properties was performed. The degree of nanoclay dispersion and morphology of the different bio-based nanocomposites was assessed using transmission electron microscopy. The effect of bio resin and nanoclay on the surface morphology of resulting tensile fracture was studied using scanning electron microscopy and is reported in an earlier work [4-6], and for brevity purposes not provided here. Results indicate synergistic behavior of bio-resin blends and nanoclay with co

show balanced n

4.3 *Experim*

Experimen

characterization

inclusions. In th

and testing are p

4.3.1 Materia

The mai

resin (UPE, Po

bio-based modi

replaced up to

compositions th

linolenate epox

wt. % methyl pa

Cloisite 30B® (S

and nanoclay) v

and 2-butanone

resin system to

was 100 parts b

Samples were cu

nanoclay with complete to partial recovery of most properties. Material combinations that show balanced multifunctional properties along with ease of processing were also identified.

4.3 Experimental Methods

Experimental determination of thermo-physical properties and material characterization were performed on bio-based polymer blends reinforced with nanoclay inclusions. In the following sections, details on materials, processing, parameters studied, and testing are provided.

4.3.1 Materials

The main component of bio-based polymer systems was ortho unsaturated polyester resin (UPE, Polylite® 32570-00, Reichhold Inc., NC), which contains 33.5 wt.% styrene. A bio-based modifier, epoxidized methyl linseedate (EML, Vikoflex® 9010, Arkema Inc., PA) replaced up to 30 wt.% of UPE. EML is a mixture of methyl esters of fatty acid compositions that construct the linseed oil. The detailed composition is 40-50 wt. % methyl linolenate epoxy, 24-26 wt. % methyl oleate epoxy, 17-22 wt. % methyl linoleate epoxy, 4-7 wt. % methyl palmitate, and 2-5% wt.% methyl stearate. The nanoclay used in this work was Cloisite 30B® (Southern Clay Products, Inc., TX). The resin system (mixture of UPE, EML and nanoclay) was processed with cobalt naphthenate (Sigma-Aldrich, MO) as a promoter and 2-butanone peroxide (Sigma-Aldrich) as an initiator. A constant ratio by weight of the resin system to the promoter and initiator was utilized to cure all samples. The mixing ratio was 100 parts by weight of the resin system to 0.03 part promoter and 1.50 part initiator. Samples were cured at 100 °C for 2 h, followed by 160 °C for 2 h.

4.3.2 Experimenta

The amount

primary resin compo

of four neat resin (n

reinforced with nano

evaluated by varying

used to describe the

and "*B*" represents t

are the weight fractio

referred to as 80/20

of EML and is r

corresponding to 0

considered the basel

4.3.3 Polymer na

The techniq

follows the findings

based clay/polyme

consists of sonicati

concentration of ap

After sonication, or

mixed continuousl

acetone. The rema

the acetone remov

4.3.2 Experimental matrix and nomenclature

The amount of bio-resin (epoxidized methyl linseedate, EML) that replaced the primary resin component UPE, was varied from 0% to 30%, in increments of 10%. A total of four neat resin (no clay) systems were obtained. Each of these resin systems were then reinforced with nanoclay inclusions of 2.5 wt.% and 5.0 wt.%. Twelve polymer systems were evaluated by varying clay and EML contents as summarized in Table 4-1. The nomenclature used to describe the polymer systems is: "*A/B/C*", where "*A*" refers to the amount of UPE and "*B*" represents the amount of EML as a percentage of the resin system, and "*C*" refers to the weight fraction of nanoclay inclusions. For example, Specimen ID 7 in Table 4-1 is referred to as 80/20/2.5, indicating that the resin system has 80 parts of UPE and 20 parts of EML and is reinforced with 2.5 wt.% of nanoclay platelets. The resin system corresponding to 0% EML content and 0% nanoclay corresponds to virgin UPE and is considered the baseline material system and was used for comparison.

4.3.3 Polymer nanocomposite processing

The technique used for processing the nanoclay reinforced bio-based resin systems follows the findings from our group's study on solvent-based processing techniques for bio-based clay/polymer nanocomposites [4-25]. The technique found to be most efficient consists of sonicating the nanoclay in acetone to an energy level of 300 kJ, using a solution concentration of approximately 50 l of acetone to 1 kg of clay, while it is constantly stirred. After sonication, only the UPE solution is added. The acetone + nanoclay + UPE solution is mixed continuously on a hot plate at approximately 55 °C to remove a majority of the acetone. The remaining acetone is removed by vacuum extraction at 55 °C for 24 h. During the acetone removal process the styrene present in the UPE is also removed. Thus, after

acetone removal the
solution is cooled t
followed by curing. A

4.3.4 Testing and

Tensile tests
speed of 5 mm/ mi
the study (Table 4-
corresponding to th
Also, it was suspe
Moreover, the rese
components using
included in the ther
identification numb
expansion above a
mechanical analysis
room temperature
throughout the te
coefficient of ther
intersection of the
tested per case stud

Moisture ab
equipment that al
maintained at 50

acetone removal the bio-resin, EML, is added along with the lost styrene. The processed solution is cooled to room temperature and blended with the initiator and promoter followed by curing. A flow chart depicting the process is shown in Figure 4-1.

4.3.4 Testing and characterization

Tensile tests were performed according to ASTM D638 standards with a testing speed of 5 mm/min. Six tensile specimens were tested for each case of polymer system in the study (Table 4-1). Experimental thermal tests were performed only on key designs corresponding to the extreme bio-resin (0 and 30%) and nanoclay (0 and 5 wt.%) contents. Also, it was suspected that the phase separation starts beyond 10% bio-resin content. Moreover, the research in our group aims at manufacturing large scale load bearing components using 10% bio-resin content. Hence, samples with 10% EML were also included in the thermal studies. Overall, thermal tests were performed on six specimens with identification numbers 1, 2, 4, 9, 10 and 12 (Table 4-1). The linear coefficient of thermal expansion above and below the glass transition temperature was obtained by thermo-mechanical analysis using a TA Instruments TMA 2940. The samples were heated from room temperature to 140 °C at a rate of 4°C/min. Strain and temperature was measured throughout the test. The linear slope of strain-temperature curve is reported as the coefficient of thermal expansion. The glass transition temperature was obtained from the intersection of the two linear portions of the strain-temperature curve. Two specimens were tested per case studied.

Moisture absorption testing was performed using a Fisher Scientific Versa bath®-138 equipment that allows immersion of samples in a distilled water bath with temperature maintained at 50 °C. The nanocomposites samples used for moisture measurements were rectangular bars and

specimens were coate

and limit the diffusio

to ensure flat and pa

80 °C for 24 h to re

12 h for the first 3

achieved. Moisture d

plots for various bi

notched Izod tests

inclusions in resulti

(TEM). Ultramicrot

included angle of 4

with LaB6 filament

4.4 Results

The polyme

virgin UPE and is

sections are compa

4.4.1 Tensile tes

Tensile modulus

Tensile mo

contents are provi

of the baseline U

reinforced bio-bas

rectangular bars and had average dimensions of 75.0 mm x 12.5 mm x 3.0 mm. The specimens were coated with impervious two-part epoxy on all edges to eliminate edge effects and limit the diffusion only through the thickness of the sample. All samples were polished to ensure flat and parallel surfaces. The polished samples were placed in a vacuum oven at 80 °C for 24 h to remove residual moisture. The weight of the samples was measured every 12 h for the first 3 days, followed by once every week until steady state (equilibrium) was achieved. Moisture diffusivity coefficients were obtained from the moisture-gain versus time plots for various bio-based nanocomposites. Impact strength was obtained by performing notched Izod tests as per ASTM D256. The dispersion and morphology of nanoclay inclusions in resulting polymer systems was assessed with transmission electron microscopy (TEM). Ultramicrotomy at room temperature was carried using a diamond knife with an included angle of 4° to produce sections approximately 70 nm thick. A JEOL 100CX TEM with LaB6 filament with 120 kV acceleration was used to obtain bright field images.

4.4 Results

The polymer system corresponding to 0% EML and 0% nanoclay corresponds to virgin UPE and is considered the baseline material system. All results in the following sections are compared to this baseline.

4.4.1 Tensile tests and properties

Tensile modulus

Tensile modulus for virgin (UPE) and bio-based polymer systems with varying clay contents are provided in Figure 4-2. A dashed horizontal line corresponding to the modulus of the baseline UPE is also shown to highlight the relative performance of the nanoclay reinforced bio-based polymer systems. As expected the trend of average tensile modulus

values suggests redu
(EML). The average
20 and 30% EML s
increase in average
and 5.0 wt.% nanoc
25 and 55%, respect

Similarly, fo
(both 2.5 wt.% and
average by 25%. Fo
wt.% nanoclay led
The reduction in av
50% for neat poly
30%. This indicates
fully recover the lo
30% EML the av
detrimental effect
gains provided by
observed.

Ultimate tensile streng

The ultima
plotted in Figure
resin (EML) reduc
low strength of th
was observed tha

values suggests reduction in average tensile modulus values with addition of bio-resin (EML). The average reduction was approximately in the range of 10, 50 and 65% for the 10, 20 and 30% EML systems, respectively. The addition of nanoclay inclusions revealed an increase in average tensile modulus values. For virgin UPE (no EML), the addition of 2.5 and 5.0 wt.% nanoclay revealed improvements in the average tensile modulus in the range of 25 and 55%, respectively.

Similarly, for UPE/EML blends with 10% EML content, the addition of nanoclay (both 2.5 wt.% and 5.0 wt.%) seems to have improved the tensile modulus values on an average by 25%. For UPE/EML blends with 20% EML content, the addition of 2.5 and 5.0 wt.% nanoclay led to an approximate reduction of 20% in average tensile modulus values. The reduction in average tensile modulus value due to the addition of 20% EML was around 50% for neat polymers and the enhancement due to 5 wt.% nanoclay was in the range of 30%. This indicates a partial recovery and that the amount of nanoclay was insufficient to fully recover the lost properties due to the addition of EML. Similarly, for bio-blends with 30% EML the average improvement due to nanoclay addition was insignificant. The detrimental effect of bio-resin (EML) on stiffness at 30% EML content was larger than the gains provided by nanoclay reinforcement and hence no significant improvement was observed.

Ultimate tensile strength

The ultimate tensile strengths (UTS) of the developed bio-based nanocomposites are plotted in Figure 4-3. The trend of average UTS values suggests that the addition of bio-resin (EML) reduces the ultimate tensile strength of the composite. This is attributed to the low strength of the bio-resin and the reduced cross-link density of the bio-blend polymer. It was observed that the addition of EML reduced the average UTS values by approximately 40

and 60% for polyme
was observed that na
This is attributed to
virgin UPE (no bio-
reduction in the ave
with 10%, 20% and
wt.%) revealed a r
respectively. For E
insignificant, as the
with respect to th
reducing the UTS
nanoclay seems to
polymer nanocomp

Elongation at failure

The ultima
nanocomposite sys
tensile failure stra
composites more
average value of t
system was lower t
EML, increase in t
specimen, which
concentration (80
at break due to ad

and 60% for polymer systems with 20 and 30% EML content, respectively. Additionally, it ws observed that nanoclay inclusions also reduced the average ultimate tensile strengths. This is attributed to the embrittlement of the polymer due to the addition of nanoclay. For virgin UPE (no bio-resin), the addition nanoclay (both 2.5 wt.% and 5.0 wt.%) revealed a reduction in the average UTS values by approximately 50 to 60%. Similarly for resin systems with 10%, 20% and 30% EML contents, the addition of nanoclay (both 2.5 wt.% and 5.0 wt.%) revealed a reduction in average UTS values by approximately 55, 70 and 80%, respectively. For EML contents up to 10%, the reduction of UTS due to EML content was insignificant, as the average UTS values of 10% EML composites had only a minor variation with respect to the neat UPE nanocomposites. EML plays a more significant role in reducing the UTS for its content is beyond 10%,. The combination of bio-resin and nanoclay seems to produce a detrimental effect that significantly reduces the UTS of the polymer nanocomposite.

Elongation at failure

The ultimate tensile strains (elongation at tensile test failure) for the tested bio-based nanocomposite systems are shown in Figure 4-4. The overall trend considering the average tensile failure strain values suggests that the addition of bio-resin makes the resulting composites more ductile and hence increased elongations at failure were observed. The average value of the ultimate tensile strain for the neat (no nanoclay) 20% EML polymer system was lower than its 10% EML counterpart. This deviation from the trend (increase in EML, increase in tensile strains) is attributed to the presence of shrinkage cracks in the test specimen, which occur while curing and were found to be prominent only at this concentration (80/20/0). Nonetheless, the overall trend indicates increase in the elongation at break due to addition of bio-resin.

The trend of average tensile strain values suggests that the addition of nanoclay reduced the elongations at failure. For virgin UPE (no EML), the addition of 2.5 and 5.0 wt.% nanoclay reduced the average failure elongations by a range of approximately 50 to 75%. For nanoclay reinforced UPE/EML blends (considering both 2.5 wt.% and 5.0 wt.%), the addition of nanoclay seems to reduce the average tensile failure strains by approximately 50 and 35% for 10% and 20% EML contents, respectively. For UPE/EML/clay blends with 30% EML content, the average tensile strain values were observed to be equal or better than the baseline virgin UPE composite, indicating complete recovery of the lost ducitility due to addition of nanoclay by addition of 30% EML.

4.4.2 Thermal properties

The linear coefficient of thermal expansion (CTE) above and below the glass transition temperature (T_g) are provided in Figure 4-5 and Figure 4-6, respectively for the key polymer systems, namely specimen numbers: 1, 2, 4, 9, 10 and 12 (see Table 4-1). For structural applications, the CTE above T_g is not of much importance, as the load carrying capacity is considerably reduced past T_g As a result, only the CTE results below T_g are discussed next. Nonetheless, CTE values above and below T_g follow similar trends and hence the discussions of CTE trends below T_g are valid for CTE values above T_g.

The trend of the average values of CTE below T_g suggests that the addition of bio-resin (EML) increased the average values of CTE. The average CTE values below T_g increased by approximately 10 and 15% for polymer systems with 10 and 30 % EML, respectively. The addition of 5 wt.% clay to virgin UPE (no EML) seems to reduce the

average CTE value
polymers with 10
approximately 10%
reduction in thermal
were partially recove

The variatio
nanoclay content is
glass transition temp
bio-resin (EML) co
reduction in the ra
decrease of T_g is at
blend [4-17]. Additi
UPE (0% EML) a
10%. The polymer
value similar to tha
blend with no nan
UPE. Overall, it se
to addition of bio-

average CTE value by approximately 20%. The addition of 5 wt.% clay to bio-based polymers with 10 and 30% EML content reveals average CTE values below T_g of approximately 10% higher than baseline UPE, respectively. Overall trends suggest that the reduction in thermal properties (represented by the increased CTE) due to addition of EML were partially recovered by the addition of nanoclay.

The variation of average T_g values for nanocomposites with varying EML and nanoclay content is shown in Figure 4-7. The T_g of virgin UPE was 98.5 °C. The average glass transition temperature values were observed to decrease proportionally with increasing bio-resin (EML) content. The average T_g values for neat polymers (no clay) revealed average reduction in the range of 5-10% with the addition of 10 to 30% EML, respectively. The decrease of T_g is attributed to the reduction in cross-link density of the bio-based polymer blend [4-17]. Addition of 5 wt.% nanoclay revealed increase in average T_g values of both neat UPE (0% EML) and the 10% EML bio-based polymers, on an average by approximately 10%. The polymer system with 5 wt.% nanoclay and 30% EML content had an average T_g value similar to that of the baseline UPE. This is an improvement from similar neat resin blend with no nanoclay, which had approximately 10% lower average T_g value than baseline UPE. Overall, it seems that the addition of 5 wt.% nanoclay helped recover the T_g lost due to addition of bio-resin (EML).

4.4.3

were

meas

amou

amou

nano

26, I

bio-n

The

M_t

wher

state,

syste

0.98,

subst

of th

user

in vi

4.4.3 Moisture absorption

Moisture absorption properties for the nanoclay reinforced bio-based composites were obtained by water immersion tests where the weight gain at any given time (M_t) was measured until steady state was achieved. Due to thickness variations in the specimens the amount of moisture absorbed by each was different. Thus, instead of simply assessing the amount of moisture absorbed, the speed of moisture absorption in polymers and nanocomposites was quantitatively compared by determining their diffusion coefficient [4-26]. Hence, moisture diffusivity coefficient was used as the parameter to assess the effect of bio-resin (EML) and nanoclay content on the different bio-based polymer nanocomposites. The diffusivity coefficient, D, was computed from the initial slope of the moisture gain, M_t/M_∞ versus time ($\sqrt{t}/d$) as:

$$D=\frac{\pi}{16}\left(\frac{M_t/M_\infty}{\sqrt{t}/d}\right)^2 \tag{4-1}$$

where M_t is the mass gain at any time t, M_∞ is the maximum mass gain at equilibrium/steady state, and d is the thickness of the specimen.

Figure 4-8 shows the plots of moisture gain versus time for neat (no clay) polymer systems. The experimental data is shown in symbols and exponential fits (average R^2 value = 0.98) are superimposed as solid lines. The diffusivity coefficients were obtained by substituting the initial slope from the curves in Figure 4-8 into Equation (4-1). The variation of the diffusivity coefficients D, with increasing bio-resin (EML) content are shown as an inset in Figure 4-8. The diffusion coefficients indicate the effect of bio-resin (EML) content in virgin UPE. The diffusivity coefficient of virgin UPE was found to be $3.67\text{x}10^{-12}$ m^2/s.

Pritcha

slightly

test co

approx

essenti

with a

In this

coeffic

reduct

diffusi

wt.%

20% E

UPE

diffus

nanoc

averag

wt.%

comp

averag

250%

diffus

the b

E.M.

Pritchard [4-27] reports a value of 3.0×10^{-12} m^2/s for ortho-unsaturated polyester. The slightly higher value obtained in this work may be due to the differences in the resins and test conditions. The average values of the diffusivity coefficients show an increase of approximately 70, 115 and 250% with the addition of 10, 20 and 30% EML. This is essentially a linear increase with EML content, as confirmed by a linear regression analysis with an R^2 value of 0.96.

The diffusivity coefficients of all the nanoclay-reinforced bio-based nanocomposites in this study are summarized in Figure 4-9. The study of average values of diffusion coefficients reveals that addition of nanoclay improved the barrier properties, observed as a reduction in the average diffusion coefficient values. A reduction in average values of diffusion coefficients of approximately 35 and 20% was observed due to addition of 2.5 wt.% nanoclay to neat UPE and 10% EML/UPE blend, respectively. For resin system with 20% EML and 2.5 wt.% nanoclay, the average diffusivity coefficients were similar to baseline UPE composite. Similar to resin systems with 2.5 wt.% nanoclay, a reduction in average diffusivity coefficients of approximately 70, 45 and 30% was observed due to 5 wt.% nanoclay inclusions in polymer systems with 0, 10, and 20% EML content, respectively. The average diffusion coefficient values for polymer systems with 30% EML reinforced with 5 wt.% nanoclay were approximately 130% higher than the value for the baseline UPE composite. Nonetheless, this is an improvement of approximately 120% considering that the average diffusivity coefficient for the neat UPE/EML blend (no clay) with 30% EML was 250% more than that of the baseline UPE. Thus, the loss in barrier properties (increased diffusivity) due to the adding bio-resin (EML) was recovered by the addition of nanoclay for the bio-based polymer systems using up to 20% EML. For bio-based polymers with 30% EML the detrimental effect of the bio-resin on diffusion properties was greater than the enha

degra

4.4.4

nano

stren

nano

cont

toug

At l

prop

beca

sugg

toug

stre

Add

poly

stif

toug

wit

ave

tha

enhancement provided by nanoclay reinforcement and hence only partial recovery of the degraded property was possible.

4.4.4 Impact strength

The relative comparison of toughness for the various bio-based polymer nanocomposites in this study was performed by notched Izod impact tests. The impact strength test results are shown inFigure 4-10. It can be observed that toughness of the nanocomposites increased with increasing EML content and decreased with increasing clay content. Research has shown that the addition of nanoclay inclusions can enhance the toughness of nanocomposites, but it depends on the morphology of the clay platelets [4-28]. At low nanoclay contents well-exfoliated clay morphology leads to increased toughness properties; while at higher loading partially exfoliated and interacted clay morphologies have better toughness performance [4-28].

The overall trend considering only the average values of the impact strengths suggests that the addition of bio-resin increased the impact strength, and thereby the toughness, of the resulting polymer systems. It was observed that the average Izod impact strength values increased in the range of 2 - 10% for EML contents of 10 - 30%. Additionally, there seems to be little improvement in impact strengths on bio-based polymers with 20 and 30% EML contents. The addition of nanoclay seems to increase the stiffness and reduce the toughness (impact strength) of the polymer nancomposites. For virgin UPE (no EML), the average impact strengths seem to reduce by approximately 5% with addition of nanoclay (both 2.5 and 5.0 wt%). In general, it was expected that the average impact strength values of nanocomposites with 5.0 wt.% nanoclay would be lower than those with 2.5 wt.% loading, since the increase in nanoclay content generally found to reduces toughness. Nevertheless, the average impact strength values of the 2.5 and 5.0 wt.% bio-based polymer/clay nanocomposites were reasonably similar. This could be due to the nanoclay morphology. Since a similar processing technique (equal sonication energy) was used for all clay contents, increased clay concentration (in this case 5 wt.%) would result in more intercalated particles. It is commonly accepted that intercalated particles increase toughness [4-28]. As a result, the impact strength lost due to the increased clay content seems to be balanced by the enhancement due to the presence of intercalated galleries. Such a balance may not occur for all clay contents, but seems to coincide for the processing technique used in this study and for the specific nanoclay loading cases considered. Overall, the average impact strength of nanoclay-reinforced bio-based polymer systems was 4 and 2% lower than that of the baseline UPE for 10 and 20% EML content, respectively. The average impact strength of nanoclay reinforced bio-based polymers containing 30% EML was lower than its counterparts with 10 and 20% EML contents. A reason behind this result could be the processing method. Polymer systems with high bio-resin content have a relatively lower amount of UPE and higher clay content. This requires higher amount of solvent for processing, leading to prolonged exposure to heat for solvent removal. This may finally cause thermal degradation of the polymer and thus a decrease in strength. The improvement in average impact strength values due to addition of 20% EML in UPE was around 10% while addition of 5 wt.% clay in neat UPE reduced the average impact strength values by 5%. Thus, the combination of 20% EML and 5 wt.% nanoclay seems to provide a synergistic stiffness-toughness balance in the performance of the bio-based polymer nanocomposite.

4.4.5 Nanoclay dispersion and morphology

Figure 4-11 shows the bright field TEM (transmission electron microscopy) micrographs of representative nanoclay bio-based reinforced polymer systems. Overall, the morphologies displayed in the images indicate excellent nanoclay dispersion with a combination of exfoliated and intercalated arrangement. As expected, nanocomposites with low nanoclay concentrations (2.5 wt.%) revealed a better degree of exfoliation (Figure 4-11a), while those with higher loading (5 wt.%) revealed an increased degree of intercalation.(Figure 4-11 d). It was also observed that the degree of intercalation seemed to increase with bio-resin content (compare Figure 4-11 a and Figure 4-11b). One of the reasons for such increased intercalation may be due to the lower amount of UPE available during the processing of bio-nanocomposites with high bio-resin contents, as bio-resin is added at the final step of process (Figure 4-1).

The roughness of the fracture surface has generally been associated to fracture properties and critical strain energy release rates. A smooth featureless fracture surface is attributed to brittle failures, and rougher fracture surfaces are attributed to tougher nanocomposites [4-29]. Thus, the effect of bio-resin and nanoclay loading on fracture toughness can be supported by studying the fracture surfaces from the tensile tests through scanning electron microscopy (SEM) imaging. This has been shown and discussed by the authors in a study of bio-based polymer/clay nancomposites using epoxidized methyl soyate (EMS) as the bio-resin [2-6]. Although that prior study used EMS instead of EML, the SEM images had similar features and are thus not repeated here. Nonetheless, the knowledge gained from that study is still relevant here. Overall, it has been shown [2-6] that fracture surfaces roughness increased with increasing bio-resin and increasing clay content. This suggests that the combination of bio-resin and clay will provide tougher composites.

Neverthe

propaga

roughne

4.5 D

unsatura

(EML,

revealed

experim

specific

strength

variatio

constr

conside

obtaine

result

proper

by the

proces

incorp

thereb

materi

proper

Nevertheless, further understanding of micro-structural parameters, such as crack propagation mechanisms and interface studies, is still required to relate fracture and toughness measures to surface morphologies.

4.5 Discussion

Experimental characterization of bio-based nanocomposites obtained from blends of unsaturated polyester (UPE, primary petro-based resin) and epoxidized methyl linseedate (EML, secondary bio-resin), and reinforced with layered silicates (Cloisite 30B®, nanoclay) revealed a wide variety of improvements in multiple properties. As expected, the experimental data revealed scatter/variations in measured parameters. These variations were specifically larger for failure-dependent parameters, such as tensile failure strains, tensile strengths and impact strengths. Detailed statistical analyses taking into account these variations should be performed to quantitatively and precisely obtain the effects of constituents, namely EMS and nanoclay. In this work, only the average values were considered and hence a qualitative effect and overall trends based on average values could be obtained. Overall, it was observed that the combination of bio-based resin and nanoclay result in synergistic behavior of constituents producing bio-based nanocomposites with properties similar or superior than the virgin UPE (0% EML, 0% nanoclay). An earlier study by the authors [2-6] could incorporate only 10% bio-resin and 1.5 wt.% nanoclay due to processing limitations. This study used an improved processing technique that enabled incorporation of high amounts of bio-resin (30% EML) and nanoclay (5 wt.%) content, thereby increasing the environmental appeal of the resulting composites. A test array of 12 material compositions allowed studying effects of individual constituents on various material properties and finding limits to the synergistic behavior offered by these materials.

45.1

EML

with E

recove

was c

recov

EML

provi

EML

addi

to be

to n

sepa

was

redu

resu

stres

in t

cons

have

4.5.1 Properties and synergistic behavior

Direct tensile tests revealed a decrease in tensile modulus due to the addition of EML, and a recovery of lost stiffness with the addition of nanoclay. For polymer systems with EML contents up to 10 wt.%, the loss of stiffness due to EML addition was not only recovered but enhanced by nanoclay addition. Significant enhancement in tensile modulus was observed with nanoclay addition for resin systems with 20% EML. However, full recovery of the losses from EML addition was not possible. Finally, the detrimental effect of EML on stiffness properties at 30% EML contents was higher than the enhancement provided by nanoclay and hence limited improvement was observed at this high level of EML content.

The ultimate tensile strength (UTS) results revealed a reduction in UTS due to addition of both EML and nanoclay. The reduction in UTS due to EML addition was found to be minimal for EML contents up to 10 wt.%, as the UTS results were found to be similar to neat UPE counterparts. This may be due to good crosslink density and absence of phase separation between UPE and EML. For EML contents higher than 10% a reduction in UTS was observed with increasing EML content. Additionally, nanoclay inclusions were found to reduce the UTS. Nanoclay addition improves the stiffness but also the brittleness of the resulting nanocomposites, thereby reducing toughness. The authors attribute this to the stress concentrations created by the stiff nanoclay sheets in the brittle polymer matrix, which in turn leads to lower tensile strength and lower ductility. While there is no general consensus on this point of view, computational studies by a parallel effort to this work [4-30] have shown evidence to this mechanism.

The ductility (tensile failure strains) and toughness of nanoclay reinforced bio-based composites increased with addition of bio-resin and reduced with increasing nanoclay content. This increase in ductility and toughness is due to the reduction in cross-link density in bio-based polymer, leading to increased plastic deformations [2-7]. Results of tensile strengths and failure strains showed a large variation. This may be due to several factors, including processing issues such as the effect of residual acetone, EML-UPE phase interaction, nanoclay-matrix interaction, etc. Nonetheless, it was observed that the increase in brittleness due to nanoclay inclusions could be balanced by the increase in ductility due to EML addition. Stiffness and toughness are opposing performance parameters and a proper balance is required for an efficient composite. The combination of bio-resin and nanoclay provides a synergistic effect producing bio-based nanocomposites with good stiffness-toughness balance. The advantage of hybrid combinations (UPE + EML + nanoclay) is not limited to mechanical performance, as similar enhancements were observed in thermal and moisture properties.

The thermal and barrier properties of the polymer systems in the study showed trends similar to the tensile elastic modulus results. The addition of EML increased the moisture diffusivity of the resulting bio-based composite. However, results indicate that the adverse effects of EML blends on moisture absorption can be recovered through the enhanced barrier properties provided by the nanoclay inclusions in bio-based polymer systems with up to 20% EML content. Similarly, a reduction in thermal properties with the addition of EML was observed, by considering increased CTE values and a decrease in T_g In this case, the thermal property lost (represented by an increase in CTE) due to the addition of EML was partially recovered by the nanoclay loading. Similarly, with respect to glass transition temperature, the degraded thermal property (indicated by a reduction in T_g)

due to blending of 30% EML was essentially recovered (~2% lower relative to the baseline UPE) by the addition of 5.0 wt.% nanoclay. While the thermal properties (specifically CTE) of bio-based polymers where only partially recovered with nanoclay reinforcement; moisture diffusion properties showed complete recovery for EML contents up to 20%. This could be explained by considering the physical aspects of the transient phenomena. In the diffusion process the clay platelets are impervious barriers to permeant molecules, thereby forcing a tortuous diffusion path that improves moisture barrier properties. Use of a similar analogy to CTE suggests that the expansion of the polymer due to heat is higher than restraining action provided by the nanoclay, which results in the nanoclay platelets moving along with the polymer under temperature expansion. Thus, although the nanoclay platelets provide resistance to thermal-induced strains, the effect is not as pronounced as its role in curtailing moisture diffusion. Hence only partial recovery in CTE was possible for the bio-based polymers.

4.5.2 Performance limits and optimized material design

The test matrix allowed studying the effect of EML and nanoclay on the resulting properties for EML and nanoclay contents up to 30 and 5 wt.%, respectively. Optimal material combination(s) that result in a balance of multiple properties, along with ease in processing were thus identified. In general, nanoclay reinforcement had little or no effect on bio-based polymers with 30% EML content. This suggests that the detrimental effects of EML blending were beyond the recovery offered by the nanoclay. Complete recovery by nanoclay reinforcement was possible in most properties for bio-based polymers with EML contents up to 10%. Similarly, partial recovery of most properties was possible bio-based polymers with EML contents of 20%. It should be noted that aforementioned comments are made in a general sense. For instance, moisture diffusivity was fully recovered in 20% EML nanocomposites reinforced with 5 wt.% clay. Yet such recovery was not possible for other properties. Overall, bio-based nanocomposites with up to 20% EML content and reinforced with 2.5% clay (90/10/2.5 and 80/20/2.5) were identified as optimized material compositions as they show promise in their processing ease and balanced properties.

Overall, results from the experimental characterization of UPE/EML/clay nanocomposites revealed synergistic behavior of constituents with improvements in multiple properties; wherein the decrease in some properties due to the addition of bio-resin or clay was completely or partially recovered by the synergistic effect of the hybrid material system. The effect of EML or nanoclay on the resulting thermo-mechanical properties was found to compliment the other, such that the detrimental effect on performance due an individual constituent was overcome by the enhancement provided by the other. Hence, the hypothesis of this work to develop eco-friendly bio-based nanocomposites by recovering the properties lost due to bio-resin addition by nanoclay inclusions was found to be feasible, efficient and promising.

4.6 Conclusions

Results from this study indicate that synergistic behavior of material constituents can be used to produce novel bio-based nanocomposites with properties similar or better than the virgin base petroleum-based polymer. In this work, blends of unsaturated polyester (UPE, petro-resin) and epoxidized methyl linseedate (EML, bio-resin) were reinforced with nanoclay inclusions. Improved processing enabled incorporation of up to 5 wt.% nanoclay and 30% EML in virgin UPE, thereby considerably improving the environmental appeal of the nanocomposite. Detailed experimental characterization and the effect of material constituent concentrations on the resulting properties were studied. Material combinations that produced overall balanced or enhanced properties, including proper stiffness-toughness balance, were identified. The degradation of thermo-mechanical properties (e.g., stiffness, thermal, diffusion) due to addition of EML were completely and partially recovered for EML contents of 10 and 20%, respectively; indicating excellent synergistic behavior of the constituents. However, such synergy was not observed for bio-based nanocomposites with 30% EML content, as they showed little or no improvement in most properties due to nanoclay reinforcement. This indicates that the adverse effects of EML were beyond the enhancements offered by nanoclay reinforcement. Including ease of processing along with the resulting balanced or enhanced properties, bio-based polymers with EML contents of 10 and 20% reinforced with 2.5 wt.% nanoclay were identified as optimal designs. The synergistic behavior of the showcased bio-based polymer nanocomposites shows promise for optimized high-performance materials with an environmentally conscious appeal.

4.7 Tables and Figures

Table 4-1. Experimental matrix showing specimen identification numbers and variation in clay and EMS contents

Clay Content (wt.%)	Amount of EML replacing UPE in UPE-EML blend. (as % of UPE)			
	0	10	20	30
0.0	1	2	3	4
2.5	5	6	7	8
5.0	9	10	11	12

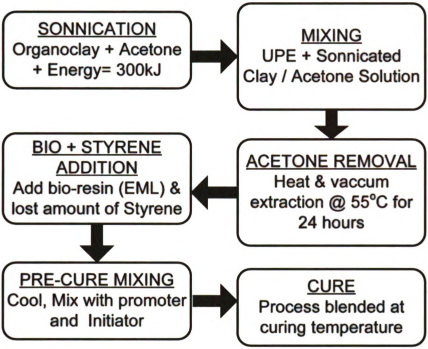

Figure 4-1. Processing of nanoclay reinforced bio-based (UPE/EML) resins.

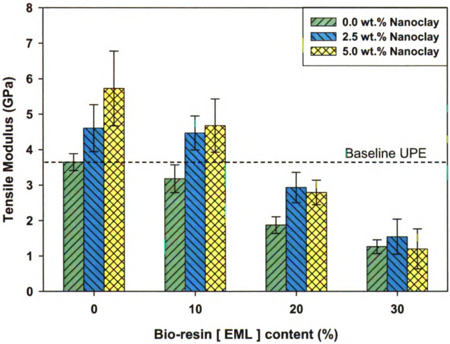

Figure 4-2. Experimental tensile modulus of bio-based polymer systems with varying nanoclay content.

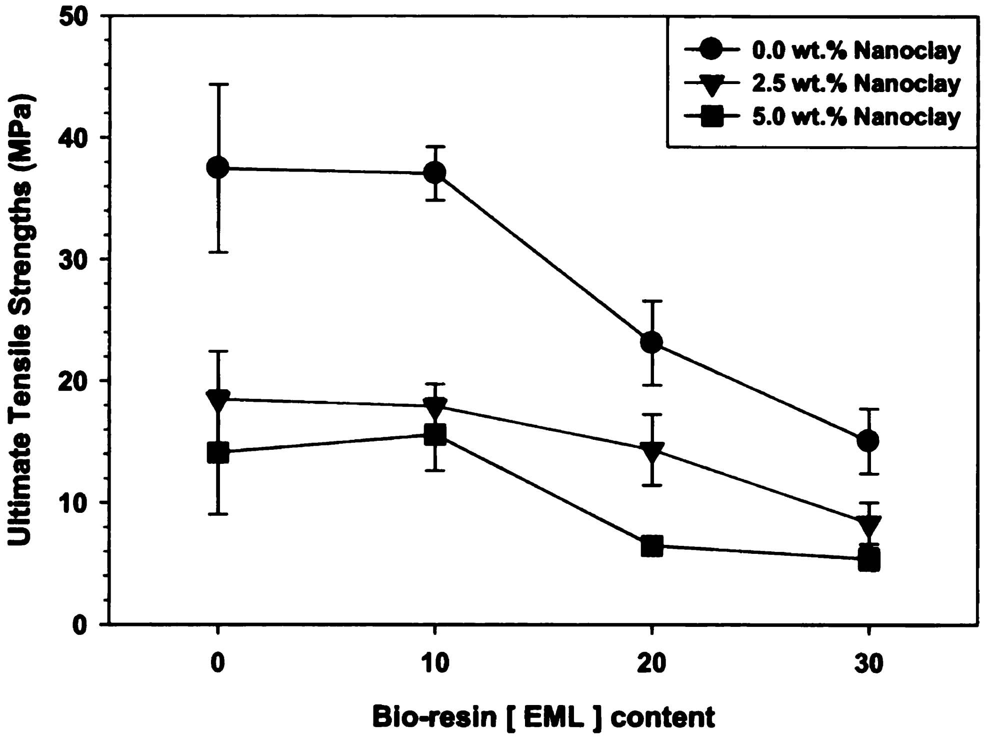

Figure 4-3. Experimental ultimate tensile stresses for various bio-based polymer/clay nanocomposites.

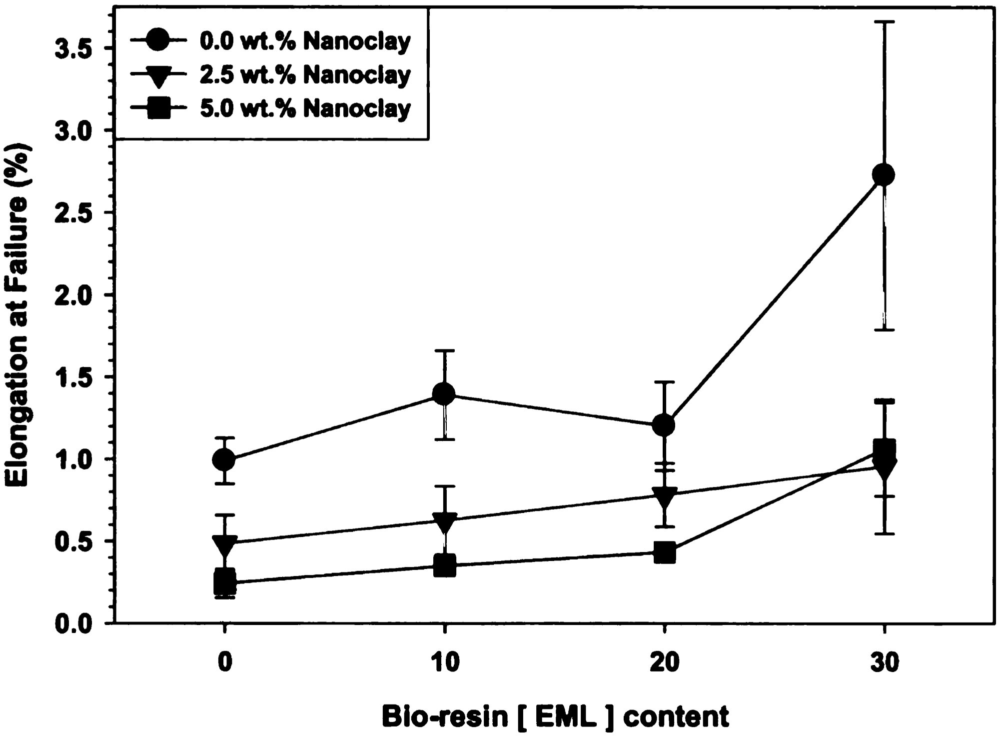

Figure 4-4. Experimental tensile test elongations at failure for various bio-based polymer/clay composites.

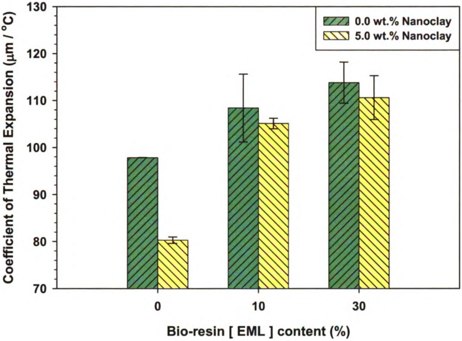

Figure 4-5. Variation of CTE below T_g with varying bio-resin (EML) and nanoclay content.

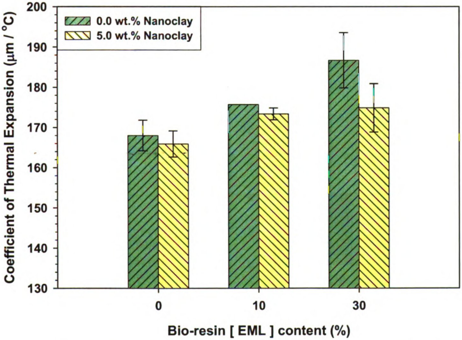

Figure 4-6. Variation of CTE above T_g with varying bio-resin (EML) and nanoclay content.

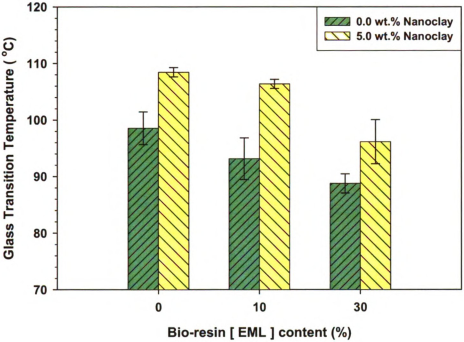

Figure 4-7. Variation of glass transition temperature (T_g) with varying EML and nanoclay content.

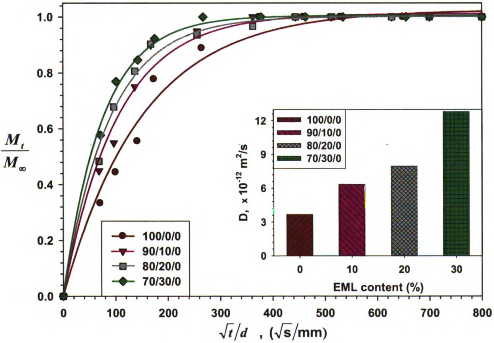

Figure 4-8. Moisture diffusivity of neat resins (no clay).

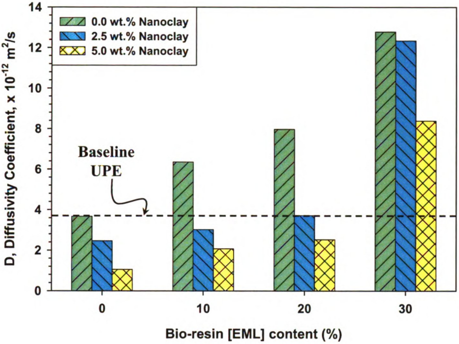

Figure 4-9. Experimental diffusivity coefficients for all bio-based polymer/clay nanocomposites in study.

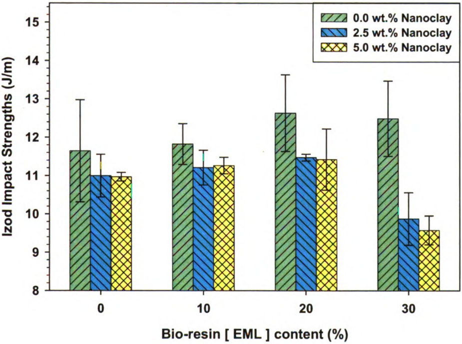

Figure 4-10. Variation of Izod Impact strength with varying bio-resin (EML) and nanoclay concentration.

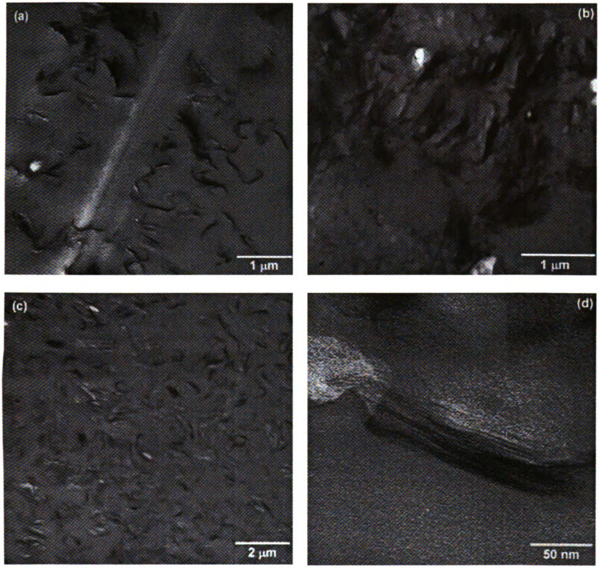

Figure 4-11. TEM micrographs showing degree of dispersion and morphology: a) 100/0/2.5-well dispersed, partially exfoliated and intercalated (scale = 1μm), b)70/30/2.5 – well dispersed, but higher degree of intercalation relative to 100/0/2.5 (scale = 1μm), c) 100/0/5 – Well dispersed, partially exfoliated and intercalated (scale = 2μm), and d) 100/0/5.0 – high magnification of an intercalated gallery (scale = 50 nm).

4.8 References

[4-1]. Uyama H, Kuwabara M, Tsujimoto T, Nakano M, Usuki A, Kobayashi S. Green nanocomposites from renewable resources: Plant oil-clay hybrid materials. Chem Mater 2003; 15:2492-2494.

[4-2]. Mohanty AK, Misra M, Hinrichsen G. Biofibers, Biodegradable polymers and biocomposites: an overview. Macromol Mater Eng 2000; 276/277:1-24.

[4-3]. Burgueño R, Quagliata MJ, Mohanty AK, Mehta GM, Drzal LT, Misra M. Load bearing natural fiber composite cellular beams and panels. Composites Part A 2004; 35:645-656.

[4-4]. Nickel J, Riedel U. Activities in biocomposites. Mater Today 2003; 6:44-48.

[4-5]. Miyagawa H, Mohanty AK, Burgueño R, Drzal LT, Misra M. Novel bio-based resins from blends of functionalized soyabean oil and unsaturated polyester resin. J Polym Sci, Part B: Polym Phys 2007; 45:698-704.

[4-6]. Haq M, Burgueño R, Mohanty AK, Misra M. Bio-based unsaturated polyester/layered silicate nanocomposites: characterization and thermo-physical properties. Composites Part A 2009; 40:540-547.

[4-7]. Ratna D. Mechanical properties and morphology of epoxidized soyabean oil-modified epoxy resin. Polym Int 2001; 50:179-184.

[4-8]. Pinnavaia TJ, Beall GW. Polymer-Clay Nanocomposites, John Wiley & Sons, Ltd., 2001.

[4-9]. Liu Z, Erhan SZ, Xu J. Preparation, characterization and mechanical properties of epoxidized soybean oil/clay nanocomposites. Polymer 2005; 46:10119-10127.

[4-10]. Song B, Chen W, Liu Z, Erhan S. Compressive properties of epoxidized soybean oil/clay nanocomposites. Int J Plast 2006; 22:1549-1568.

[4-11]. Lu B, Larock RC. Bio-Based nanocomposites from corn oil and functionalized organoclay prepared by cationic polymerization. Macromol Mater Eng 2007; 292:863-872.

[4-12]. Alexandre M, Dubois P. Polymer-layered silicate nancomposites: preparation, properties and uses of a new class of materials. Mater Sci Eng R 2000; 28:1-63.

[4-13]. Le Baron PC, Wang Z, Pinnavaia, TJ. Polymer – layered silicate nanocomposites: an overview. Appl Clay Sci 1999; 15:11-29.

[4-14]. Hussain F, Hojjati M, Okamoto M, Gorga RE. Polymer-matrix Nanocomposites, Processing, Manufacturing and Application: An Overview. J Comp Mats 2006; 17: 1511-1575.

[4-15]

[4-16]

[4-17]

[4-18]

[4-19]

[4-20]

[4-21]

[4-22

[4-23

[4-24

[4-25

[4-2

[4-2

[4-15]. Miyagawa H, Mohanty AK, Burgueño R, Drzal LT, Misra M. Characterization and thermophysical properties of unsaturated polyester-layered silicate nanocomposites. J Nanosci Nanotechnol 2006; 6:464-471.

[4-16]. Bakar M, Djaider F. Effect of plasticizers content on the mechanical properties of unsaturated polyester resin. J Thermoplast Compos Mater 2007; 20:53-64.

[4-17]. Miyagawa H, Mohanty AK, Burgueño R, Drzal LT, Misra M. Development of biobased unsaturated polyester containing functionalized vegetable oils. Ind Eng Chem Res. 2006; 45:1014-1018.

[4-18]. Mohanty AK, Miyagawa H, Burgueño R, Misra M. Biobased nanocomposites from organoclay and blends of unsaturated polyester and functionalized vegetable oil. ANTEC, Conference Proceedings. 2005; 4: 52-56.

[4-19]. Ratna D, Banthia AK. Epoxidized soybean oil toughened epoxy adhesive. J Adhes Sci Technol 2000; 14:15-25.

[4-20]. Miyagawa H, Mohanty A, Misra M, Drzal LT. Thermo-physical and impact properties of epoxy containing epoxidized linseed oil, 1: Anhydride cured epoxy. Macromol Mater Eng 2004; 289:629-635.

[4-21]. Miyagawa H, Mohanty A, Misra M, Drzal LT. Thermo-physical and impact properties of epoxy containing epoxidized linseed oil, 2: Amine cured epoxy. Macromol Mater Eng 2004; 289:636-641.

[4-22]. Haq M, Burgueño R, Mohanty AK, Misra M. Hybrid bio-based composites from blends of unsaturated polyester and soybean oil reinforced with nanoclay and natural fibers. Compos Sci Technol 2008; 68(15-16):3344-3351.

[4-23]. Shabeer A, Chandrashekhara K, Schuman T, Phan N, Nguyen T. Mechanical, thermal and flammability properties of pultruded soy -based nanocomposites. SAMPE, Conference Proceedings. 2007; 52:71/1-71/12.

[4-24]. Shabeer A, Sundaraman S, Chandrashekhara K, Dharani LR. Physicochemical properties and fracture behavior of soy-based resin. J Appl Polym Sci 2007; 105(2):656-663.

[4-25]. Haq M, Burgueño R, Mohanty AK, Misra M. Processing Techniques for Bio-based Unsaturated-Polyester/Clay Nanocomposites: Tensile Properties, Efficiency, and Limits. Composites – Part A 2009; 40:394-403.

[4-26]. Vlasveld DPN, Groenewold J, Bersee HEN, Picken SJ. Moisture absorption in polyamide-6 silicate nanocomposites and its influence on mechanical properties. Polymer 2005; 46:12567-12576.

[4-27]. Pritchard, G., Reinforced Plastics Durability. CRC Press, FL, USA. 1999.

[4-28]. Nair SV, Goettler LA, Lysek, B.A. Toughness of nanoscale and multiscale polyamide -6,6 composites. Polym Eng Sci. 2002; 42:1872-1882.

[4-29]. Wang L, Wang K, Chen L, Zhang Y, He C. Preparation, morphology and thermal/mechanical properties of epoxy/clay nanoclay composite. Composites Part A. 2006; 37:1890-1896.

[4-30]. Haq M, Burgueño R. Modeling and simulation of bio-based polymer/clay nanocomposites through a multi-level FE approach. In: Proceedings of Sixth International conference on Computation of Shell & Spatial Structures. New York, May, 2008. SessionT-2-E.

Chap

5.1

Indu

while

unsat

comp

with

barri

syne

origi

impr

thus

and

5.2

man

or n

natu

envi

---

[1] Ha
Usa
and

Chapter 5. Multiscale Hybrid Biocomposites: I - HF / UPE / EMS [1]

5.1 *Abstract*

Hybrid bio-based composites that exploit the synergy between natural fibers (industrial hemp) in a nano-reinforced bio-based polymer can lead to improved properties while maintaining environmental appeal. Bio-based resins obtained by partial substitution of unsaturated polyester (UPE) with epoxidized soybean oil (EMS) increase toughness but compromise stiffness and hygro-thermal properties. Reinforcement of the bio-based resin with nanoclays permits to retain stiffness without sacrificing toughness, while also improving barrier and thermal properties. Characterization of different hybrid composites verified this synergistic behavior in which systems with 10 % EMS and 1.5 wt. % nanoclay retained the original stiffness, strain to failure, and hygrothermal properties of the original resin while improving toughness. Optimum designs that maximize the synergy of the constituents are thus possible and the presented results provide an initial benchmark to identify such balance, and thus increase the potential applications of bio-based composites.

5.2 *Introduction*

Environmental concerns related to the use of synthetic, or petroleum-based, polymer matrix composites has propelled the development of composite materials based on natural or renewable sources [5-1][5-2]. Biocomposites, composed of natural fibers in synthetic or natural polymer matrices have recently gained much attention due to their low cost, environmental friendliness, and their potential to compete with synthetic composites [5-3]-

---

[1] Haq, M., Burgueño, R., Mohanty, A.K., and Misra, M., "Hybrid Bio-based Composites from blends of Unsaturated Polyester and Soy Bean Oil Reinforced with Nanoclay and Natural Fibers," Composites Science and Technology. 2008; 68:3344-3351

[5-7]. Nonetheless, the use of bio-based composites has been limited due to their lower mechanical and thermo-physical properties compared to synthetic composites and conventional structural materials [5-6][5-7].

A promising compromise between environmental friendliness and performance are bio-based resins, or bio-blends, obtained by replacing part of a petroleum-based resin with natural bio-resin. In addition to higher natural content, bio-based resins improve toughness of the resulting resin blend [5-8][5-9]. However, this increase in toughness compromises stiffness, barrier and thermal properties [5-8][5-9]. Stiffness and toughness are opposing performance parameters and a proper balance is required for an efficient composite. One way to attain this balance is the addition of layered silicates, or nanoclays.

Polymers reinforced with nanoclays have been shown to exhibit enhancements in mechanical, thermal and barrier properties at low concentrations [5-10]. Nanoclays consist of stacks of sheet like silica platelets with thickness of ~1 nm and extremely large surface areas and aspect ratios. The enhancement of mechanical and barrier properties in polymers with addition of small concentrations of nanoclays is well reported, and a good review on polymer clay hybrid nanocomposites is provided by Le Baron et al. [5-10]. The reinforcement of bio-based polymers with nanoclays has been shown to recover the decrease in stiffness, thermal and barrier properties due to the addition of bio-resin and can lead to improved stiffness-toughness balance [5-11][5-12]. Thus, the synergy between nanoclay reinforcement in a bio-blend produces a polymer nanocomposite with similar or enhanced properties than the virgin polymer and holds great promise for use in wide applications.

The true value of layered silicate nanocomposites is, however, not solely the enhancement of the neat resin but rather the value-added properties it provides to a fiber-reinforced composite. Thus, in a biocomposite, natural fibers must remain as the main reinfo

and k

modu

or ev

fibers

nanoc

while

barrie

fiber

comp

to en

glass

stren

24]

mult

micr

epox

prop

carb

incre

bee

bio

no

reinforcement for stiffness and strength. Natural fibers such as flax, industrial hemp, jute and kenaf have been found to have specific strengths comparable to E-glass; and the elastic modulus and specific modulus of natural fiber composites has been found to be comparable or even superior to E-glass composites [5-1]. The incorporation of nanoclays and natural fibers in resin systems thus provides reinforcements to resin systems at two scales. The nanoclay enhances the bio-based polymer system in stiffness and hygrothermal properties, while the natural fibers provide the main stiffness and strength. In addition, the enhanced barrier properties of the nano-reinforced resin retard moisture from reaching the natural fibers, thereby providing a synergetic effect between scales for an efficient bio-based composite. Similar multiscale reinforcement concepts have been studied for synthetic fibers to enhance mechanical and electrical properties [5-13]-[5-16]. Tsai and Wu [5-13] reinforced glass/epoxy composites with nanoclay and found a reduction in longitudinal tensile strengths and mode I fracture toughness with increasing nanoclay content. Kinloch et al. [5-14] report improvement in the interlaminar toughness of a carbon-fiber composite with multiphase toughened epoxy matrix. The epoxy matrix was reinforced with nanosilica and microsized rubber particles. Kinloch et al. [5-15] report that this multiphase toughened epoxy matrix provides increase in toughness without significant loss in modulus and thermal properties. Gojny et al. [5-16] reinforced the epoxy matrix of glass fiber composites with carbon black and carbon nanotubes and report improvements in electrical conductivity and interlaminar shear strength. Thus, while different concepts of multiscale reinforcement have been studied for synthetic composites, the study of multiscale/multiphase reinforcements on bio-based composites is limited.

This work provides an overview of a study aimed at developing and characterizing novel multiscale hybrid biocomposites from bio-based polymer blends of unsaturated polyester (UPE) and epoxidized methyl soyate (EMS) reinforced with nanoclay and chopped industrial (unprocessed) hemp. An optimum or synergistic balance of the various constituents in the resulting hybrid biocomposites is essential to achieve increased environmental friendliness and proper stiffness-toughness balance, along with the other tailorable features that they offer, such as enhanced and/or controlled moisture and thermal properties. This work aims at demonstrating that this synergistic balance can be achieved. Material systems that varied the bio-resin (EMS) content in UPE and the concentration of nanoclay while maintaining a constant amount of natural fibers were fabricated by compression molding. Mechanical and thermophysical properties were evaluated through standard tests. The degree of dispersion and exfoliation of nanoclay in the resins systems was characterized using transmission electron microscopy and the features of fracture surfaces were characterized using scanning electron microscopy. The results provide a benchmark to identify the synergistic balance of the constituents such that efficient, novel and multifunctional hybrid biocomposites can be designed.

5.3 Experimental methods

The developed hybrid bio-based composites were compared in terms of basic thermo-physical properties and qualitative material distribution features. Details on materials, processing, parameters studied and testing are provided in this section.

5.3.1 Materials

Industrial unprocessed raw hemp (Stemergy Inc, London, Ontario, Canada) was used as natural fiber reinforcement. The fibers were hand chopped to an average length of 25 mm. The primary component of the resin blend was ortho unsaturated polyester resin (*UPE*, Polylite® 32570-00, Reichhold Inc., NC), which contains 33.5 wt. % styrene. The secondary component that replaced parts of the UPE was a bio-based modifier: epoxidized methyl soyate (*EMS*, Vikoflex® 7010, Arkema Inc, PA). EMS is a mixture of methyl ester of fatty acid compositions that construct soybean oil. The detailed composition is 5-11% methyl epoxy linolenate, 43-56% methyl epoxy linoleate, 24-26% methyl epoxy oleate, and 7-11% methyl epoxy palmitate. The nanoclay used to reinforce the resin system was Cloisite 30B® (Southern Clay Products, Inc. TX). The nanoclay was chosen by trial and error to be compatible with EMS and no detailed study on surfaces and interfaces of the constituents was performed. Compatibility is assumed to be due to the carbonyl groups of UPE/EMS and free hydroxyl group of organic modifier part (methyl tallow bis-2-hydroxyethyl quaternary ammonium) in the organoclay Cloisite 30B®.The resin blend was processed with cobalt naphthenate (Sigma Aldrich, MO) as a promoter and 2-butanone peroxide (Sigma Aldrich) as an initiator. A constant mixing ratio of 0.03 parts promoter and 1.50 parts initiator to 100 parts of resin system was used for all resin systems. Table 1 provides the nomenclature, composition, concentration of constituents and densities of the five biocomposite systems studied. Biocomposite A, manufactured of only virgin UPE (no EMS and no nanoclay) is considered the benchmark biocomposite and hence, the performance of all biocomposites is compared with this benchmark composite.

5.3.2 Nanocomposite processing

The resin system (UPE +EMS +nanoclay) had varying amounts of nanoclay and EMS content that replaced UPE. For nanoclay reinforced resin systems, the processing technique is similar to that reported in references [5-11][5-12]. Nanoclay was sonicated in acetone using a solution concentration of approximately 50 liters of acetone to 1 kilogram of clay, while it was constantly stirred by a magnetic stirrer. The amount of energy spent on sonication was maintained at 30 kJ for all resin systems. The UPE and EMS were then added to the acetone-clay solution and mixed with a magnetic stirrer on a hot plate for 3 to 4 hours to remove the majority of acetone. The remaining acetone was removed by vacuum extraction at approximately 55 °C for 12-24 hours. During the acetone removal process, along with acetone, the styrene present in resin system was also removed. The lost styrene was thus added after the acetone removal process. During vacuum extraction of the acetone, and at higher concentrations of EMS and clay, processing issues such as phase separation in UPE/EMS blend and cross linking were observed. The above mentioned problems were not observed at nanoclay contents of 1.5 wt. % or less and bio-blends of 10% EMS or less. Hence, nanoclay reinforced resins with 20 % EMS was not feasible in this study. Studies by our group on bio-based nanocomposite processing have shown that the aforementioned issues can be overcome by modifications in the above process [5-17].

The styrene content in the UPE used in this study was 33.5 wt. %. The replacement of parts of UPE with bio-resins reduced the overall styrene content of the resulting resin blend. It was suspected that premature curing of the resin blend during acetone removal was due to the reduced styrene content. Hence, styrene was added to the bio-based blend to maintain the overall styrene content at 33.5 wt. % for the resin system. The processed polymer nanocomposite (UPE + EMS + nanoclay) was used as the matrix for natural fibers in hybrid biocomposite material systems.

5.3.3 Manufacturing of hybrid biocomposite plates

Flat biocomposite plates for five material systems described in Table 5-1 were manufactured using compression molding. Before use, the fibers were dried in vacuum oven at 80 °C and 100 kPa of pressure for 12 hours. The nano-reinforced resin system (UPE +

EM

imp

imp

fre

cir

wit

'C

5.4

sar

stre

Dy

coe

me

fro

the

tak

wa

cur

env

ap

Th

Mo

EMS + nanoclay) was mixed with the promoter and initiator. The fibers were then impregnated with the resin system by hand until the material was consistent. The impregnated fibers were then placed in a frame mold. Care was taken to evenly distribute the fiber material in the mold to ensure a uniform sample, since natural fibers have a tendency to clump and tangle together. The frame mold was placed between two steel plates covered with Teflon paper. The sample was then cured in a press under 550 kPa of pressure at 100 °C for 2 hours, followed by 150 °C for 2 hours.

5.4 Testing & characterization

Testing and characterization of the hybrid bio-based composites was performed on samples taken from the compression molded plates. The tensile properties (modulus, strength and elongation at failure) were measured on six to eight samples as per ASTM D638, while impact strength was measured on five samples as per ASTM D256. The coefficient of thermal expansion was measured on two to three samples by thermo-mechanical analysis using TA instruments TMA 2940 analyzer. The specimens were heated from room temperature to 140 °C at a rate of 4 °C/minute. The strain and temperature of the samples were measured throughout the test. The coefficient of thermal expansion was taken as the linear slope of the strain-temperature curve. The glass transition temperature was obtained from the intersection of the two linear portions of the strain-temperature curve. Moisture absorption testing was performed by storing the samples in an environmental chamber at 30 °C and 90 % relative humidity. Two rectangular samples of approximate dimensions: 63.5 mm x 12.7 mm x 3.2 mm were used for each biocomposite. The weight increase of the samples was measured until steady state was reached (~50 days). Moisture absorption was evaluated as the percent weight gained at steady state. The dispersion and morphology of clay inclusions in the resin systems was assessed with transmission electron microscopy (TEM). A JEOL 100CX TEM with LaB_6 filament and 120 kV acceleration was used to obtain bright field images from sections approximately 70 nm thick. Tensile failure surfaces of biocomposites were pre-coated with a thin gold film and observed in a JEOL 6400 field emission scanning electron microscope (SEM) at 10 kV acceleration voltage.

5.5 Results

The addition of EMS or nanoclay may have a beneficial or detrimental effect depending on the parameter studied. All results in the following sections are thus relative to benchmark biocomposite A, consisting of 100 % UPE (0 % EMS and 0 % nanoclay).

5.5.1 Tensile modulus and ultimate tensile strength

Results for tensile modulus and strength are provided in Figure 5-1. The overall trend considering only the average values suggests that the addition of bio-resin in UPE reduced tensile modulus and ultimate tensile strength of reslting biocomposites, which is attributed to the low stiffness of the bio-resin. The average values of tensile modulus for biocomposites B (10 % EMS) and C (20 % EMS), were reduced by approximately 5 % and 40 %, respectively. Similarly, for biocomposites B and C, the average tensile strengths values decreased around 5 % and 20 %, respectively. Tensile modulus is primarily dependent on the micro-scale natural fiber reinforcement and hence a major increase in tensile modulus due to 1.5 wt. % of nanoclay was not expected. Nevertheless, biocomposite D, which had 1.5 wt. % nanoclay in UPE (no EMS) showed an increase in the range of 5% in the average tensile modulus. A similar increase for biocomposite materials with 10 % EMS (B, E) was expected. Nevertheless, it seems that the reduction in tensile modulus due to addition of 10 % EMS was more than the recovery provided by adding 1.5 wt. % nanoclay. Regarding strength, the addition of nanoclay in the resin blends showed a decrease in the average values of ultimate tensile strength in the range of 20 % and 25 % for biocomposites D and E, respectively. This decrease may be attributed to the embrittlement of the resin system. It can be seen from Figure 5-1 that there is large variance in test results. The variance could be due to many reasons including processing, presence of voids and impurities, improper fiber distribution, variation in fiber lengths, distribution of nanoclay etc. Detailed statistical analyses taking into account these variations should be performed to quantitatively and precisely obtain the effects of constituents, namely EMS and nanoclay. In this work, only the average values were considered and hence a qualitative effect and overall trends based on average values could be obtained. Overall, the addition of bio-resin reduces the tensile modulus and strength of the composite. The addition of nanoclay leads to a recovery in modulus but reduces the tensile strength.

5.5.2 Elongation at failure and notched Izod impact strengths

Figure 5-2 summarizes the results of elongations at failure from tensile tests and notched Izod impact strengths. The overall trend considering only the average values suggests that the addition of EMS increased the toughness of the biocomposites, which was observed experimentally as increase in average values of elongations at failure and impact strengths. For resin blends with no nanoclay inclusions an average increase in ultimate strain values of approximately 30 % and 65 % was observed for biocomposites B (10 % EMS) and C (20 % EMS), respectively. Similarly, the average impact strength values increased by approximately 10 % and 15 % for biocomposites B and C, respectively. The addition of nanoclay seems to make the resin blends more brittle and hence reduces the ductility, con

uti

20

the

10

bio

uti

sug

an

co

5.5

m

th

w

E

re

ap

(9

d

T

n

correspondingly the elongations at failure and impact strengths. The average values of ultimate strains and impact strengths showed an approximate reduction of around 25 and 20% in ultimate tensile strains and impact strengths, respectively for biocomposite D due to the addition of 1.5 wt. % clay in neat UPE. Biocomposite E, which has a combination of 10% EMS and 1.5 wt. % nanoclay showed a synergistic effect. The overall performance of biocomposite E was very similar to baseline composite A, with the average values of ultimate strains and the impact strengths within 5% of those of baseline bicomposite A. This suggests that the combination of bio-resin and nanoclay can balance individual deficiencies and the resulting hybrid composites will have the beneficial effects of each of the constituents resulting in good stiffness-toughness balance.

5.5.3 Thermal properties and moisture absorption

Figure 5-3 summarizes the results of coefficient of thermal expansion (*CTE*) and moisture absorption (*MA*) tests. The overall trend considering the average values suggests that both *CTE* and *MA* increased with increasing bio-resin (EMS) content and decreased with the addition of nanoclay. The increase in average *CTE* values due to addition of 10 % EMS (biocomposite B) and 20 % EMS (biocomposite C) was around 10 % and 25 %, respectively. The average glass transition temperature (T_g) value of virgin UPE was approximately 98 °C. The average T_g values of hybrid biocomposites D (100/0/1.5) and E (90/10/1.5) were 102 °C and 84 °C, respectively. The T_g of hybrid biocomposites was dominated by the properties of the resin system, and as such, the effect of nanoclay on the T_g of bio-based resins is reported in reference [5-12]. Similar to CTE, the increase in average moisture absorption value for biocomposite C was around 20 %. The addition of 1.5 wt. %

nanoclay reduced the average values of *MA* of biocomposite D by approximately 10 %. Biocomposite E, with 10 % EMS and 1.5 wt. % nanoclay, showed results similar to benchmark biocomposite A. Overall, it was observed that the reduction of average thermal and barrier properties due to the addition of bio-resin were recovered by addition of nanoclay.

5.5.4 Nanoclay dispersion and exfoliation.

Transmission electron microscopy (TEM) was used to observe the dispersion and morphology of nanoclay in the resin system (no fibers). Figure 5-4 shows the bright field TEM micrographs of UPE/clay nanocomposites. It was observed that the nanoclay platelets were well distributed with partially exfoliated and intercalated morphologies. Figure 5-4a shows a general view of clay platelets distributed in UPE matrix and, Figure 5-4b shows an intercalated gallery containing three to four platelets. Similar micrographs were obtained for bio-based matrices (EMS blends) as the same amount of sonication energy was spent on all resin systems. Improved nanoclay exfoliation can be achieved with increased sonication energy. Nonetheless, excessive sonication energy/time can break the clay platelets and reduce their aspect ratios, leading to inferior composite properties. A study on the effect of processing techniques, with varying sonication energies and solvents, on the resulting morphology and properties of bio-based polymer nanocomposites is reported in reference [5-17].

5.5.5 Fracture surface observations.

Scanning electron microscopy (SEM) was used to observe the features of tensile fracture surfaces and interfacial fiber-matrix. This approach has been used by others to evaluate the stiffness strength and toughness performance of biocomposites [2-4]-[2-6].

Three types of failure mechanisms have been identified in literature for natural fiber reinforced polymers: matrix failure, fiber fracture, and fiber-matrix interfacial failure [2-6]. A weak interface or improper compatibility between fiber and matrix may lead to fiber pull-out instead of fracture, and may reduce the resulting mechanical properties. In this study, combinations of these failures were observed depending on the composition of the biocomposite. Figure 5-5d shows a representative SEM micrograph corresponding to biocomposite E with 10 % EMS in UPE and 1.5 wt. % nanoclay. The encircled region shows fiber pull-out and the boxed region shows fiber fracture. It was observed that the interfacial gaps around pulled-out fibers increased with increasing bio-resin content, suggesting weaker adhesion characteristics between fiber and the bio-based matrix.

The interfacial characteristics of pullout failures were thus studied. Figure 5-5a and Figure 5-5b show that the interfacial gap increases with increasing bio-resin contents for 10 % EMS (biocomposite B) and 20 % EMS (biocomposite C), respectively. The interface gap for biocomposite E, with 10 % EMS and 1.5 wt. % clay revealed a similar interface gap as its counterpart neat resin biocomposite B, with 10 % EMS and no clay (Figure 5-5c). This would indicate that nanoclay reinforcement does not seem to alter the adhesion features between fiber and matrix. Tensile test results support the hypotheses that weaker interface leads to a more pronounced pull-out phenomenon, as reduction in tensile modulus and strength were observed with an increase of bio-resin. Fiber pull-out enables dissipation of more energy along the interface, which is consistent with higher impact strength and ductility values obtained when increasing bio-resin content.

The final study in tensile fracture morphologies was the study of the matrix surface. Figure 5-6 shows matrix morphologies in the tensile fracture surfaces of biocomposites A, B, D and E (see Table 5-1 for nomenclature). The roughness of a fracture surface has generally been associated with fracture properties and critical strain energy release rates [5-18]. Smooth featureless fracture surface is attributed to brittle failures and rougher fracture surfaces are attributed to tougher nanocomposites [5-18]. SEM micrographs for biocomposites A (Figure 5-6a) and B (Figure 5-6b), with no nanoclay, revealed fracture surfaces that were relatively smooth and featureless. The roughness of the fracture surfaces increased with increasing bio-resin and nanoclay content. For neat resins (no clay), an increase in bio-resin content resulted in increased surface roughness in the form of reduced spacing of the fractal planes. Increase in surface roughness due to addition of clay (Figure 5-6c and Figure 5-6d) was more obvious. The increase in surface roughness due to combination of bio-resin and nanoclay suggests resulting hybrid biocomposites are tougher than benchmark biocomposite A. Research has shown that changes in fracture morphologies suggest different toughening mechanism at low and high clay loading [5-18]. It is difficult to quantitatively relate the fracture surface to toughness of the composites [5-18]. This requires better understanding of micro-structural parameters, crack propagation mechanisms and interface studies to relate fracture and toughness measures to the fracture surface morphologies.

5.6 Discussion

The characterization of hybrid biocomposites made of natural fibers, petroleum based resin (UPE), bio-resin (EMS) and nanoclay inclusions (Cloisite 30B®) showed a variety of multifunctional properties. As expected, the experimental data revealed scatter/variations in measured parameters. These variations were specifically larger for failure-dependent parameters, such as tensile failure strains, tensile strengths and impact strengths. Detailed statistical analyses taking into account these variations should be performed to quantitatively and precisely obtain the effects of constituents, namely EMS and nanoclay. In this work, only the average values were considered and hence a qualitative effect and overall trends based on average values could be obtained. It was observed that the combination of layered silicates and bio-based resin systems provide biocomposites with similar or better properties than the benchmark biocomposite manufactured from natural fibers and UPE. Mechanical testing revealed a decrease in stiffness-related parameters such as tensile modulus and ultimate tensile stress, and an increase in toughness related parameters, such as ductility (elongation at failure) and impact strengths, with increasing bio-resin content. The addition of nanoclay increased stiffness but reduced toughness of the composites. The improvement in toughness of the resulting biocomposites was thus compromised with the addition of nanoclay. The advantages of combining EMS and nanoclay provides a synergistic effect that is not limited to only achieving a stiffness-toughness balance for the resulting bio-based composites, as similar enhancements were observed in barrier and thermal properties.

The addition of EMS increased moisture absorption and the coefficient of thermal expansion of the resulting biocomposite. However, results indicate that the adverse effects of bio-resin on permeability and thermal properties can be recovered with the enhancement provided by the nanoclay. The moisture absorption results also show that the biocomposite material systems absorb less moisture than the natural fibers alone. Biocomposite A (benchmark) absorbed approximately 3 % moisture, while the hemp fibers alone are reported to absorb 8 % moisture [5-7]. The matrix thus serves as a barrier, reducing the moisture absorbed by the natural fibers. In a bio-based polymer, bio-resin is more permeable than its synthetic counterpart. The incorporation of nanoclay inclusions introduces a tortuous path for moisture movement thereby enhancing barrier properties of the matrix and enabling the recovery of the negative effects from bio-resin addition.

The enhancements provided by nanoclay were more pronounced in UPE biocomposites than UPE/EMS biocomposites. This indicates that the negative effect from EMS addition was larger than the benefit provided by nanoclay and raises questions on the compatibility of EMS and nanoclay. The authors believe that the compatibility was adequate. In a parallel numerical study, material layout optimization of the three-phase system (UPE, EMS, and nanoclay) was carried out to identify their distribution by matching the numerically homogenized tensile modulus to experimental data. Results indicate that the bio-resin tends to accumulate around the nanoclay platelet, suggesting affinity between them. This deposition of the more complaint EMS around the clay platelet affects the stress transfer and hence supports the lower degree of enhancements in mechanical properties.

Transmission electron microscopy on the matrix revealed partially exfoliated and intercalated galleries. Improvements in nanocomposite processing can enable better exfoliation thereby leading to better stiffness and barrier properties [5-17]. Meanwhile, an intercalated morphology gives better toughness properties [5-17]. This suggests that a balance of exfoliation and intercalation is best suited for stiffness/toughness balance of the nanocomposite. However, since mechanical properties are governed by macro-fibers, exfoliated nanoclay morphology is preferred as it enhances barrier and thermal properties.

Scanning electron microscopy lead to interesting observations related to the toughness and the adhesion between the natural fibers and the nanoclay reinforced bio-based resin. While the effects of nanoclay and bio-resin additives on fiber adhesion are not fully understood, the interfacial properties can be improved by surface treatment of the fibers. Industrial raw (unprocessed) fibers were used in this work to characterize an initial benchmark towards a synergistic balance of the constituents. In this way, a lower performance bound for this type of hybrid bio-based composite was obtained.

Improvements in nanocomposite processing, incorporation of higher amounts of nanoclay and bio-resin along with the use of "engineered," or treated, fibers would lead to environmentally friendly composites with competitive thermo-mechanical properties.

5.7 Conclusions

Results from this study indicate that novel multiscale hybrid bio-based composites can be obtained from a combination of industrial hemp and blends of unsaturated polyester with epoxidized methyl soyate and nanoclay inclusions. The properties of the resulting biocomposites are tailorable and dictated by the amount and distribution of the constituents. Experimental characterization studies showed that the addition of bio-resin lowers mechanical parameters, such as stiffness and ultimate tensile stress, but increases toughness parameters, such as impact strengths and ductility. The addition of nanoclay enhances stiffness but seems to decrease toughness. Thus, the study shows that a proper stiffness/toughness balance can be obtained by controlling the amount of bio-resin and nanoclay content. Moreover, the multiphase hybrid biocomposites have multifunctional properties, such as improved barrier and thermal properties. Incorporation of higher concentrations of bio-resins and nanoclay along with improvements in processing will enable maximizing the multifunctional properties that the hybrid biocomposites offer. The study shows that bio-based composites with proper stiffness/toughness balance can be obtained while preserving environmental friendliness and cost effectiveness. The improved multifaceted features possible for these sustainable bio-based materials are likely to increase their appeal for use in transportation and housing structural applications.

5.8 Tables and Figures

Table 5-1. Biocomposite material identification and composition.

Specimen Identification	Composition (%)			Fiber Fractions (%)		Density (g/cc.)	
	UPE	EMS	Clay	Weight Fraction W_f	Volume Fraction V_f	Resin ρ_m	Composite ρ_c
A	100	0	0	21	18	1.177	1.257
B	90	10	0	21	17	1.161	1.234
C	80	20	0	21	17	1.157	1.157
D	100	0	1.5	22	18	1.196	1.245
E	90	10	1.5	21	17	1.178	1.201

Density of Fiber (ρ_f) = 1.48 g/cc [7].

The nomenclature is also referred as: [UPE / EMS / Clay / W_f/ V_f], For example, specimen ID "D" can be referred as [100 / 0 / 1.5 / 22 / 18].

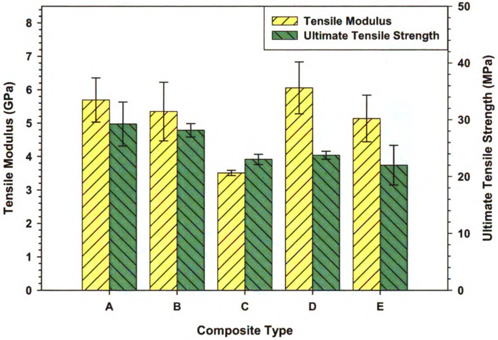

Figure 5-1. Tensile modulus and ultimate tensile strengths.

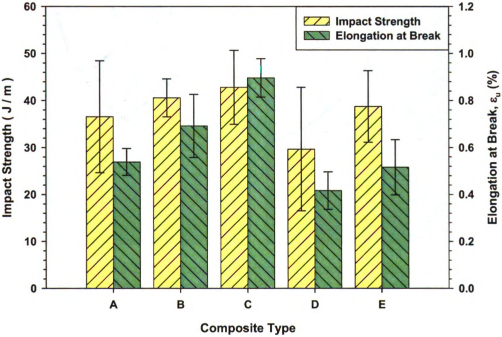

Figure 5-2. Impact strengths from notched Izod tests and tensile strains at failure.

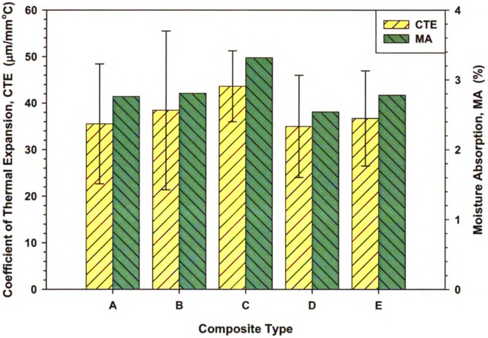

Figure 5-3. Linear coefficient of thermal expansion (CTE) and moisture absorption (MA).

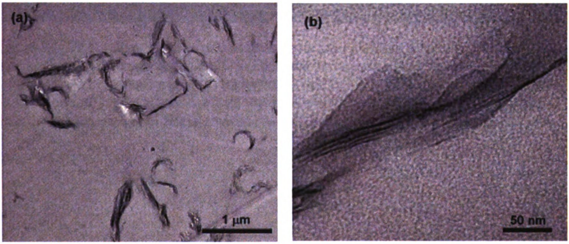

Figure 5-4. Bright-field TEM micrographs revealing homogenous dispersion with partially exfoliated and intercalated clay particles in UPE matrix. a) low magnification, scale bar = 1 µm, b) high magnification, scale bar = 50 nm, approximately 3 to 4 particles per gallery of intercalated particle

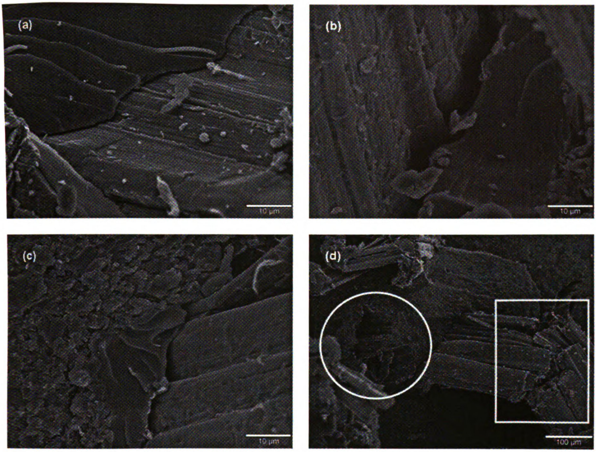

Figure 5-5. SEM micrographs of tensile fracture surfaces showing interfacial gaps between fiber and matrix. (a) biocomposite B: 10 % EMS and no nanoclay in UPE, (b) biocomposite C: 20 % EMS and no nanoclay in UPE, (c) biocomposite E: 10 % EMS and 1.5 wt. % nanoclay in UPE, and (d) representative fracture surface showing both pull-out (circled region) and fracture (boxed region) of fibers, scale bar = 100 µm. Images (a) to (c): scale bar =10 µm.

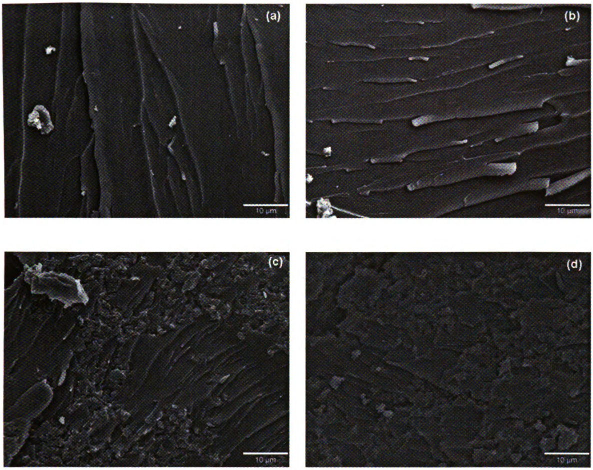

Figure 5-6. SEM micrographs showing matrix region in tensile fracture surface of biocomposites. Micrographs (a), (b), (c) and d represent biocomposites A, B, D, E, respectively. All images have a magnification scale bar of 10 µm.

5.9 References

[5-1]. Mohanty, A.K, Misra M, Hinrichsen, G. Biofibers, Biodegradable Polymers and Biocomposites: An Overview. Macromol Mater Eng 2000; 276/277:1-24.

[5-2]. Nickel J, Riedel U. Activities in biocomposites. Mater Today 2003; 6:44-48.

[5-3]. O'Donnell A, Dweib MA, Wool RP. Natural fiber composites with plant oil based resin. Compos Sci Technol 2004, 64:1135-1145.

[5-4]. Shibata M, Ozawa K, Teramoto N, Yosomiya R, Takeishi H. Biocomposites made from short abaca fiber and biodegradable polyesters. Macromol Mater Eng 2003; 288:35-43.

[5-5]. Morye SS, Wool RP. Mechanical properties of glass /flax hybrid composites based on a novel modified soyabean oil matrix material. Polym Compos 2005, 26:407-146.

[5-6]. Bodros E, Pillin I, Montrelay N, Baley C. Could biopolymers reinforced by randomly scattered flax fibers be used in structural applications. Compos Sci Technol 2007; 67:462-470.

[5-7]. Burgueño R, Quagliata, MJ, Mohanty AK, Mehta GM, Drzal LT, Misra M. Load bearing natural fiber composite cellular beams and panels. Composites: A 2004; 35:645-656.

[5-8]. Miyagawa H, Mohanty AK, Burgueño R, Drzal LT, Misra M. Novel bio-based resins from blends of functionalized soyabean oil and unsaturated polyester resin. J Polym Sci, Part B: Polym Phys 2007; 45: 698-704

[5-9]. Miyagawa H, Mohanty AK, Burgueño R, Drzal LT, Misra M. Development of bio-based unsaturated polyester containing functionalized vegetable oils. Ind Eng Chem Res 2006; 45:1014-1018.

[5-10]. Le Baron PC, Wang Z, Pinnavaia TJ, Polymer – layered silicate nanocomposites: an overview. Appl Clay Sci. 1999; 15:11-29

[5-11]. Miyagawa H, Mohanty AK, Burgueño R, Drzal LT, Misra M. Characterization and thermophysical properties of unsaturated polyester-layered silicate nanocomposites. J Nanosci Nanotech 2006; 6:464-471.

[5-12]. Haq M, Burgueño R, Mohanty AK, Misra M. Bio-based unsaturated polyester/layered silicate nanocomposites: characterization and thermo-physical properties. Composites: A, Communicated.

[5-13]. Tsai JL, Wu MD. Organoclay effect on mechanical responses of glass/epoxy nanocomposites. J Compos Mater 2008; 42:553-568.

[5-14]. Kinloch AJ, Mohammed RD, Taylor AC, Sprenger S, Egan D. The interlaminar toughness of carbon fibre reinforced plastic composites using 'hybrid-toughened' matrices. J Mater Sci 2006; 41:5043-5046.

[5-15]. Kinloch AJ, Mohammed RD, Taylor AC, Sprenger S, Egan D. The effect of silica nano particles and rubber particles on the toughness of multiphase thermosetting epoxy polymers. J Mater Sci 2005; 40:5083-5086.

[5-16]. Gojny FH, Wichmann MHG, Fiedler B, Bauhofer W, Schulte K. Influence of nano-modification on the mechanical and electrical properties of conventional fiber-reinforced polymers. Composites: A 2005; 36:1525-1535.

[5-17]. Haq M, Burgueño R, Mohanty AK, Misra M. Processing techniques for bio-based unsaturated-polyester/clay nanocomposites: tensile properties, efficiency and limits. Polymer, Communicated.

[5-18]. Wang L, Wang K, Chen L, Zhang Y, He C. Preparation, morphology and thermal/mechanical properties of epoxy/clay nanoclay composite. Composites: A 2006; 37:1890-1896.

Chapter 6. Multiscale Hybrid Biocomposites: II - HF / UPE / EML [1]

6.1 Abstract

Environmentally friendly bio-based composites with enhancements in multiple properties can be obtained by harnessing the synergy offered by hybrid constituents such as multiscale (nano- and micro- scale) reinforcement in bio-based polymers composed of blends of synthetic and natural resins. Multiscale reinforcement offers synergy of constituents at various length scales, and when combined with bio-based resins provide stiffness-toughness balance, improved thermal and barrier properties, and increased environmental appeal to the resulting composites. Bio-based composites consisting of unsaturated polyester (UPE, petroleum-based resin), epoxidized methyl linseedate (EML, bio-resin), natural fibers (industrial hemp), and nanoclay inclusions were developed. The effects of EML and nanoclay content, and optimal material compositions that maximize synergy of resulting biocomposites were studied through experimental characterization of 12 biocomposites with EML and nanoclay contents of upto 30% and 5 wt.%, respectively. Results show synergistic behavior of resulting biocomposites with the effects of bio-resin addition being complimented by nanoclay, and vice versa. Moreover, these hybrid materials are tailorable in performance and in environmental impact, and show potential for wide applications.

6.2 Introduction

Hybrid bio-based composites consisting of multiscale reinforcements, namely natural fibers and nanoclay embedded in blends of petroleum based (unsaturated polyester) and

---

[1] Haq, M., Burgueño, R., Mohanty, A.K., and Misra, M., "Multifunctional Biocomposites from Hybrids of Hemp fibers, Nanoclay, Linseed oil and Unsaturated Polyester." Draft – to be submitted to Journal of Biobased Materials and Bioenergy.

vegetable oil based resins (derivatives of vegetable oils, e.g soybean, linseed oil etc.), were found to produce composites that exhibit synergistic behavior, including stiffness-toughness balance, improvements in thermal and barrier properties, and increased environmental appeal [6-1]. Biocomposites, composed of natural fibers in synthetic or natural polymer matrices have recently gained much attention due to their low cost, environmental friendliness, and their potential to compete with synthetic composites [6-2]-[6-6]. Nonetheless, the use of bio-based composites has been limited due to their lower mechanical and thermo-physical properties compared to synthetic composites and conventional structural materials [6-5][6-6]. Nanoclay reinforcement in matrices of biocomposites enhances the thermal and barrier properties, and prevents moisture from reaching the natural fibers, thereby help maintain the integrity of the biocomposites and enhance its durability. The advantage of multiscale reinforcement is not limited to barrier properties, but when combined with bio-based resins provide stiffness-toughness balance, increase environmental appeal and provide multi-property improvements of resulting biocomposites [6-1].

Environmental concerns related to the use of synthetic, or petroleum-based, polymer matrix composites has propelled the development of composite materials based on natural or renewable sources [6-8][6-9]. Bio-based resins, or bio-blends, obtained by replacing part of a petroleum-based resin with natural bio-resin have been found to be a promising compromise between environmental friendliness and performance [6-1], as the use of all natural bio-resins has been limited due to performance concerns [6-7]. In addition to higher natural content, bio-based resins improve toughness of the resulting resin blend [6-1] [6-8][6-10]. However, this increase in toughness compromises stiffness, barrier and thermal properties [6-8][6-10]. Stiffness and toughness are opposing performance parameters and a proper balance is required for an efficient composite. Hence, one way pursued by the authors to obtain stiffness-toughness balance and recover the lost barrier and thermal properties due to bio-resin addition is by addition of layered silicates (nanoclay).

The reinforcement of petroleum-based polymers with nanoclay has been shown to impart multifunctionality to the resulting polymers with enhancements not only on stiffness but improvements in thermal, barrier, flammability and ablation resistance properties [6-11]. Polymer-clay nanocomposites are well understood and considerable literature and review articles [6-11]-[6-14] exist on this topic. The advantage of nanoclay reinforcement in bio-based polymers is that it enables the recovery of the properties lost due to bio-resin addition, and produce bio-based nanocomposites with improved stiffness-toughness balance [6-15][6-16]. Thus, the synergy between nanoclay reinforcement in a bio-blend produces a polymer nanocomposite with similar or enhanced properties than the virgin polymer and holds great promise for use in wide applications [6-16]. The application of nanoclay reinforced bio-based polymers to fiber reinforced composites provides value added properties to resulting biocomposites [6-1]. Thus, in a biocomposite, natural fibers remain the main reinforcement for stiffness and strength, while the nanoclay enhances the resin properties thereby improving the transient properties [6-1]. The incorporation of nanoclay and natural fibers in resin systems thus provides reinforcements to resin systems at two scales. Although, different concepts of multiscale reinforcement have been studied for synthetic composites [6-17]-[6-20], similar studies on multiscale/multiphase reinforcements of bio-based composites are limited [6-1].

An initial attempt to use the multiscale reinforcements for biocomposites and to evaluate the synergy of the constituents was performed on bio-based resins containing blends of unsaturated polyester (UPE) and epoxidized methyl soyate (EMS), reinforced with hemp fibers and nanoclay [6-1]. The study incorporated up to 10% of EMS, 1.5 wt.% of nanoclay and an average volume fraction of 17% of short hemp fibers. The study showed promising results but was limited by the nanocomposite processing that allowed relatively less amounts of bio-resin (10%) and nanoclay (1.5 wt.%). In order to exploit the synergy offered by these materials and improve the environmental appeal, higher amounts of bio-resin and nanoclay were recommended [6-1]. Also, a study on blends of neat resins (no clay), by replacing parts of UPE with EMS [6-16] and EML [6-21] suggests UPE/EML composites perform relatively better than similar composites from UPE/EMS blends.

In this work, the shortcomings and recommendations from the UPE/EMS nanocomposites study [6-16] were addressed and improvements were made. Firstly, the bio-resin used in this work is EML instead of EMS, as it has been reported to perform better [6-21]. Secondly, an improved manufacturing method identified from a detailed processing study [6-22], and which allowed incorporation of up to 30 wt.% EML and 5.0 wt.% nanoclay was used. Thirdly, the average volume fraction of natural fibers (hemp fibers) used in this work (27%) was higher than that from UPE/EMS study (17%) [6-1]. Finally, the possibility of incorporating relatively large amounts of nanoclay and bio-resin allowed detailed experimental characterization on 12 biocomposites, unlike UPE/EMS study wherein only five biocomposite systems were studied. Such detailed characterization allowed studying the effects of constituent materials on resulting biocomposite properties and enabled finding optimized material designs that maximize the synergy of these constituents. Biocomposites with material systems that varied the bio-resin (EML) content in UPE and the concentration of nanoclay while maintaining a constant amount of natural fibers were fabricated by compression molding. Mechanical and thermo-physical properties were evaluated through standard tests. The degree nanoclay dispersion and morphology in the resin systems was characterized using transmission electron microscopy and the features of fracture surfaces were characterized using scanning electron microscopy. Results show synergistic behavior of constituents in the biocomposite with improved stiffness-toughness balance and enhancements in multiple properties of resulting environmental friendly and cost effective biocomposites. The resulting biocomposites are tailorable both in performance and in environmental impact and have potential for wide applications.

6.3 Experimental methods

Experimental determination of thermo-physical properties and material characterization was performed on biocomposite plates made from bio-based resin blends and reinforced with nanoclay inclusions and natural fibers. In the following sections, details on materials, processing, parameters studied, and testing are provided.

6.3.1 Materials

Industrial unprocessed raw hemp (Stemergy, Ontario, Canada) was used as natural fiber reinforcement. The fibers were hand chopped to an average length of 25mm. The primary component of the resin blend was ortho unsaturated polyester resin (*UPE*, Polylite® 32570-00, Reichhold Inc., NC), which contains 33.5 wt.% styrene. The secondary component that replaced parts of UPE was a bio-based modifier, epoxidized methyl linseedate (*EML*, Vikoflex® 9010, Arkema Inc, PA).. EML is a mixture of methyl esters of fatty acid compositions that construct the linseed oil. The detailed composition is 40-50 wt % methyl linolenate epoxy, 24-26 wt % methyl oleate epoxy, 17-22 wt % methyl linoleate epoxy, 4-7 wt % methyl palmitate, and 2-5% methyl stearate. The nanoclay used to reinforce the resin system was Cloisite 30B® (Southern Clay Products, Inc. TX). The resin blend was processed with cobalt naphthenate (Sigma Aldrich, MO) as a promoter and 2-butanone peroxide (Sigma Aldrich) as an initiator. A constant ratio by weight of the resin system to the promoter and initiator was utilized to cure all of the biocomposites. The mixing ratio was 100 parts by weight of the resin system to 0.03 parts promoter and 1.50 part initiator.

6.3.2 Experimental matrix and nomenclature

All biocomposite material systems were composed of natural fibers and a set of UPE-EML bio-based resin blends. The amount of bio-resin (epoxidized methyl linseedate, EML) that replaced the primary resin component UPE, was varied from 0% to 30%, in increments of 10%. A total of 4 neat resin (no clay) systems were obtained. Each of these resin systems were then reinforced with nanoclay inclusions of 0 wt.%, 2.5 wt.% and 5.0 wt.%. A total of 12 resin systems were obtained which were then reinforced with natural hemp fibers. A summary of the experimental matrix including nomenclature, composition, concentration of constituents and densities of the 12 biocomposite material systems studied are provided in Table 3-1.

6.3.3 Polymer nanocomposite processing

The technique used for processing the nanoclay reinforced bio-based resin systems follows the findings from our group's study on solvent-based processing techniques for bio-based clay/polymer nanocomposites [6-22]. The technique found to be most efficient consists of sonicating the nanoclay in acetone to an energy level of 300 kJ, using a solution concentration of approximately 50 l of acetone to 1 kg of clay, while it is constantly stirred. After sonication, only the UPE solution is added. The acetone + nanoclay + UPE solution is mixed continuously on a hot plate at approximately 55 °C to remove a majority of the acetone. The remaining acetone is removed by vacuum extraction at 55 °C for 24 h. During the acetone removal process the styrene present in the UPE is also removed. Thus, after acetone removal the bio-resin, EML, is added along with the lost styrene. The processed solution is cooled to room temperature and blended with the initiator and promoter followed by curing. A flow chart depicting the process is shown in Figure 6-1. The processed resin system with UPE, EML and nanoclay was used in the manufacturing of biocomposite plates.

6.3.4 Manufacturing of hybrid biocomposite plates

Flat biocomposite plates for the twelve biocomposite material systems as described in Table 3-1 were manufactured using compression molding. The natural fibers were chopped to an average length of approximately 25 mm. These fibers were washed in distilled water and dried at room temperature for 12 hours. The fibers were then dried in a vacuum oven at 80°C and 100 kPa of pressure for at least 12 hours before compression molding. The resin system obtained from nanocomposite processing as described in earlier section was mixed with cobalt naphthenate (Sigma Aldrich, MO) as a promoter (0.03% by weight of resin blend) and 2-butanone peroxide (Sigma Aldrich) as an initiator (1.5 wt.% of resin blend). The measured quantity of fibers were then impregnated with resin system (UPE + EML + nanoclay + initiator + promoter) by hand mixing until the material was consistent (by visual evaluation). The impregnated fibers were then placed in a frame mold. Care was taken to evenly distribute the fiber material in the mold to ensure a uniform sample since natural fibers have a tendency to clump and tangle together when mixed. The frame mold was placed between two steel plates covered with Teflon paper. The sample was then cured in a press under 550 kPa of pressure for a total of 4 hours using a time-temperature profile of 100 °C for 2 hours, followed by 150 °C for 2 hours. An overview of biocomposite manufacturing is provided inFigure 6-2.

6.3.5 Testing and characterization

Characterization of the biocomposite material systems was done through ASTM testing of coupon samples taken from the compression molded plates. The tensile properties (modulus, strength and elongation at failure) were measured on 6 to 8 samples as per ASTM D638. The impact strength was measured on 5 samples using notched Izod tests as per ASTM D256. Moisture absorption testing was performed using Fisher Scientific Versa bath®-138 equipment that allowed immersion of samples in a distilled water bath with temperature maintained at 50 °C. The samples used for moisture measurements were rectangular bars and had average dimensions of 60.0 mm x 12.5 x 3.0 mm. The specimens were coated with impervious two-part epoxy on all edges to eliminate edge effects and limit the diffusion only through the thickness of the sample. All samples had flat and parallel surfaces as obtained from compression molded plate. The samples were placed in a vacuum oven at 80 °C for 24 hours to remove any residual moisture. The initial dry weights were recorded and the samples were immersed in water. The weight of the samples was measured every 12 hours for the first 3 days, followed by once every week until steady state (equilibrium, no further increase in weight of sample) was achieved. Moisture diffusivity coefficients were obtained from the moisture gain versus time plots for various biocomposites. The dispersion and morphology of clay inclusions in the resin systems was assessed with transmission electron microscopy (TEM). A JEOL 100CX TEM with LaB6 filament and 120 kV acceleration was used to obtain bright field images from sections approximately 100 nm thick. Tensile failure surfaces of biocomposites were pre-coated with a thin gold film and observed in a JEOL 6400 field emission scanning electron microscope (SEM) at 10 kV acceleration voltage.

6.4 Results

The incorporation of EML and nanoclay may have a beneficial or detrimental effect on the resulting biocomposite properties, depending on the property considered. Since the amount of natural fibers were relatively similar (Weight fraction of ~32%), the effects of bio-resin (EML) and nanoclay could be directly compared. All results in the following section are thus compared to benchmark biocomposite A, containing 100% UPE (0% EML and 0% nanoclay). Also, in the relative comparison in the following results, the biocomposite under consideration is provided in parentheses (See Table 3-1 for nomenclature).

6.4.1 Material characterization study

(a) *Tensile modulus:* Results for the tensile modulus are provided in Figure 6-3. Considering only the average values, the overall trend suggests that the modulus of biocomposite materials decreased with increasing bio-resin content. The average tensile modulus of biocomposites B (10% EML), C (20% EML) and D (30% EML) was reduced approximately by 5, 30 and 50%, respectively. The addition of nanoclay enhances the properties of the resin system thereby increasing the overall composite properties. A major enhancement in modulus due to addition of nanoclay was not observed in our previous work as only 1.5 wt.% of nanoclay could be processed [6-1]. In this work, nanoclay content of up to 5 wt.% was used and hence relatively, a more pronounced effect of nanoclay was observed. The sole effect of nanoclay was studied by comparing virgin UPE (no EML) biocomposites reinforced with nanoclay (E and I) with benchmark biocomposite. The average tensile modulus values improved approximately by 20% (E) and 30% (I) for nanoclay contents of 2.5 wt.% and 5.0 wt.%, respectively.

Similarly, for biocomposites containing 2.5 wt.% nanoclay, the biocomposite F (10% EML) had an average tensile modulus value approximately 5% higher than benchmark bicomposite. Similarly biocomposites with 20% (G) and 30% (H) EML contents showed reduction in average tensile modulus values of approximately 10% (G) and 45% (H), respectively. Finally, for biocomposites containing 5.0 wt.% nanoclay, biocomposites with 10% EML blend (J) showed an enhancement in average tensile modulus values of approximately of 15% (J), while addition of 20% (K) and 30% (L) EML contents showed reduction in average tensile modulus values by approximately 5% (K) and 30% (L), respectively. The biocomposites containing 10% EML and reinforced with nanoclay, revealed not only a complete recovery, but improvement in lost stiffness due to EML addition. Overall trend considering the average values of tensile modulus suggests that the addition of bio-resin (EML) reduces the tensile modulus and addition of nanoclay improves the tensile modulus.

(b) *Ultimate tensile strength:* Results for the ultimate tensile strength are summarized in Figure 6-4. Similar to modulus, the sole effect of nanoclay on UTS was studied by comparing virgin UPE (no EML) biocomposites reinforced with nanoclay (E and I) with benchmark biocomposite. The biocomposite E, had average tensile strengths similar to baseline biocomposite A. Nevertheless, biocomposite I, showed an average reduction of approximately 20%. The effect of EML was studied by comparing neat resin (no clay) biocomposites. The biocomposites B (10% EML) and C (20% EML) showed an improvement in average UTS values by approximately 20% (B) and 30% (C), respectively. Similarly for biocomposites reinforced with 2.5 wt.% nanoclay, improvements in average UTS values of approximately 20% (both F and G) was observed. Also, for biocomposites reinforced with 5.0 wt.% nanoclay, improvement in average UTS values of approximately

10% (J) and 20% (K) were observed. Finally, biocomposites with 30% EML content revealed reduction in average UTS values relative to counterparts with 10% and 20% EML contents but were higher than the baseline biocomposite (A). Biocomposites with 30% EML, namely, D (0% nanoclay) had average UTS values higher by approximately 10%, while biocomposites H (2.5 wt.% nanoclay) and L (5.0 wt.% nanoclay), on average had UTS values similar to benchmark biocomposite.

Overall, the addition of nanoclay seems to reduce the UTS values of resulting biocomposites while addition of bio-resin (EML) seems to enhance the UTS values. Nevertheless, reduction in average UTS values was observed for biocomposites with EML contents beyond 20%. Finally, all hybrid biocomposites that had both EML and nanoclay, showed average UTS values similar or higher than baseline biocomposite (A), indicating that the lost UTS properties due to nanoclay addition were recovered by EML addition, suggesting a synergistic behavior of the hybrid constituents.

(c) *Elongation at failure:* The summary of tensile elongation at failure results is provided in Figure 6-5. The overall trend considering the average values of tensile failure strains suggests that the EML addition increases the ductility of the resulting biocomposite. For neat resin (no nanoclay) biocomposites, increase in average tensile failure elongation values of approximately 45% (B), 110% (C), and 150% (D) was observed. The nanoclay addition seems to make the resin systems more brittle, thereby reducing the ductility and corresponding tensile failure elongations. A reduction in average tensile failure elongations of approximately 20% was observed for nanoclay reinforced neat UPE (no EML) biocomposites (E and I). For biocomposites containing 2.5 wt.% nanoclay, the average tensile failure elongations improved by approximately 20% (F), 55% (G) and 130% (H).

Similarly for biocomposites containing 5.0 wt.% nanoclay, the average tensile failure elongations increased by approximately 15% (J), 75% (K) and 90% (L).

Overall nanoclay addition seems to make the resin system brittle and reduces the elongations at tensile failure of resulting biocomposites. The loss of ductility due to the addition of nanoclay seems to not only be recovered but improved by addition of EML in all biocomposites in this study.

(d) *Notched Izod impact strength:* Figure 6-6 summarizes the results from the notched Izod impact strength testing. The overall trend considering the average impact strength values suggests that impact strengths of resulting biocomposites increased with increasing EML content and decreased with the nanoclay addition. The increase in average impact strength values of neat resin (no clay) biocomposites due to addition of EML was approximately 70% (B), 105% (C) and 125% (D). The addition of nanoclay reduced the average impact strengths, as observed in virgin UPE (no EML) biocomposites reinforced with nanoclay. The impact strengths of biocomposites E and I, on an average reduced by approximately 20% due to addition of nanoclay.

For biocomposites containing 2.5 wt.%, EML addition revealed enhancements in average impact strength values by approximately 65% (F), 90% (G) and 100%(H). Similarly for biocomposites containing 5.0 wt.% nanoclay, EML addition revealed increase in average impact strength values by approximately 60% (J), 80% (K) and 95% (L). Overall, the loss in impact strengths (toughness) due to addition of nanoclay seems to not only be fully recovered but enhancements were obtained by addition of EML content. A summary of the experimental tensile and impact strength results are provided in Table 6-2.

(f) *Moisture absorption (MA):* Moisture absorption properties for the biocomposites were obtained by water immersion tests where the weight gain at any given time (M_t) was measured until steady state was achieved. Due to thickness variations in the specimens the amount of moisture absorbed by each was different. Thus, instead of simply assessing the amount of moisture absorbed, the speed of moisture absorption in polymers and nanocomposites was quantitatively compared by determining their diffusion coefficient [6-23]. Hence, moisture diffusivity coefficient was used as the parameter to assess the effect of bio-resin (EML) and nanoclay content on the different bio-based polymer nanocomposites. The diffusivity coefficient, D, was computed from the initial slope of the moisture gain, M_t/M_∞ versus time ($\sqrt{t}/d$) as:

$$D=\frac{\pi}{16}\left(\frac{M_t/M_\infty}{\sqrt{t}/d}\right)^2 \tag{6-1}$$

where M_t is the mass gain at any time t, M_∞ is the maximum mass gain at equilibrium/steady state, and d is the thickness of the specimen.

Figure 6-7 shows the plots of moisture gain versus time for neat (no clay) resin systems. The experimental data is shown in symbols and the exponential fits are superimposed as solid line. The diffusivity coefficients were obtained by substituting the initial slope from the curves in Figure 6-7 into Equation (6-1). The variation of the diffusivity coefficients D, with increasing EML content are shown as an inset in Figure 6-7. Due to the absence of nanoclay, the diffusion coefficients obtained show the effect of blending bio-resin (EML) in virgin UPE. The overall trend considering the average values of diffusivity coefficients of biocomposites suggests increase in diffusivity with increasing EML content. For neat resins (no nanoclay), the average diffusivity coefficient values increased by approximately 20% (B), 85% (C) and 200% (D).

The addition of nanoclay seems to improve the barrier properties, thereby reducing the diffusion coefficient values. For neat UPE (no EML) biocomposites, the addition of 2.5 wt.% and 5.0 wt.% nanoclay show reduction in average diffusion coefficient values by approximately 25% (E) and 35% (I), respectively. It is clear that the increase in moisture diffusivity coefficients due to addition of EML is higher than the reduction offered by nanoclay. For biocomposites containing 2.5 wt.% nanoclay, the average diffusivity coefficients values were higher by approximately 5% (F), 65% (G) and 190% (H) for EML contents of 10% (F), 20%(G), and 30%(H), respectively. The barrier properties lost due to addition of EML were only partially recovered by addition of 2.5 wt.% nanoclay. Nevertheless, for biocomposite J (10% EML, 5.0 wt.% nanoclay), average diffusion coefficient values were reduced by approximately 5%, indicating recoveryof loast barrier properties. Similarly, for biocomposites containing 5 wt.% nanoclay, the addition of 20% and 30% EML contents revealed increase in average diffusion coefficient values by approximately 20% (K) and 160% (L), respectively, thereby offering only partial recovery. Considerable enhancement in moisture diffusion properties were observed due to the addition of nanoclay. Nevertheless, the detrimental effect of EML was more than the enhancement provided by nanoclay. As a result a partial recovery was obtained in all biocomposites with EML contents more than 10%. Full recovery of lost barrier properties due to EML addition was observed only in biocomposite J(10%EML, 5 wt.% nanoclay). The diffusivity coefficients of all biocomposites in this study are summarized in Figure 6-8.

(g) *Nanoclay dispersion and exfoliation:* Transmission electron microscopy (TEM) was used in this study to observe the dispersion and morphology of nanoclay in the polymer system (no fibers). Figure 6-9 (a) and (b) shows the bright field TEM micrographs of clay / UPE composites. Figure 6-9 (a) shows a general distribution of nanoclay particles in UPE matrix. It was observed that the clay platelets were well distributed and had partially exfoliated and intercalated morphologies. Figure 6-9 (b) shows a high magnification micrograph of an intercalated clay gallery in a UPE matrix containing 5 wt.% nanoclay. Similar micrographs were observed for UPE/EML blends reinforced with nanoclay. In order to obtain better exfoliation, additional energy must be spent in sonication of clay along with improvements in the functionalization of the nanoclay and the polymer.

(h) *Fracture surface observations:* Scanning electron microscopy (SEM) was used to observe the features of tensile fracture surfaces and fiber-matrix interfaces. Such an approach has been used by others to study the fiber-distribution, stiffness and toughness performance of biocomposites [6-3][6-4][6-5].Three types of failure mechanisms have been identified in literature for natural fiber reinforced polymers: matrix failure, fiber fracture and fiber-matrix interfacial failure [6-5]. Similar failure morphologies were observed in the tensile fracture surfaces of the biocomposites in this study.

The natural fibers used for all biocomposites in this study had same fiber quantity, average lengths, surface characteristics and manufacturing procedures. Hence, the observed distribution of fibers was similar for all biocomposites. Figure 6-10 (a) and (b) show epresentative tensile fracture surfaces from biocomposite A. Figure 6-10 (a) is a low magnification (scale = 200 μm) fracture surface showing the distribution of fibers and the various failure types. The fiber pull-out failure is observed by cavities left in the matrix (encircled regions) and fiber fracture is observed by loose fiber ends in the fracture surface (arrow regions). Similarly, Figure 6-10 (b) shows the failure morphologies such as pull-out (encircled), fiber fracture (boxed) and fiber-matrix interface (arrow). Also, clumping / bunching of some fibers was observed. This may be due to two reasons: a) natural fibers have an inherent tendency to clump together, and b) the fibers used were not surface-treated, and hence may have relatively poor adhesion characteristics with the polymer. Improvements of surface characteristics may avoid clumping of fibers and lead to better enhancement in material properties. Many studies have been performed to study the effect of surface treatments and a good review of the same is provided by Mohanty et. al [6-24].

SEM micrographs have also been used to observe interfacial performance or pullout characteristics of the fiber [6-3]. A weak interface, weaker matrix, improper compatibility between natural fiber and the matrix and/or improper adhesion characteristics may lead to fiber pull-out instead of fracture and may reduce the resulting mechanical properties. In short random fiber composites, a fracture surface may generally show a combination of fiber pull-out, fiber fractures and fracture of matrix regions. The fiber pull-out is observed in tensile fracture surfaces by three main characteristics: a) observation of cavity with shape and diameter of the fiber indicating fiber pull-out, b) existence of long pulled-out fibers, which may have pulled out of the other half of the tensile specimen not viewed in SEM, and c) the interface gap - the gap between the fiber and the matrix in pulled-out fibers. It is generally possible to see the first two factors, (a) and (b) in all short-fiber composite tensile fracture surfaces. The pull-out strength of the fibers depends mainly on the embedment length of the fibers. In all randomly oriented short fiber composites, it is possible that at the cross section of failure, there are some fibers that do not have enough embedment length and hence may pull out of the resin. This embedment length depends mainly on fiber-matrix adhesion property. Hence surface treatments may enhance the adhesion property and reduce the embedment length and corresponding pull-out type failure. A well embedded fiber may have adequate bonding and lead to tensile fracture of the fiber. In general, SEM micrographs of tensile fracture surface will hence show a combination of the above mention failure mechanisms.

In an earlier study by our group the interfacial gap (gap between the fiber and matrix) was studied for varying contents of bio-resin and nanoclay [6-1]. A similar study was performed in this work by comparing the interfacial characteristics of specific biocomposites in the experimental matrix. The biocomposites with extreme values of bio-resin and nanoclay content within the experimental matrix under consideration (A, D, I and K) were selected. Figure 6-10 (c) shows the interfacial gap for the benchmark biocomposite A with no clay and no EML. Figure 6-10 (d) shows the increase in interfacial gap due to addition of 30% EML (D). The interface gap for biocomposite (I) with 0% EML and 5 wt.% clay is shown in Figure 6-10 (e) and was observed to be similar or better (smaller interfacial gap) than benchmark biocomposite (A). A larger interface gap would have been expected if the nanoclay used and its morphology was having an adverse effect on interfacial properties. Also, the addition of nanoclay improves the overall matrix properties, thereby enabling fiber fracture instead of fiber pull-out and hence reduction in fiber-matrix interfacial gap. Finally, the biocomposite (L) with 30%EML and 5.0 wt.% nanoclay showed increase in interfacial gap relative to its counterpart biocomposite (I) and the benchmark composite (A). The study of interface and the effect of clay on fiber-matrix adhesion are not fully established and are beyond the scope of this work and hence no definite conclusions can be drawn at this time. The experimental tensile test results support this weaker interface and pull-out phenomena, as reduction in tensile modulus and strength was observed. The pull-out phenomena enables dissipation of more energy along the interface and hence higher impact strengths and higher ductility was observed for increasing bio-resin content.

The final study in tensile fracture morphologies was the study of matrix in biocomposites. The roughness of fracture surface has generally been associated fracture properties and critical strain energy release rates. A smooth featureless fracture surface is attributed to brittle failures and rougher fracture surfaces are attributed to tougher nanocomposites [6-25]. The matrix region in the fracture surface for biocomposite A (0% EML, 0% nanoclay), was found to be relatively smooth and featureless (Figure 6-11 a). Figure 6-11 (b) shows the well-blended (UPE/EML) matrix region of biocomposite D (30%EML, 0% clay). Figure 6-11 (c) shows the phase-separated, EML enriched matrix region of biocomposite D. Such phase separation was observed only in biocomposite (D) and not it other biocomposites in this study. Overall, the roughness of the fracture surfaces increased with increasing bio-resin (EML) content. Figure 6-11 (d) and (e) shows the matrix region of biocomposites with 5 wt.% nanoclay containing 0% EML (I) and 30% EML (L), respectively. The addition of nanoclay also increased the surface roughness of the matrix region. This suggests that the combination of EML blend and clay will provide tougher composites. Research has shown that change in fracture morphologies suggest different toughening mechanism at low and high clay loading. It is difficult to quantitatively relate the fracture surface to toughness of the composites [6-25]. This requires better understanding of micro-structural parameter, crack propagation mechanisms and interface studies to relate the fracture and toughness to the surface morphologies.

6.5 Discussion

Experimental characterization of hybrid biocomposites containing multiscale reinforcements of nanoclay and natural fibers (unprocessed hemp) in bio-based resins (blends of petroleum based UPE and bio-resin, EML) reveal synergistic behavior and multifunctional properties. As expected, the experimental data revealed scatter/variations in measured parameters. These variations were specifically larger for failure-dependent parameters, such as tensile failure strains, tensile strengths and impact strengths. Detailed statistical analyses taking into account these variations should be performed to quantitatively and precisely obtain the effects of constituents, namely EMS and nanoclay. In this work, only the average values were considered and hence a qualitative effect and overall trends based on average values could be obtained. Overall, it was observed that hybrid combination of layered silicates and bio-based resin systems provide biocomposites with similar or better properties than the baseline biocomposite containing natural fibers and virgin UPE (0% EML, 0% nanoclay).

This work was an improvement of an earlier study [6-1] that had limitations on the amounts of bio-resin (EMS, 10%) and nanoclay (1.5 wt.%) used. The study [6-1] showed promise with respect to synergistic behavior of biocomposites and recommended incorporation of high amounts of bio-resin and nanoclay to fully exploit the benefits offered by these biocomposites. This work used improved processing that allowed incorporation of 30% of bio-resin (EML) and 5 wt.% nanoclay, thereby allowing to find limits to the synergistic performance of these materials. Mechanical testing revealed enhancement in toughness related parameters such as impact strengths and ductility, and reduction of stiffness related parameters such as tensile modulus, with addition of bio-resin. Similarly, the nanoclay addition increased stiffness but reduced toughness of resulting biocomposites. An interesting observation was made in tensile strength results: the study on neat resins (no reinforcements) revealed decrease in tensile strengths with addition of bio-resin in UPE, which was attributed to the inherent weak nature of the bio-resin [6-16]. A similar trend was expected when such bio-based resins were used for biocomposites. Nevertheless, the biocomposites evaluated in this work showed increase in tensile strengths for EML contents up to 20%, and then a drop in tensile strengths for EML contents of 30%. This trend was consistent for nanoclay reinforced resin systems (Figure 6-4). Additonally, the nanoclay reinforced biocomposites had lower strengths than respective neat resin (no clay) counterparts. Similar reduction in tensile strengths was also observed for nanoclay reinforced (no natural fibers) resins. The authors believe that the failure initiates in the flaws and imperfections in the matrix and thus attribute the reduction in tensile strengths and ductility of nanoclay reinforced bio-based composites to the stress concentrations created by the nanoclay reinforcement in the relatively brittle polymer matrix. While there is no general consensus on this point of view, computational studies by a parallel effort to this work [6-26] have shown evidence to this mechanism.

It should be noted that most mechanical properties are governed primarily by the macro-reinforcement, (hemp fibers). Also, the fiber content in all the biocomposites was similar and the increase in tensile strengths due to increase in EML contents (up to 20%) suggests better synergy of the constituents. The addition of bio-resin makes the resin system ductile and less brittle. Such compliance offered by bio-resin addition allows the natural fibers to take more stresses and hence the improvement in strengths. Finally, the decrease in tensile strengths at 30% EML content is attributed to phase separation of UPE and EML, thereby creating EML rich regions that lead to premature failure due to their inherent weak nature. Moreover, large variations in tensile strength values were observed which may be due to many factors including manufacturing defects like fiber-distribution or voids, impurities such as the wood-like core material present in the untreated natural fibers which may lead to premature tensile failure and cause scatter in the results. These defects and impurities may act as crack initiators, or lead to poor fiber-matrix adhesion. In spite of the scatter, consistent trends (Figure 6-4) were observed with variations of nanoclay and bio-resin addition. Overall, mechanical characterization revealed that addition of EML enhanced toughness but reduced stiffness, while nanoclay improved stiffness but compromised toughness of the resulting biocomposites. The combination of nanoclay and EML provides a synergistic effect such that the detrimental effects of each constituent are complimented by the other and beneficial properties are revealed in resulting biocomposites. The advantages of hybrid combinations of EML and nanoclay and the synergy they offer is not limited to stiffness-toughness balance but similar enhancements were observed in barrier properties.

The study on moisture diffusion of biocomposites revealed that addition of EML increased moisture diffusivity while excellent barrier properties enhancements provided by nanoclay inclusions helped in recovering the barrier properties lost due to EML addition. However, the increase in moisture diffusivity due to addition of EML was higher than the barrier resistance offered by nanoclay. Hence, complete recovery was possible only in biocomposites with 10% EML contents with 5 wt.% nanoclay. Nevertheless, nanoclay inclusions resulted in partial recovery in all other biocomposites. Also, it was observed that biocomposite material systems absorb less moisture than natural fibers alone. Similar results were reported in an earlier study [6-1]. The matrix serves as a barrier for the moisture reaching the natural fibers. Hence, the merit of using nanoclay in the biocomposites is that it improves the barrier properties of the matrix by preventing/delaying the moisture from reaching the natural fibers by introducing a tortuous path for moisture movement, thereby help maintaining integrity of biocomposites and improving its durability.

The improved processing and incorporation of high amounts of EML (30%) and nanoclay (5 wt.%) allowed to obtain limits to synergistic performance and the effects of each of the constituents on the resulting properties of the hybrid biocomposites. It was found that biocomposites with EML contents beyond 30% showed least synergy among constituents. Although partial recovery was observed in most properties, the loss in properties due to the addition of EML was beyond the recovery provided by nanoclay. Biocomposites with 10% EML contents and nanoclay showed complete recovery with superior properties than the baseline biocomposites. Finally, biocomposites with 20% EML and nanoclay showed balanced properties, with properties similar or lower than baseline biocomposites. Considering ease of nanocomposites processing and synergistic performance of resulting biocomposite, EML contents of 10% and 20% EML reinforced with nanoclay (2.5 wt.% and 5.0 wt.%) have been identified as optimized material layouts.

The nanocomposites processing technique used in this work were found to produce nanoclay platelets with a combination of exfoliated and intercalated morphologies with excellent dispersion. Exfoliated morphologies lead to better stiffness and barrier properties, while intercalated morphology gives better toughness properties. A proper balance of exfoliation and intercalation would be suggested for the desired stiffness - toughness balance. However, in biocomposites, and in general fiber reinforced composites, since mechanical properties are mostly governed by fibers, exfoliated nanoclay morphologies are preferred for non-mechanical enhancements such as barrier and thermal properties. The study of tensile fracture surfaces of biocomposites revealed interesting observations on toughness and adhesion between natural fibers and hemp. The addition of bio-resin (EML) led to increased fiber pull-outs and increased fiber-matrix interfacial gap, resulting in increased toughness and ductility. The addition of nanoclay and its effect on fiber-matrix adhesion is beyond the scope of this work. Overall, the fracture surface observations support the experimental observation of synergistic behavior and the resulting stiffness-toughness balance due to the combination of EML and nanoclay. Meanwhile, the interfacial

properties and resulting properties of biocomposites can be improved by surface treatment of the fibers [6-1]. Unprocessed industrial raw fibers were used in this work to characterize the resulting biocomposites such that lower performance bounds were obtained. The use of "engineered," or treated, fibers with nanoclay reinforced bio-resins would lead to novel environmentally friendly hybrid biocomposites with competitive and improvements in multiple properties.

6.6 Conclusions

Results from this study indicate that novel environmentally friendly bio-based composites with improvements in multiple properties can be obtained from combination of multiscale reinforcements of nanoclay and industrial hemp fibers in resin blends of unsaturated polyester (UPE) and epoxidized methyl linseedate(EML). Experimental characterization revealed addition of EML increases toughness parameters like impact strengths and ductility, but reduces stiffness. Addition of nanoclay improves stiffness but decreases toughness. Thus synergistic behavior of the hybrid biocomposite constituents resulted in excellent stiffness-toughness balance. Similar synergistic behavior was observed in moisture barrier properties where barrier properties lost due to bio-resin addition of EML were recovered by nanoclay. The incorporation of large amounts of bio-resin (30%) and nanoclay (5 wt.%) enabled finding optimized material layouts that maximize the synergy of these materials and also find the effect of the constituents resulting properties. It was found that biocomposites with EML contents beyond 30% showed least synergy, and properties lost due to bio-resin addition were not reasonably recovered by nanoclay inclusions. Biocomposites with 10% EML contents and nanoclay showed complete recovery with superior properties than the baseline biocomposites. Finally, biocomposites with 20% EML and nanoclay showed balanced properties, with properties similar or slightly lower than baseline biocomposites. Considering ease of nanocomposite processing and synergistic performance of resulting biocomposite, EML contents of 10% and 20% EML reinforced with nanoclay (2.5 wt.% and 5.0 wt.%) were identified as optimized material layouts. The mechanical properties of biocomposites are governed mostly by natural fibers while nanoclay inclusions improve matrix properties, thereby enhancing transient properties like moisture diffusion and thermal properties. Thus the use of multiscale reinforcements provides enhancements and synergistic behavior at different scales resulting in efficient bio based materials. Finally, these materials are tailorable in performance and environmental impact by controlling the constituent concentrations. Such tailorable nature along with the use of "engineered," or treated, fibers with nanoclay reinforced bio-resins would lead to novel, environmentally friendly hybrid biocomposites with enhanced and competitive properties, thereby increasing the potential applications of such composites.

6.7 *Tables and Figures*

Table 6-1. Biocomposite material properties, Composition and Identification

Specimen Identification	Composition (%)			Fiber Fractions (%)		Density (g/cc.)	
	UPE	EML	Clay	Weight Fraction W_f	Volume Fraction V_f	Resin ρ_m	Composite ρ_c
A	100	0	0.0	33	29	1.221	1.255
B	90	10	0.0	29	24	1.194	1.239
C	80	20	0.0	33	28	1.167	1.161
D	70	30	0.0	32	27	1.140	1.227
E	100	0	2.5	33	29	1.234	1.229
F	90	10	2.5	32	28	1.207	1.214
G	80	20	2.5	32	27	1.180	1.209
H	70	30	2.5	32	27	1.153	1.194
I	100	0	5.0	29	25	1.247	1.277
J	90	10	5.0	32	28	1.220	1.227
K	80	20	5.0	31	27	1.194	1.214
L	70	30	5.0	32	27	1.167	1.179

Density of Fiber (ρ_f) = 1.48 g/cc.

The nomenclature is also referred as: [UPE / EML / Clay / W_f / V_f], For example, specimen ID "6" can be referred as [90 / 10 / 2.5 / 32 / 28].

Table 6-2. Measured properties of biocomposite material systems

Material	MOE (GPa)		UTS (MPa)		EF (%)		IS (J/m)	
ID-[UPE / EML / Clay / W_f / V_f]	$\bar{x}$	σ	$\bar{x}$	σ	$\bar{x}$	σ	$\bar{x}$	σ
A-[100 / 0 / 0.0 / 33 / 29]	6.11	1.52	19.85	2.12	0.37	0.02	26.11	5.50
B-[90 / 10 / 0.0 / 29 / 24]	5.75	0.50	25.53	2.41	0.54	0.08	44.73	6.33
C-[80 / 20 / 0.0 / 33 / 28]	4.26	0.53	28.45	3.21	0.77	0.08	53.60	11.08
D-[70 / 30 / 0.0 / 32 / 27]	3.18	0.61	22.37	4.49	0.92	0.14	58.22	3.28
E-[100 / 0 / 2.5 / 33 / 29]	7.45	0.34	20.55	1.04	0.28	0.05	21.02	5.08
F-[90 / 10 / 2.5 / 32 / 28]	6.55	2.23	24.47	1.85	0.45	0.08	43.48	4.79
G-[80 / 20 / 2.5 / 32 / 27]	5.57	1.17	25.27	1.50	0.58	0.03	49.94	5.29
H-[70 / 30 / 2.5 / 32 / 27]	3.45	0.60	19.53	2.12	0.85	0.18	52.67	19.82
I-[100 / 0 / 5.0 / 29 / 25]	7.95	1.93	16.40	3.17	0.32	0.14	20.24	3.14
J-[90 / 10 / 5.0 / 32 / 28]	6.88	0.66	21.89	3.24	0.42	0.08	42.12	7.53
K-[80 / 20 / 5.0 / 31 / 27]	5.70	0.72	25.31	1.79	0.64	0.09	46.52	5.57
L-[70 /30 / 5.0 / 32 / 27]	4.43	0.17	20.34	2.15	0.71	0.07	50.92	2.49

E : Tensile modulus, σ_u: Ultimate tensile strength, ε_u: Elongation at failure, IS: Impact Strength

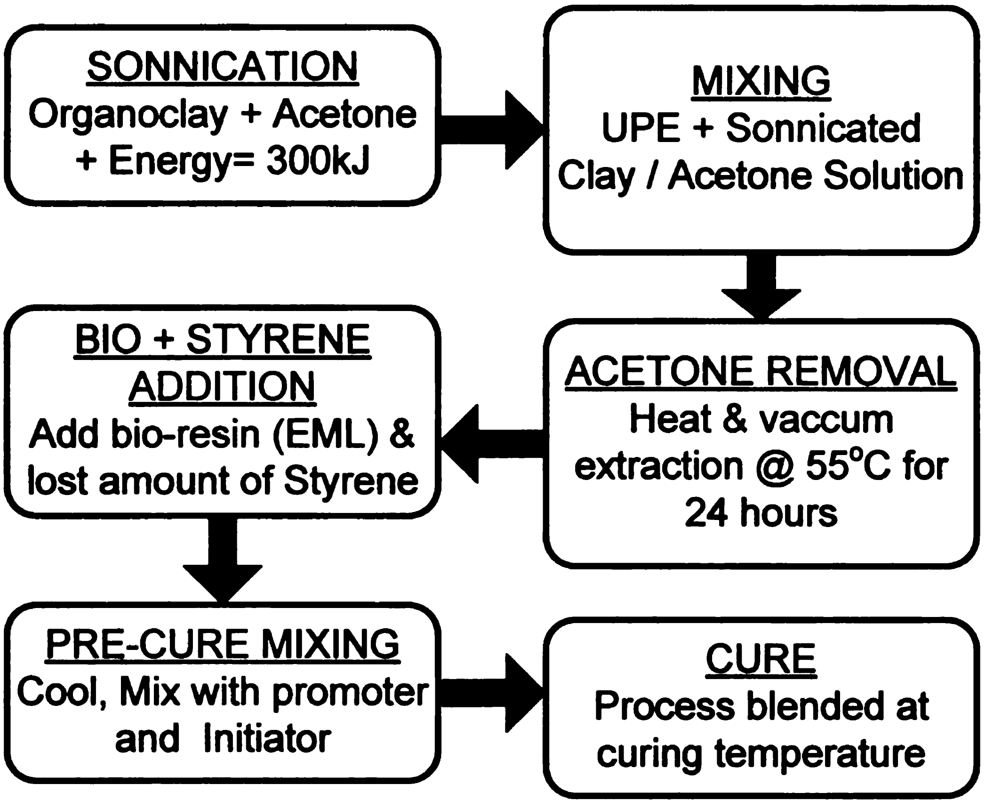

Figure 6-1. Schematic of processing technique of nanoclay reinforced UPE + bio-resin blends

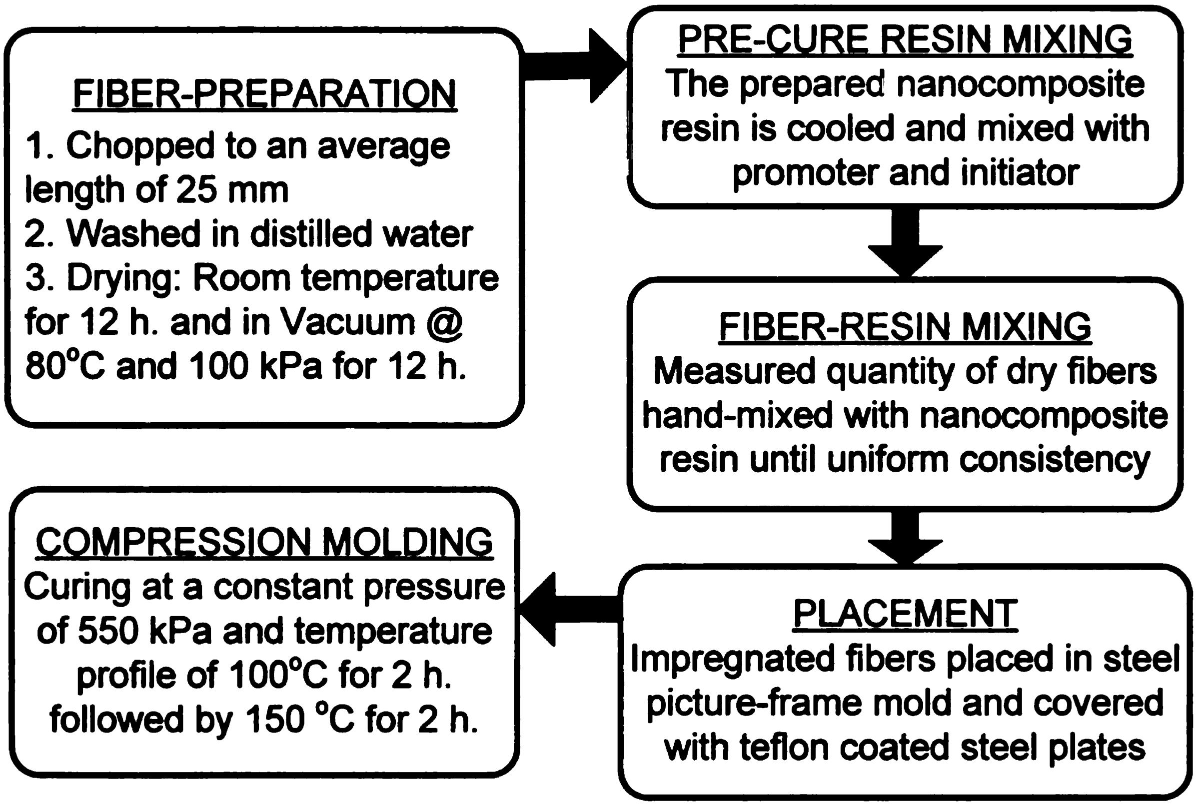

Figure 6-2. Manufacturing of nanoclay reinforced biocomposites

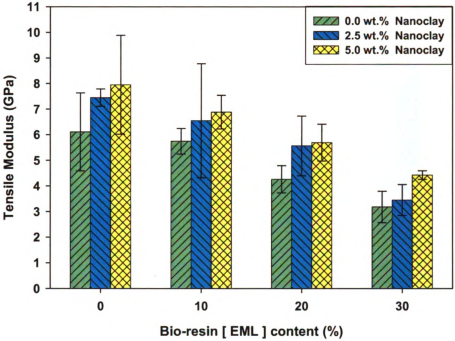

Figure 6-3. Experimental tensile modulus of biocomposite.

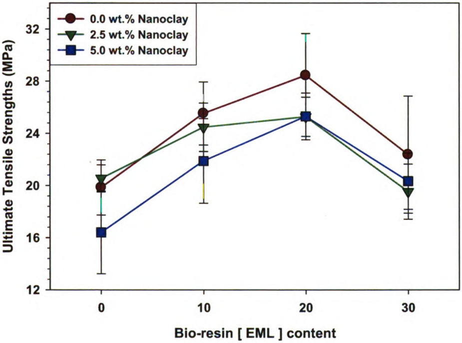

Figure 6-4. Experimental ultimate tensile strengths of biocomposites

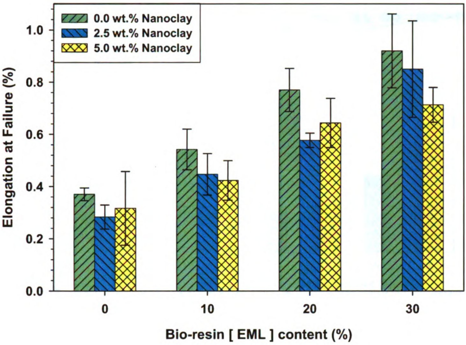

Figure 6-5. Experimental elongations at tensile failure of biocomposites

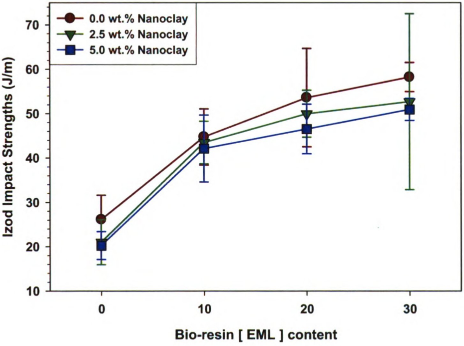

Figure 6-6. Impact strengths of biocomposites from notched Izod tests

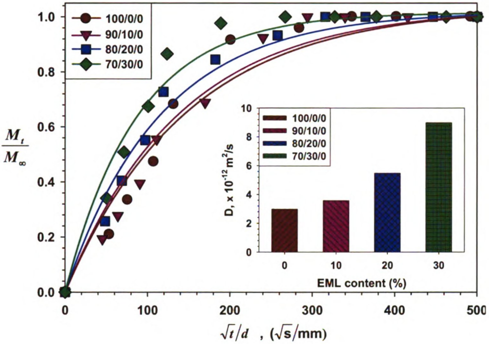

Figure 6-7. Moisture diffuisivity of neat resin (no nanoclay) biocomposites.

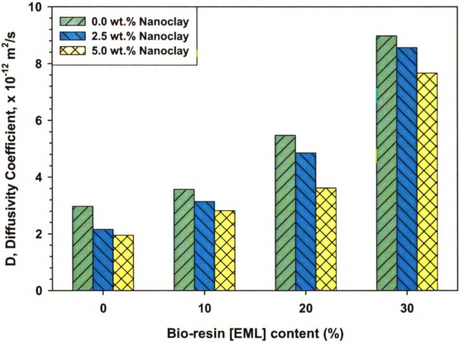

Figure 6-8. Summary of diffusion coefficients of various biocomposites.

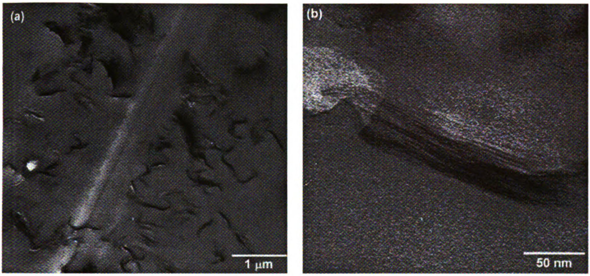

Figure 6-9. TEM micrographs showing nanoclay dispersion and morphology. a) Nanocomposite resin in Biocomposite E (100/0/2.5) showing good dispersion with partially exfoliated and intercalated morphology in a resin system (scale = 1µm), and b) High magnification image of an intercalated gallery in nanocomposite resin of Biocomposite I (100/0/5.0) (scale = 50 nm).

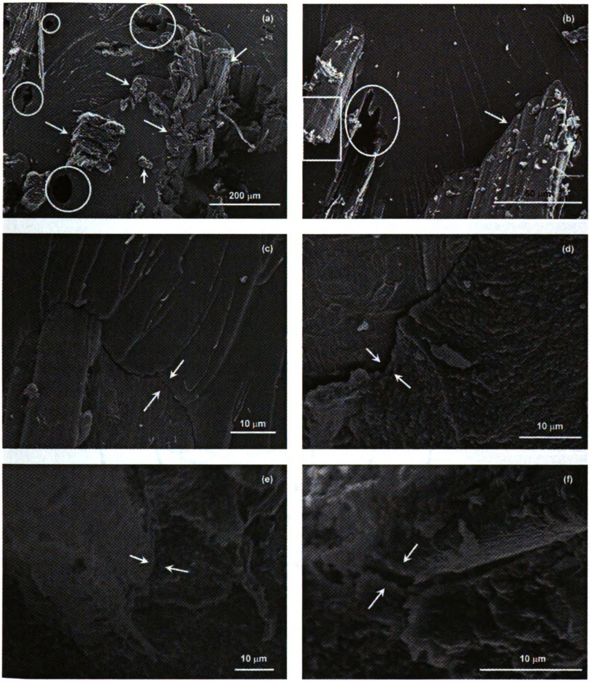

Figure 6-10. Tensile fracture surface analysis: a) Generic low magnification failure surface showing fiber-pull-out (encircled) and fiber fracture (arrows) regions, (scale bar = 200 μm), b) Magnified regions showing fiber-pull-out (encircled), fiber fracture (boxed) regions and fiber-matrix interfacial gap (arrows), (scale bar = 50 μm). Fiber-matrix interfacial gap: c) Biocomposite A (100/0/0), d) Biocomposite D (70/30/0), e) Biocomposite I (100/0/5.0), and f) Biocomposite L (70/30/5.0). (Images c to e, Scale bar = 10 μm).

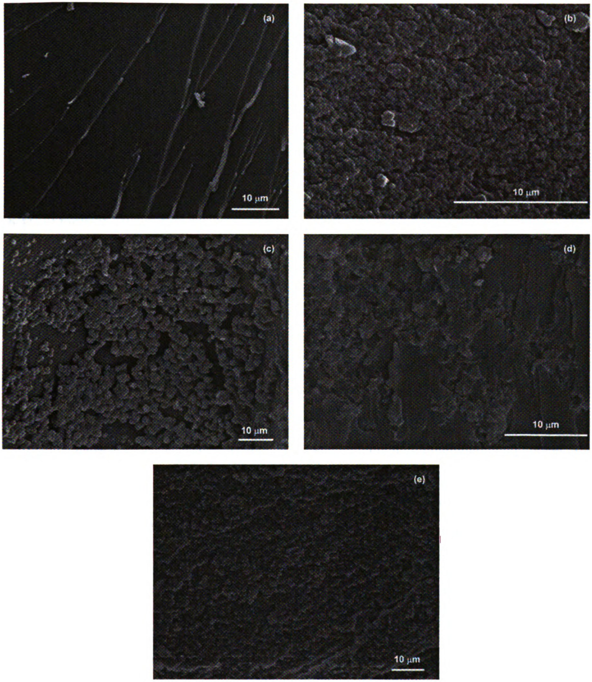

Figure 6-11. Matrix regions of Tensile fracture surfaces: a) Biocomposite A (100/0/0), b) Biocomposite D (70/30/0), well blended UPE/EML region, c) Biocomposite D (70/30/0), phase-separated, bio-resin enriched region, d) Biocomposite I (100/0/5.0), and f) Biocomposite I (70/30/5.0).

6.8 References

[6-1]. Haq M, Burgueño R, Mohanty AK. Misra, M. Hybrid Bio-based Composites from blends of Unsaturated Polyester and Soy Bean Oil Reinforced with Nanoclay and Natural Fibers," Compos Sci Technol 2008, 68:3344-3351.

[6-2]. O'Donnell A, Dweib MA, Wool RP. Natural fiber composites with plant oil based resin. Compos Sci Technol 2004, 64:1135-1145.

[6-3]. Shibata M, Ozawa K, Teramoto N, Yosomiya R, Takeishi H. Biocomposites made from short abaca fiber and biodegradable polyesters. Macromol Mater Eng 2003; 288:35-43.

[6-4]. Morye SS, Wool RP. Mechanical properties of glass /flax hybrid composites based on a novel modified soyabean oil matrix material. Polym Compos 2005, 26:407-146.

[6-5]. Bodros E, Pillin I, Montrelay N, Baley C. Could biopolymers reinforced by randomly scattered flax fibers be used in structural applications. Compos Sci Technol 2007; 67:462-470.

[6-6]. Burgueño R, Quagliata, MJ, Mohanty AK, Mehta GM, Drzal LT, Misra M. Load bearing natural fiber composite cellular beams and panels. Composites: A 2004; 35:645-656.

[6-7]. Miyagawa H, Mohanty AK, Burgueño R, Drzal LT, Misra M. Novel bio-based resins from blends of functionalized soyabean oil and unsaturated polyester resin. J Polym Sci, Part B: Polym Phys 2007; 45: 698-704

[6-8]. Mohanty, A.K, Misra M, Hinrichsen, G. Biofibers, Biodegradable Polymers and Biocomposites: An Overview. Macromol Mater Eng 2000; 276/277:1-24.

[6-9]. Nickel J, Riedel U. Activities in biocomposites. Mater Today 2003; 6:44-48.

[6-10]. Miyagawa H, Mohanty AK, Burgueño R, Drzal LT, Misra M. Development of bio-based unsaturated polyester containing functionalized vegetable oils. Ind Eng Chem Res 2006; 45:1014-1018.

[6-11]. Pinnavaia TJ, Beall GW. Polymer-Clay Nanocomposites, John Wiley & Sons, Ltd., 2001.

[6-12]. Le Baron PC, Wang Z, Pinnavaia TJ, Polymer – layered silicate nanocomposites: an overview. Appl Clay Sci. 1999; 15:11-29

[6-13]. Alexandre M, Dubois P. Polymer-layered silicate nancomposites: preparation, properties and uses of a new class of materials. Mater Sci Eng R 2000; 28:1-63.

[6-14]. Hussain F, Hojjati M, Okamoto M, Gorga RE. Polymer-matrix Nanocomposites, Processing, Manufacturing and Application: An Overview. J Comp Mats 2006; 17: 1511-1575.

[6-15]. Miyagawa H, Mohanty AK, Burgueño R, Drzal LT, Misra M. Characterization and thermophysical properties of unsaturated polyester-layered silicate nanocomposites. J Nanosci Nanotech 2006; 6:464-471.

[6-16]. Haq M, Burgueño R, Mohanty AK, Misra M. Bio-based unsaturated polyester/layered silicate nanocomposites: characterization and thermo-physical properties. Composites: A 2009; 40:540-547.

[6-17]. Tsai JL, Wu MD. Organoclay effect on mechanical responses of glass/epoxy nanocomposites. J Compos Mater 2008; 42:553-568.

[6-18]. Kinloch AJ, Mohammed RD, Taylor AC, Sprenger S, Egan D. The interlaminar toughness of carbon fibre reinforced plastic composites using 'hybrid-toughened' matrices. J Mater Sci 2006; 41:5043-5046.

[6-19]. Kinloch AJ, Mohammed RD, Taylor AC, Sprenger S, Egan D. The effect of silica nano particles and rubber particles on the toughness of multiphase thermosetting epoxy polymers. J Mater Sci 2005; 40:5083-5086.

[6-20]. Gojny FH, Wichmann MHG, Fiedler B, Bauhofer W, Schulte K. Influence of nano-modification on the mechanical and electrical properties of conventional fiber-reinforced polymers. Composites: A 2005; 36:1525-1535.

[6-21]. Haq M, Burgueño R, Mohanty AK, Misra M. Development and Thermophysical Characterization of Clay Nanocomposites from Blends of Linseed oil and Unsaturated Polyester. Composites: A Communicated.

[6-22]. Haq M, Burgueño R, Mohanty AK, Misra M. Processing techniques for bio-based unsaturated-polyester/clay nanocomposites: tensile properties, efficiency and limits. Composites: A 2009; 40:394-403.

[6-23]. Vlasveld, D.P.N., Groenewold, J., Bersee, H.E.N., Picken, S.J. Moisture absorption in polyamide-6 silicate nanocomposites and its influence on mechanical properties. Polymer 2005; 46:12567-12576.

[6-24]. Mohanty AK, Misra M, Drzal LT. Surface Modifications of Natural Fibers and Performance of the Resulting Biocomposites: An Overview. Compos Interfaces 2001; 8:313-343.

[6-25]. Wang L, Wang K, Chen L, Zhang Y, He C. Preparation, morphology and thermal/mechanical properties of epoxy/clay nanoclay composite. Composites: A 2006; 37:1890-1896

[6-26]. Haq M, Burgueño R. Modeling and simulation of bio-based polymer/clay nanocomposites through a multi-level FE approach. In:Proceedings of Sixth

International conference on Computation of Shell & Spatial Structures. New York, May, 2008. SessionT-2-E.

Chapter 7. Analytical and Numerical Modeling of Mechanical and Barrier Properties of Clay/Polymer Nanocomposites

7.1 Introduction

Polymeric materials are often reinforced by stiff fillers to improve mechanical properties. The efficiency of reinforcement depends on the filler aspect ratio, the filler mechanical properties and the adhesion between the matrix and the filler [7-1]. Nanocomposites consisting of highly anisotropic clay platelets (layered alumino silicates, LAS) dispersed in polymeric matrix material are of interest for many important industrial applications [7-2]. Clays, or LAS, are composed of extremely thin (~1 nm) sheet like platelets that possess very large specific surface areas (SSA) and high aspect ratios. In addition, these platelets have an exceptionally high modulus in tension relative to most polymers and even many other types of fillers. Such properties enable the platelets, when dispersed in a polymer matrix, to carry a significant component of the applied load. Because of the high surface area and the small inter-particle distances, the platelets can, in principle, significantly alter the properties of the polymer matrix [7-3]. Research has shown that at very low concentrations (~5% by weight) the modulus has been increased by 100%. Considerable research has been performed on polymer/clay nanocomposites and apart from an increase in modulus, it has been observed that clay nanocomposites exhibit multi-functionality by exhibiting enhancement in many other physical properties including thermal, barrier, flammability resistance and tribological performance.

In order to efficiently exploit all the benefits that clay/polymer nanocomposites can offer it is important to understand the challenges that are faced relative to conventional fillers. The challenges include:

a) Appropriate dispersion of reinforcements in the resin systems

b) Interfacial issues: bonding, modeling, prediction of properties in the interfacial regime, interactions and functionalizations etc, and

c) Obtaining nano–structural influences and representative information about the clay structure property relationship and nano-mechanical mechanisms. Issues include stress transfer mechanisms and theoretical predictions to validate or explain the experimental results taking into considerations possible mechanisms at the nano-scale.

As discussed earlier, one of the major attractions of clay in polymers is the high SSA that provides exceptional enhancement of mechano-physical properties due at lower concentrations. At the same time, high SSA can induce undesirable effects. It introduces strong attractive forces between the clay particles, leading to excessive agglomeration. Hence, it becomes essential to separate them for the resin to penetrate/infiltrate between them. On the contrary, if the clay particles are not completely exfoliated, it may lead to intercalated morphologies that have lower aspect ratios and less SSA relative to an exfoliated case. Due to the lower aspect ratios and lower SSA, intercalated clay particles have relatively less ability to effectively transfer stresses and hence lead to lower mechanical properties. Hence the role of dispersion is essential to obtain proper SSA and high aspect ratios that increase the efficiency of the system. In this work, the dispersion is performed by using an ultra-sonnicator.

The next main issue in clay based composites is the interfacial adhesion between the matrix and clay particles. Sufficient stress transfer needs to take place to efficiently exploit the potential of clay as structural reinforcement. The interfacial bonding can be improved by proper functionalization of the clay surface. The choice of resin system and its compatibility with the nanoinclusion (in this case clay) is very essential to obtain the benefits offered by the nano-dimension. Research has shown that the surface modification of clay surface provides compatibility with resin systems and helps in efficient interfacial strengths [7-4].

The third main issue is the need nano-mechanical models or theories that can address the outstanding issues of the polymer - clay interface. Although several theories have been developed, it is important to efficiently relate the nano-mechanical mechanisms to the experimental results. This would help in optimizing mechanical performance and the development of tailorable materials.

The polymer nanocomposites used in this research have four major components: polyester based resin, bio-based resin, natural fibers, and nano-clay inclusions. Bio-based resin is included as it enhances the toughness of the resulting composite. More importantly, it is added as a replacement to the conventional petroleum based resins so as to make the resulting composites more eco-friendly. The purpose of this research is the development of load bearing components made of such biocomposites. In order to achieve this goal, it becomes essential to have a fundamental understanding of each component, its arrangement, proportion, and its effect on each of the mechanical parameter (stiffness, hygro-thermal properties, flammability, etc.) considered. Hence, it is required to find an optimal balance between the components that exhibit the best collective properties while hiding their intrinsic bad behavior. This understanding can be made possible by analytical and computational modeling.

As discussed earlier, the interfacial region plays an important role in the enhancement of the mechanical and physical properties of the resulting composite. The addition of bio-resin is suspected to introduce a layer around the nano-inclusions thereby reducing the efficiency of the stress transfer and hence a reduction in the overall mechanical properties. It is thus essential to have proper modeling techniques to efficiently model, design and optimize such materials.

In this study the modeling of biocomposites can be classified into two main categories: a) modeling of polymer nanocomposites (clay + resin system and no natural fibers), and b) modeling of natural fiber reinforced biocomposites.

Prediction of the mechanical properties of discontinuous fiber/flake composite materials has been a subject of extensive study. As discussed earlier, the modeling of heterogeneous materials (in our case, resin system and clay particles) involves many complexities that should take into account the morphologies of the inclusion and resin system. The models should also take into account the various physico-chemical mechanisms at the various scales. Numerous micromechanical models have been proposed to predict the elastic constants of discontinuous fiber/flake composites. These models generally depend on parameters including particle/matrix stiffness ratio Ep/Em, particle volume fraction fp, particle aspect ratio l/t, and orientation. Ep and Em denote the elastic modulii of the particle and the matrix, respectively. The prediction of homogenized properties of heterogeneous materials has been widely discussed in literature, and good overview is provided by Bohm [7-5]. Various theories and models have been proposed, and each of these models has its own advantages and limitations. Overall, the homogenization techniques can be classified into [7-5]: mean field approaches (MFA), variational bound methods, periodic microfield approaches (PMA's) / unit cell methods (UCM), embedded cell approaches (ECA), windowing approaches (WA), rules of mixtures and empirical formulae, such as Halpin-Tsai (H-T) methods etc.

In this chapter, section 7.2 will focus on micromechanical modeling of PNC's using MFA's and empirical methods. Section 7.3 will focus on modeling of these PNCs with UCM or Finite Element homogenization schemes, RVE studies etc. Lastly, Section 7.4 will compare some experimental results

7.2 Micromechanical Modeling of PNC's

As discussed earlier, it is essential to obtain the overall properties of a heterogeneous material. Various homogenization techniques exist and have been used widely in the past. The process of homogenization involves finding the average properties at a lower scale due to the macroscopic homogeneous deformations. In other words, it involves finding elastic constants and stress-strain (constitutive) relations that relate the two scales. Homogenization procedures aim at finding a volume element's (local) response to prescribed mechanical loads (macroscopic). The resulting homogenized behavior is idealized as statistically isotropic or statistically transversely isotropic. The classification of different models is based on the way they analyze / treat the local microscopic responses and then relate it with the macroscopic behavior.

The most commonly used analytical models are Halpin-Tsai and Mori Tanaka (Tandon-Weng and Hui-Shia) models. In this section, these models are briefly compared and discussed. These theories/models differ in regard to their treatment of the filler geometry; however, they show analogous responses to how composite modulus responds to the filler properties.

7.2.1 Mori Tanaka Estimates

Mori-Tanaka (M-T) estimates are popular micromechanical modeling techniques quite successful for conventional composites based on the mean field approach (MFA), namely the Eshelby Equivalent Inclusion method [7-6]. M-T average stress theory was derived on the principles of Eshelby's inclusion model for predicting an elastic field in and around an ellipsoidal particle in an infinite matrix [7-3]. To account for finite filler concentrations, Mori and Tanaka, however, considered a non-dilute composite consisting of many identical spheroidal particles that cause the matrix to experience an average stress different from that of the applied stress. To satisfy equilibrium conditions the volume average over the entire composite was forced to equal the applied stress [7-3].

One way for achieving the accountability of inter-particle interaction/stresses consists of approximating the stresses acting on an inclusion, which may be viewed as the perturbation stresses caused by the presence of other inclusions superimposed on the applied far field stress, by an appropriate average matrix stress. Effective field theories of this type are generically called Mori-Tanaka (M-T) methods or Equivalent Inclusion Average Stress (EIAS) approaches [7-5].

Although M-T model is successful, it has some concerns regarding its application to nanocomposites. The first is that although the M-T method is predominantly an energy method, it is based on the Eshelby equivalent inclusion method which assumes a dilute suspension of particles; that is, the particles do not interact. Thus, particle interactions are accounted for only at high volume fractions, but are effectively ignored for low volume fractions. For clay polymer nanocomposites (CPNC)s, although reinforcement volume fractions are very low, the large number of particles with high aspect ratio suggests that particle interactions will have a significant influence on mechanical properties. Another concern is that the assumption of a completely random flake orientation suggests that the nano-composite is isotropic, which is not often the case [7-6].

The Tandon – Weng model and Hui-Shia models are the two most commonly cited methods in the literature which are based on the Mori-Tanaka estimates and are briefly discussed in the following sections.

Tandon - Weng Model

As discussed earlier, Tandon-Weng used the average stress assumption and Eshleby's solution to derive complete analytical solutions for the elastic moduli of an isotropic matrix filled with aligned spheroidal inclusions [7-3]. With the inclusions aligned along the x_1 direction, there are five independent elastic constants associated with the transversely isotropic composites. These are the longitudinal elastic modulus E_{11}, the transverse elastic modulus E_{22}, the in-plane shear modulus G_{12}, the out of plane shear modulus G_{23}, and the plane strain bulk modulus K_{23},. Their results for the five elastic constants are as follows [7-7]:

a) Longitudinal Elastic Modulus (E_{11})

$$\frac{E_{11}}{E_m} = \frac{A}{A + \phi_f(A_1 + 2\nu_m A_2)} \tag{7-1}$$

b) Transverse Elastic Modulus (E_{22})

$$\frac{E_{22}}{E_m} = \frac{2A}{2A + f_p[-2\nu_m A_3 + (1-\nu_m)A_4 + (1+\nu_m)A_5 A]} \tag{7-2}$$

c) In-plane Shear Modulus (G_{12})

$$\frac{G_{12}}{G_m} = 1 + \frac{f_p}{\dfrac{G_m}{G_p - G_m} + 2(1-f_p)S_{1212}} \tag{7-3}$$

d) Out of-plane Shear Modulus (G_{23})

$$\frac{G_{23}}{G_m}=1+\frac{f_p}{\dfrac{G_m}{G_p-G_m}+2(1-f_p)S_{2323}} \tag{8-4}$$

e) Plane Strain Bulk Modulus (K_{23})

$$\frac{K_{23}}{K_m}=\frac{(1+\nu_m)(1-2\nu_m)}{1-\nu_m(1+2\nu_{12})+f_p\{2(\nu_{12}-\nu_m)A_3+[1-\nu_m(1+2\nu_{12})]A_4\}/A} \tag{7-5}$$

f) Major direction Poisson's ratio of the composite (ν_{12})

The major direction Poisson's ratio ν_{12} of the composite is not an independent modulus; it is related to the other elastic constants by:

$$\nu_{12}{}^2=\frac{E_{11}}{E_{22}}-\frac{E_{11}}{4}\left(\frac{1}{G_{23}}+\frac{1}{K_{23}}\right) \tag{7-6}$$

After finding E_{11}, E_{22} and G_{23} from the above equations, ν_{12} is directly related to K_{23} and hence Equation (7-5) is implicit and can be solved by a simple iterative procedure.

In the above equations, f_p is the filler volume fraction, ν_m is the poisson's ratio of the matrix, ν_{12} is the major Poisson's ratio of the composite and A_1, A_2, A_3, A_4, A_5, *and* A are the functions of the Eshelby's tensor and the properties of the filler. It is obvious that in the above equations when f_p is equal to zero the effective modulus of the composite reduce to that of the matrix and when $f_p=1$ each quantity reduces to that of the inclusions.

Equations (7-1) and (7-2) are dependent upon the shape of the filler, e.g., fiber-like versus disk like ellipsoids, which are accounted for in Eshelby's tensor. Moreover, Equation (7-2) is used instead of Equation (7-1) when predicting modulus parallel to either major axis of a disk-like spheroid. Figure 7-1 shows the Mori–Tanaka physical representation of glass fibers and disk-like platelets and Table 7-1 lists the different equations used to calculate composite modulii along the three principal orthogonal directions.

Hui - Shia Model

Hui-Shia's model was derived from the Tandon-Weng model. Although Tandon-Weng model provides exact solution, it is rarely used in practice, perhaps due to its complexity [7-8]. Hui and Shia [7-8] developed simplified expressions for the effective moduli of unidirectionally aligned two-phase composites from Tandon and Weng's exact solution by making the assumptions that the Poisson's ratios of the inclusion and the matrix are the same and are equal to 0.5. Of the five independent elastic constants, only E_{11}, E_{22} are given here; since these are the most complex equations. For other constants, the same equations of the Tandon-Weng model are used as they are already very simple.

All modulii depend on a geometrical parameter g, which depends on the aspect ratio α. The geometrical parameter g is given by:

$$g = \begin{cases} \dfrac{\alpha}{(\alpha^2-1)^{\frac{3}{2}}}\left[\alpha(\alpha^2-1)^{\frac{1}{2}} - \cosh^{-1}(\alpha)\right] & \alpha \geq 1 \\ \dfrac{\alpha}{(1-\alpha^2)^{\frac{3}{2}}}\left[-\alpha(1-\alpha^2)^{\frac{1}{2}} - \cos^{-1}(\alpha)\right] & \alpha \leq 1 \end{cases} \tag{7-7}$$

It can be shown that $g(\alpha = 1) = 2/3$. The case of $\alpha \succ\succ 1$ corresponds to fiber like inclusions whereas $\alpha \prec\prec 1$ corresponds to flake like or disc-shaped inclusions (see Figure 7-1). The simplified Hui-Shia equations for longitudinal and transverse tensile modulii are as follows:

Longitudinal Tensile Modulus (E_{11})

$$\frac{E_{11}}{E_m} = \frac{1}{1 - \frac{f_p}{\xi}} \tag{7-8}$$

where

$$\xi = f_p + \frac{E_m}{E_p - E_m} + 3(1 - f_p)\left[\frac{(1-g)\alpha^2 - (g/2)}{\alpha^2 - 1}\right] \tag{7-9}$$

Transverse Tensile Modulus (E_{22})

$$\frac{E_{22}}{E_m} = \frac{1}{1 - \frac{f_p}{4}\left[\frac{1}{\xi} + \frac{3}{\xi + \Lambda}\right]} \tag{7-10}$$

where

$$\Lambda = (1 - f_p)\left[\frac{3(\alpha^2 + 0.25)g - 2\alpha^2}{\alpha^2 - 1}\right] \tag{7-11}$$

The formulae used for the derivation of the above modulii are similar to Tandon-Weng's and are described in detail in the literature [7-7][7-8].

Empirical Models - Halpin Tsai Models

Halpin and Tsai developed a well known composite theory for predicting the stiffness of unidirectional composites as a function of aspect ratio. This theory is based on the early micromechanics works of Hermans and Hill [7-5]. Hermans generalized the form of Hill's self-consistent theory by considering a *single fiber* encased in a cylindrical shell of matrix that is embedded an infinite medium assumed to possess the average properties of the composite. Halpin and Tsai reduced Hermans' results into a simpler analytical form adapted for a variety of reinforcement geometries, including discontinuous filler reinforcement [7-3]. The material properties by Halpin-Tsai (H-T) model are as follows:

a) Stiffness estimate in the fiber direction (E_{11})

$$\frac{E_{11}}{E_m}=\frac{1+\zeta\eta f_p}{1-\eta f_p} \tag{7-12}$$

where E_{11} and E_m represent the Young's modulus of the composite and matrix, respectively; ζ is a shape parameter dependent upon filler geometry and loading direction, f_p is the volume fraction of filler; and η is given by:

$$\eta=\frac{\dfrac{E_p}{E_m}-1}{\dfrac{E_p}{E_m}+\zeta} \tag{7-13}$$

where E_p represents the Young's modulus of the filler, and the shape parameter ζ is related to the aspect ratio (l/t), where, l and t are the length and thickness of the fiber respectively:

$$\zeta=2\left(\frac{l}{t}\right) \tag{7-14}$$

The longitudinal modulus E_{11} is very sensitive to the aspect ratio (see Figure 7-2) relative to other properties.

b) In-plane shear modulus estimate (G_{12})

G_{12} is estimated by noting that it must lie between the shear stiffness of the filler (G_p) and the shear stiffness of the matrix (G_m). G_{12} is not sensitive to the (l/t) ratio and hence may be approximated as [7-9]:

$$\frac{G_{12}}{G_m} = \frac{1+\zeta\eta f_p}{1-\eta f_p} \tag{7-15}$$

where,

$$\eta = \frac{\frac{G_p}{G_m}-1}{\frac{G_p}{G_m}+\zeta} \tag{7-16}$$

$$\zeta = 1 \tag{7-17}$$

Hence, the modulus perpendicular to the fiber direction (transverse to the fiber direction) E_{22}, in-plane Shear Modulus G_{12}, and in-plane Poisson's ratio are insensitive to the aspect ratio and are obtained from Equations (7-12) to (7-15) by substituting the aspect ratio of (l/t =1).

c) Stiffness estimate transverse to the fiber direction (E_{22})

Similar to G_{12}, E_{22} is least dependent on aspect ratio and can be obtained from Equations (7-12) to (7-15) by substituting the aspect ratio (l/t =1).

c) Poisson coefficient estimate (ν_{12})

Similar to the discussion of G_{12}, ν_{12} is bounded between the filler (ν_p) and matrix ν_m) Poisson ratios. For large values of (l/t), ν_{12} is close to the rules of mixtures, (Equation (7-18)) but probably above this estimate. Errors introduced by this estimate are not critical as most lamination calculations are not sensitive to ν_{12}[7-9]

$$\nu_{12} \sim \nu_p f_p + \nu_m f_m \tag{7-18}$$

where f_p and f_m are the volume fractions of the filler and the matrix respectively.

It should be noted that in the Halpin-Tsai equations, the parameters least sensitive to the shape factor ζ are obtained by making the shape factor $\zeta = 1$. It should be noted as ζ tends to zero, the Halpin-Tsai theory converges to inverse rule of mixtures (lower bound) and as ζ tends to infinity, the theory reduces to the rule of mixtures (upper bound). Furthermore, the Halpin–Tsai equations retain the same form for discontinuous cylindrical fibers and lamellar shape reinforcements, such as ribbons or rectangular platelets. However, when calculating elastic moduli E_{11} and E_{22} in the case of ribbons or rectangular platelets, ζ is equal to (l/t) and (w/t) respectively, where 'l' is the length, 'w is the width and 't' is the thickness of the dispersed phase. Figure 7-1 shows the two types of fillers examined in this work, their orientation with respect to orthogonal axes and their corresponding Halpin–Tsai quantities. Dispersed clay platelets are expected to resemble disks as depicted in Figure 7-1, where **E | |** and **E î** are the composite modulus parallel (longitudinal) and perpendicular (transverse) to the major axis of the filler.

Comparison of Models, Limitations

A number of assumptions are inherent to both M-T estimates and HT methods. The filler and matrix are linearly elastic, isotropic, and firmly bonded. The filler is perfectly aligned, asymmetric, and uniform in shape and size. Particle – particle interactions are not explicitly considered. Of course, for all composite theories the properties of the matrix and filler are considered to be identical to those of the pure components. In addition to these assumptions, there are number of differences between the two theories that are worth noting. First, the Mori–Tanaka theory treats fibers and disks as ellipsoidal particles, whereas the Halpin–Tsai equations treat a fiber as a fiber and disk as a rectangular platelet; the later disparity in the Halpin–Tsai equations is of some concern, since the length and, in turn, aspect ratio across a disk is not constant as shown in Figure 7-3. Second, the Halpin–Tsai equations for E_{11} and E_{22} are independent of the Poisson's ratio of the filler or the matrix. Third, the Halpin–Tsai equations for transverse modulus, i.e., perpendicular to the filler's major axis, are independent of aspect ratio. Last, it is important to emphasize that numerous complexities arise when comparing composite theories to experimental data, particularly for polymer layered silicate nanocomposites. Table 7-2 summarizes some of the issues involved. In addition to physical disparities between theory and experiment, the choice of composite theory will also dictate how well the predicted and observed properties agree [7-3].

Comparison of Theoretical Models & Validation:

The following section compares / validates the existing models by recreating the models in the literature. This was done by writing custom algorithms in Matlab® and recreating the plots in the literature, thereby validating the code. The validation of the algorithms enable comparison of analytical model predictions with experimental and FE models. Since the validation of the algorithm was done with results from the literature [7-7], the material properties of the constituents were taken from the literature [7-7] as well. Figure 7-4 to Figure 7-15 provide some results from the algorithm. The predicted results agreed well with published results [7-7]. For brevity, the plots from the literature [7-7] are not provided, but are exactly the same as those provided here. The properties used in the validation of the model are as follows [7-7]:

E_m = Elastic Modulus of Matrix = 2.76 Gpa,

E_p = Elastic Modulus of Inclusion = 72.4 Gpa,

ν_m = Poisson's Ratio of Matrix = 0.35,

ν_p = Poisson's Ratio of Inclusion = 0.20.

Sub-Conclusions of Analytical Modeling

The analytical models of Halpin- Tsai and Mori-Tanaka theories have been widely used in the literature and these theories have been found to satisfactorily capture the clay characteristics. The two theories differ in regard to their treatment to filler geometry; however, they both show analogous responses to how the composite modulus responds to filler aspect ratio, modulus and orientation [7-3].

7.3 Unit Cell Methods / FE - RVE based method

As discussed in earlier sections, various homogenization techniques exist and have been used widely in the past. With the advancement and availability of computational power unit cell methods (UCM) or periodic microfield approaches (PMA) are gaining importance. In UCM, the real inhomogeneous material is approximated by an infinitely extended model material with a periodic phase arrangement. The corresponding periodic microfields are usually evaluated by analyzing unit cells also known as representative volume elements (RVEs). These RVEs may describe microgeometries that may be rather simplistic or highly complex and are solved via analytical, numerical or finite element methods [7-5].

"Unit cell methods are typically used for performing materials characterization of inhomogeneous materials in the nonlinear range, but they can also be employed as micromechanically based constitutive models. The high resolution of the microfields provided by PMAs can be very useful for studying the initiation of damage at the microscale. However, because they inherently give rise to periodic configurations of damage, PMAs are not well suited for investigating phenomena such as the interaction of the microstructure with macroscopic cracks. Periodic microfield approaches can give detailed information on the local stress and strain fields within a given unit cell, but they tend to be computationally expensive [7-5]."

Moreover, the concept of homogenization in the MFA's has certain limitations due to the inherent assumptions like the particles being perfectly aligned, perfectly bonded, etc. The unit cell (RVE) methods allow for an easier account of complex micro structural morphology and enabling the investigation of the influence of different geometrical features of the overall response. In discrete microstructures, homogenization is carried out by selecting a local Representative Volume Element (RVE) that closely represents the actual structure. The macroscopic properties are then derived from proper analyses of the RVE

In this work RVEs of polymer nanocomposites were created and analyzed. The initial task was to validate the results from these analyses with results from literature [7-1]. RVE selection is very important for the efficiency of the analyses. Initially, RVEs from literature were replicated [7-1] and validated. The following sections summarizes these studies.

7.3.1 Representative Volume Element (RVE)- Selection and Boundary Conditions

As discussed in the previous section, RVE analyses assume a periodic repetition of the RVE itself in an infinite media to replicate the macroscopic behavior. Hence, it is essential to select a proper RVE as the success of a micro mechanical model depends on the selection of RVE. The RVE should be selected such that the local microscopic material structure can be considered as the RVE is surrounded by copies of itself. Adjacent RVE's should not overlap. No voids (discontinuities) should exist between boundaries of adjacent RVE's. Most importantly, the RVE should be large enough to represent the microstructure with enough detail and small enough to allow efficient computational modeling.

Periodic Boundary Conditions (PBCs)

In this work periodic boundary conditions (PBCs) are assumed for micromechanical modeling of polymer/clay nanocomposites. For micromechanical modeling through RVE analyses, proper boundary conditions should be provided to the RVE's such that they represent the actual loading conditions of the macroscopic state. BC's should be provided in such a way that all deformation modes appropriate for the load cases can be attained in the RVE.

For periodic boundary conditions, the following compatibility demands with respect to opposite edges should be met. Two adjacent RVES should show identical deformations without overlapping or separation. Compatibility implies that the shape of both boundaries remain identical and stresses acting along boundaries are opposite in sign (stress equilibrium). The deformation boundary conditions are represented schematically in Figure 7-16 [7-5].

For heterogeneous materials, as in the case of most composite materials, the distribution of the materials is mostly random. For the present case, the clay particles are randomly distributed in the RVE. Although the particles are randomly distributed, the volume fraction of the RVE is maintained. A series of analyses with same volume fractions is performed with different random distributions and the average of such analyses was taken as the representative result for the particular reinforcement volume fraction.

As discussed earlier, a RVE must closely describe the composite. During the random distribution, the particles may be placed closed to the edge of the RVE, in which case, part of the inclusions are lost (Figure 7-17a). This causes reduction in the particle volume fraction inside the RVE. In order to overcome this problem, the inclusions that are randomly generated, and which are truncated at the edges, need to be placed back in to the RVE. This is done by bringing back the truncated part of the inclusion in to the RVE at the same level (y-axis) of the RVE (Figure 7-17b). This process ensures that the desired volume fraction is achieved and introduces periodicity in the particle distribution. Figure 7-18 shows the particle periodicity applied to the RVEs studied in this work (encircled regions in Figure 7-18).

The RVEs similar to those shown in Figure 7-18 were created and analyses were performed to obtain thermo-mechanical properties. The studies and results are described in the following section.

RVE Studies & Limitations

As discussed in earlier sections, proper selection of RVE is essential for the success of the analyses performed. Also, the RVE should be selected in a way that it is large enough to represent the actual structure and small enough to have computational efficiency. In this work, the initial RVE size was obtained from literature [7-1], wherein plane-strain analyses were performed on a rectangular RVE having dimensions of length and breadth that were 1000 and 500 times of the thickness of the clay particle, respectively. A sample RVE used in the work is shown in Figure 7-19.

Creation of the RVE with random distribution of clay particles, periodicity in distribution and associated modeling was done in a custom program written in Matlab® environment. Also, the program generated an input file for the respective clay distribution for a finite element program (ABAQUS®). The generated input file was used to perform plane strain finite element (FE) analyses on different distributions and volume fractions. Figure 7-19a shows the RVE generated from the custom Matlab program and its associated FE model is shown in Figure 7-19b.

7.3.2 RVE Analyses

The objective of the RVE analyses is to obtain the homogenized properties or the elastic tensor of the resulting composite. Apart from the mechanical stresses, the RVE analyses could also be used to obtain thermal and barrier properties. The following parameters (in 2D, plane strain) were sought from the RVE analyses:

a) Longitudinal Modulus (E_{11})

b) Transverse Modulus (E_{22})

c) Poisson's ratio (ν_{12}) and resulting Shear modulus (G_{12})

d) Linear Coefficient of thermal expansion in principal directions (α_{11} and α_{22})

e) Diffusion / permeability parameters.

The modulus parameters have been extensively studied and the results from RVE analyses were found to compare reasonably with those in literature [7-1]. Figure 7-20 shows the stress contours of one of the RVE analyses.

As discussed earlier, the RVE must represent the actual composite as close as possible. The polymer/clay morphologies can be broadly classified into four types: a) agglomerated b) exfoliated, c) intercalated and d) partly exfoliated and intercalated. The agglomerated case is not considered as it does not offer the benefits of PNCs.

The exfoliated case offers the highest enhancement of the properties and is achieved with proper processing techniques, especially at low concentrations. The RVEs corresponding to exfoliated cases have been discussed and shown in Figure 7-18 to Figure 7-20. At the same time, at higher concentrations it is difficult to obtain exfoliated morphologies. In most cases, there is a combination of exfoliated and intercalated morphologies. Hence, the RVE should be capable of modeling and analyzing a combination of exfoliated and intercalated morphologies.

Figure 7-19 shows an RVE for the exfoliated case. Similarly, Figure 7-20 shows FE model for an intercalated case. It can also be seen in Figure 7-20, the mesh used in FE model is very fine compared to that shown in Figure 7-19. In the RVE studies, mesh thickness was also studied. Finer mesh thickness will reduce FE associated problems of element distortion etc. (see Figure 7-21 to Figure 7-24).

The next main concern in the modeling of RVEs for PNCs is the modeling of interface. Research has shown that interfacial region plays a vital role in the stress transfer from the particle to the matrix. Research has also shown that the greatest difficulty in modeling PNCs comes in modeling these interfaces as the properties of the interfacial zone are questionable [7-1].

Moreover in this research, the addition of bio-based resin to petroleum based resin introduces a third phase into already existing two phase heterogeneous system. Also, research from our group has shown lower mechanical properties for bio based resins [7-10]. It is hypothesized that the bio-resins form a rubbery layer around the clay particles thereby affecting the stress transfer between the clay reinforcement and the polymer matrix. Even in the absence of the bio-resin, research has shown concerns about the anonymity of properties in the interface region [7-1]. It's commonly agreed that the properties in the interface are lower than that of the pristine resin in itself [7-1].

In order to model the interface of the PNCs, a third phase was introduced around the existing clay particles. The properties of the interface were modified as a function of the pristine polymer and the effect of interface properties. The results of the interface studies are shown in Figure 7-27

7.3.3 Results of RVE Analyses

Although, the RVE size analyses were performed, the study did not provide insight as linear elastic materials were used. Hence the RVE used by Sheng et al. [7-1] was used and the models were validated with results from this study. Not all RVE analyses and results are shown in this work, instead a few results on parameters of stiffness, effect of interface and coefficient of thermal expansion are provided.

Figure 7-25 shows the comparison of the stiffness obtained from RVE analyses and Mori-Tanaka (MT) estimates. MT estimates is used as the literature shows that MT methods provide a better comparison with experimental results. Figure 7-26 shows the variation of longitudinal stiffness with varying aspects ratios. Figure 7-27 shows the effect of interface properties on the longitudinal modulus of the resulting composite. The interface properties were varied as a percentage of the virgin matrix properties. It was observed that a reduction in the resulting stiffness of the composite occurs when the interface stiffness is lower that 20% of that of the virgin polymer. Although more studies need to be performed on this, it is clear that the interface properties of the bio-based polymer/clay nanocomposites being studied here are much lower than the actual resin system, as suggested by experimental results [7-10]. Similarly, Figure 7-28 shows the variation of thermal expansion with varying clay volume fraction.

The study on micromechanical modeling through RVE analyses was validated with results from reference [7-1] and the results were found to agree very well. Hence it can be concluded that RVE analyses such as those presented here can be used in future for prediction of mechanical and hygro-thermal properties of PNCs.

7.4 Comparison of Tensile Modulus Results with Theoretical and FE predictions.

As discussed earlier, the theoretical predictions by mean field approaches (Mori-Tanaka estimates) and empirical methods (Halpin-Tsai) have been used extensively and have been well documented [7-5]. Also, the unit cell method / RVE analysis using finite element has been gaining importance due to the availability of computational power and the ability to overcome the limitations of MFA and the assumptions in the theory [7-5].

In this work, the experimentally obtained tensile modulus was compared with the theoretical predictions of and RVE-FE results. For theoretical calculations, the modified Halpin-Tsai model was used. It has been shown and observed that the modified H-T model agrees very well with M-T models. The modified H-T model is mainly used for random inclusion composites. Figure 7-29 shows the comparison of the experimental results with theory and FE predictions for neat UPE (no bio-resin) with varying concentration. It can be observed that the experimental results are well predicted by our current RVE analyses.

7.5 Theoretical Models for Diffusion / Heat Transfer Problems

The mechanism of moisture diffusion in polymer-clay nanocomposites has been extensively studied [7-14]-[7-17][7-20][7-22]. Chen et al. [7-23] provide a good review of barrier properties of flake-filled membranes. In this work a brief theoretical background on the computation of diffusivity coefficients is explained.

The moisture absorption speed in polymers and nanocomposites can be compared quantitatively by determining the diffusion coefficient [7-15]. Moisture diffusion in a polymer with constant diffusivity, D, can be represented by Fick's second law, which describes the non-steady state diffusion of a substance, and can be represented in Cartesian coordinates x, y, z as [7-14]:

$$\frac{\partial c}{\partial t} = D\left(\frac{\partial^2 c}{\partial x^2} + \frac{\partial^2 c}{\partial y^2} + \frac{\partial^2 c}{\partial z^2}\right) \tag{7-19}$$

where c, is the concentration of the permeant, and t is the time. For one dimensional diffusion problem of an infinite plate with thickness d, Equation (7-19) reduced to:

$$\frac{\partial c}{\partial t} = D\frac{\partial^2 c}{\partial x^2} \tag{7-20}$$

The analytical solution of Equation (7-20) with constant boundary conditions and expressed in terms of moisture uptake (increase in sample mass) can be expressed as [7-14][7-16]:

$$\frac{M_t}{M_\infty} = 1 - \sum_{n=0}^{\infty}\frac{8}{(2n+1)^2\pi^2} \text{ x } \exp\left[\frac{-D(2n+1)^2\pi^2 t}{d^2}\right] \tag{7-21}$$

where M_t is the mass gain at any time t, and M_∞ is the maximum mass gain at equilibrium/steady state. At initial stages of diffusion, up to approximately $M_t/M_\infty \cong 0.5$, the increase in mass shows a linear relationship with the square root of time [7-15]. Also, at initial stages, Equation (7-21) can be approximated as [7-14][7-16]:

$$\frac{M_t}{M_\infty} = 4\sqrt{\frac{Dt}{\pi d^2}} \tag{7-22}$$

Therefore, the diffusivity coefficient, D, can be computed from the initial slope of the moisture gain, M_t/M_∞ versus time ($\sqrt{t}/d$) as:

$$D = \frac{\pi}{16}\left(\frac{M_t/M_\infty}{\sqrt{t}/d}\right)^2 \tag{7-23}$$

The diffusion coefficients, D, can be used to compare the diffusion speed in neat polymers and nanoclay reinforced resin systems [7-15]. When diffusion takes place through a polymer containing nanoclay platelets, or in general, flake like impervious particles, the diffusing molecules have to go around these platelets. The morphology that is likely to be most efficient is when these platelets are well exfoliated, aligned parallel to the thickness and the moisture diffusion takes place perpendicular to these platelets [7-16]. Using such simplifications, many models have been developed to predict moisture permeability in platelet filled polymers. Chen et al. [7-23] provide a good overview and comparison of these models. Nielsen [7-24] derived the relationship of diffusivity coefficient with the increased path the molecules have to travel due to the presence of impervious platelets [7-15][7-23]:

$$\frac{D_c}{D_0} = \frac{1}{1+(L/2W)V_f} \tag{7-24}$$

where D_c and D_0 represent the diffusion coefficient of composite and resin, respectively; L/W indicates the aspect ratio of the platelets and V_f is the volume fraction of platelets in the composite. The factor $\left(1+(L/2W)V_f\right)$ is termed as the tortuousity factor and denotes the extra distance to be travelled by the permeant [7-14]. In Equation (7-24), the solubility is assumed to be constant and hence, permeability coefficients can be replaced by diffusion coefficients [7-23]. Nielsen's model has been widely used but has many simplifications and hence its accuracy is limited to low volume fractions [7-15][7-23]. Nielsen's model assumes two-dimensional particle arrangement, with the platelets extending infinitely in the third direction. Moreover, the platelets are well-aligned and perfectly overlapped. Therefore Nielsen's model is conservative and provides diffusion coefficients that are lower than actual measurements [7-15]. In real nanocomposites, the platelets are randomly oriented, and do not exhibit perfect overlaps. Van Es [7-20] addressed the issue of overlap in two-dimensional composites by incorporating a overlap factor, γ :

$$\frac{D_0}{D_c} = \left(V_f \beta + 1 - V_f\right)\left[V_f \beta \gamma \left(1 - \gamma\right) + 1\right] \qquad (7\text{-}25)$$

$$\beta = \frac{8}{5\pi}\frac{L}{W}; \quad \frac{L}{W} = \text{length/thickness} = \text{aspect ratio} \qquad (7\text{-}26)$$

where γ is the overlap factor with $\gamma = \mathbf{0.5}$ for perfect overlap, $\gamma = \mathbf{0}$ for no overlap and $\gamma = \mathbf{0.25}$ for random oriented composites. Equation (7-25) still assumes impenetrable platelets parallelly aligned in a polymer matrix with varying overlap factors. Equation (7-25) has been found to agree reasonably for a larger range of particle concentration [7-15]. Moreover, it has been found that random placement of sheets leads to an overlap factor γ of 0.25 in Equation (7-25) [7-15]. In this work, the diffusivity coefficients of various bio-based nanocomposites were compared with the Van Es model as given in equation (7-25).

7.6 FE-RVE based Diffusion Modeling and Comparison with Experiments

The RVEs developed to model mechanical properties as explained in earlier sections were used to compute diffusivity coefficients. In this study, diffusion models for only neat UPE (no EML) were considered. Experimental data reveals considerable increase in diffusivity due to bio-resin addition. Hence in order to accurate model the diffusion behavior of nanoclay reinforced bio-based resins, the individual phases of UPE and bio-resin (EML) is essential. An optimization-based material layout study that determines the bio-resin distribution by matching effective model properties with presecribed thermo-elastic properties was performed (see Chapter 9). In the current work, the moisture properties were not used in the determination of material layout, and hence diffusion properties of only neat UPE polymer is modeled. The same approach can easily be extended to bio-based nanocomposites by using an enhanced RVEs that models three distinct phases, namely petro-, bio-resins and nanoclay.

7.7 Moisture Diffusion Results

The moisture diffusivity of nanoclay reinforced bio-based composites with varying bio-resin [EML] and nanoclay contents as described in Table 7-3 were studied. As described in Chapter 4, in order to accelerate the diffusion process the samples were placed at 50 °C instead of room temperature. Hence the resulting diffusion coefficient will be slightly larger than those observed at room temperature. Nevertheless, since all the bio-based nanocomposites were maintained at the same condition, the relative comparison and trends are assumed to remain the same and hence valid. The resin system corresponding to 0% EML content and 0% nanoclay corresponds to virgin UPE and is considered the baseline composite. Hence, results were compared relative to the baseline UPE. Table 7-4 summarizes the values of diffusion coefficients of the various nanocomposites in this study. Table 7-5 provides the comparison of moisture diffusion coefficients of various nanoclay reinforced bio-based composites (in %) in this study relative to virgin UPE.

7.7.1 Moisture diffusivity through neat resins (no clay)

Figure 7-31 shows the plots of moisture gain M_t/M_∞ versus time $\sqrt{t}/d$ for neat (no clay) resin systems. The experimental data is shown in symbols and the exponential fit is superimposed. The diffusivity coefficients were obtained by substituting the initial slope in Equation (8-23). The variation of the diffusivity coefficients D, with increasing bio-resin (EML) content are shown as an inset in Figure 7-31. Due to the absence of nanoclay, the diffusion coefficients obtained show the effect of blending bio-resin in virgin UPE. The diffusivity coefficient of virgin UPE was found to be 3.67×10^{-12} m^2/s. Pritchard [7-25] reports a lower value of diffusivity coefficient (3.0×10^{-12} m^2/s) for ortho-unsaturated polyester. The slightly higher experimental diffusion coefficient obtained in this work may be due to the differences in the resins and test conditions. The diffusivity coefficients increased with increasing bio-resin content. The increase in D due to increase in EML content followed a linear relationship. This was confirmed with a linear regression analysis that fit a line with a good R^2 value (0.96). The diffusivity coefficients increased by approximately 70%, 115% and 250% with addition of 10%, 20% and 30% EML content in UPE, relative to virgin UPE.

7.7.2 Moisture diffusivity in virgin UPE reinforced with nanoclay

The addition of nanoclay to virgin UPE, without addition of bio-resin (EML), was taken to represent the effect of nanoclay on diffusion properties. Figure 7-32 shows the plots of moisture gain M_t/M_∞ versus time $\sqrt{t}/d$ for neat (no clay) resin systems. The experimental data is shown in symbols and the exponential fit is superimposed in Figure 7-32. As expected, the diffusivity coefficients decreased with increasing nanoclay content. The diffusivity coefficients decreased by approximately 35% and 70% with addition of 2.5

wt.% and 5 wt.% nanoclay respectively. The reduction in diffusion coefficients indicates enhanced barrier properties due to the addition of nanoclay.

7.7.3 Moisture diffusivity in UPE/EML blends reinforced with nanoclay

Similar to the results of the neat UPE explained in previous section, the results of UPE/EML blends are presented here by studying the effect of nanoclay on different UPE/EML blends.

UPE/EML blend, 10%EML:

Figure 7-33 shows the plots of moisture gain M_t/M_∞ versus time $\sqrt{t}/d$ for UPE/EML blends containing 10% EML. The diffusion coefficient of 10% EML blend resin with no clay was approximately 70% higher relative to virgin UPE. Nevertheless, the addition of 2.5 wt.% and 5 wt.% nanoclay resulted in diffusion coefficients lower than virgin UPE by approximately 20% and 45% respectively. In other words, the nanoclay inclusions not only recovered the lost barrier properties due to the addition of 10% EML blend but enhanced it by approximately 44% at 5 wt.% nanoclay content.

UPE/EML blend, 20%EML:

Figure 7-34 shows the plots of moisture gain M_t/M_∞ versus time $\sqrt{t}/d$ for UPE/EML blends containing 20% EML. The diffusion coefficient of 20% EML blend resin with no clay was approximately 115% higher relative to virgin UPE. The addition of 2.5 wt.% nanoclay had diffusion coefficient similar to virgin UPE, while addition of 5 wt.% nanoclay resulted in diffusion coefficient lower than virgin UPE by approximately 30%. Similar to 10% EML blends, nanoclay reinforcements recovered the lost barrier properties due to the addition of 20% EML.

UPE/EML blend 30%EML:

Figure 7-35 shows the plots of moisture gain M_t/M_∞ versus time $\sqrt{t}/d$ for UPE/EML blends containing 30% EML. The diffusion coefficient of 30% EML blend resin with no clay was approximately 250% higher relative to virgin UPE. The addition of 2.5 wt% and 5 wt.% nanoclay resulted in diffusion coefficients 235% and 130% higher than virgin UPE. Although an improvement in barrier properties was observed with the addition of nanoclay, the enhancement was insufficient to recover the lost barrier properties from the addition of 30% EML.

7.8 Comparison of Diffusion Results: Experiment and Theory

The diffusion coefficients of various nanoclay reinforced bio-based composites in this study are summarized in Table 7-3 and Figure 7-36. The experimental diffusion coefficients were compared with the theoretical model by Van Es [7-20] as given in Equation (7-25). The experimental values of diffusion coefficients for neat resins (no clay) were used for D_0 values in Equation (7-25). An aspect ratio of 130 obtained from transmission electron microscopy observation, was used in theoretical predictions. Results indicated a large variation in model predictions and experimental results for samples with EML content of 30%. For better schematic representation, results corresponding to 30% EML content are not shown in figures, but are summarized in respective tables.

Figure 7-37 and Figure 7-38 provide a comparison of experimental results with the model predictions for clay contents of 2.5 wt.% and 5.0 wt.%, respectively, for various particle overlap factors. The particle overlap factor, γ, takes values of 0.5, 0.25 and 0, representing perfect overlap, random orientation and no overlap, respectively. In this section, results corresponding to $\gamma = 0.25$ and representing random orientation are discussed. For clay concentrations of 2.5 wt.%, theoretical prediction of diffusion coefficients for neat UPE, and 10% and 20% EML blends were lower by approximately 35%, 10% and 5% respectively. This Van Es theoretical model [7-20] assumes perfectly exfoliated and aligned clay morphology, whereas in reality, partially exfoliated and intercalated morphologies with random orientation exist. Hence the experimental diffusion coefficients are generally higher than theoretical predictions. Similarly for 5 wt.% clay, the theoretical predictions were lower by approximately 13%, 24% and 22% for neat UPE, 10% EML and 20% EML blends, respectively.

The experimental diffusion coefficients for 30% EMS blends were much higher than theoretical predictions and this discrepancy is attributed to the phase separation of the resins in the blend. The bio-resin seems to facilitate faster transport of water molecules through them and hence for phase-separated resins (30% EML), the experimental diffusivities were found to be much higher. The comparison of diffusion coefficients with theoretical predictions for all nanocomposites, including 30% EML blends are provided in Table 7-6 and Table 7-7 for clay contents of 2.5 wt.% and 5.0 wt.% respectively. Overall, up to 20% EML blends, the barrier properties lost due to addition of bio-resin were not only recovered, but enhanced by addition of nanoclay.

7.9 Discussion of Diffusion Results

Bio-based resins reinforced with nanoclay produce nanocomposites with synergistic, multifunctional properties [7-10][7-26]. It is preferred to increase the amount of bio-resin that can be blended with petroleum based resin, in order to make environmentally friendly composites. Nevertheless, the addition of bio-resin reduces stiffness, thermal and barrier properties [7-10][7-26]. As a result, the global objective of the research is to recover the properties lost due to the addition of bio-resin by reinforcing the resin blends with nanoclay. This work focused on moisture diffusion properties of nanoclay reinforced UPE/EML blends. Relative to virgin UPE, the addition of bio-resin increased the moisture diffusion, while addition of nanoclay reduced the moisture diffusion. The combination of bio-resin and nanoclay provides a synergy between the bio-resin and nanoclay.

The increase in the value of diffusion coefficient due to the addition of bio-resin (EML) was linear for EML contents up to 20% (Figure 7-36). For EML contents up to 20%, the barrier properties were not only recovered but enhanced by addition of nanoclay. Nevertheless, for EML contents of 30% phase separation of UPE/EML blend seems to dominate the moisture diffusion properties. Due to phase separation, the bio-resin (EML) acts as a weak material and a plasticizer, allowing faster path for the permeant molecules to travel. As a result, a sudden increase in diffusion coefficients was observed at 30% EML content. Enhancement due to nanoclay reinforcement was observed on samples with 30% EML contents, but the adverse effect of bio-resin dominated the enhancement provided by the nanoclay and hence total recovery was not possible.

The experimental results were compared with the theoretical Van Es model [7-20] as governed by Equation (7-25). Equation (7-25) assumes impenetrable platelets aligned parallel in a polymer matrix with varying overlap factors. In spite of these limitations, Van Es model [7-20] was chosen as it was reported to be valid for a wide range of clay concentrations [7-15], unlike Nielsen's model [7-24] which is valid for low nanoclay contents [7-15][7-23]. The theoretical model in equation (7-25) includes a particle overlap factor γ that defines the platelet morphology. The particle overlap factor takes values of 0.25, 0.5 and 0 corresponding to random orientation, perfect overlap and no overlap, respectively. In this work, experimental diffusivity coefficients were compared with all three values of γ. Figure 7-37 and Figure 7-38 provide the comparison of theoretical predictions and experimental results for clay contents of 2.5 wt.% and 5.0 wt.% respectively.

Theoretical predictions with perfect particle overlap ($\gamma = 0.5$) were farthest away from experimental results. The perfect overlap suggests that the permeant molecule has the greatest tortuous path, leading to lower diffusivity. In actual nanocomposites, perfect particle overlap does not exist and hence experimental results are generally higher than those predicted by the model. For randomly oriented particles in two dimensions, a particle overlap factor of 0.25 has been reported [7-15]. The theoretical predictions with $\gamma = 0.25$ were slightly lower than experimental values. In reality, the nanocomposites have a combination of both exfoliated and intercalated morphologies, but the model assumes exfoliated, aligned and randomly overlapped morphologies. Hence, experimental results are slightly higher than the model.

Finally, the theoretical predictions with $\gamma = 0$ showed relatively good agreement with experimental results compared to γ =0.25 and 0.5, especially for high bio-resin contents (>10% EML). A particle overlap factor $\gamma = 0$, suggests that no overlap occurs, indicating that through paths consisting of only polymer exists in between the particles. Although such morphology does not exist in reality, it seems that the presence of bio-resin allows the permeant molecules to travel faster. Moreover, the presence of intercalated morphologies, considerably reduces the particle overlap and tortuous path. The combination of intercalation and the presence of a faster permeant path due to the presence of bio-resin seems like a through path analogous to a no particle overlap. This is supported by the good agreement between theoretical predictions and experimental results for bio-based nanocomposites. Moreover, for particle overlap factor $\gamma = 0$, the model predictions were higher than experimental results for all nanocomposites except neat UPE with 2.5 wt.%. The theoretical model used does not hold for EML contents of 30% or more. The Van Es model [7-20] is not intended to model nanoclay reinforced bio-blends. Nevertheless, understanding the tortuous path and the effect of bio-resin addition on the permeant path can help in understanding diffusion phenomena taking place in the bio-based nanocomposites.

Overall, the diffusion study showed promise in the use of environmental friendly bio-based resin systems reinforced with nanoclay. The loss in barrier properties due to incorporation of bio-resin were not only recovered but enhanced by addition of nanoclay. Moreover, the results are indicative that the barrier properties of resulting nanocomposites can be tailored by controlling the concentrations of bio-resin and nanoclay content. The ability to recover the lost barrier properties due to bio-resin addition by incorporating nanoclay can allow the use of higher amounts of bio-resin, making the resulting nanocomposites more environmental friendly without sacrificing performance.

7.10 Conclusion

Modification of polymers at the nanoscale by addition of nano-inclusions has been shown to enhance mechanical properties and provide multifunctionality to the resulting polymer nanocomposites . However, quantitative evaluation of the mechanisms leading to these property enhancements as well as those that limit the performance of polymer nanocomposites is still limited due to experimental constraints. Computational simulation seems to be a good way to fill this gap. However, the simulation approach must be able to account for features of these materials at the nano- and micro- scales.

Mechanics-based models have proved to be successful in predicting homogenized properties where the filler length scale is in the order of tens of microns or larger. In nanoclay reinforced composites, depending on the processing, the clay morphology varies significantly. Exfoliated clays may be in range of nanometers and highly intercalated clay agglomerations may be in the order of micrometers. Moreover, it is commonly agreed that polymer clay nanocomposites exhibit both exfoliated hierarchical morphologies. Clearly, mechanics-based models cannot handle this complexity. The final and most important issue in modeling of polymer/clay nanocomposites is the particle-polymer interface. Depending on the chemical compatibility / functionalization of the nanoclay and polymer, the resulting interfacial properties will vary considerably. Additionally, in intercalated clay morphologies the properties of the material in galleries is not fully understood. The above mentioned issues specific to polymer/clay nanocomposites make modeling of such composites challenging. Finite element (FE) based modeling and simulation can address some of these issues and enable modeling of interfaces, different particle sizes and morphologies, nonlinear material properties and complex loading.

In this chapter, the analytical models were implemented and finite element models were developed to model polymer clay nanocomposites. Simulations were compared with experimental results for mechanical and diffusion properties. The accuracy of the simulations and the analytical model depends upon the detailed modeling of the microstructure. The models with least assumptions and most realistic modeling, as expected yielded better agreement with experiments.

7.11 Tables & Figures

Table 7-1. Modulus along different filler orientations (fibers and platelets) – Mori – Tanaka

Direction of Applied Load	**Mori Tanaka Composite Modulus**	
	Fibers	**Platelets**
1	E_{11}=E|| Equation (7-1)	E_{11}= Eî Equation (7-2)
2	E_{22}=Eî Equation (7-2)	E_{22}=E|| Equation (7-12)
3	E_{33}=Eî Equation (7-2)	E_{33}=E|| Equation (7-12)

Table 7-2. Important issues limiting ability to model the nanocomposites [7-3]

ISSUE	THEORY	EXPERIMENTAL
Filler Shape and Size	▪ Uniform shape ▪ Constant dimensions	▪ Non-uniform shape ▪ Distribution of lengths and thickness ▪ Imperfect exfoliation
Filler Orientation	▪ Unidirectional	▪ Some degree of misalignment
Filler Interface	▪ Filler and matrix are well bonded	▪ Imperfect bonding between filler and matrix
Filler Modulus	▪ Assumes filler modulus is same in all directions	▪ Filler is anisotropic
Matrix considerations	▪ Assumes matrix is isotropic	▪ Polymer chain orientation ▪ Presence of polymer crystallites
Filler concentration Effects	▪ No particle – particle interactions ▪ Ignores changes in viscosity ▪ No particle agglomeration	▪ Particle – particle interactions and agglomerations ▪ Changes in viscosity can alter morphology during injection molding ▪ Changes in crystalline morphology

Table 7-3. Experimental matrix showing specimen identification numbers and variation in clay and EML contents

Clay Content (wt.%)	Amount of EML replacing UPE in UPE-EML blend. (as % of UPE)			
	0	10	20	30
0.0	1	2	3	4
2.5	5	6	7	8
5.0	9	10	11	12

Table 7-4. Diffusivity coefficients of UPE/EML nanoclay composites.

Diffusivity Coefficients, D x 10^{-12} m^2/s				
Clay Content (wt.%)	Amount of EML replacing UPE in UPE-EML blend. (as % of UPE)			
	0	10	20	30
0.0	3.666	6.350	7.965	12.781
2.5	2.458	3.019	3.714	12.341
5.0	1.050	2.071	2.522	8.385

Table 7-5. Comparison of diffusivity coefficients of various nanocomposites with virgin UPE, expressed in percentage. Highlighted region shows nanocomposites that had equal or better barrier properties than virgin UPE.

Percentage increase of Diffusivity Coefficients, D relative to virgin UPE				
Clay Content (wt.%)	Amount of EML replacing UPE in UPE-EML blend. (as % of UPE)			
	0	10	20	30
0.0	0	73	117	249
2.5	**-33**	**-18**	**1**	237
5.0	**-71**	**-44**	**-31**	129

Table 7-6. Comparison of experimental results and theoretical predictions for various particle overlap factors, at nanoclay content of 2.5 wt.%

Diffusivity Coefficients, D x 10^{-12} m^2/s Clay Content = 2.5 wt.%, aspect ratio=130				
	Amount of EML replacing UPE in UPE-EML blend (as % of UPE)			
	0	10	20	30
Experiments	2.458	3.019	3.714	12.341
Theory, γ = 0.25	1.583	2.742	3.439	5.519
Theory, γ = = 0.50	1.505	2.608	3.271	5.249
Theory, γ = = 0.00	1.872	3.242	4.067	6.526

Table 7-7. Comparison of experimental results and theoretical predictions for various particle overlap factors, at nanoclay content of 5 wt.%

Diffusivity Coefficients, D x 10^{-12} m^2/s Clay Content = 5.0 wt.%, aspect ratio=130				
	Amount of EML replacing UPE in UPE-EML blend (as % of UPE)			
	0	10	20	30
Experiments	1.050	2.071	2.522	8.385
Theory, γ = 0.25	0.912	1.580	1.982	3.180
Theory, γ = = 0.50	0.837	1.450	1.818	2.918
Theory, γ = = 0.00	1.248	2.162	2.712	4.352

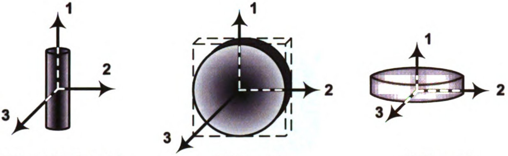

H-T and M-T model H-T model M-T model

α »1 – prolate shaped / fiber-like α « 1 – oblate shaped / disc-like

Figure 7-1. Physical representations, coordinate systems, Mori-Tanaka model – filler orientations [7-3]

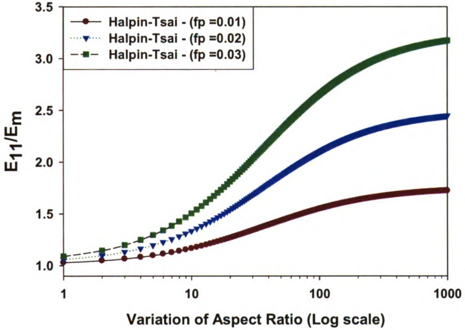

Figure 7-2 Variation of Longitudinal Modulus with Aspect ratio.

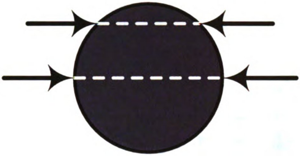

Figure 7-3. Variation in length and subsequently aspect ratio, across a dish-like platelet [7-3].

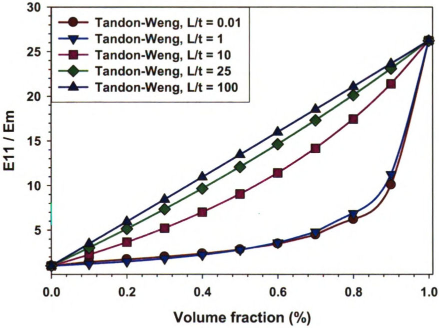

Figure 7-4. Variation of Longitudinal Modulus (E_{11}) with variation in f_p and (L/t) [7-7].

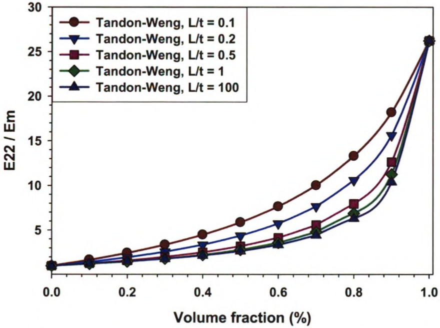

Figure 7-5. Variation of Transverse Modulus (E_{22}) with variation in f_p and *(L/t)* [7-7]

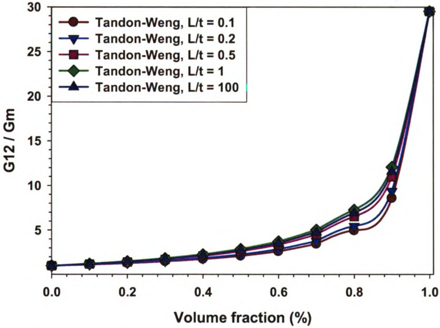

Figure 7-6. Variation of In-Plane Shear Modulus (G_{12}) with variation in f_p and *(L/t)* [7-7]

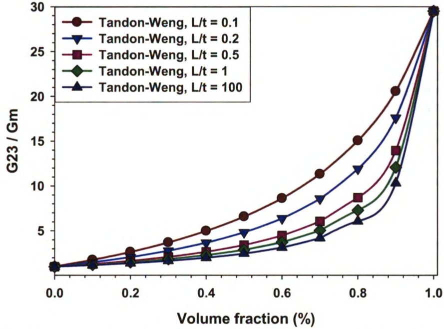

Figure 7-7. Variation of Out of-Plane Shear Modulus (G_{23}) with variation in f_p and *(L/t)* [7-7]

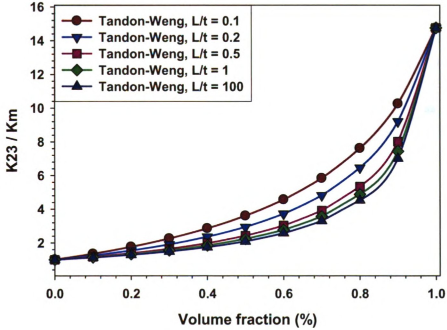

Figure 7-8. Variation of Plane Strain Bulk Modulus (K_{23}) with variation in f_p and *(L/t)* [7-7].

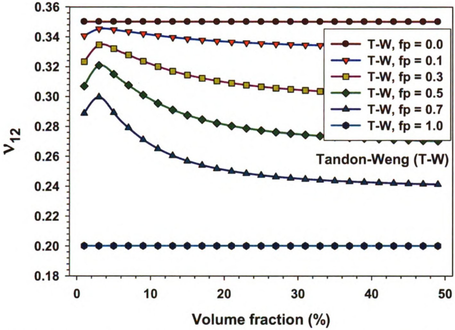

Figure 7-9. Variation of Major Poisson's Ratio (ν_{12}) with variation in f_p and (L/t) [7-7]

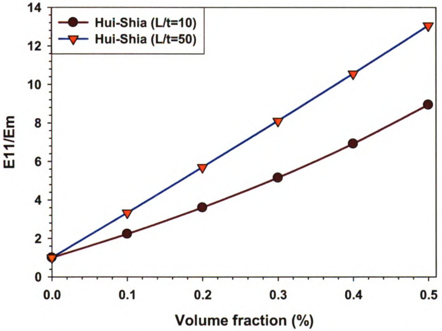

Figure 7-10. Variation of Longitudinal Modulus (E_{11}) with variation in f_p and (L/t)- Hui-Shia Fiber Like inclusions, (L/t = 10, 50) [7-7].

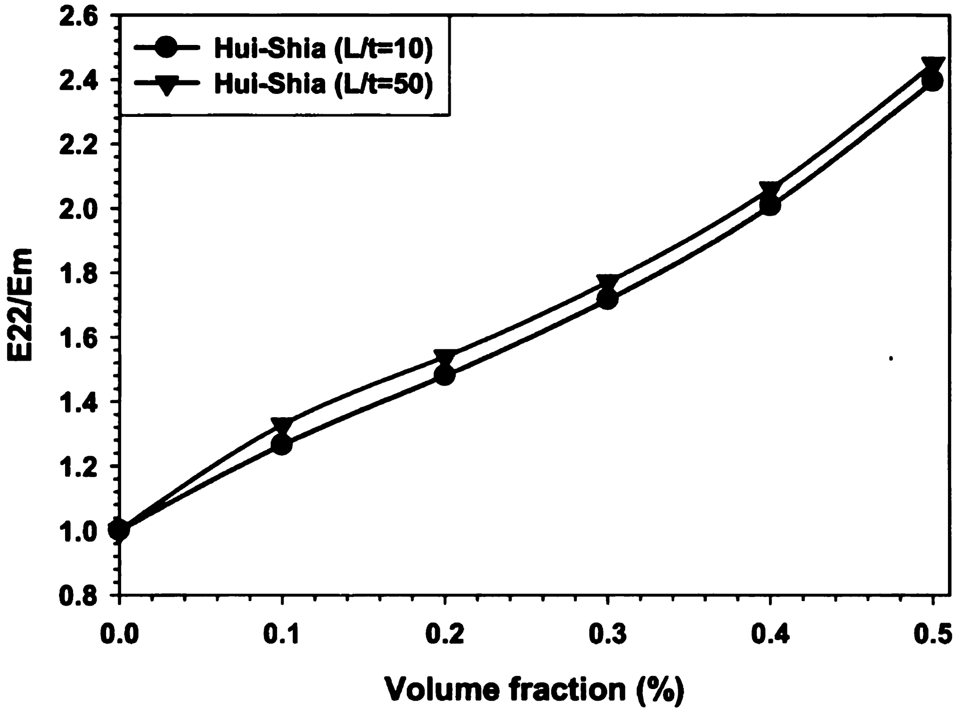

Figure 7-11. Variation of Transverse Modulus (E_{22}) with variation in f_p and *(L/t)*- Hui-Shia Fiber Like inclusions, (L/t = 10, 50) [7-7].

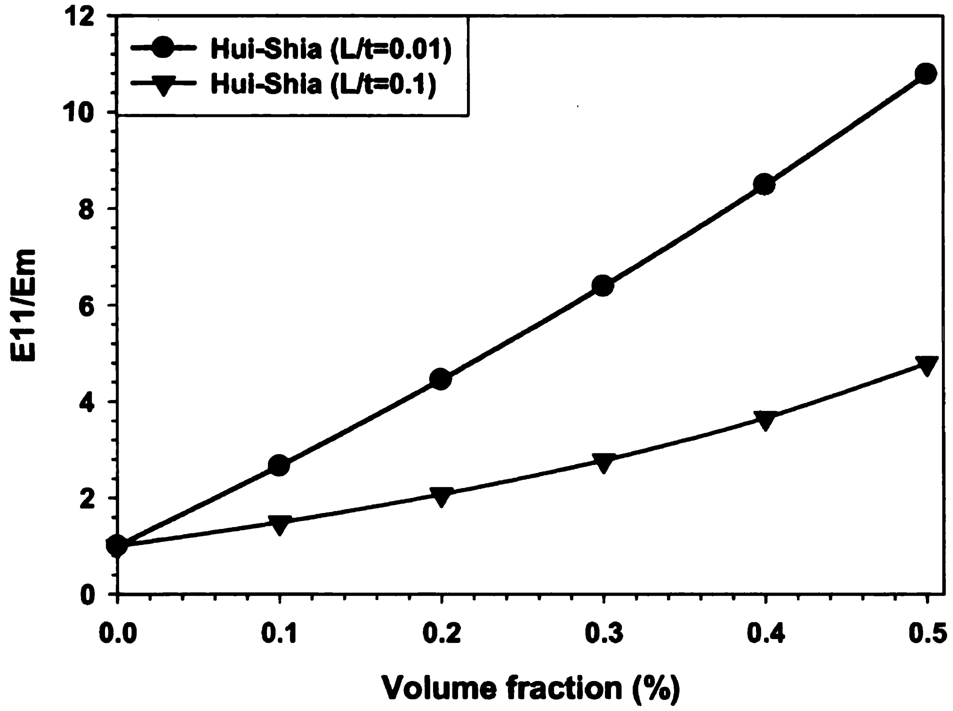

Figure 7-12. Variation of Longitudinal Modulus (E_{11}) with variation in f_p and *(L/t)*- Hui-Shia Flake Like inclusions, (L/t = 0.01, 0.1) [7-7].

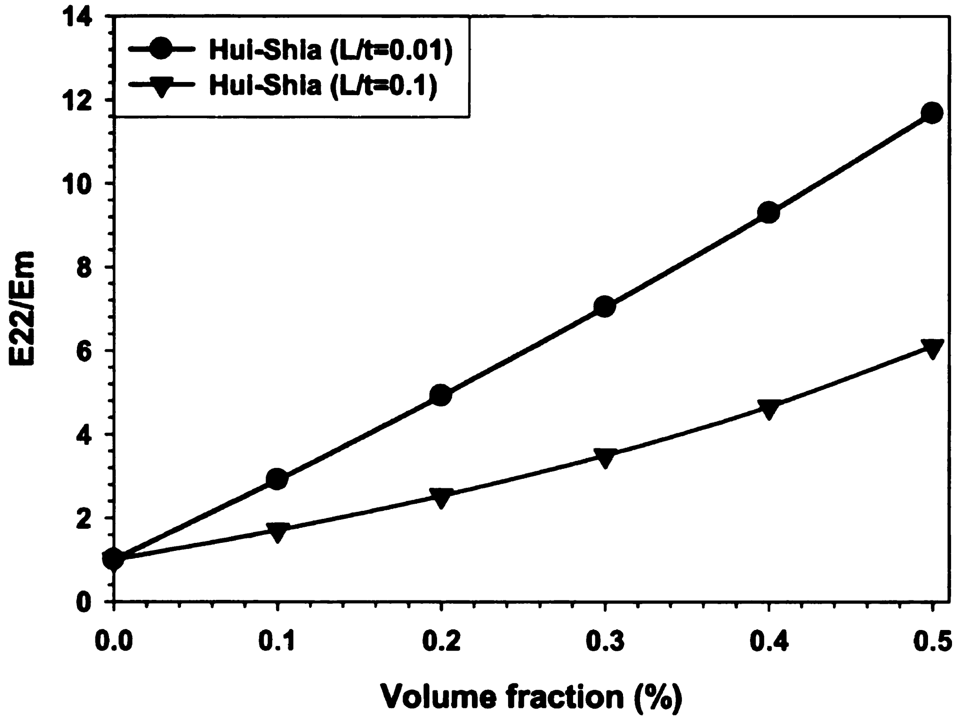

Figure 7-13. Variation of Transverse Modulus (E_{22}) with variation in f_p and *(L/t)*- Hui-Shia Flake Like inclusions, (L/t = 0.01, 0.1) [7-7]

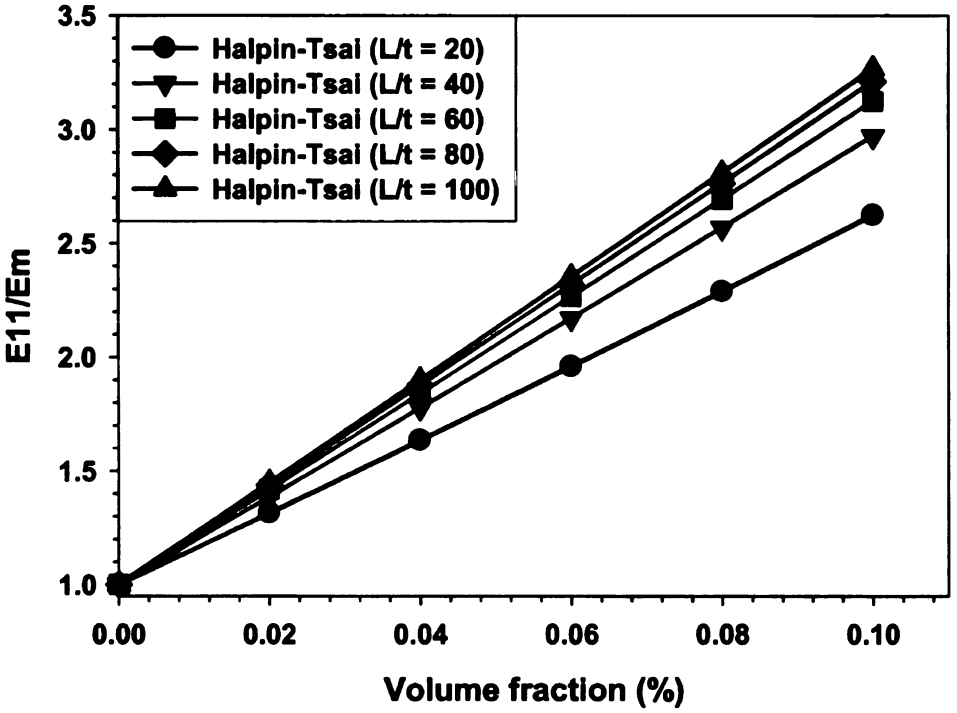

Figure 7-14. Variation of E_{11} with respect to particle volume fraction(f_p) – Halpin-Tsai model [7-7]

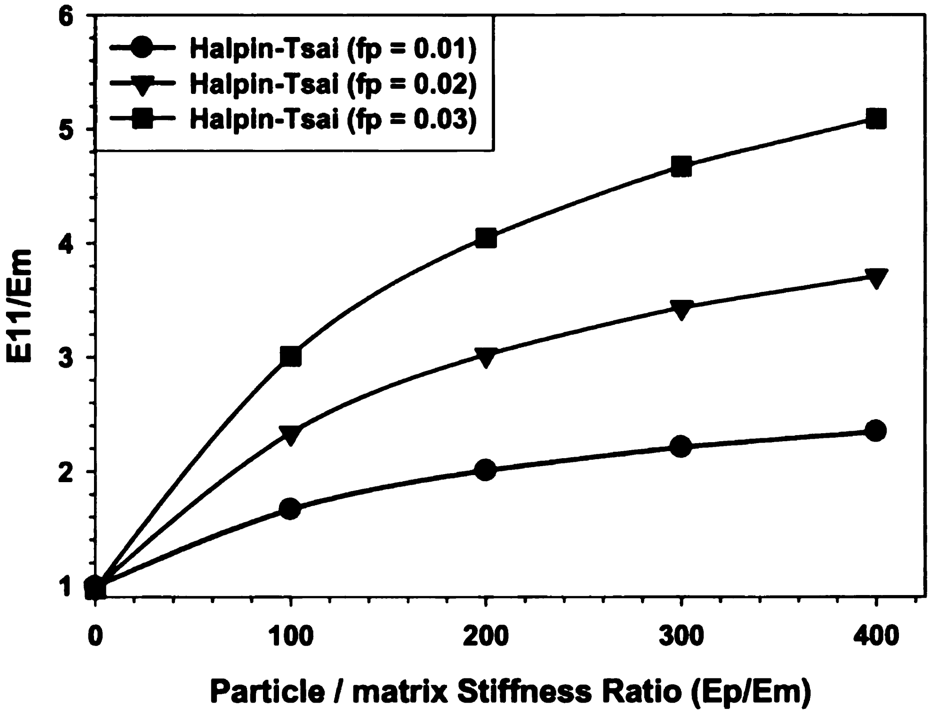

Figure 7-15. Variation of E_{11}/E_m. Halpin –Tsai model [7-1]

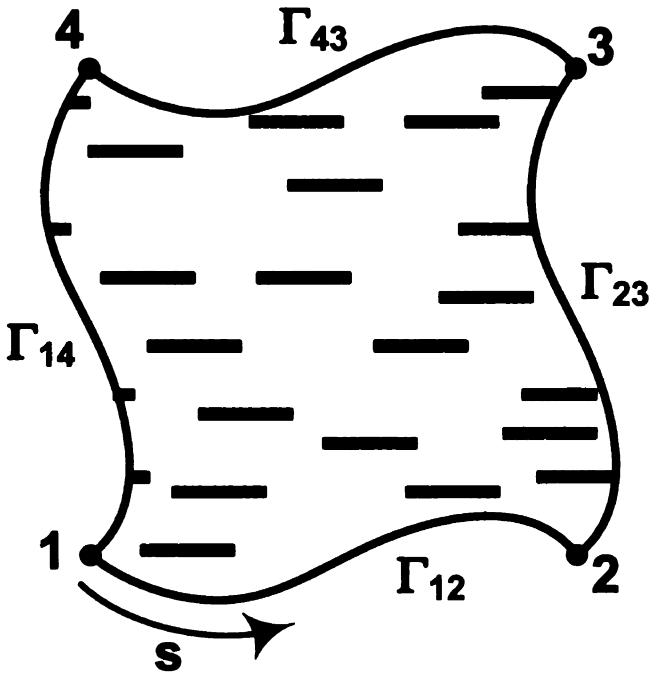

Figure 7-16. Kinematic Periodic Boundary Conditions

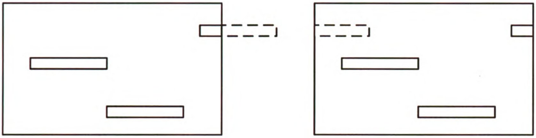

a) Truncated inclusion at the edge of RVE

b) Applying the particle periodicity by including the truncated particle on the other edge

Figure 7-17. Schematic Representation of Particle Periodicity in RVE

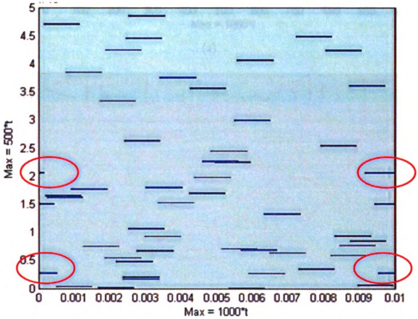

Figure 7-18. Particle Periodicity. Circled regions show the inclusions of the truncated particles. RVE dimension of 500 x1000 nm

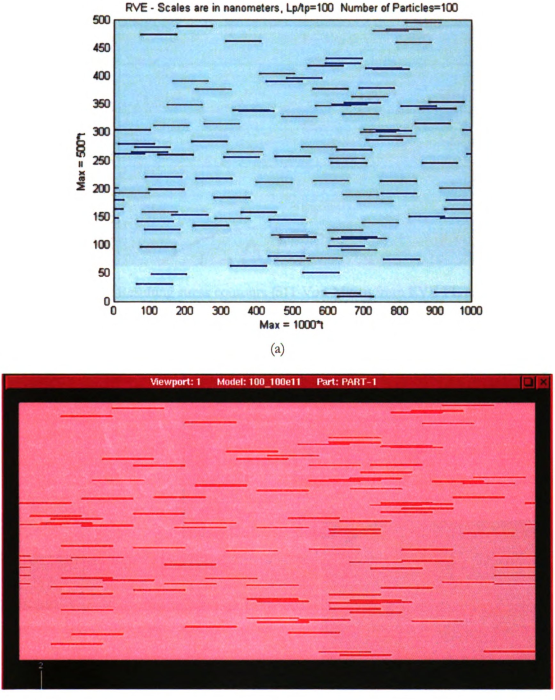

(a)

(b)

Figure 7-19. a) Sample RVE with 2% wt. clay concentration, and, b) equivalent FE model

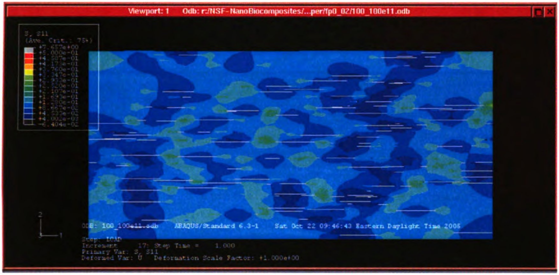

```
ODB: 100_100e11.odb    ABAQUS/Standard 6.3-1    Sat Oct 22 09:46:43 Eastern Daylight Time 2005
Step: LOAD
Increment     17: Step Time =    1.000
Primary Var: S, S11
Deformed Var: U   Deformation Scale Factor: +1.000e+00
```

Figure 7-20. Resulting stress contours (S11-Von-Mises) from RVE FE analyses

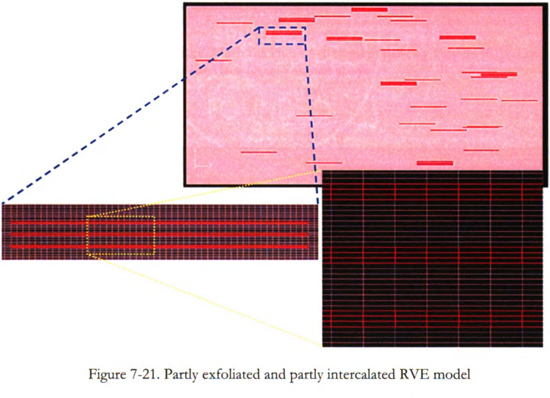

Figure 7-21. Partly exfoliated and partly intercalated RVE model

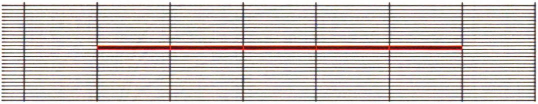

Figure 7-22. RVE with Mesh thickness = 1 element per clay particle (RED)

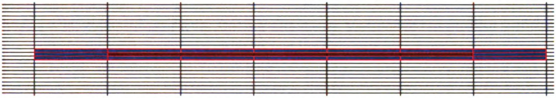

Figure 7-23. RVE with interface, Mesh thickness = 1 element per clay Particle (RED) and Interface (green) shown above

Figure 7-24. RVE with Interface, Mesh thickness= 4 elements per Clay Particle and Interface (red)

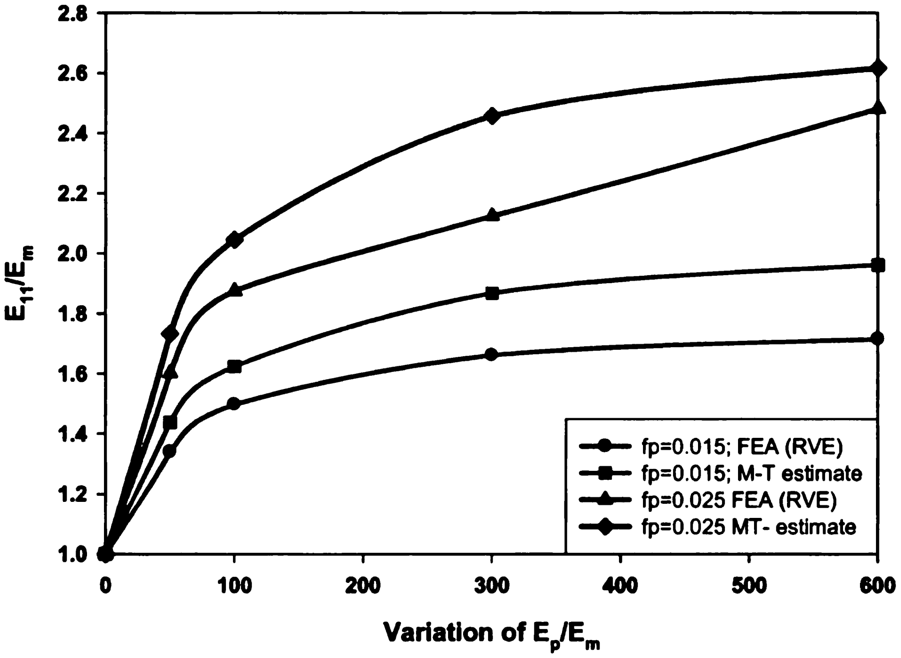

Figure 7-25. Comparison of RVE Analyses with theory, Variation of Longitudinal Stiffness with varying E_p/E_m

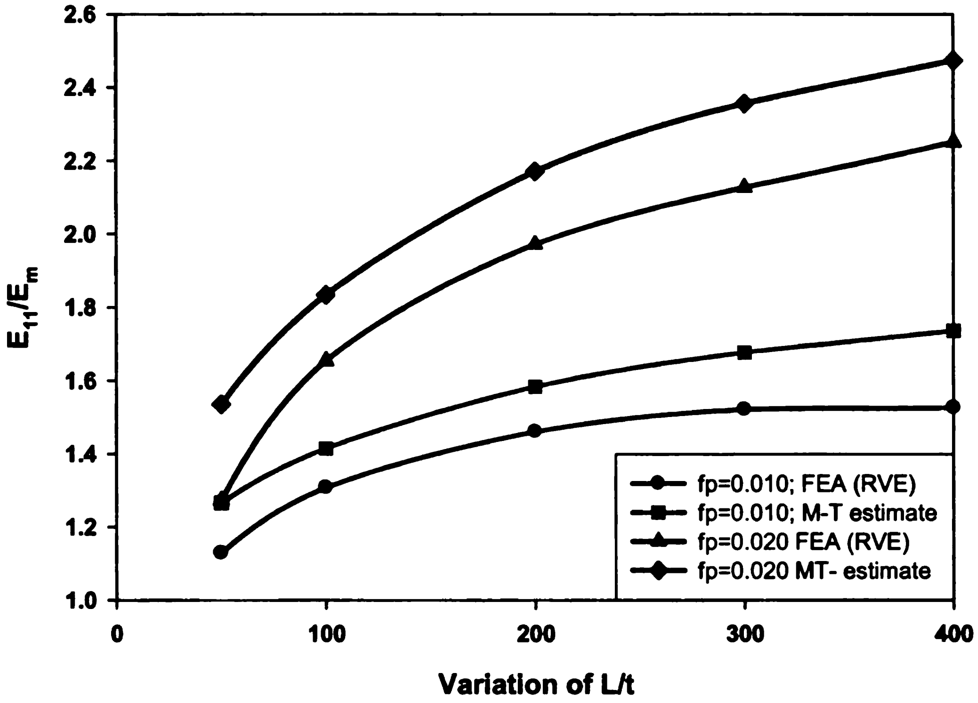

Figure 7-26. Comparison of RVE Analyses with theory, Variation of Longitudinal Stiffness with varying aspect ratios

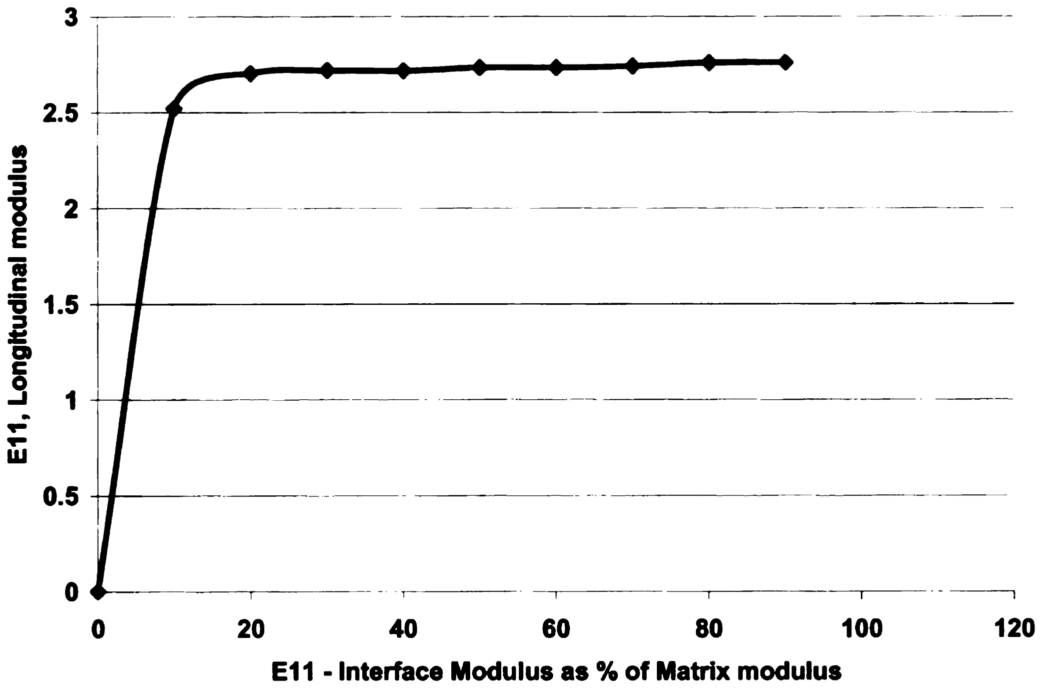

Figure 7-27. Study of Interface properties through RVE Analyses

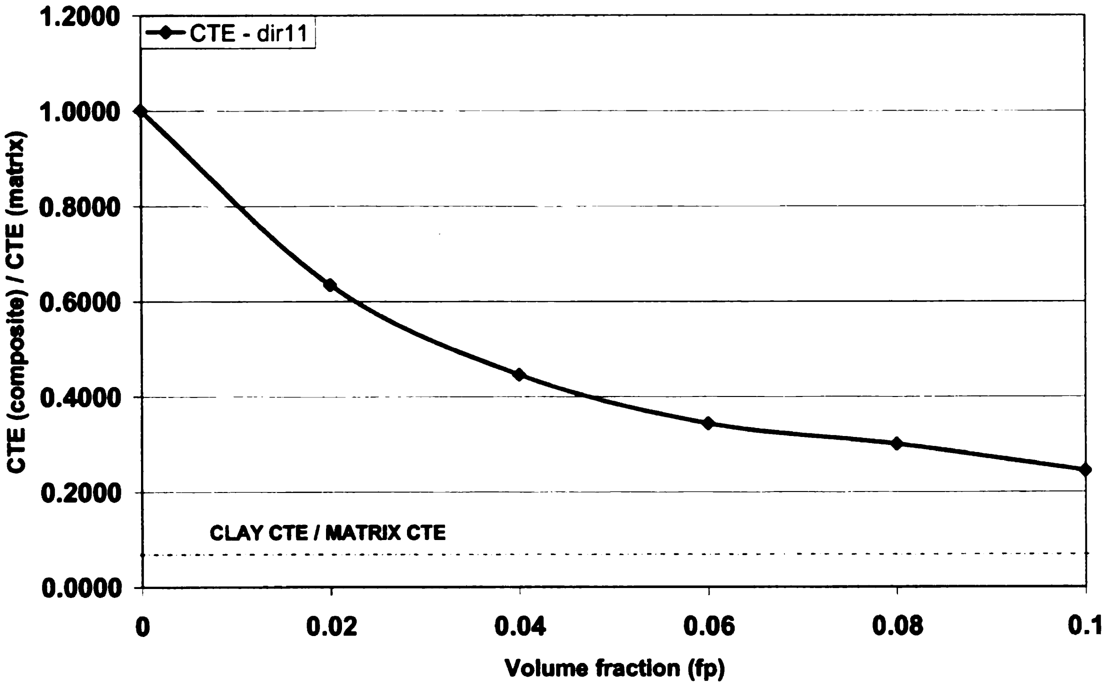

Figure 7-28. Study of CTE through RVE analyses

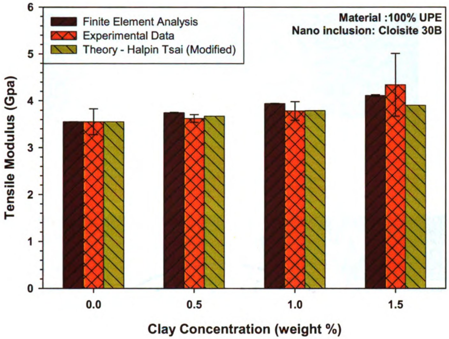

Figure 7-29. Comparison of Tensile Modulus from theory, FEA – UCM and Experimental Results for 100% Neat UPE with varying clay content

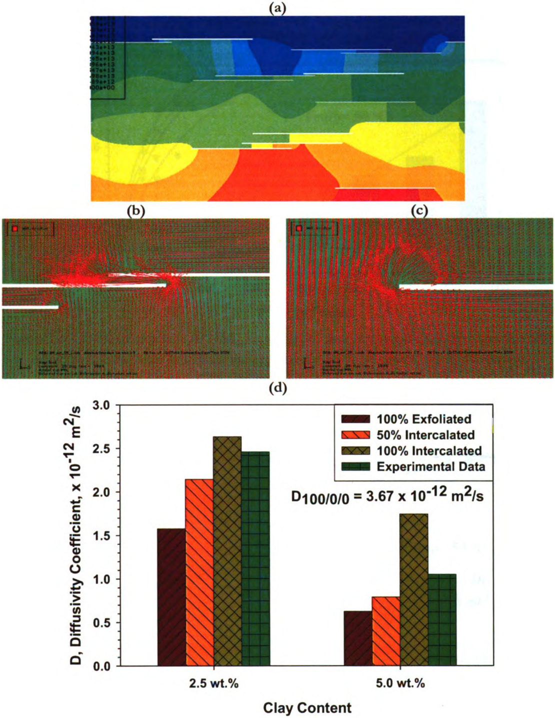

Figure 7-30. Diffusion modeling using FE-based RVEs. a) concentration contours showing diffusion of water from bottom to top, b) tortuous flow path simulation, low magnification, c) tortuous flow path simulation, high magnification, and d) Simulation and Experimental results comparison.

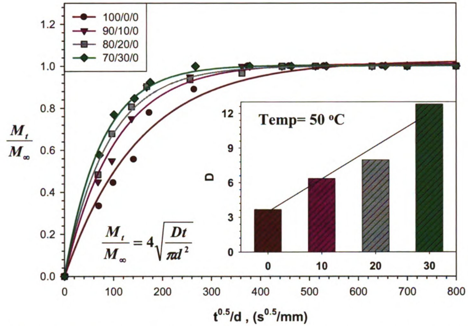

Figure 7-31. Diffusivity plots (M_t/M_∞ vs. $\sqrt{t}/d$) of neat resins (no clay). Symbols indicate experimental data and solid lines the exponential fit. Inset shows, the initial slope / diffusivity coefficients (D x 10^{-12} m^2/s) as a function of bio-resin content

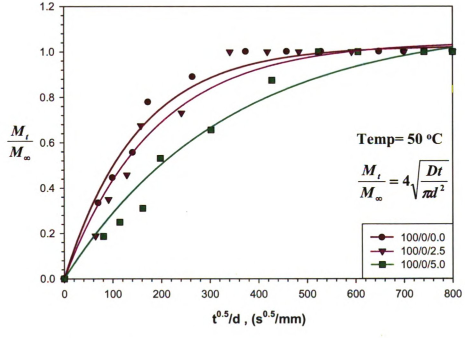

Figure 7-32. Diffusivity plots (M_t/M_∞ vs. $\sqrt{t}/d$) of UPE (no EML) with varying clay contents. Symbols indicate experimental data and solid lines the exponential fit.

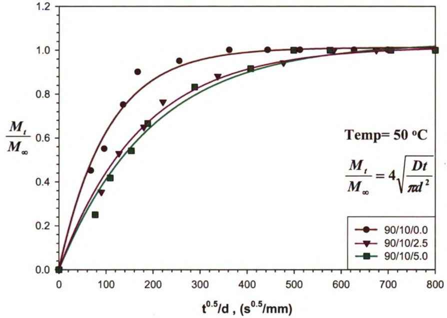

Figure 7-33. Diffusivity plots (M_t/M_∞ vs. $\sqrt{t}/d$) of UPE/EML blend containing 10%EML, with varying clay contents. Symbols indicate experimental data and solid lines the exponential fit.

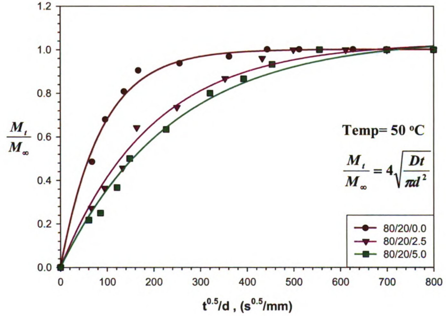

Figure 7-34. Diffusivity plots (M_t/M_∞ vs. $\sqrt{t}/d$) of UPE/EML blend containing 20%EML, with varying clay contents. Symbols indicate experimental data and solid lines the exponential fit.

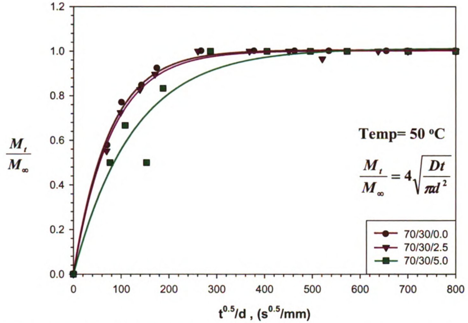

Figure 7-35. Diffusivity plots (M_t/M_∞ vs. $\sqrt{t}/d$) of UPE/EML blend containing 30% EML, with varying clay contents. Symbols indicate experimental data and solid lines the exponential fit.

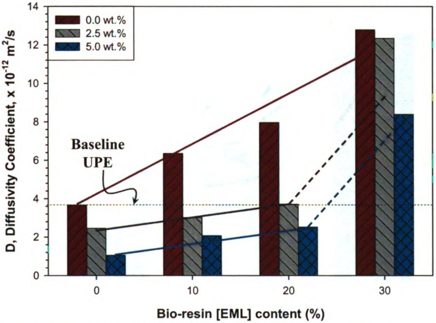

Figure 7-36. Summary of diffusivity coefficients of all bio-based nanoclay composites in this study

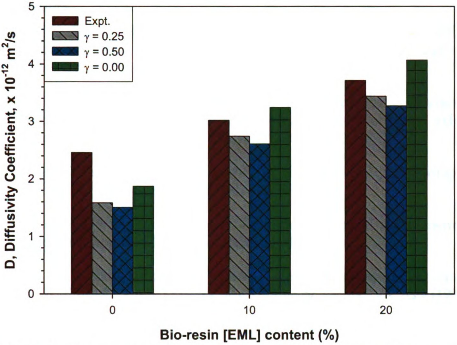

Figure 7-37. Comparison of experimental results and theoretical predictions for various particle overlap factors, corresponding to clay content of 2.5 wt. %.

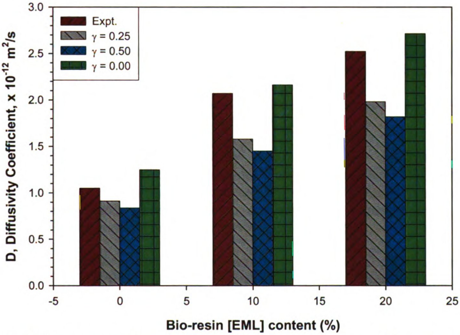

Figure 7-38. Comparison of experimental results and theoretical predictions for various particle overlap factors, corresponding to clay content of 5 wt. %.

7.12 References

[7-1] Sheng N, Boyce MC, Parks DM, Rutledge GC, Abes JI, Cohen RE. Multiscale micromechanical modeling of polymer/clay nanocomposites and the effective clay particle. Polymer 2004, 45:487-506.

[7-2] Brune DA, Bicerano J. Micromechanics of nanocomposites: comparison of tensile and compressive elastic modulii and prediction of incomplete exfoliation and imperfect alignment modulus. Polymer. 2002, 43:369-387.

[7-3] Fornes TD, Paul DR. Modeling properties of nylon6 / clay nanocomposites using composite theories. Polymer. 2003, 44:4993 – 5013.

[7-4] Le Baron PC, Wang Z, Pinnavaia TJ. Polymer – layered silicate nanocomposites: an overview. Applied Clay Science 1999; 15:11-29

[7-5] Bohm HJ. A short introduction to basic aspects of continuum micromechanics, A CDL-FMD Report 3-1998, Vienna Institute of Technology, Italy (1998).

[7-6] Fertig III RS, Garnich MR. Influence of constituent properties and microstructural parameters on the tensile modulus of a polymer / clay nanocomposite. Composite Science and Technology. 2004, 64:2577-2588.

[7-7] Tandon GP, Weng GJ. The effect of aspect ratio of inclusions on the elastic properties of unidirectionally aligned composites. Polymer composites. 1984, 5:327-333.

[7-8] Hui CY Shia D. Simple Formulae for the Effective Modulii of Unidirectional Aligned Composites. Polymer Engineering and Science. 1998, 38:774-782.

[7-9] Halpin JC. Stiffness and expansion estimates for oriented short fiber composites. Journal of Composite Materials. 1969, 3:732-735.

[7-10] Haq M, Burgueño R, Mohanty AK, Misra M. Bio-based unsaturated polyester/layered silicate nanocomposites: characterization and thermo-physical properties." Composites – Part A. 2009; 40:540-547Gusev AA. Representative volume element size for elastic composites: a numerical study. Journal of Mechanics and .Physics of Solids1997, 45:1449-1459.

[7-11] Feyel F. A multilevel finite element method (FE^2) to describe the response of highly nonlinear strucutures using generalized continua. Computational Methods in Applied Mechanical Engineering. 2003, 192: 3233-3244.

[7-12] Smit RJM, Brekelmans WAM, Meijer HEH. Prediction of the mechanical behavior of nonlinear heterogeneous systems by multi-level finite element modeling. Computational methods in Applied Mechanical Engineering. 1998, 155: 181-192.

[7-13] Olson GB. Computational design of hierarchically structured materials. Science. 1997, 277:1237-42.

[7-14] Kim JK, Hu C, Woo RSC, Sham ML. Moisture barrier characteristics of organoclay-epoxy nanocomposites. Composites Science and Technology. 2005; 65:805-813.

[7-15] Vlasveld DPN, Groenewold J, Bersee HEN, Picken SJ. Moisture absorption in polyamide-6 silicate nanocomposites and its influence on mechanical properties. Polymer 2005; 46:12567-12576.

[7-16] Rana HT, Gupta RK, GangaRao HVS, Sridhar LN. Measurement of moisture diffusivity through layered-silicate nanocomposites. Materials, Interfaces, and electrochemical phenomena, AIChE Journal. 2005; 51:3249-3256.

[7-17] Gorassi G, Tortora M, Vittoria V, Galli G, Chiellini E. Transport and mechanical properties of blends of poly (ε-caprolactone) and a modified montmorillonite poly (ε-caprolactone) nanocomposites. Journal of Polymer Science; Part B: Polymer Physics. 2002; 40:1118-1124.

[7-18] Pourabas B, Raeesi V. Preparation of ABS/montmorillonite nanocomposite using a solvent / non solvent method. Polymer. 2005; 46: 5533-5540.

[7-19] Ludueña LN, Alvarez VA, Vazques A. Processing and microstructure of PCL/clay nanocomposites. Materials Science and Engineering A. 2007; 460-461:121-129.

[7-20] Van Es MA, Polymer clay nanocomposites. The importance of particle dimensions. PhD Thesis. Delft Institute of Technology; 2001.

[7-21] Haq M, Burgueño R., Mohanty AK, Misra M. Processing techniques for bio-based unsaturated-polyester/clay nanocomposites: tensile properties, efficiency, and limits. Composites: A, 2009, 40:540-547.

[7-22] Drozdov AD, Christiansen J deC, Gupta RK, Shah AP. Model for Anomalous Moisture Diffusion through a Polymer–Clay Nanocomposite. Journal of Polymer Science: Part B: Polymer Physics. 2003; 41:476–492.

[7-23] Chen X, Papathanasiou TD. Barrier Properties of Flake-Filled Membranes: Review and Numerical Evaluation. Journal of Plastic Film and Sheeting. 2007; 23:319-346.

[7-24] Nielsen LE. Models for the Permeability of Filled Polymer Systems. Journal of Macromolecular Science, Part A. 1967; 1(5):929-942.

[7-25] Pritchard G. Reinforced Plastics Durability. CRC Press, FL, USA. 1999.

[7-26] Haq M, Burgueño R, Mohanty AK, Misra M. Hybrid Bio-based Composites from blends of Unsaturated Polyester and Soy Bean Oil Reinforced with Nanoclay and Natural Fibers. Composites Science and Technology. 2008, 68:3344-3351.

Chapter 8. FE-based Multiscale Homogenization[1,2]

8.1 Abstract

Multi-level finite element (FE) methods have gained importance for modeling heterogeneous materials as they offer the ability to model microgeometries in detail and permit incorporating nonlinear material behavior. A multi-level FE computation does not require any constitutive equations to be written at the macroscopic scale as all non-linearites are obtained from separate FE analyses at lower hierarchical (micro/nano) scales. In this work, a multi-level FE algorithm was implemented to model the tensile response of hybrid bio-based materials. A two-level (nano-micro) multi FE scheme was used to predict the tensile response of two-phase (nanoclay + matrix) and three-phase (nanoclay + petro-resin + bio-resin) bio-based nanocomposites. Also, a three-level multi-FE (nano-micro-macro) algorithm was implemented to predict the tensile behavior of biocomposites (natural fiber + nanoclay + petro-resin + bio-resin). The nanocomposite geometry was modeled as realistic as possible using a FE based representative volume element (RVE) taking into account random nanoclay distribution and hierarchical nanoclay morphologies. The three-level multi-FE scheme modeling the hybrid fiber-reinforced composite was aimed to show the robustness of the multi-FE approach and not necessarily to model the material with high accuracy, and hence a simplified RVE was used. The multi-FE simulations agreed very well with the average experimental response in the initial stiffness regime and seem to deviate

---

[1] Partial results from this chapter were presented in a conference proceeding: Haq, M. and Burgueño, R. "Modeling and simulation of bio-based polymer/clay nanocomposites through a multilevel FE approach," Computation of Shell & Spatial Structures, Spanning Nano to Mega, IASS-IACM 2008. Ithaca, New York, USA. May 2008.

[2] Complete results to be submitted to Journal of Composites Science and Technology.

away near ultimate, for nanocomposiets (two-level) and hybrid composites (three-level). The RVEs that depict the material more realistically, namely intercalated morphologies and three-phase idealized RVEs, performed better than exfoliated and two-phase RVEs. One of the main drawbacks of the multi-FE algorithm is that it basically is a sophisticated homogenization/averaging scheme, which can account for non-linearities but cannot model damage. Once damage occurs the periodicity of the RVE ceases to exist and violates the assumptions of multi-FE method. Also, stress-concentration and numerical anomalies (if any) are averaged out and hence the scheme may over-predict the response. Overall, multi-FE algorithms hold great promise in modeling different length scales within the continuum regime.

8.2 Introduction

Modification of polymers at the nanoscale, by addition of nano-inclusions has been shown to enhance mechanical properties and provide multifunctionality to the resulting polymer nanocomposites [8-1]. However, quantitative evaluation of the mechanisms leading to these property enhancements as well as those that limit the performance of polymer nanocomposites is still limited due to experimental restrictions. Computational simulation seems to be a good way to fill this gap. However, the simulation aiming to determine overall macro-scale properties must be able to account for features of these materials at the nanoscale.

The enhancement gained from nanoscale fillers (e.g. nanotubes, silica, layered silicates, etc.) is experimentally well established. Many analytical and numerical models are available to predict the overall effective/homogenized properties of these heterogeneous polymer-filler systems. It is commonly accepted that the overall effective physico-mechanical properties of a polymer-filler material depends on the type of the filler, its aspect ratio, modulus of the filler, modulus of the matrix, concentration of the filler, etc. Hence, prediction of the homogenized properties of heterogeneous materials is widely documented in literature. Various theories and models have been proposed, each with their own advantages and limitations. Overall, homogenization techniques can be classified into [8-2]: mean field approaches, variational bound methods, periodic microfield approaches /unit cell methods, embedded cell approaches, windowing approaches, rules of mixtures and semi-empirical formulae such as Halpin-Tsai methods, etc.

The simplest method of homogenization is the rule of mixtures wherein the overall properties are calculated as an average over the respective properties of the constituents weighed by their volume fractions. Clearly, this method takes into account only one microstructural property, the volume fraction, and is applicable for simple geometries and linear material properties [8-1][8-2]. A more sophisticated method is the self-consistent or effective-medium theories developed by Eshelby [8-3]. Eshelby's theory was further developed by various researchers including Hashin [8-4], Hashin and Shtrikman [8-5], Hill [8-6], and others [8-7]. Effective overall properties are obtained as an analytical solution of a boundary value problem for a spherical/ellipsoidal particle in an infinite matrix. In order to take into account for the particle-particle interactions, Mori-Tanaka [8-2] modified the Eshelby inclusion theory. Mori-Tanaka estimates are commonly used to estimate elastic properties of particulate composites and are found to agree reasonably with experimental results. Extended, or modified, Mori-Tanaka schemes have been proposed that also take into account variations in fiber orientations and fiber lengths using probability distribution functions [8-2][8-8].

Another mathematical approach is the asymptotic homogenization method reported by Bensoussan et al. [8-9] and Sanchez [8-10]. In this method "natural length parameter," which is the ratio of characteristic size of the heterogeneities to a measure of macrostructure, is used in an asymptotic expansion of the displacement and stress fields. Variational principles are then used to create a link between the scales [8-2][8-7]. Among the computational methods, unit cell methods have become widely used. The success of these methods depends on the selection of the unit cell or the representative volume element (RVE). The RVE should be selected such that it is large enough to represent the microstructure and small enough to allow efficient computational modeling. The corresponding RVE's are then analyzed with proper loading and boundary conditions via analytical or numerical methods. Unit cell methods allow modeling of micro-scale geometries in great detail (specifically in finite element based unit cell methods) and enable investigation of the influence of different geometrical features, interfaces, interparticle interactions, etc., on the overall material response. However, since these approaches formulate the macroscopic constitutive relations based on the behavior of a single RVE subjected to a given loading history, they are in fact successful only for small deformations [8-2][8-7].

Unlike most conventional fillers, the modeling of nanoclays, or layered silicates, pose new and unique modeling issues such as: a) particle size, b) hierarchical modeling, and c) interface and gallery properties [8-11]. Analytical micromechanical models have proved to be successful in predicting homogenized properties of conventional composites where the filler length scale is in the order of tens of microns or larger [8-11]. In nanoclay reinforced composites, depending on the processing, the clay morphology varies significantly. Exfoliated clays may be in range of nanometers and highly intercalated clay agglomerations may be in the order of micrometers. Moreover, it is commonly agreed that polymer/clay nanocomposites exhibit both exfoliated and intercalated (hierarchical) morphologies. Clearly, most micromechanical models cannot handle this complexity [8-11]. More importantly, it shows the limitation in modeling hierarchical morphologies that can vary by orders of magnitudes. The concepts of "matrix" and "particle" that are well-defined in micromechanical models can no longer be directly applied to polymer-clay nanocomposites. Researchers have tried to address this issue by defining an "effective particle" or a "pseudo inclusion." Sheng et al. [8-11] employ an "effective particle" in analytical and numerical (finite element) micromechanical models. Similarly, Brune and Bicerano [8-12] developed a pseudo inclusion model using the Halpin-Tsai empirical model by substituting the effective pseudo inclusion size. Miyagawa et al. [8-13] used the same concept in Mori-Tanaka models. The aforementioned studies with the concept of "effective particle" have shown to model the hierarchical nature of polymer/clay nanocomposites successfully and have reported good agreement with experimental data [8-11][8-12][8-13]. The final and most important issue in modeling of polymer/clay nanocomposites is the particle-polymer interface. Depending on the chemical compatibility, or functionalization, of the nanoclay and polymer the resulting interfacial properties will vary considerably [8-14]. Additionally in intercalated clay morphologies, wherein the clay platelets are in stacks (called galleries), the properties of the material in the galleries is not fully understood [8-11].

The above mentioned issues specific to polymer/clay nanocomposites make modeling of such composites challenging. Finite element (FE) based modeling and simulation address these issues and enable modeling of interfaces, different particle sizes and morphologies, non-linear material properties and complex loading [8-2]. Due to the complex hierarchical nature of polymer/clay nanocomposites multiscale models are considered in this work. Not limited to polymer/clay nanocomposites, multiscale models or direct micro-macro methods have been used for homogenization of different heterogeneous materials[8-7][8-15]-[8-19]. These models have also been termed as "multiscale methods[8-15][8-16][8-17]," "FE^2 methods [8-18]," "integrated methods[8-19]," and "multi-level methods[8-18]". These methods do not use a material model for the macrostructure, but rather estimate the relevant macroscopic stress-strain relationship by performing numerical homogenization on representative volume elements (RVEs) that define lower scale heterogeneities. The link between the macro and micro behavior is then obtained by volume averaging [8-7][8-15][8-16]. Thus, computational multi-level approaches using finite element procedures offer the ability to model micro- and nano-scale geometries in greater detail and incorporate non-linear material behavior with minimal assumptions of inter-particle behavior or macro-scale constitutive response.

In the multi-level FE approach presented here, a unique RVE is assigned to each macroscopic finite element integration point. The macroscopic deformation gradient at the respective integration point is applied as boundary conditions to the associated RVE. The tangential stiffness matrix is also derived from the RVE using a computational homogenization procedure as presented by Breuls et al. [8-15]. . This multi-level approach has been validated for a perforated sheet of hypoelastic material by Smit et al [8-16], bending of porous aluminum by Kouznetsova et al. [8-7] and study of local tissue deformations by Breuls et al[8-15]. In this study, two types of composites, namely: a) nanocomposites, consisting of petro-resin (unsaturated polyester, UPE), bio-resin (epoxidized methyl linseedate, EML) and nanoclay (Cloisite 30 B®), and b) hybrid biocomposites, consisting of micro-sized (~25 mm long) industrial hemp fibers and nanoclay in blends of petro- (UPE) and bio-resin (EML), were modeled using the multi-level FE approach. The non-linear material behavior of bio-based polymers used in this work is defined in the form of hyperelastic models (obtained from experimental data) at the nanoscale RVEs. The tensile behavior of nanoclay reinforced bio-based polymer systems and fiber reinforced hybrid biocomposites is evaluated using this multi-level finite-element approach and its performance is compared with experimental data.

8.3 Multi-level Approach

8.3.1 Materials

The nanocomposite under consideration is an environmentally friendly material that aims at replacing parts of a petroleum based polymer (unsaturated polyester, UPE) with natural bio-resin (epoxidized linseed oil, EML) [8-20]. The resulting bio-based resin system has been shown to attain increased toughness but its stiffness is reduced [8-20]. The lost stiffness was improved by addition of nanoscale layered silicates (nanoclay), which are sheet-like layers approximately 1 nm thick and with aspect ratios of 50-1000. Depending on the processing technique, the nanoclay in the nanocomposite exists as exfoliated (well separated), intercalated (stacks of layers with equal spacing) and a combination of both. The FE based RVE for microstructures in this study modeled these morphologies based on observations from transmission electron microscopy (TEM) images of manufactured nanocomposites, which indicated common occurrence of three platelets stacked in an intercalated gallery(see Figure 8-4c). This morphology was thus used in the RVEs(Figure 8-4b, d). Two types of composites, namely: a) nanocomposites, consisting of petro-resin (unsaturated polyester, UPE), bio-resin (epoxidized methyl linseedate, EML) and nanoclay (Cloisite 30 B®), and b) hybrid biocomposites, consisting of micro-sized (~25 mm long) industrial hemp fibers and nanoclay in blends of petro- (UPE) and bio-resin (EML), were modeled using the multi-level FE approach. Additionally, the nanocomposites were modeled as two-phase material (nanoclay + effective matrix) and three-phase material (nanoclay + petro-resin + bio-resin). Experimental data is based on bio-based clay/polymer nanocomposite (Chapter 4), and hybrid biocomposites (Chapter 6), with 20% bio-resin (EML) and 2.5 wt. % nanoclay. The material layout study (Chapter 9) also resulted in idealized RVE for nanocomposite with 10% EML and 2.5 wt.% nanoclay, and was hence used as an additional comparison for the nanocomposite example. This material composition was not used for hybrid biocomposites. Also, for the hybrid biocomposites, the idealized RVE (Chapter 9) with three-phase materials was used to describe the properties of the matrix. The properties of the natural fiber were back-calculated from the experimental data using rules of mixtures. Experimental tensile tests were performed according to ASTM D638 standards (See Chapter 4 and Chapter 6 for details).

8.3.2 Computational Homogenization Hypotheses

The material considered in this work is a polymer nanocomposite consisting of layered silicates (nanoclay) embedded in a polymer matrix. The material is considered to be macroscopically homogeneous, such that continuum mechanics theory is applicable at that scale. At the microscale the material is heterogeneous and consists of distinguishable components, namely nanoclay platelets with varying spatial distribution. Also, the microscopic length scale considered is much larger than the molecular dimensions, such that continuum approach is applicable to all components at that scale, but much smaller than the characteristic length of macroscopic sample considered, and hence periodicity of the microstructure is acceptable [8-7].

The assumption of local periodicity follows the work of Breuls et al. [8-15] and Kouznetsova [8-7]. Instead of assuming global periodicity of the microstructure, wherein the whole macroscopic material consists of spatially repeated unit cells, a more realistic assumption of local periodicity is followed. The microstructure can have different morphologies corresponding to different macroscopic points, while it repeats itself in the vicinity of the each individual macroscopic point [8-7][8-15] . This assumption allows us to model the random nanoclay morphology in a more realistic manner. The repetitive microstructural deformations suggest that the macroscopic stresses and strains around a macroscopic point can be obtained by averaging microstructural stresses and strains in a small representative part of the microstructure assigned to the macroscopic material point. In this work, a two-dimensional (2D) representative volume element (RVE) is used to model the microstructure. The use of periodic constraints and stress/strain averaging for 2D models used in this work follow the derivation provided by Breuls et al. [8-15] and are briefly presented in the following section.

8.3.3 Periodic Boundary Conditions (PBC)

A two-dimensional (2D) representative volume element defining the local microstructure of an assigned macroscopic material point is considered (Figure 8-1). For a 2D RVE, throughout the deformation processes, the PBCs indicate: a) shapes of any two opposite edges remain identical, and b) stress vectors on opposite edges are equal and opposite in direction to satisfy stress continuity. In Smit et al. [8-16], appropriate derivations of the boundary conditions are presented and were later used by Breuls et al. [8-15] and Kouznetsova [8-7]. The final expressions:

$$\vec{y}_{14} = \vec{y}_{23} - \vec{y}_2 + \vec{y}_1 \tag{8-1}$$

$$\vec{y}_{43} = \vec{y}_{12} - \vec{y}_1 + \vec{y}_4 \tag{8-2}$$

where $\vec{y}_{ij}$ is the displacement vector for any material point on the corresponding boundary Γ_{ij} and $\vec{y}_i$ is the displacement vector for corresponding vertex *i*. In addition, for vertex 3, a constraint equation is formulated, such that the vertex 3 displacements are tied with the other vertices [8-17]:

$$\vec{y}_3 - \vec{y}_2 = \vec{y}_4 - \vec{y}_1 \tag{8-3}$$

The rigid body motions can be eliminated by enforcing $\vec{y}_i = 0$, for either $i \in \{1,2,4\}$. In this work, displacements on vertex 1 were enforced to be zero, i.e. $\vec{y}_1 = 0$. From the periodicity Equations (8-1) to (8-3) it can be observed that variables $\vec{y}_{12}, \vec{y}_{23}, \vec{y}_1, \vec{y}_2$ and $\vec{y}_4$ are independent, where as $\vec{y}_{14}, \vec{y}_{43}, \vec{y}_3$ are tied (dependent). Hence it is sufficient to prescribe displacements on the three vertices $\vec{y}_1, \vec{y}_2$ and $\vec{y}_4$ [8-15].

8.3.4 Coupling Macrostructure and Microstructure

Deformation: According to the homogenization assumption stated above, the local macroscopic deformation gradient tensor F_{macro} equals the averaged deformation gradient tensor over the RVE volume (F_{RVE}). The volume averaging is performed over the initial volume (V_0), since the deformation tensor is computed from the undeformed RVE configuration [8-15]:

$$F_{macro} = F_{RVE} = \frac{1}{V_0} \int_{y_0 \in V_0} \left(\vec{\nabla}_0 \vec{y}\right) dV_0 \tag{8-4}$$

where $\left(\vec{\nabla}_0\vec{y}\right)$ denotes the deformation tensor at any point $\vec{y}_0$ of the undeformed RVE. Equation (8-4) also states that the strain energy in the macroscopic point equals the strain energy of the corresponding RVE. The volume integral in Equation (8-4) can be transformed into a surface integral using Gauss divergence theorem, and can be simplified for a 2D RVE. For implementation in finite element program it is written as [8-15]:

$$\{u\}_{RVE} = [u_1 \quad u_2 \quad u_4] = [F_{RVE} - I][y_{01} \quad y_{02} \quad y_{04}] \tag{8-5}$$

where u_i denotes the displacement of RVE vertex point *i*. Using the equality condition from Equation (8-4), the RVE vertex point displacements due to macroscopic loads can be obtained directly from F_{macro}.

Stress: Similar to the deformation assumption, the stress at any macroscopic material point equals the volume averaged RVE stresses. Stress averaging is done over the current volume (V) of the RVE [8-15].

$$\sigma_{macro} = \sigma_{RVE} = \frac{1}{V} \int_{y \in V} \sigma(\vec{y})\, dV \tag{8-6}$$

Using Gauss divergence theorem, and simplifying for a 2D RVE, the average stresses can be obtained as [8-15]:

$$\sigma_{RVE} = \frac{1}{A} sym\left[\left(\overrightarrow{y_4} - \overrightarrow{y_1}\right)\overrightarrow{f_4} + \left(\overrightarrow{y_2} - \overrightarrow{y_1}\right)\overrightarrow{f_2}\right] \tag{8-7}$$

Equation (8-7) relates the vertex forces (f_i) acting on vertex point *i* to the vertex displacements y_i. Since $\sigma_{macro} = \sigma_{RVE}$, Equation (8-7) is taken as a constitutive equation at the corresponding macroscopic material point [8-7][8-15]. Overall, the macroscopic deformation gradients at any macroscopic material point are transferred to a 2D RVE as vertex displacements, and the RVE averaged stresses are utilized as the resulting stress at the respective material point (Figure 8-3).

8.3.5 FE Implementation

The macroscopic homogenized tensile behavior is of interest and is decoupled with the micro structural heterogeneities in a computational sense by using two separate finite element models at each scale (Figure 8-3)[8-7][8-15]. These two models are linked using the concepts of local periodicity of the microstructure and stress/strain averaging as described in 8.3.4.

The macroscopic body is discretized into finite elements. A RVE, representing the heterogeneous microstructure, is modeled in detail as a separate FE model and assigned to each integration point in the macroscopic finite element mesh. It should be noted that a unique RVE can be assigned to each integration point, depending on the heterogeneity and morphology at that point. A step by step explanation of the computational approach to multi-level FE problem is given in the following

- The external macroscopic loads are applied in an incremental manner and the macroscopic FE problem is solved with an incremental procedure. The solution of the macroscopic FE problem yields macroscopic deformation gradients at respective integration points (ip), $F_{macro,ip}$.
- For each macroscopic integration point, the deformation gradient $F_{macro,ip}$ RVE vertex displacements $\{u\}_{RVE}$, corresponding to vertices 1, 2 and 4 are computed using Equation (8-5). These vertex displacements combined with the periodic boundary

constraints complete the set of boundary conditions required to solve the micro/nano-FE model [8-15].

- Each RVE is solved using a separate incremental iterative procedure. After convergence, the macroscopic stresses, σ_{macro}, and macroscopic tangential stiffness matrix, ${}^4S_{macro}$, are returned to the respective integration point. The macroscopic stress, σ_{macro}, is obtained using Equation (8-7) and ${}^4S_{macro}$ is obtained from the variation of the averaged RVE stress using a computational homogenization approach and is explained briefly in the Appendix (Section 8.8) to this chapter. The RVE solution also provides the local stresses and strains inside the RVE, thereby enabling to study the effect of heterogeneities in detail.
- The macroscopic stresses assigned to each macroscopic integration point are used to compute the internal nodal forces. If these internal forces are in balance with the externally applied macroscopic loads, convergence has occurred and the next load step is applied. If convergence has not yet been reached, the macroscopic iteration continues with updated macroscopic deformations.

A schematic explaining the iterative multi-level FE procedure is provided in Figure 8-2. A detailed description of microscopic morphologies, micro and macro FE models, and numerical aspects are explained in the following section.

8.4 Multi-level FE Model of bio-based Polymer/Clay Composites

The tensile behavior of nanoclay reinforced bio-based polymer composite was simulated using the multi-level FE approach. Two-dimensional plane strain RVEs were used at the nanoscale to model the nanocomposites. The success of the computational scheme depends on detailed modeling such that the FE based RVEs represent the microstructure in a realistic manner. Hence, actual transmission electron microscopy imaging was used to observe the nanoclay morphology, which revealed random dispersion of nanoclay with a combination of exfoliated and intercalated particles. The intercalated galleries had around 3 silicate layers in each gallery (Figure 8-4c and Figure 8-4d). As a result, two types of nanoclay morphologies were studied: a) completely exfoliated (Figure 8-4a), and b) partially exfoliated (50%) and partially intercalated (50%) nanoclay particles (Figure 8-4b). A unique RVE, with different random clay distributions, was assigned to each macroscopic integration point, with the intent of better representing the actual microstructure. Ideally, the matrix consists of blends of bio-resin and petro-resin. In this study, two RVEs were used to model the bio-based polymer nanocomposites. One containing two phases namely nanoclay and matrix; while the other consists of three-phases, namely: nanoclay, petro-resin and bio-resin. A brief description of the models is provided in the following.

8.4.1 Macromesh, RVE (micromesh), Material Models and Computational Aspects

The macroscopic tensile behavior of polymer/clay nanocomposites is of interest. The multi-level approach used in this work, and presented earlier, can be applied to any number of macroscopic elements under arbitrary loads. Yet, for simplicity, in this study the macro mesh was assumed to represent a region within the gauge length of a tensile coupon with dimensions of 1 mm x 1 mm (Figure 8-3), and hence assumed to be subjected to pure tension. This could then be modeled by a single plane strain quadrilateral element with four integration points.

Material Models & Assumptions:

Nanoclay: The nanoclay sheets were modeled as a linear elastic material (E = 170 GPa [8-21][8-22]) with exfoliated sheets having aspect ratios of 130. Electron microscopy revealed partially exfoliates and partially intercalated galleries, with approximately three platelets per gallery and inter-platelet spacing of 3 nm. Figure 8-4c and Figure 8-4d show the TEM micrograph of an intercalated gallery and its corresponding model in an RVE, respectively.

Matrix Properites:

a) Neat UPE: Tensile tests showed that neat UPE (no clay and no bio-resin) had essentially a linear elastic response. Addition of bio-resin makes the resulting bio-based polymer more ductile and non-linear, while addition of nanoclay makes the resulting nanocomposite stiffer and less ductile. Neat UPE was thus modeled as a linear elastic material (E = 3.65 GPa [8-20]).

b) Two-phase models (nanoclay + bio-based matrix): The initial attempt of multi-FE algorithm was applied using two-phase models wherein the bio-based matrix was assumed to be a homogeneous, effective matrix. In this case, the neat bio-based polymer (UPE/EML blend without nanoclay) was modeled as a hyperelastic material using an Ogden strain energy potential with parameters determined from experimental data. Figure 8-4a and Figure 8-4b show sample two-phase RVEs for exfoliated and intercalated morphologies, respectively.

c) Three-phase models (nanoclay + UPE + bio-resin). The experimental characterization of bio-based nanocomposites revealed reduction in stiffness parameters due to addition of bio-resin [8-20]. It was hypothesized that bio-resin addition affects the stress-transfer between the stiff nanoclay particle and the matrix. Additionally visual observation of manufactured nanocomposites and scanning electron images of tensile fracture surfaces revealed phase-separation of petro-resin and bio-resin. The distribution of the bio-resin around a nanoclay platelet could not be observed experimentally and hence an adhoc approach was adopted to determine the bio-resin distribution (Chapter 9). In order to model the material realistically at the lower/nano-scale, three phase RVEs having distinct clay, petro-resin and bio-resin phases were used. The three phase RVES were obtained from the material layout optimization study, as discussed in Chapter 9. The three-phase idealized RVEs were used in the multi-FE algorithms. Since the RVEs developed through the material layout procedure (Chapter 9) have only one clay particle, the concept of an idealized RVEs was used in a random way to better represent the nanoclay distribution. Figure 8-5 shows: a) the single platelet idealized RVE, (b) an RVE containing randomly distributed platelets with exfoliated platelets and c) an RVE with random intercalated clay morphology for three-phase material modeling for compositions of 10% EML and 2.5 wt.% nanoclay. Similar models for 20% EML and 2.5 wt.% nanoclay are shown in Figure 8-6. The next challenge was the determination of properties of pure bio-resin (100% EML), which are not available, as blends of only up to 30% EML content in UPE could be manufactured. Additionally, the properties of 100% bio-resins found in literature cannot be used as they do not match the chemical compositons of the bio-resin used in this work. Nevertheless, the experimental tensile modulus data studying the effect of EML concentration in UPE revealed a sigmoidal trend. Figure 8-7 shows the tensile modulus data and the sigmoidal fit (R^2 value = 1). This suggests that beyond 30% bio-resin content, the reduction in tensile properties would be minimal. Hence, experimental data of bio-based resin with 30% EML content was used to model pure bio-resin. It should be noted that this assumption may lead to an over-estimation of properties as the pure bio-resin properties will be lower than 30% bio-blend. The commercial FE program Abaqus® [8-23] allows fitting non-linear hyperelastic models for any given experimental data. For the provided data, a hyper-elastic Marlow model was found to be the most stable fit for all strains and hence was used to model the bio-resin. The model was validated by comparing the simulated response with experimental data for a neat RVE (no nanoclay), and, as expected, was found to be an exact match.

d) RVE Description:

The selection of an RVE plays a vital role in the effectively modeling the heterogeneous material. The RVE should be selected such that it is large enough to represent the microstructure realistically and small enough to allow efficient computations. The bio-based nanocomposites in this work were modeled in two ways: a) two-phase RVEs (nanoclay + effective matrix), and b) three-phase RVEs (nanoclay + petro-resin +bio-resin). All RVEs were modeled using plane strain elements. The two-phase RVEs had dimensions of 500 nm x 250 nm and each element having a size of 1nm x 1nm.. For a clay content of 2.5 wt.%, and exfoliated clay aspect ratios of 130, approximately 13 particles were randomly dispersed in the RVE. For three-phase models idealized RVEs were obtained from a material layout study (Chapter 9). In order to facilitate the computational speed, the RVE size was reduced to 500 nm x 125 nm with element size of 1 nm x 1 nm. These RVEs resulted in 7 particles for a clay content of 2.5 wt.%. This reduction in size was found to have no influence on resulting tensile predictions.

A custom Matlab® algorithm was used to create RVEs with randomly distributed clay platelets and generate the input file for its analysis using the general purpose FE program ABAQUS® [8-23]. The macro FE analysis was performed by a custom FE code in Matlab® and the nanoscale RVE FE analysis was performed in ABAQUS® [8-23]. A schematic of the implemented multi-level FE approach with an exfoliated RVE is shown in Figure 8-3.

8.5 Multi-level FE Model of Hybrid Biocomposites:

The macroscopic tensile behavior of hybrid biocomposites was modeled similarly to the nanocomposites, as discussed in the earlier section. A simplified model assumed to be within the gage length of the tensile coupon was used at the macroscopic scale, and a unique lower-scale RVE was assigned to each macroscopic integration point. The macroscopic model consists of nine plane strain quadrilateral element with four integration points each (Figure 8-8). The dimension of the fiber element was assigned as half the diameter of the raw industrial hemp fiber [8-24]. The dimensions of the matrix elements were assigned such that it satisfied the volume fraction of fiber/matrix, of the material test used for validation. The material under consideration has an average volume fraction of natural fibers of 21% with 20% EML content in UPE and 2.5 wt.% nanoclay.

As discussed earlier, in the multi-level FE approach no constitutive relationship is defined at the macroscale, instead all nonlinearities are obtained from the lower scale. The material properties of the nanocomposite models were described in the earlier section. In order to facilitate computational speed, a single particle RVE with three-phase material (Figure 8-8) was used. The material properties of natural hemp fiber were back-calculated from experimental results (Chapter 6), and using rule of mixtures. The average elastic modulus of the fibers was computed to be 12.5 GPa with a standard deviation of 3.0 GPa. The modulus of hemp fiber has been reported to be 70 GPa [8-24] whereas the average back-calculated modulus value was only 12.5 GPa. The lower value of computed modulus was expected as the experiment data represents short fibers while reported modulus uses aligned/single hemp fiber [8-24]. The efficiency of short fibers is considerably lower than aligned fully bonded fiber composites thereby supports the lower computed values of the modulus. Also, it should be noted that the modulus of natural fibers generally have significant scatter due to varying fiber quality. Finally, the hemp fiber was modeled as a linear elastic material with a modulus of 12.5 GPa.

8.6 Results and Discussion

Tensile behavior of bio-based nanocomposites (UPE+EML+clay) and hybrid biocomposites (hemp fiber+UPE+EML+clay) was simulated through the multi-FE approach and the simulations were compared with experimental data. The comparison of the predictions and the experiments was performed by studying the following parameters: a) initial stiffness, b) strain deviation parameter (ε_d), and c) stresses at average experimental ultimate strain. These parameters are schematically represented in Figure 8-9 and are explained in the following.

The strain deviation parameter (ε_d), or the strain level at which simulations starts to significantly deviate from the experimental response (ε_d) is computed as:

$$\varepsilon_d = \frac{\varepsilon_{d,start}}{\varepsilon_{u,\exp}} (\%) \tag{8-8}$$

where $\varepsilon_{d,start}$ is the value of the strain at which the start of significant deviation of simulation and average experimental response was observed, and $\varepsilon_{u,\exp}$ is the average experimental ultimate tensile strain. Additionally, $\sigma_{u,\exp}$, which is the average experimental stress corresponding to $\varepsilon_{u,\exp}$, is compared with the stress-predictions from multi-FE models ($\sigma_{\max,FE}$) corresponding to $\varepsilon_{u,\exp}$. The FE simulations in this study do not model damage and hence the simulations were terminated at $\varepsilon_{u,\exp}$.

8.6.1 Bio-based Polymer Nanocomposites

Two-phase models:

Figure 8-10 compares the simulated and experimental tensile stress-strain responses for two-phase RVEs. A nomenclature of A(%)/B(%)/C(wt.%) is used to indicate the concentration of UPE/bio-resin/clay content. The high correlation between simulated and experimental responses for neat resins (no nanolay) in Figure 8-10a simply shows that the assumptions of information transfer (deformation gradient and effective stiffness) between the micro and macro levels is adequate. Two material compositions namely 100/0/2.5 and 90/10/2.5 were studied. The 100/0/2.5 material composition represents neat UPE (no bio-resin) reinforced with nanoclay, and has a linear average experimental response (Figure 8-10b). Since both UPE and nanoclay were modeled as linear elastic, the simulated response was also linear elastic. The main purpose of performing this analysis was to study the effect of nanoclay morphology. It was observed (Figure 8-10b) that models with partially intercalated and exfoliated morphologies exactly matched average experimental response. Additionally, transmission electron imaging revealed that the actual microstructure had partially exfoliated and intercalated nanoclay morphology. This supports the good agreement of the simulations from partially intercalated model with experimental data, conversely indicating the need to realistically model the microstructure.

Similar to material composition 100/0/2.5, the models with exfoliated and partially intercalated morphologies were studied for material composition 80/20/2.5. As described in earlier section, the bio-based matrix was modeled as a non-linear hyperelastic material. The simulations for 80/20/2.5 material compositions from both exfoliated and partially intercalated models seem to capture the non-linear behavior (Figure 8-10b). Both models (exfoliated and partially intercalated) match the average experimental data in initial stiffness. The exfoliated model had a strain deviation value of 35% while the partially intercalated model had a strain deviation value of 50%. This indicates better agreement of the partially intercalated model with average experimental data, as similarly observed with material composition of 100/0/2.5. At $\varepsilon_{u,\exp}$ the exfoliated model prediction exceeds the average ultimate experimental stress ($\sigma_{u,\exp}$) by approximately 45%, while the partially intercalated model exceeds it by only 35%. Additionally, the experimental ultimate stress values ($\sigma_{u,\exp}$) have a deviation of around 10%. Overall, it was found that the multi-FE simulations agree well with the average experimental response in initial stiffness, and the intercalated RVE models gave better predictions compared to the models with exfoliated morphology.

Three-phase models:

The single particle idealized RVE obtained from the material layout study (Chapter 9) was used along with random distribution in exfoliated and intercalated morphologies. Additionally, since two idealized RVEs for 10% and 20% EML contents were obtained from the material layout study, both RVEs were used in the multi-FE simulations. Hence, for a given material composition, three models were studied, namely: a) single-particle idealized RVE, b) RVE with multi-particles and exfoliated morphology, and c) RVE with multi-particles and intercalated morphology. Figure 8-11 and Figure 8-12 compare the average experimental response of the multi-FE simulated tensile response of the aforementioned three models for bio-resin contents of 10% and 20% EML, respectively.

The comparison of multi-FE simulations for material composition 90/10/2.5 and the average experimental response is provided in Figure 8-11. The initial stiffness of all three models (single-particle idealized RVE, multi-particle+exfoliated and multi-particle+ intercalated) matched the average experimental data. The simulations from the single-particle idealized model and the multi-particle intercalated model were found be very similar. The exfoliated platelets model had a strain deviation value around 20%, while the intercalated and single-particle idealized models had strain deviation values of 60%. This suggests that the single-particle idealized and intercalated platelet models performed better than the exfoliated platelet model. Finally, the stresses at $\varepsilon_{u,\exp}$ for the intercalated platelets model were approximately 30% higher than $\sigma_{u,\exp}$. For the single-particle idealized RVE and the intercalated platelets model, the predictions exceeded $\sigma_{u,\exp}$ by around 15%. It should be noted that the $\sigma_{u,\exp}$ value has a deviation of around 15%. The above-mentioned comparisons were made only with respect to the average experimental data and the deviations were not considered. This suggests that in spite of the simulations appearing to deviate slightly from the average experimental response at ultimate, consideration of the deviation in the data would indicate reasonable agreement with experiments. Additionally, the material compositions with 10% bio-content are relatively brittle, which is what is thought to lead to the larger deviations near ultimate. Considering these variations and the assumptions made in the idealized RVE, it can be concluded that, overall, the simulations perform well and that the results reasonably agree with the average experimental response. Specifically, the models matched the average experimental response in initial stiffness, and both single-particle idealized RVE and the intercalated platelets models gave better predictions relative to the exfoliated platelet model.

The comparison of multi-FE simulations for material composition 80/20/2.5 and average the experimental response is provided in Figure 8-12. . The initial stiffness of the three models (single-particle idealized RVE, multi-particle + exfoliated and multi-particle + intercalated) matched the average experimental data. The strain deviation values were approximately 15, 40, and 70% for the exfoliated, intercalated and single-platelet idealized models, respectively. The model predicted stress values at $\varepsilon_{u,\exp}$ were approximately 62, 50 and 15% higher than $\sigma_{u,\exp}$. These results suggest that the single-particle idealized RVE performed the best, followed by the intercalated model. The exfoliated model did not show good agreement beyond the initial stiffness and strain deviation values of 15%. Additionally, the single-particle model had strain deviation values of 70% or more, suggesting that the model predicted the response reasonably well for more than 70% of the average experimental response. Finally, $\sigma_{u,\exp}$ value has a deviation of around 10% and the single-particle model exceeded it by only 15%. The reasons attributed for the single-particle idealized RVE performing better than the multi-particle models are discussed in the following section. The above comparisons were made only with respect to the average experimental data and the deviations were not considered. Considering the data deviations and the assumptions made in the idealized RVE, it can be concluded that, overall, the simulations performed well and that the results agree reasonably well with the average experimental response. Specifically, the models matched the average experimental response in initial stiffness, and both the single-particle idealized RVE and the intercalated platelets models gave better predictions compared to the exfoliated platelets model.

Comparison of two-phase and three-phase models:

Figure 8-13 shows the comparison of the simulations using two-phase and three-phase RVEs. Only models with intercalated morphology and 20% EML content were compared, as intercalated morphologies were found to agree better with experiments.

Additionally, since the initial stiffness from all models matched the experimental response reasonably well, only the stresses at $\varepsilon_{u,\exp}$ are compared. The two-phase and three -phase models exceed $\sigma_{u,\exp}$ by 35% and 50%, respectively. It appears that for multi-platelet RVEs, the two-phase model performed better than the three-phase RVE. However, this observation should be dealt with carefully. The model is as good as the assumptions at the lower scale. In the two-phase model the non-linear behavior of the bio-based matrix was modeled as a homogenized hyperelastic material fitted to the experimental data. In the three-phase models, UPE was assumed to be linear elastic and an upper-estimate of bio-resin material properties was assumed (refer to Section 8.4.1). Improved accuracy in material properties for each constituent would improve the performance of three-phase models, which additionally have more versatility by not requiring the fitting of a material model to the homogenized bio-based polymer.

The three-phase single-particle model had better agreement with the average experimental response with strain deviation values beyond 70% and stresses at $\varepsilon_{u,\exp}$ exceeding $\sigma_{u,\exp}$ by approximately 15%. For three-phase models, the multi-particle intercalated model would be expected to perform better than the single-particle model, as it seemingly models the material more realistically. Nevertheless, the single-particle idealized RVE was obtained by matching elastic experimental properties with the effective properties from the model (see Chapter 9). The material layout study in Chapter 9 was not performed with multiple platelets, as it would require large models that would be computationally too expensive to perform the material layout optimization. Additionally, the multi-particle distribution obtained as an extension of idealized RVEs violates the periodicity assumption used in the actual development of such idealized single particle RVE. For the same reason, the single-particle idealized RVE performed better than other models, as it was obtained by fitting experimental data.

8.6.2 Hybrid Bio-based Composites.

The multi-level FE approach used to model the bio-based nanocomposites as described in earlier sections of this chapter was extended to model hybrid biocomposites (hemp fiber + UPE + EML + nanoclay. The objective of modeling hybrid biocomposites in this study was mainly to show the feasibility and robustness of the multi-level FE scheme and not to accurately predict the response. Hence, simplified bio-based nanocomposite RVEs (with linear elastic UPE, hyperelastic discrete EML and linear elastic nanoclay) were used along with a simplified segment of a linear elastic fiber (hemp). The comparison of multi-FE simulations and average experimental data was evaluated similar to the bio-based nanocomposites (see Section 8.6.1). Figure 8-14 compares the tensile response from multi-FE simulations and experiments for virgin UPE biocomposites (0% EML, 0% clay). The response is linear elastic as all the properties were assumed to be linear elastic. As expected, the initial stiffness matched the experiments. The strain deviation value was approximately 25%. The model predicted stress value at $\varepsilon_{u,\exp}$ was approximately 40% higher than $\sigma_{u,\exp}$. Figure 8-15 compares the tensile-response of a hybrid biocomposite with 20% EML and 2.5 wt.% nanoclay. Similar to a virgin UPE biocomposite, the predicted initial stiffness agrees well with the experimental data. The strain deviation value was approximately 35%. The model predicted stress value at $\varepsilon_{u,\exp}$ was approximately 30% higher than $\sigma_{u,\exp}$. The models that had 20% bio-resin used a non-linear material model for bio-resin, and seem to agree average experimental response for up to 35%, while similar linear elastic model (100/0/0) agreed only up to 25% of respective $\varepsilon_{u,\exp}$. This suggests that material non-linearity helps in capturing the non-linear behavior, but is not the only source of non-linearity. The deviation of the simulation from the experimental data is due to many factors, including material non-linearity, random distribution of the short hemp fibers, interaction of the short-fibers, fiber pull-out, straightening of the curved fibers, interfacial properties, etc. Hence, relying purely on material non-linearity will still be unable to capture the non-linear response accurately, particularly near ultimate response. Nonetheless, properly designed multiscale FE simulations can shed light in understanding the aforementioned complexities and sources of non-linearity. Again, the accuracy of the model is as good as the assumptions and modeling of the actual phenomena. If all sources of non-linearities are properly modeled at the lower-scale, these multi-level schemes hold great promise for use in hierarchical materials.

8.7 Conclusion

A multi-level finite element approach was implemented and evaluated for simulating the tensile behavior of both bio-based-polymer/clay nanocomposites and biocomposites (fiber+bio-blend+nanoclay). The approach derives macro-scale constitutive relations from numerically homogenized micro/nano-scale behavior. Two-phase and three-phase models, each having a) a single-particle idealized RVE, b) an exfoliated multi-platelet RVE, and c) intercalated multi-platelet RVE were studied. All simulations were in good agreement with the initial stiffness. The intercalated platelet models performed better than the exfoliated platelet models (at ultimate). The idealized single-particle model had the best performance of all models with good agreement up to 70% of the ultimate strain observed from average experimental response. Also, considering the deviations in the experimental data, the stresses predicted by the single-particle idealized RVE, corresponding to the average experimental ultimate tensile strain, were within 5% of the average experimental ultimate tensile stresses. Overall, the simulated responses agreed reasonably well with experimental results and were able to capture the nonlinear response. The models can be improved by more accurate definition of the material properties at the micro- and nano-scale level. The approach holds great promise in understanding the behavior of polymers reinforced with nano-particles and, in general, the behavior of hybrid hierarchical materials.

8.8 Appendix-Derivation of Tangential Stiffness Matrix

The objective of the appendix is to briefly report the derivation of the tangential stiffness matrix used in the multi-level FE scheme used in this work. The material that follows is directly from the work of Breuls et al. [8-15].

The effective macroscopic behavior for the problem at hand is computed in the form of the tangential stiffness matrix, which provides the relationship between infinitesimal stress and incremental strain variations as follows:

$$\delta\sigma_{macro} = {}^{4}S_{macro} : \delta\varepsilon_{macro} \tag{8-9}$$

where, ${}^{4}S_{macro}$ is the fourth order macroscopic tangential stiffness matrix, consisting of three terms, which are obtained from the linearization of the geometrical nonlinear deformation tensor, the volume ration factor and the constitutive equation. Linearization of the constitutive equation yields to the extra stress term, ${}^{4}S_{extra}$ This extra stress term, ${}^{4}S_{extra}$, is obtained by a computational homogenization procedure as follows:

The extra-stress term ${}^4S_{extra}$ to the macroscopic tangential stiffness matrix relates the macroscopic stress variations to strain variations

$$\delta\sigma_{macro} = {}^4S_{extra} : \left(\vec{\nabla}\,\overrightarrow{\delta x}\right)^T \tag{8-10}$$

wherein $\vec{x}$ is the position vector of the macroscopic integration point. The macroscopic stress tensor at any integration point equals the averaged stress tensor in the corresponding RVE, as per Equation (8-7):

$$\sigma_{macro} = \sigma_{RVE} = \frac{1}{A} sym\left[\left(\overrightarrow{y_4} - \overrightarrow{y_1}\right)\overrightarrow{f_4} + \left(\overrightarrow{y_2} - \overrightarrow{y_1}\right)\overrightarrow{f_2}\right] \tag{8-7}$$

in which, *A* is the current RVE area, $\overrightarrow{y_i}$, the local position vector of RVE vertex point *i*; and $\overrightarrow{f_i}$ is the local force vector acting in vertex point *i*. Taking the variation of Equation (8-7) yields:

$$\begin{aligned} \delta\vec{\sigma}_{RVE} = &\underbrace{-\sigma_{RVE}\frac{\delta A}{A}}_{I} + \underbrace{\frac{1}{A} sym\left[\delta\left(\overrightarrow{y_4} - \overrightarrow{y_1}\right)\overrightarrow{f_4} + \delta\left(\overrightarrow{y_2} - \overrightarrow{y_1}\right)\overrightarrow{f_2}\right]}_{II} + \\ &\underbrace{\frac{1}{A} sym\left[\left(\overrightarrow{y_4} - \overrightarrow{y_1}\right)\delta\overrightarrow{f_4} + \left(\overrightarrow{y_2} - \overrightarrow{y_1}\right)\delta\overrightarrow{f_2}\right]}_{III} \end{aligned} \tag{8-11}$$

Parts I, II and III in the above equation are re-written in forms of deformation tensor δF. Also, in order to store the three components of the three parts in the r.h.s of the above equation, the following are used:

$$\delta\tilde{\sigma}^{I}_{RVE} = \begin{bmatrix} \delta\tilde{\sigma}^{I}_{RVE,xx} \\ \delta\tilde{\sigma}^{I}_{RVE,yy} \\ \delta\tilde{\sigma}^{I}_{RVE,xy} \\ \delta\tilde{\sigma}^{I}_{RVE,yx} \end{bmatrix}; \quad \delta\tilde{\sigma}^{II}_{RVE} = \begin{bmatrix} \delta\tilde{\sigma}^{II}_{RVE,xx} \\ \delta\tilde{\sigma}^{II}_{RVE,yy} \\ \delta\tilde{\sigma}^{II}_{RVE,xy} \\ \delta\tilde{\sigma}^{II}_{RVE,yx} \end{bmatrix}; \quad \delta\tilde{\sigma}^{III}_{RVE} = \begin{bmatrix} \delta\tilde{\sigma}^{III}_{RVE,xx} \\ \delta\tilde{\sigma}^{III}_{RVE,yy} \\ \delta\tilde{\sigma}^{III}_{RVE,xy} \\ \delta\tilde{\sigma}^{III}_{RVE,yx} \end{bmatrix}; \tag{8-12}$$

Similarly, we create vectors δF and F^{-1} to store the components of the deformation tensor.

$$\delta\tilde{F} = \begin{bmatrix} \delta F_{xx} \\ \delta F_{yy} \\ \delta F_{xy} \\ \delta F_{yx} \end{bmatrix}; \quad F^{-1} = \begin{bmatrix} F_{xx}^{-1} \\ F_{yy}^{-1} \\ F_{xy}^{-1} \\ F_{yx}^{-1} \end{bmatrix} \tag{8-13}$$

PART - I

Part I can be re-written as:

$$-\bar{\sigma}_{RVE}\frac{\delta A}{A} = -\bar{\sigma}_{RVE}tr\left(\delta F \cdot F^{-1}\right) \tag{8-14}$$

Equation (8-14) can be elaborated to

$$\tilde{\sigma}^{I}{}_{RVE} = B_I \delta F \tag{8-15}$$

with

$$B_I = \begin{bmatrix} -\sigma_{xx} \cdot F_{xx}^{-1} & -\sigma_{xx} \cdot F_{yy}^{-1} & -\sigma_{xx} \cdot F_{yx}^{-1} & -\sigma_{xx} \cdot F_{xy}^{-1} \\ -\sigma_{yy} \cdot F_{xx}^{-1} & -\sigma_{yy} \cdot F_{yy}^{-1} & -\sigma_{yy} \cdot F_{yx}^{-1} & -\sigma_{yy} \cdot F_{xy}^{-1} \\ -\sigma_{xy} \cdot F_{xx}^{-1} & -\sigma_{xy} \cdot F_{yy}^{-1} & -\sigma_{xy} \cdot F_{yx}^{-1} & -\sigma_{xy} \cdot F_{xy}^{-1} \\ -\sigma_{yx} \cdot F_{xx}^{-1} & -\sigma_{yx} \cdot F_{yy}^{-1} & -\sigma_{yx} \cdot F_{yx}^{-1} & -\sigma_{yx} \cdot F_{xy}^{-1} \end{bmatrix} \tag{8-16}$$

The components σ_{ij} are the components of the macroscopic stress tensor σ_{macro} as obtained from Equation (8-7).

PART - II

To rewrite part II in terms of δF the following is used:

$$\delta\vec{y}_i = \delta F \cdot \vec{y}_i^{\,0} \tag{8-17}$$

in which $\vec{y}_i^{\,0}$ is the vertex position of the RVE in the reference configuration.

Then,

$$\delta\tilde{\sigma}_{RVE}^{II} = B_{II}\delta F \tag{8-18}$$

with

$$B_{II} = \begin{bmatrix} p_1 & 0 & p_2 & 0 \\ 0 & p_4 & 0 & p_3 \\ \frac{1}{2}p_3 & \frac{1}{2}p_2 & \frac{1}{2}p_4 & \frac{1}{2}p_1 \\ \frac{1}{2}p_3 & \frac{1}{2}p_2 & \frac{1}{2}p_4 & \frac{1}{2}p_1 \end{bmatrix} \tag{8-19}$$

and

$$\begin{aligned} p_1 &= \frac{1}{A}\left[f_{2,x}\left(y_{2,x}^{0} - y_{1,x}^{0}\right) + f_{4,x}\left(y_{4,x}^{0} - y_{1,x}^{0}\right)\right] \\ p_2 &= \frac{1}{A}\left[f_{2,x}\left(y_{2,y}^{0} - y_{1,y}^{0}\right) + f_{4,x}\left(y_{4,y}^{0} - y_{1,y}^{0}\right)\right] \\ p_3 &= \frac{1}{A}\left[f_{2,y}\left(y_{2,x}^{0} - y_{1,x}^{0}\right) + f_{4,y}\left(y_{4,x}^{0} - y_{1,x}^{0}\right)\right] \\ p_4 &= \frac{1}{A}\left[f_{2,y}\left(y_{2,y}^{0} - y_{1,y}^{0}\right) + f_{4,x}\left(y_{4,y}^{0} - y_{1,y}^{0}\right)\right] \end{aligned} \tag{8-20}$$

In which $f_{i,x}$ is the *x* component of the vertex force, acting on the vertex *i*; $y^{0}{}_{i,x}$ denotes the *x* component of the reference position of point *i*

PART - III

Part III is reformulated to:

$$\begin{aligned} &\frac{1}{A} sym\left[\left(\overrightarrow{y_4} - \overrightarrow{y_1}\right)\overrightarrow{\delta f_4} + \left(\overrightarrow{y_2} - \overrightarrow{y_1}\right)\overrightarrow{\delta f_2}\right] \\ &= \frac{1}{2A}\left(\overrightarrow{y_1}\overrightarrow{\delta f}_1 + \overrightarrow{\delta f}_1\overrightarrow{y_1} + \overrightarrow{y_2}\overrightarrow{\delta f}_2 + \overrightarrow{\delta f}_2\overrightarrow{y_2} + \overrightarrow{y_4}\overrightarrow{\delta f}_4 + \overrightarrow{\delta f}_4\overrightarrow{y_4}\right) \end{aligned} \tag{8-21}$$

By making use of

$$\delta \vec{f}_1 = -\delta \vec{f}_4 - \delta \vec{f}_2 \tag{8-22}$$

Equation 8-22 is written in matrix form as:

$$\frac{1}{A} sym\left[\left(\overrightarrow{y_4} - \overrightarrow{y_1}\right)\delta \overrightarrow{f_4} + \left(\overrightarrow{y_2} - \overrightarrow{y_1}\right)\delta \overrightarrow{f_2}\right]$$

$$= \frac{1}{A} \underbrace{\begin{bmatrix} y_{1,x} & 0 & y_{2,x} & 0 & y_{4,x} & 0 \\ 0 & y_{1,y} & 0 & y_{2,y} & 0 & y_{4,y} \\ \frac{1}{2} y_{1,y} & \frac{1}{2} y_{1,x} & \frac{1}{2} y_{2,y} & \frac{1}{2} y_{2,x} & \frac{1}{2} y_{4,y} & \frac{1}{2} y_{4,x} \\ \frac{1}{2} y_{1,y} & \frac{1}{2} y_{1,x} & \frac{1}{2} y_{2,y} & \frac{1}{2} y_{2,x} & \frac{1}{2} y_{4,y} & \frac{1}{2} y_{4,x} \end{bmatrix}}_{C} \cdot \begin{bmatrix} \delta f_{1,x} \\ \delta f_{1,y} \\ \delta f_{2,x} \\ \delta f_{2,y} \\ \delta f_{4,x} \\ \delta f_{4,y} \end{bmatrix} \tag{8-23}$$

The vertex force variations δf are rewritten in terms of displacement variations as:

$$\delta f = K_{RVE} \delta u_{vertex} \tag{8-24}$$

The reduced RVE stiffness matrix K_{RVE} is found by partitioning the RVE stiffness matrix:

$$\begin{bmatrix} K_{rr} & K_{rp} \\ K_{pr} & K_{pp} \end{bmatrix} \cdot \begin{bmatrix} \delta u_r \\ \delta u_p \end{bmatrix} = \begin{bmatrix} 0 \\ \delta f_p \end{bmatrix} \tag{8-25}$$

wherein δu_p refers to the iterative displacements of prescribed vertices 1, 2, and 4, and δu_r denotes the iterative displacements of the remaining nodes in the RVE. The vertex force variation δf_p is expressed in terms of prescribed displacements as:

$$\delta f_p = K_{RVE} \delta u_p \tag{8-26}$$

with

$$K_{RVE} = K_{pp} - K_{pr} K_{rr}^{-1} K_{rp} \tag{8-27}$$

The displacement δu_p is written in terms of δF

$$\delta u_p = \underbrace{\begin{bmatrix} y^0_{1,x} & 0 & y^0_{1,y} & 0 \\ 0 & y^0_{1,y} & 0 & y^0_{1,x} \\ y^0_{2,x} & 0 & y^0_{2,y} & 0 \\ 0 & y^0_{2,y} & 0 & y^0_{2,x} \\ y^0_{4,x} & 0 & y^0_{4,y} & 0 \\ 0 & y^0_{4,y} & 0 & y^0_{4,x} \end{bmatrix}}_{D} \delta F \tag{8-28}$$

Hence,

$$\delta\sigma^{III}_{RVE} = CK_{RVE}\delta F \tag{8-29}$$

Combining the terms from part I to III yields:

$$\delta\tilde{\sigma}_{RVE} = [B_I + B_{II} + CK_{RVE}D]\delta F \tag{8-30}$$

Finally, δF is rewritten in terms of $\left(\vec{\nabla}\,\overrightarrow{\delta x}\right)^T$ using

$$\delta F = GH \tag{8-31}$$

with

$$G = \begin{bmatrix} F_{xx} & 0 & F_{yx} & 0 \\ 0 & F_{yy} & 0 & F_{xy} \\ F_{xy} & 0 & F_{yy} & 0 \\ 0 & F_{yx} & 0 & F_{xx} \end{bmatrix} ;\ \mathrm{H} = \begin{bmatrix} \left(\vec{\nabla}\,\overrightarrow{\delta x}\right)^T_{xx} \\ \left(\vec{\nabla}\,\overrightarrow{\delta x}\right)^T_{yy} \\ \left(\vec{\nabla}\,\overrightarrow{\delta x}\right)^T_{xy} \\ \left(\vec{\nabla}\,\overrightarrow{\delta x}\right)^T_{yx} \end{bmatrix} \tag{8-32}$$

Hence, the matrix representation of the extra stress term contribution ${}^4S_{extra}$, to the macroscopic tangential stiffness matrix ${}^4S_{macro}$ can be written as:

$$\delta\tilde{\sigma}_{macro} = [B_I + B_{II} + CK_{RVE}D]\cdot GH \tag{8-33}$$

8.9 Tables & Figures

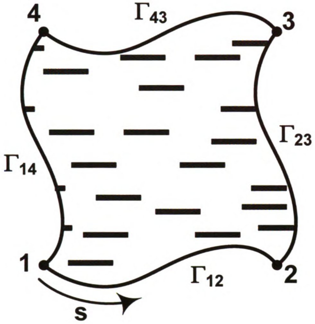

Figure 8-1. A schematic of a typical 2D periodic RVE used in the current multiscale approach. Adapted from [8-15].

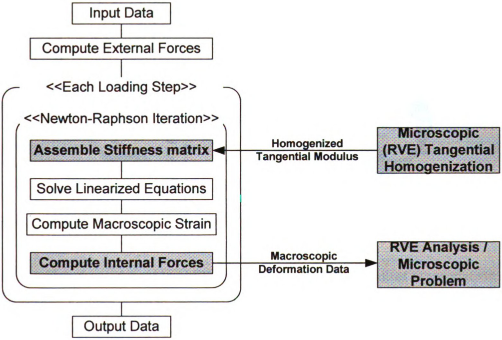

Figure 8-2. Schematic of Iterative Computational Procedure. Adapted from [8-19]

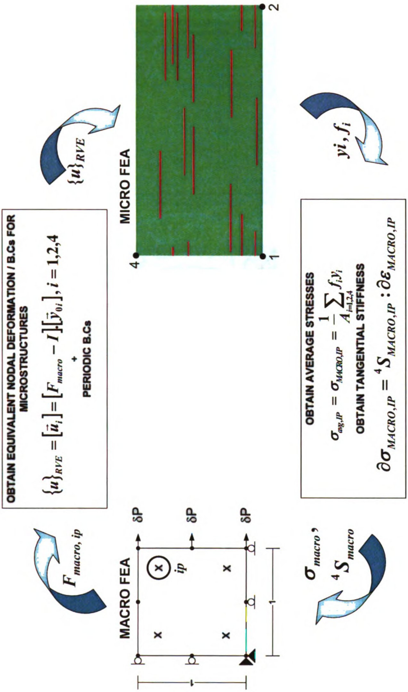

Figure 8-3. Flowchart of multi-level FE approach. Deformation gradient at any macroscopic FE integration point, $F_{macro,ip}$ is transferred to microFEA models as vertex displacements $\{u_i\}$. Macroscopic stresses $\sigma_{macro,ip}$, and tangential stiffness $^4S_{macro}$, are returned to macroscopic integration points from microscopic models.

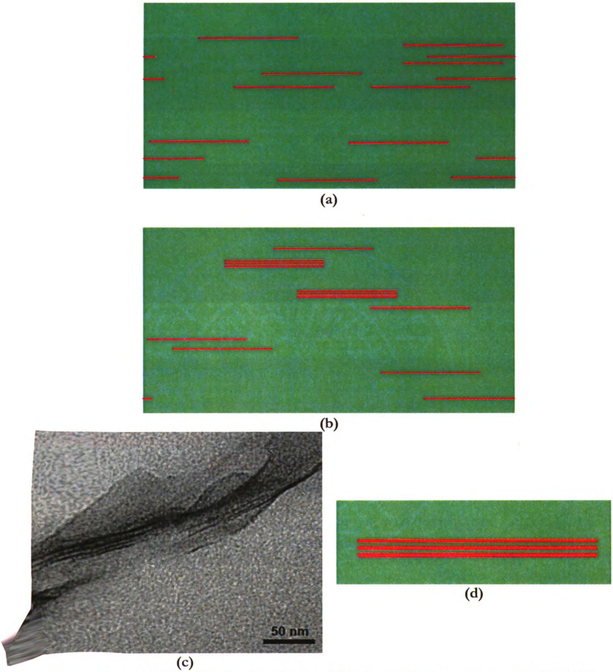

(a)

(b)

(c)

(d)

Figure 8-4. a) A FE-RVE showing 100% exfoliated nanoclay morphology, b) A FE-RVE showing 50% exfoliated and 50% intercalated nanoclay particles, c) actual TEM micrograph showing intercalated gallery, and d) zoom in of the intercalated gallery in FE based RVE model.

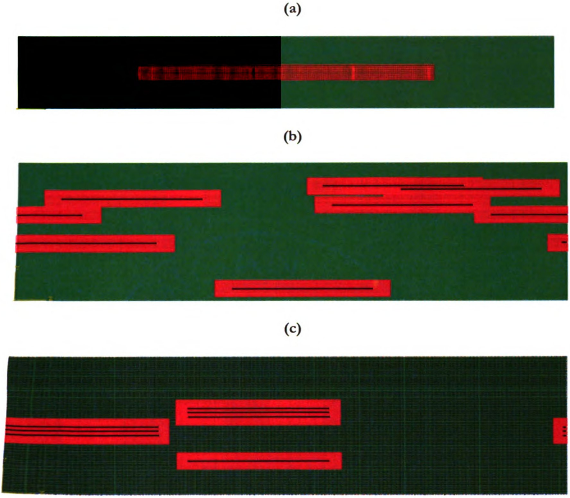

Figure 8-5. Three phase RVEs for materials with 10% EML (red) in UPE (green) with 2.5 wt.% nanoclay (black), (a) Single platelet idealized RVE, b) multi-particle, exfoliated morphology RVE c) multi-particle, intercalated morphology RVE

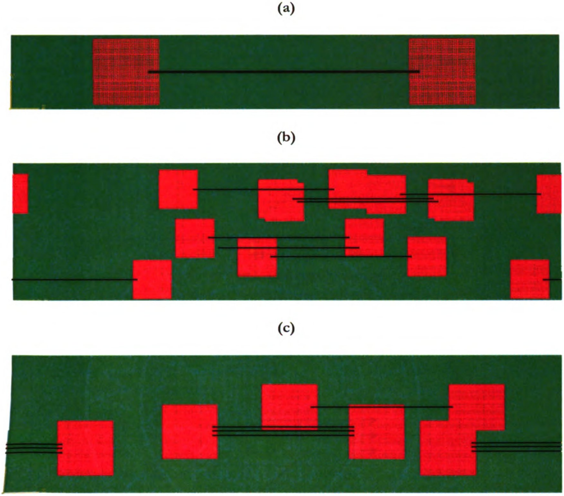

Figure 8-6. Three phase RVEs for materials with 20% EML (red) in UPE (green) with 2.5 wt.% nanoclay (black), (a) Single platelet idealized RVE, b) multi-particle, exfoliated morphology RVE c) multi-particle, intercalated morphology RVE

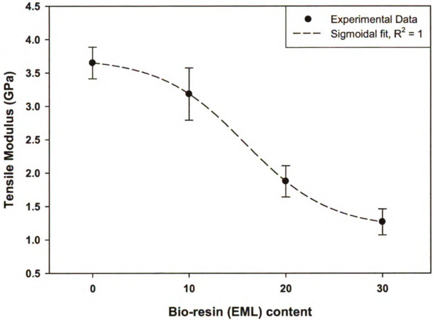

Figure 8-7. Experimental tensile modulus for neat bio-blends (no clay). The dotted line is a sigmoidal fit to the experimental data.

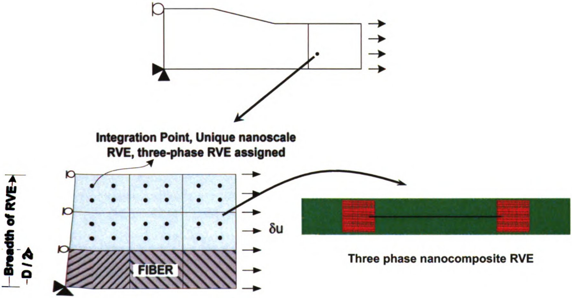

Figure 8-8. Schematic of multi-FE model used for fiber-reinforced hybrid composites.

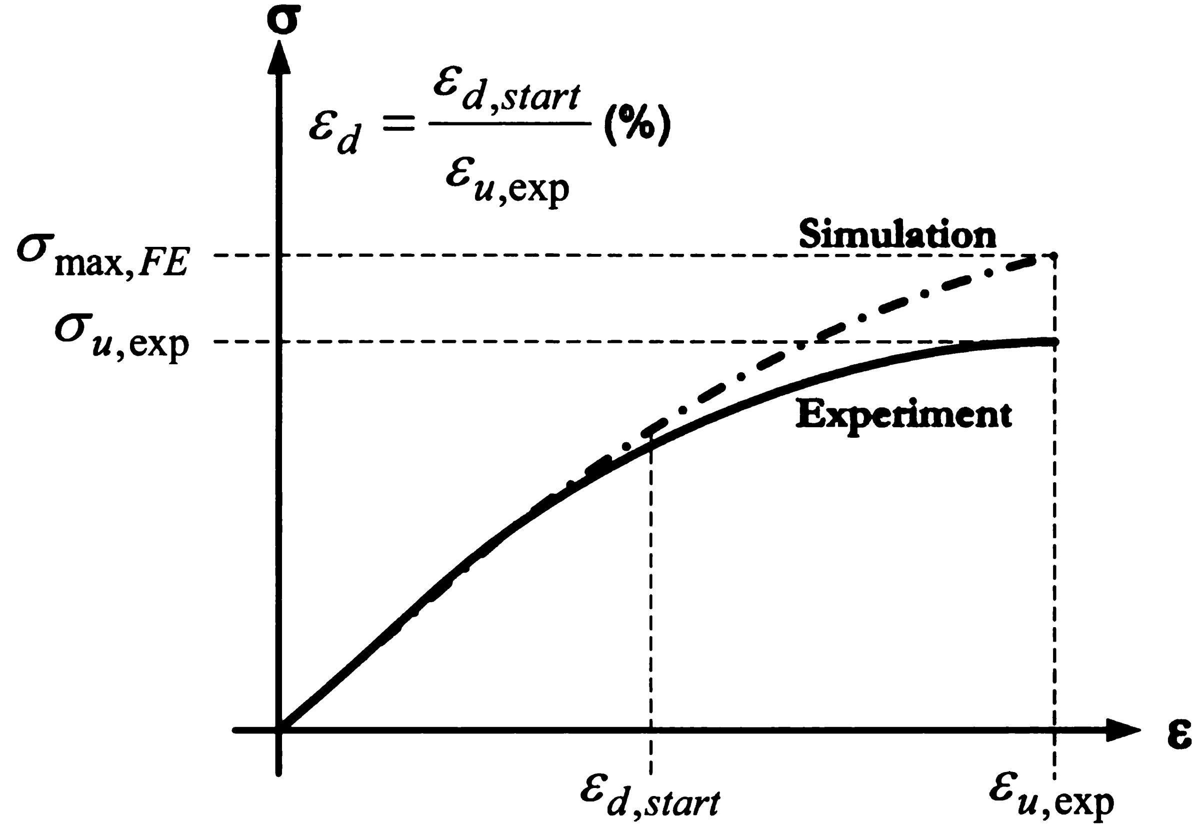

Figure 8-9. Parameters considered to compare simulations and average experimental response

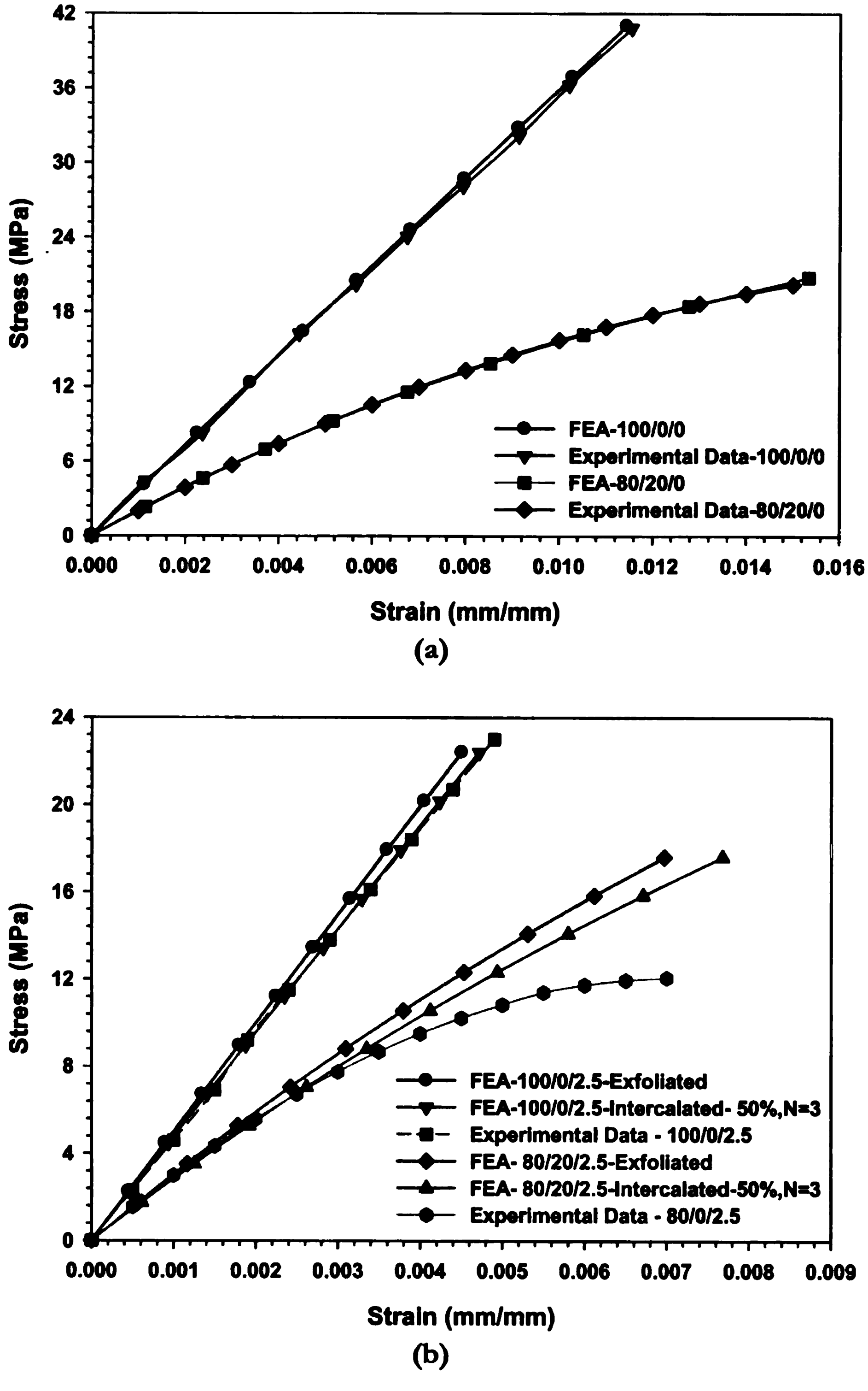

Figure 8-10. Tensile stress-strain response of two-phase RVEs: a) Neat (no clay) resins, b) Nanocomposite with 2.5 wt.% clay.

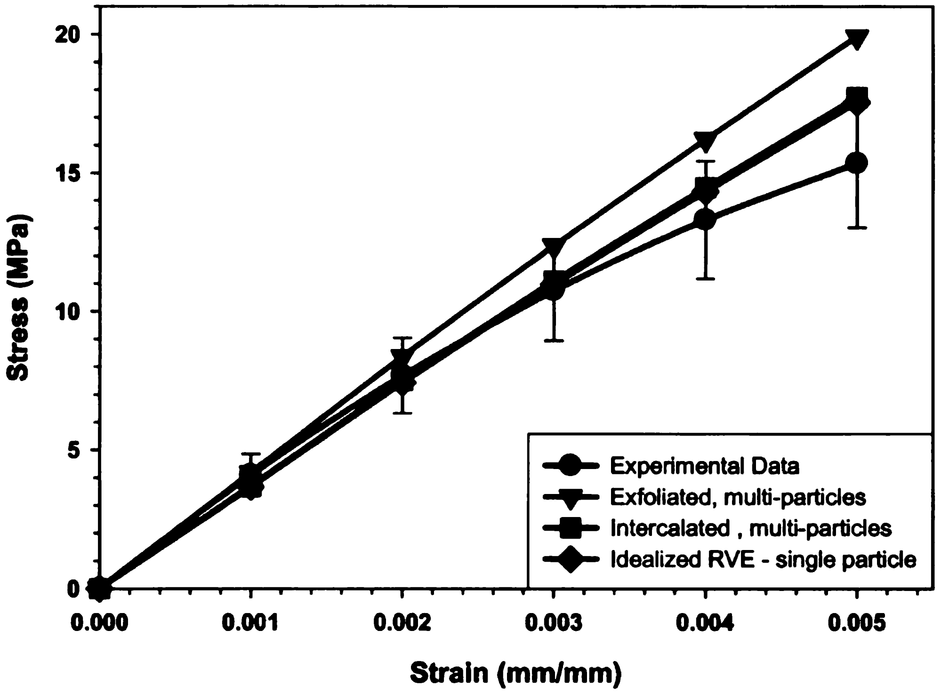

Figure 8-11. Comparison of tensile response from multi-FE simulations and experiments for biocomposites with 10% EML and 2.5wt.% nanoclay in UPE

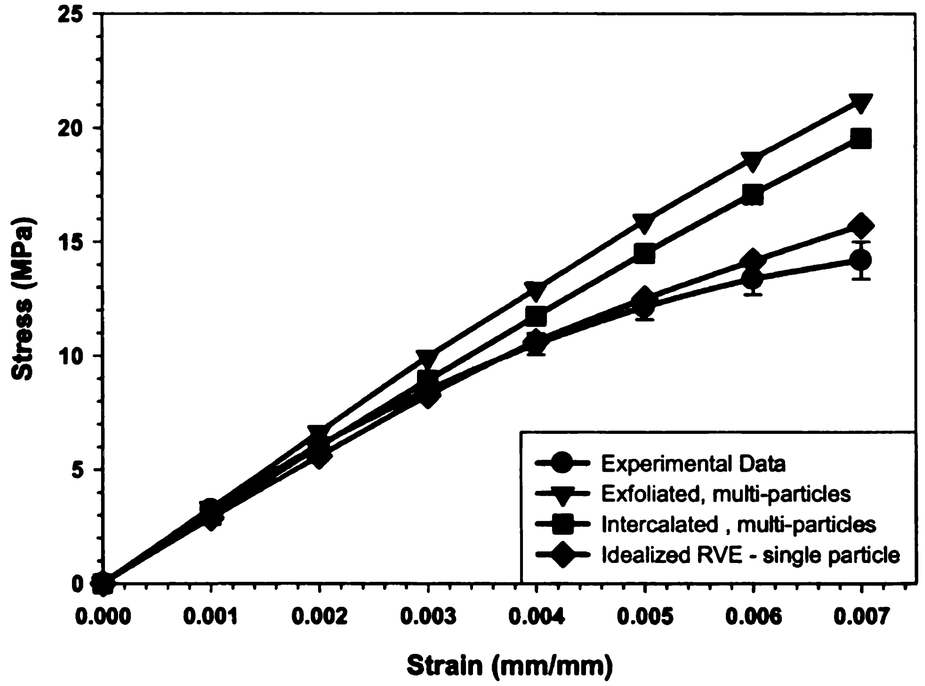

Figure 8-12 Comparison of tensile response from multi-FE simulations and experiments for biocomposites with 20% EML and 2.5 wt.% nanoclay in UPE

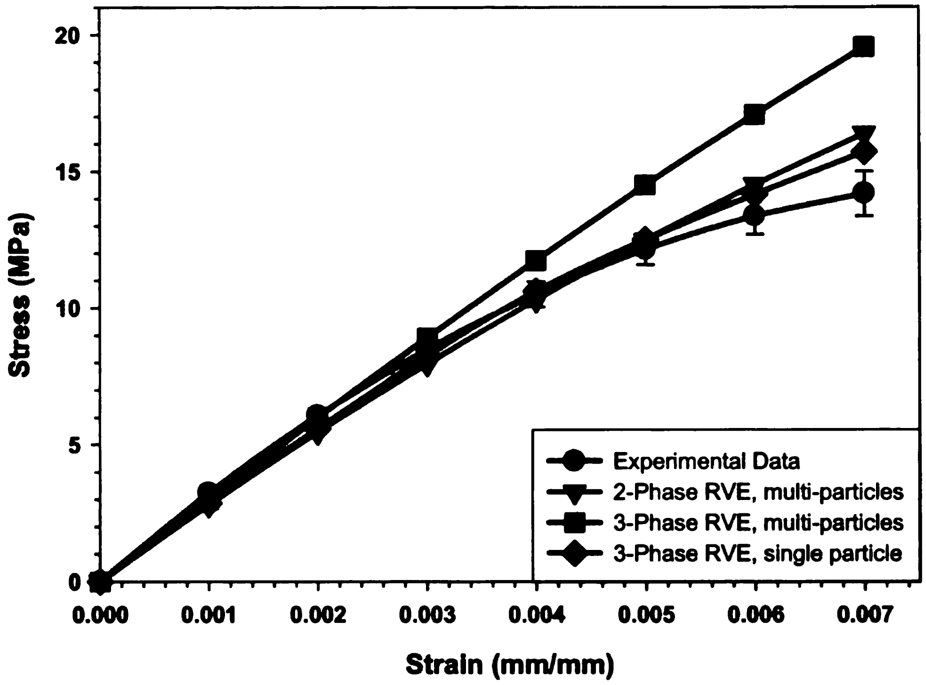

Figure 8-13. Comparison of tensile response from multi-FE simulations using two-phase and three-phase RVEs. All models have intercalated morphologies

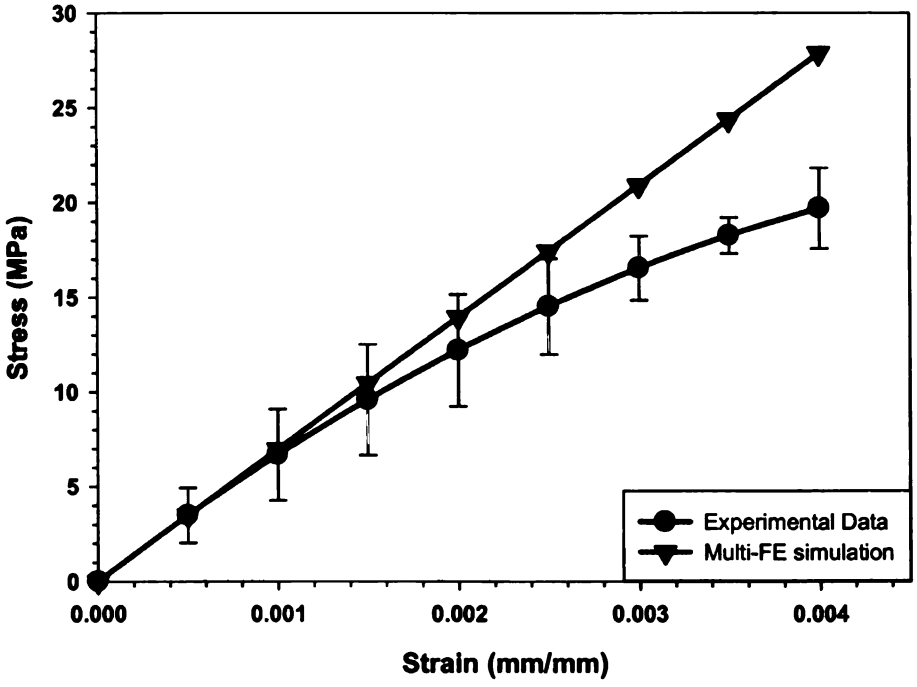

Figure 8-14. Comparison of tensile response from multi-FE simulations and experiments for virgin UPE (0% bio-resin and 0% nanoclay) biocomposites

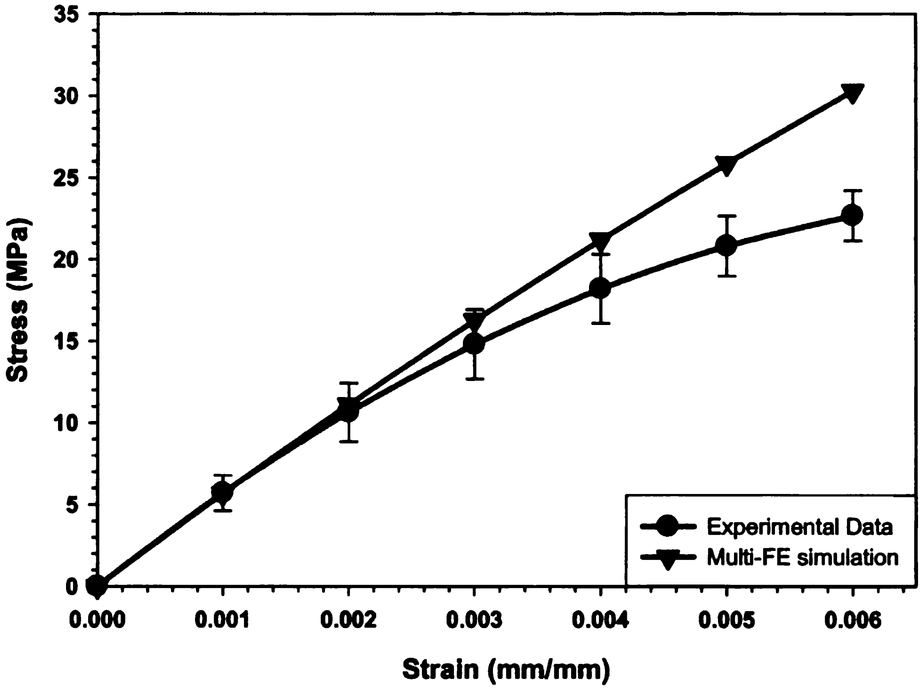

Figure 8-15. Comparison of tensile response from multi-FE simulations and experiments for hybrid composites with 20% EML and 2.5 wt.% nanoclay.

8.10 References

[8-1]. Le Baron PC, Wang Z, Pinnavaia TJ. Polymer – layered silicate nanocomposites: an overview. Applied Clay Science 1999; 15:11-29

[8-2]. Bohm, HJ. A Short Introduction to Basic Aspects of Continuum Mechanics." CDL-FMD Report, 3 (1998). Vienna Institute of Technology.

[8-3]. Eshelby JD. The determination of the field of an ellipsoidal inclusion and related. Proceedings of the Royal Soceity of London, Part A. 1957, 241:376-296.

[8-4]. Hashin Z. The elastic modulii of heterogenous materials. Journal of Applied Mechanics. 1962, 29:143-150.

[8-5]. Hashin Z, Shrikman S. A variational approach to the theory of elastic behavior of multiphase materials. Journal of the Mechanics and Physics of Solids. 1963, 11:127-140,

[8-6]. Hill R. A self-consistent mechanics of composite materials. Journal of the Mechanics and Physics of Solids. 1965, 13: 213-222.

[8-7]. Kouznetsova V, Brekelmans WAM, Baaijens FPT. An approach to micro-macro modeling of heterogeneous materials. Computational Mechanics 2001; 27:37-48.

[8-8]. Duschlbauer D, Bohm HJ, Petermann HE. Computational Simulation of Composites Reinforced by planar random fibers: Homogenization and Localization by Unit Cell and Mean Field Approaches. Journal of Composite Materials 2006, 40:2217-2234.

[8-9]. Bensoussan A, Lionis JL, Papanicolau G. Asymptotic Analysis for Periodic Structures, 1978. North Holland, Amsterdam.

[8-10]. Sanchez-Palencia E. Non-homogeneous Media and Vibration Theory. Lecture Notes in Physics, 1980. Springer-Verlag, Berlin.

[8-11]. Sheng N, Boyce MC, Parks DM, Rutledge GC, Abes JI, Cohen RE. Multiscale micromechanical modeling of polymer/clay nanocomposites and the effective clay particle. Polymer 2004, 45:487-506.

[8-12]. Brune DD, Bicerano J. Micromechanics of nanocomposites: Comparison of tensile and compressive elastic modulii, and prediction of effects of incomplete exfoliation and imperfect alignment on modulus. Polymer 2002, 43:369-387.

[8-13]. Miyagawa H, Rich MJ, Drzal LT. Amine-cured epoxy/clay nanocomposites. II. Effect of the nanoclay aspect ratio. Journal of Polymer Science PartB: Polymer Physics, 42:4391-4400.

[8-14]. Drown EK, Mohanty AK, Parulekar Y, Hasija D, Harte BR, Misra, M, Kurian JV. The surface characteristics of organoclays and their effect on the properties of poly(trimethylene terephtahalate) nanocomposites. Composites Science and Technology, 2007, 67:3168-3175.

[8-15]. Breuls RGM, Sengers BG, Oomens CWJ, Bouten CVC, Baaijens FPT. Predicting local cell deformations in engineered tissue constructs: A multi-level finite element approach. Transactions of the ASME 2002; 124:198-207.

[8-16]. Smit RJM, Brekelmans WAM, Meijer HEH. Prediction of the mechanical behavior of nonlinear heterogeneous systems by multi-level finite element modeling. Computational methods in Applied Mechanical Engineering 1998, 155:181-192.

[8-17]. Van der Sluis O, Schreurs PJG, Brekelmans WAM, Meijer HEH. Overall behavior of heterogeneous elastoviscoplastic materials: effect of microstructural modeling. Mechanics of Materials 2000, 32:449-462.

[8-18]. Feyel F, Chaboche JL. FE^2 multiscale approach for modeling the elastoviscoplastic behvior of long fiber SiC/Ti composite materials. Computational Methods in Applied Mechanical engineering. 2000, 183:309-330.

[8-19]. Matsui K, Terada K, Yuge K. Two-scale finite element analysis of heterogeneous solids with periodic microstructures. Computers and Structures 2004, 82:593-606.

[8-20]. Haq M, Burgueño R, Mohanty AK, Misra M. Bio-based polymer nanocomposites from UPE/EML blends and nanoclay: Development, experimental characterization and limits to synergistic performance," Composites: Part A. Communicated.

[8-21]. Miyagawa H, Misra M, Drzal LT, Mohanty AK. Biobased Epoxy/Layered Silicate Nanocomposites: Thermophysical Properties and Fracture Behavior Evaluation. Journal of Polymers and the Environment. 2005, 13:87-96.

[8-22]. Luo JJ, Daniel IM. Characterization and modeling of mechanical behavior of polymer/clay nanocomposites. Composites Science and Technology. 2003, 63:1607-1616.

[8-23]. ABAQUS Documentation (Version 6.8) Dassault Systèmes Simulia Corp., Providence, RI, USA, 2009.

[8-24]. Mohanty AK., Misra M, Drzal LT., Natural Fibers, Bio-polymers, and Biocomposites, 2005. CRC, Taylor & Francis Group.

Chapter 9. Modeling of Three-phase Bio-based Nanocomposites: Determining Bio-resin Distribution using an Optimization-based Material Design Problem

9.1 Abstract:

Environmentally friendly composites with material properties that can compete with conventional composites can be obtained by reinforcing blends of petroleum- and vegetable-oil-based polymers (bio-resin) with layered silicates. Such hybrid combinations have been found to produce composites that exhibit synergistic behavior with properties that are superior or similar to the primary petroleum-based polymer while the addition of bio-resin addition reduces stiffness and barrier properties of the resulting composites. The lost properties have been shown to be recoverable by the addition of nanoparticles (nanoclay). Nevertheless, the enhancement efficiency provided by the nanoclay is reduced by the presence of bio-resin. It was hypothesized that the bio-resin forms an interface around the clay particle affecting the stress transfer between the reinforcing clay particle and the polymer matrix, thereby supporting the experimental reduction of stiffness due to bio-resin addition. The distribution of bio-resin depends on its concentration and compatibility with other constituents. In order to provide a quantitative insight on the effect of bio-resin on resulting properties, the distribution of bio-resin was sought. The available experimental data on thermo-elastic parameters was used along with topology optimization to determine the distribution of bio-resin and develop an enhanced RVE for modeling the three-phase material.

The formulation of the problem followed a topology optimization method in which the objective function was minimization of the error between the model predictions and the

prescribed experimental thermo-elastic parameters subjected to constraints on bio-resin concentration. The effective properties were determined through a numerical homogenization method based on finite element discretization of the base cell. The optimization problem was solved using the method of moving asymptotes. Two-dimensional linear elasticity (small strains), perfect bonding between material phases, uniform temperature distribution and constant material properties were assumed. This chapter presents the challenges of modeling polymer-blend nanocomposites, the approach taken to address the problem, the formulation of a three-phase material layout problem, a parametric study of the optimization problem, case-studies with experimental data and the resulting material layouts for various bio-resin contents. Simplified RVEs were developed from the resulting material layout study and were used in multi-FE analyses to predict the macroscopic response. The multi-level FE simulated tensile response using the simplified RVEs from this study matched the average experimental data in initial stiffness. Additionally, the idealized RVE corresponding to 20% bio-resin content and 2.5 wt.% nanoclay, agreed reasonably with experimental data for up to 70% of the average experimental ultimate strains, and deviated from average experimental ultimate stress marginally (~5%), while the two-phase model deviated by approximately 35%. The response of this model was better than corresponding two-phase model which deviated considerably (at ultimate) by approximately 45%. This emphasizes the need to model materials as realistic as possible. Overall, the approach of validating computational models with experiments shows promise in developing models rationally, and thereby confidence in using such models in multiscale simulations linking the nanostructure with macroscopic properties.

9.2 Introduction:

Novel eco-friendly bio-based nanocomposites obtained from reinforcing layered silicates (nanoclays) in blends of petroleum and natural polymers (bio-resin) have been shown to exhibit properties that are superior or similar to base petroleum-polymer [9-1]-[9-3]. The addition of bio-resin has shown to reduce stiffness and barrier properties. The distribution of nanoclay can be observed experimentally through electron microscopy. However, similar observations on distribution of petro/bio blends are infeasible. In order to understand and model these materials efficiently, the distribution of bio/petro resin is sought. The material layout problem used in this work was aimed to develop an enhanced three-phase RVE by using experimental data along with topology optimization in an attempt to provide insight to the distribution of bio-resin in the RVE, and not necessarily to accurately solve the material design problem.

The motivation for this work follows from the desire to improve the modeling of hybrid multiscale eco-friendly composites. Environmental concerns related to the use of petroleum-based polymer matrix composites have propelled the development of composite materials based on natural or renewable sources. Bio-based resins, or bio-blends, obtained by replacing part of a petroleum-based resin with natural bio-resin increase environmental appeal along with but reduces stiffness and barrier properties of the resulting composites. A recent study [9-1]-[9-3] has shown that the property degradations due to bio-resin addition can be recovered by the addition of nanoparticles (nanoclay) [9-1]-[9-3]. Nevertheless, the enhancement efficiency provided by the nanoclay is reduced by the presence of bio-resin. It is hypothesized that the bio-resin forms an interface around the clay particle affecting the stress transfer, thereby supporting the observed reduction of stiffness due to bio-resin addition. The distribution of bio-resin depends on its concentration and compatibility with the host polymer [9-4]. In order to provide a quantitative insight on the effect of bio-resin on the resulting properties, the distribution of bio-resin is sought. Experimental data was used along with a topology optimization method to determine the mostl likely distribution of bio-resin and develop an enhanced RVE for the multiscale modeling of the three-phase material.

The use of topology optimization to solve a material design problem was introduced by Sigmund [9-5]-[9-8], whose goal was to find a periodic microstructure in which the mixture of two-distinct isotropic materials results in a composite material whose overall homogenized elastic properties match prescribed target values. The results of such material design problems is usually a spatial layout of a mixture that is optimized for prescribe objectives. Sigmund [9-8] applied the material design problem to obtain microstructures with extremal properties such as negative and zero poisson ratios. Diaz and Benard [9-9] used a similar approach to design materials with prescribed elastic properties using polygonal cells. In this work, the material design approach is used to determine the distribution of bio-resin (weak material) and petro-resin in a base cell containing a fixed stiff particle (clay). Ideally, it is a two-material spatial layout problem, wherein instead of a void, a weaker bio-resin material is present and the solid material is replaced with petro-resin.

Experimental data for various constituent concentrations (petro- and bio-resin) is available [9-3] (also refer Chapter 4). The objective is to determine the distribution of weak material (bio-resin) in a base-cell such that the effective properties of the base cell match the prescribed parameters obtained experimentally. The use of a single property (say elastic tensor) as a prescribed parameter will yield a material layout in the base cell whose effective properties would match that parameter. Using this material layout to obtain effective properties other than the prescribed parameter will most likely yield incorrect results. For the problem at hand, the material clearly has a unique bio-resin distribution for which various properties were experimentally measured. In other words using a single prescribed parameter to obtain the bio-resin distribution is not realistic. Hence, multiple material properties (elastic and thermal) are prescribed with the aim of obtaining a unique bio-resin distribution. Similar use of multiple prescribed paramaters in a material design study was used by Guest et al. [9-10][9-11] to obtain microstructures that maximize stiffness and permeability.

The topology based material design problem has also been termed as "inverse homogenization problem [9-9]." The assumption for such problems is that base cell is periodic and that the effective properties of the mixture can be obtained by analyzing only the respective base cell. The optimization problem and determination of updated design variables and sensitivities was solved by the method of moving asymptotes (MMA)[9-12][9-13]. It should be emphasized that the work attempted here aims at providing an insight to the distribution of the weaker bio-resin and not necessarily at accurately solving the material design problem.

The material under consideration is a nanocomposite bio-based material containg unsaturated polyester (UPE, primary petro-resin), epoxidized methyl linseedate (EML, bio-resin) and nanoclay. The nanoclay concentration was kept constant at 2.5 wt.% and two concentrations of bio-resin, namely, 10% and 20% were considered. Additionally, models with a single exfoliated nanoclay platelet and a single intercalated gallery were studied. The RVE size was determined by fixing the length of the RVE as twice the aspect ratio of nanoclay platelet, and the width was determined to satisfy the volume fractions. The resulting bio-resin distribution was simplified to develop idealized base cells, or representative volume elements (RVE). These idealized RVEs were then used in a multi-level FE scheme (as presented in Chapter 8) to simulate the tensile response of bio-based nanocomposites and the performance of the developed three-phase RVEs were compared with existing two-phase RVEs and experimental data. The formulation used, examples studied, the determination of target properties and results are provided in the following sections. As expected, results show affinity of the weaker material with the stiff nanoclay platelets. Additionally, multi-FE simulated tensile response from developed idealized RVEs performed better than two-phase RVEs (see Chapter 8). Also, the simulated tensile responses from idealized RVEs were found to agree with average experimental response in initial stiffness and beyond 50-70% of the average experimental ultimate strain. Detailed results and discussions of multi-FE simulations are provided in Chapter 8. Overall, idealized RVEs developed from this study were found to agree reasonably well with experiments.

9.3 Materials Design / Layout as an Optimization Problem

In typical material design problem the base cell Y is discretized using four node plane stress elements. The material property within an element is assumed to be constant and can vary from element to element. The target property tensors, in this case the elastic tensor (E^*) and thermal strain tensor (α^*) are given and the goal is to find the vector of design variables $\rho = \{\rho_1, \quad \rho_2, \ldots \quad \rho_N\}$ that results in effective tensors (E^H and α^H) that match the target properties as close as possible [9-9]. The elastic and thermal strain tensors (E, α) of the materials studied in this case are given as (E_1, α_1), (E_2, α_2) and (E_3, α_3) corresponding to petro-resin (Material-1, M1), clay inclusion(Material-2, M2) and bio-resin (Material-3, M3), respectively. In this work, the distribution of M2 (clay) is fixed. Also, ρ_e, corresponds to the material property of either M1 (petro-resin) or M3 (bio-resin). The value of

ρ_e corresponding to M1 and M3 is constrained to lie in the interval (0,1]. The problem is formulated such that for any element the value of ρ_e corresponding to 1 will lead to M3 (bio-resin). Equation (9-1) describes the assignment of material properties to the elements in the base cell. In Equation (9-1), the value of "a" is unity for all elements, except for those with clay inclusions (M2), where "a" is zero.

$$\begin{aligned} E_e &= (1-a)E_2 + a\left[\rho_e E_3 + (1-\rho_e)E_1\right] \\ \alpha_e &= (1-a)\alpha_2 + a\left[\rho_e \alpha_3 + (1-\rho_e)\alpha_1\right] \end{aligned} \tag{9-1}$$

The material design problem is formulated as a optimization problem where a prescribe amount of material is provided and the deviation from the target tensors, namely weighted mean squares, is minimized [9-9].

The problem to be solved is: to find $\rho = \{\rho_1, \quad \rho_2, \ldots \quad \rho_N\}$ such that:

$$\begin{aligned} &\min \ \phi(\rho) = \frac{1}{2} \ W_E \sum_{I=1}^{6}\left(E_I^H - E_I^*\right)^2 + \frac{1}{2} W_\alpha \ \sum_{I=1}^{3}\left(\alpha_I^H - \alpha_I^*\right)^2 \\ &sub \ \sum_{e=1}^{N} A_e \rho_e = v_{BIO} A_{mat} \\ &0 \le \rho_{\min} \le \rho_e \le 1 \end{aligned} \tag{9-2}$$

where E_I is a compact notation to denote the six independent terms of an elastic tensor in two dimensions. Similarly, α_I denotes the three independent terms of the thermal strain tensors. W_E and W_α are scalar non-negative weight factors to emphasize importance to elastic and thermal properties, respectively. A_e is the area of element e, A_{mat} is the total area occupied by the matrix elements (excluding clay), v_{BIO} is the volume fraction of bio-resin, and $\rho_{\min}$ is a prescribed lower bound for ρ_e, which was taken as 0.001 in this work.

The overall formulation of the problem as expressed in Equation (9-2), the effective thermo-elastic properties, determination of sensitivities were adapted from reference [9-8] and are provided as follows:

a) Homogenized properties:

For any microstructure which is represented by a periodic repetition of a base cell, the effective properties are obtained such that for any test strain (ε_0^i) applied to the base cell, the average strain energy matches the strain energy in the base cell when subjected to same field [9-9]. The final equations for effective/homogenized properties are [9-8]:

$$\begin{aligned}
E_{ij}^H &= \frac{1}{Y}\int_Y \left(\varepsilon_0^i - \varepsilon^i\right) E \left(\varepsilon_0^j - \varepsilon^j\right) dY \quad i,j = 1,2,3 \\
\beta_{ij}^H &= \frac{1}{Y}\int_Y \left(\alpha^i - \varepsilon^C(\Gamma)^i\right) E \left(\varepsilon_0^j - \varepsilon^j\right) dY \quad i,j = 1,2,3 \\
\alpha_{ij}^H &= \left(E_{ij}^H\right)^{-1} \beta_{ij}^H
\end{aligned} \tag{9-3}$$

where ε_0^i are linearly independent test strains, ε^i and $\varepsilon^C(\Gamma)^i$ are fluctuation strains due to applied mechanical and thermal test strains, E_{ij}^H is the effective elastic tensor, β_{ij}^H is the effective thermal stress tensor and α_{ij}^H is the effective thermal strain tensor.

(b) Sensitivity Analysis.

The detailed derivations of the sensitivities are provided in reference [9-8] and are summarized in the following. The gradient of the objective function () required for the numerical solution of Equation (9-2) was obtained as:

$$\nabla_\rho \phi = \left(E^H - E^*\right)\frac{\partial E^H}{\partial \rho} + \left(\alpha^H - \alpha^*\right)\frac{\partial \alpha^H}{\partial \rho} \tag{9-4}$$

The sensitivities of effective elastic tensor are given by:

$$\frac{\partial E^H}{\partial \rho} = -\frac{p\rho^{p-1}}{A_e}\int_e \left(\varepsilon_0^i - \varepsilon^i\right) E \left(\varepsilon_0^j - \varepsilon^j\right) dA \tag{9-5}$$

Similar to the elastic tensor, the sensitivities of the effective thermal stress tensor are given by:

$$\frac{\partial \beta^H}{\partial \rho} = -\frac{p\rho^{p-1}}{A_e}\int_e \left(\alpha^i - \varepsilon^C(\Gamma)^i\right) E \left(\varepsilon_0^j - \varepsilon^j\right) dA \tag{9-6}$$

The sensitivities of effective thermal strain tensor are obtained by differentiating Equation (9-3) as follows:

$$\begin{aligned} \frac{\partial \alpha^H}{\partial \rho} &= \frac{\partial \left(E^H\right)^{-1}}{\partial \rho}\beta^H + \left(E^H\right)^{-1}\frac{\partial \beta^H}{\partial \rho} \\ \frac{\partial \left(E^H\right)^{-1}}{\partial \rho} &= -\frac{p\rho^{p-1}}{A_e}\int_e \left(\varepsilon_0^i - \varepsilon^i\right) E^{-1} \left(\varepsilon_0^j - \varepsilon^j\right) dA \end{aligned} \tag{8-7}$$

The optimization problem at hand was solved using the method of moving asymptotes (MMA). The equality in the constraint equation as given in Equation (9-2) was changed into two inequality constraints such that an upper and lower limit to the bio-resin content could be defined. Hence, the two inequality constraints are as follows:

$$sub \ \sum_{e=1}^{N} A_e \rho_e \geq 0.95.v_{BIO} A_{mat} \tag{9-8}$$

$$sub \ \sum_{e=1}^{N} A_e \rho_e \leq 1.10.v_{BIO} A_{mat} \tag{9-9}$$

This suggests that the amount of bio-resin can vary between 95% and 110% of the actual value of the bio-resin content as prescribed in the experiments/target properties. This tolerance in the amount of bio-resin was provided as a means to indirectly take into account the variations in experimental data, since only the average properties are used in prescribing target properties.

9.4 Case Studies:

9.4.1 Introduction to the models/cases:

The examples solved in this study aimed at modeling varying bio-resin content (10% and 20%) and varying clay morphology (exfoliated and intercalated). Additionally, it was observed that phase-separation between petro- and bio-resin at bio-resin contents starts at bio-resin contents beyond 10%. This indicates that at bio-resin contents below 10% there is sufficient cross-linking between the bio- and petro-resins, and the material essentially behaves in a homogenized manner and not as discrete material distribution as assumed in this study. This would also suggests that for base cells with 20% bio-resin content only 10% is available for discrete distribution and the other 10% is cross-linked with the petro-resin in a true homogenized blend. The properties of this homogenized blend was lower than pure petro-polymer and hence reduced properties must be taken for the cross-linked blend in such cases. To address this issue, a base cell with exfoliated and intercalated morphology containing 20% bio-resin was optimized such that only 10% of bio-resin was available for discrete distribution while the remaining 10% was assumed to be cross-linked with petro-resin. Finally, for a multiple parameter objective function like the one used in this work, it has been found that providing uniform initial value of design variable may yield unsatisfactory results and it is thus suggested that the initial value of design variable be distributed linearly decreasing away from the centroid of the base cell [9-10]. Hence, two models containing 10% bio-resin contents were modeled with the aforementioned distribution of initial values. A summary of the cases studied are provided in Table 9-1.

9.4.2 Description of models

The models studied in this work can be classified into two types namely: exfoliated models (Figure 9-1a) and intercalated models (Figure 9-1b). The white region in Figure 9-1 shows the fixed location of the clay platelet and the blue region is the design domain (matrix) to consist of bio-resin and petro-resin. The RVE dimensions were taken such that the length of the RVE is twice the aspect ratio of the exfoliated platelet. The width of the RVE was computed to satisfy the clay/matrix concentration. In this study a constant clay content of 2.5 wt.% is considered. For models with exfoliated morphologies, the RVE had dimensions of 260 nm x 35 nm. Similarly, RVEs for the intercalated morphology had dimensions of 260 nm x 105 nm. Both models are discretized with square elements having dimensions of 1 nm x 1 nm. Hence the exfoliated and intercalted models have 9100 and 27300 elements. The nanoclay platelets were placed in the center of RVE thereby yielding symmetric results.

9.4.3 Determination of Target Properties

The experimental properties available for various bio-based polymer nanocomposites included tensile modulus and coefficient of thermal expansions for various material concentrations. Also, the Poisson's ratios for neat resins (no clay) were available. Additionally, the effect of bio-resin on the aforementioned properties is known. As it can be seen, the available experimental data is insufficient to exactly define all six independent values of the constitutive tensor (E^*). Hence, certain assumptions were made in defining the target properties.

The effective properties of the model considering the matrix was comprised of all UPE (no bio-resin) was first obtained (E_{UPE}^{H} and α_{UPE}^{H}). Secondly, the matrix properties of neat bio-blends (in accordance to the petro/bio ratios) were obtained. The average decrease in tensile modulus (γ) and average increase in CTE (β) due to the addition of a known concentration of bio-resin was known from experiments. It was assumed that the bio-resin affects the properties in the longitudinal direction of the clay reinforcement. Along the transverse direction the properties of bio-blends was assumed. The prediction of target properties is illustrated with the example of Case-1, namely exfoliated morphology with 10% EML content.

The homogenized properties of the model with matrix properties equal to neat UPE resin (E =3.65 GPa, ν =0.3805, α =100.1 μm/°C) are:

$$E_{UPE}^{H} = \begin{bmatrix} 5.531 & 1.634 & 0.000 \\ & 4.327 & 0.000 \\ sym & & 1.342 \end{bmatrix}; \qquad \alpha_{UPE}^{H} = \begin{bmatrix} 76.103 \\ 107.578 \\ 0.000 \end{bmatrix} \mu m/^{\circ}C \quad (9\text{-}10)$$

The homogenized properties of the model with matrix properties equal to a neat UPE/EML blend with 10% EML (E =3.18 GPa, ν =0.3923, α =105.0 μm/°C) are:

$$E_{90/10}^{H} = \begin{bmatrix} 4.950 & 1.485 & 0.000 \\ & 3.812 & 0.000 \\ sym & & 1.159 \end{bmatrix}; \qquad \alpha_{90/10}^{H} = \begin{bmatrix} 77.970 \\ 113.83 \\ 0.000 \end{bmatrix} \mu m/^{\circ}C \quad (9\text{-}11)$$

Therefore, the target propeties were defined from the combination of Equation (9-10) and (9-11) as follows

$$E^{*} = \begin{bmatrix} \gamma(5.531) & \gamma(1.634) & 0.000 \\ & 3.812 & 0.000 \\ sym & & 1.159 \end{bmatrix}; \quad \alpha^{*} = \begin{bmatrix} \beta(76.103) \\ 113.83 \\ 0.000 \end{bmatrix} \mu m/^{\circ}C \quad (9\text{-}12)$$

As explained earlier, the effect of nanoclay on transverse direction properties is assumed negligible, and hence the reduction in the elastic tensor terms involving the 1-

direction due to addition of bio-resin was applied to the terms obtained from the UPE homogenized properties. The target properties for other cases in this study were similarly determined and are reportes later along with the results of the respective cases. The values of γ for 10% and 20% bio-resin contents were 0.97 and 0.64, respectively. Similarly, the values of β for 10% and 20% bio-resin contents were 1.076 and 1.151, respectively. The description of the study cases and their results are only provided in the following. The discussions of results of the various cases follow the results (Section 9.4.12).

9.4.4 Case-1: Exfoliated, 10% bio-resin, 10% available for layout optimization

This case models an exfoliated clay morphology with 10% bio-resin content. The initial value of the design variables was distributed uniformly to all matrix elements. Figure 9-2a shows the histories of the objective function, magnitude of the design variable vector, and the values of constraints, as the design evolved. Figure 9-2b and Figure 9-2c show the bio-resin distribution at iteration steps of 50 and 200, respectively. The target properties are given in Equation (9-13) and the effective properties upon convergence are provided in Equation (9-14). The discussion of the results is provided in Section 9.4.12.

$$E^* = \begin{bmatrix} 5.365 & 1.585 & 0.000 \\ & 3.812 & 0.000 \\ sym & & 1.159 \end{bmatrix}; \qquad \alpha^* = \begin{bmatrix} 81.887 \\ 113.729 \\ 0.000 \end{bmatrix} \mu\text{m/°C} \qquad (9\text{-}13)$$

$$E^H = \begin{bmatrix} 5.323 & 1.494 & 0.000 \\ & 3.806 & 0.000 \\ sym & & 1.162 \end{bmatrix}; \qquad \alpha^H = \begin{bmatrix} 76.189 \\ 116.534 \\ -2.177 \end{bmatrix} \mu\text{m/°C} \qquad (9\text{-}14)$$

9.4.5 Case-2: Exfoliated, 20% bio-resin, 20% available for layout optimization

This case models an exfoliated clay morphology with 20% bio-resin content. The initial value of the design variables was distributed uniformly to all matrix elements. Figure 9-3a shows the histories of the objective function, magnitude of the design variable vector, and the values of constraints. Figure 9-3b and Figure 9-3c show the bio-resin distribution at iteration steps 50 and 200, respectively. The target properties are given in Equation (9-15) and the effective properties at convergence are provided in Equation (9-16). The discussion of the results is provided in Section 9.4.12.

$$E^{*}=\begin{bmatrix} 3.540 & 1.0455 & 0.000 \\ & 2.321 & 0.000 \\ sym & & 0.668 \end{bmatrix}; \qquad \alpha^{*}=\begin{bmatrix} 87.488 \\ 122.270 \\ 0.000 \end{bmatrix} \mu\text{m}/^{\circ}\text{C} \qquad (9\text{-}15)$$

$$E^{H}=\begin{bmatrix} 3.840 & 1.153 & 0.000 \\ & 3.407 & 0.000 \\ sym & & 0.987 \end{bmatrix}; \qquad \alpha^{H}=\begin{bmatrix} 94.190 \\ 119.960 \\ -0.272 \end{bmatrix} \mu\text{m}/^{\circ}\text{C} \qquad (9\text{-}16)$$

9.4.6 Case-3: Exfoliated, 20% bio-resin, 10% available for layout optimization

This case models an exfoliated clay morphology with 20% bio-resin content. It is assumed that 10% of the bio-resin in cross-linked with petro-resin (and thus well homogenized as a single matrix material), and only 10% is available for discrete material design. The initial value of the design variables was distributed uniformly to all matrix elements. Figure 9-4a shows the histories of the objective function, the magnitude of the design variable vector, and the constraints as the design evolved. Figure 9-4b and Figure 9-4c show the bio-resin distribution at iteration steps 50 and 200, respectively. The target properties are given in Equation (9-15) and the effective properties at convergence are provided in Equation (9-17). The discussion of the results is provided in Section 9.4.12.

$$E^{H} = \begin{bmatrix} 3.840 & 1.153 & 0.000 \\ & 3.407 & 0.000 \\ sym & & 0.987 \end{bmatrix}; \qquad \alpha^{H} = \begin{bmatrix} 94.190 \\ 119.960 \\ -0.272 \end{bmatrix} \ \mu\text{m}/^{\circ}\text{C} \quad (9\text{-}17)$$

9.4.7 Case-4: Exfoliated, 10% bio-resin, Initial Value Varies Linearly

This case models an exfoliated morphology with 10% bio-resin content. The initial value of the design variables was varied linearly, decaying away from the centroid of the RVE. This was done as it has been reported to improve convergence performance. Figure 9-5a shows the histories of the objective function, magnitude of the design variable vector, and the values of constraints, as the design evolved. Figure 9-5b shows the distribution of initial value of design variable. Figure 9-5c and Figure 9-5d show the bio-resin distribution at iteration steps 50 and 200, respectively. The target properties for the 10% bio-resin materials are given in Equation (9-13) and the effective properties upon convergence are provided in Equation (9-18). The discussion of the results is provided in Section 9.4.12.

$$E^{H} = \begin{bmatrix} 5.345 & 1.502 & 0.000 \\ & 3.818 & 0.000 \\ sym & & 1.153 \end{bmatrix}; \qquad \alpha^{H} = \begin{bmatrix} 75.399 \\ 115.360 \\ -1.4561 \end{bmatrix} \ \mu\text{m}/^{\circ}\text{C} \quad (9\text{-}18)$$

9.4.8 Case-5: Intercalated, 10% bio-resin, 10% available for layout optimization

This case models an intercalated clay morphology with 10% bio-resin content. The initial value of the design variables was distributed uniformly to all matrix elements. Figure 9-6a shows the histories of the objective function, magnitude of the design variable vector, and the values of constraints, as the design evolved. Figure 9-6b and Figure 9-6c show the bio-resin distribution at iteration steps 50 and 200, respectively. The target properties are provided in Equation (9-19) and the effective properties upon convergence are provided in Equation (9-20). The discussion of the results is provided in Section 9.4.12.

$$E^* = \begin{bmatrix} 5.018 & 1.591 & 0.000 \\ & 3.813 & 0.000 \\ sym & & 1.159 \end{bmatrix}; \qquad \alpha^* = \begin{bmatrix} 87.644 \\ 111.120 \\ 0.000 \end{bmatrix} \mu m/^\circ C \qquad (9\text{-}19)$$

$$E^H = \begin{bmatrix} 4.947 & 1.468 & 0.000 \\ & 3.817 & 0.000 \\ sym & & 1.182 \end{bmatrix}; \qquad \alpha^H = \begin{bmatrix} 84.002 \\ 116.090 \\ -0.237 \end{bmatrix} \mu m/^\circ C \qquad (9\text{-}20)$$

9.4.9 Case-6: Intercalated, 20% bio-resin, 20% available for layout optimization

This case models an intercalated clay morphology with 20% bio-resin content. The initial value of the design variables was distributed uniformly to all matrix elements. Figure 9-7a shows the histories of the objective function, magnitude of the design variable vector, and the values of constraints, as the design evolved. Figure 9-7b and Figure 9-7c show the bio-resin distribution at iteration steps 50 and 200, respectively. The target properties are provided in Equation (9-21) and the effective properties upon convergence are provided in Equation (9-22). The discussion of the results is provided in Section 9.4.12.

$$E^* = \begin{bmatrix} 3.311 & 1.191 & 0.000 \\ & 3.255 & 0.000 \\ sym & & 0.967 \end{bmatrix}; \qquad \alpha^* = \begin{bmatrix} 93.753 \\ 118.23 \\ 0.000 \end{bmatrix} \mu m/^\circ C \qquad (9\text{-}21)$$

$$E^H = \begin{bmatrix} 3.804 & 1.191 & 0.000 \\ & 3.255 & 0.000 \\ sym & & 0.967 \end{bmatrix}; \qquad \alpha^H = \begin{bmatrix} 97.986 \\ 120.220 \\ 0.046 \end{bmatrix} \mu m/^\circ C \qquad (9\text{-}22)$$

9.4.10 Case-7: Intercalated, 20% bio-resin, 10% available for layout optimization

This case models an intercalated clay morphology with 20% bio-resin content. It is assumed that 10% of the bio-resin in cross-linked with petro-resin (and behaving in a homogenized manner), and only 10% is available for discrete material design. The initial value of the design variables was distributed uniformly to all the matrix elements. Figure 9-8a shows the histories of the objective function, magnitude of the design variable vector, and the values of constraints, as the design evolved. Figure 9-8b and Figure 9-8c show the bio-resin distribution at iteration steps 50 and 200 respectively. The target properties are given in Equation (9-21) and the effective properties upon convergence are provided in Equation (9-23). The discussion of the results is provided in Section 9.4.12.

$$E^H = \begin{bmatrix} 3.818 & 1.301 & 0.000 \\ & 3.358 & 0.000 \\ sym & & 1.025 \end{bmatrix}; \qquad \alpha^H = \begin{bmatrix} 95.807 \\ 116.590 \\ 0.254 \end{bmatrix} \mu\text{m/}^\circ\text{C} \qquad (9\text{-}23)$$

9.4.11 Case-8: Intercalated, 10% bio-resin, Initial Value varies linearly

This case models an intercalated clay morphology with 10% bio-resin content. The initial value of the design variables was varied linearly, decaying away from the centroid of the RVE. Figure 9-9a shows the histories of the objective function, magnitude of the design variable vector, and the values of constraints, as the design evolved. Figure 9-9b shows the distribution of initial value of design variable. Figure 9-9c and Figure 9-9d show the bio-resin distribution at iteration steps 50 and 200 respectively. The target properties for 10% bio-resin materials are provided in Equation (9-19) and the effective properties upon convergence are provided in Equation (9-24). The discussion of the results is provided in the following section.

$$E^H = \begin{bmatrix} 5.345 & 1.502 & 0.000 \\ & 3.818 & 0.000 \\ sym & & 1.153 \end{bmatrix}; \ \alpha^H = \begin{bmatrix} 75.399 \\ 115.360 \\ -1.4561 \end{bmatrix} \mu\text{m/°C} \quad (9\text{-}24)$$

9.4.12 Discussion of the case-studies and Idealized RVEs

The material design based optimization study was performed on eight cases that had varying amounts of bio-resin in UPE, exfoliated and intercalated nanoclay morphology and different intial values for design variables. It was observed that for all the cases studied that the objective function reached convergence at approximately after 50 iterations. Although small variations continued to occur after 50 iterations, the change in the values of objective function and the resulting effective properties was minimal. Overall, the effective elastic tensor agreed reasonably with prescribed target properties for all cases (For e.g., E_{11} was within 0 - 14% of target property). The same agreement was not observed for the thermal strain tensor. One reason could be that the values of thermal strain tensors are in the order of 10^{-6} lower than the individual elastic tensor properties, and hence the sensitivities due to thermal properties may be having a minimal influence on the objective function and thereby resulting material layout. Guest et al. [9-10] report similar problems with a bi-objective problem wherein the maximize stiffness and permeability. They suggest that the weight factors be modified to address these issues. In this work, models that varied the weight factors of elastic and tensor parts of the objective function, and models that had the elastic and thermal parts of objective function normalized with respective target properties were studied. Results similar to the one reported here were obtained. Nevertheless, additional analyses should be performed to address the non-zero parameter in the thermal strain tensor (α_{12}^H). Diaz and Benard [9-9] used a formulation wherein they scaled the matrial properties

and also include weight factors for each of the individual components of the elastic tensor. It is possible that such approaches would allow better control of target properties and thereby the resulting material layouts..

The models with 20% bio-resin contents had effective properties whose objective function did not fully reach global minima. The problem at hand is an error-minimization problem and hence the global minima should occur at zero, indicating a perfect match of target and effective properties. It should be noted that the target properties used in this work had many assumptions. This could be one of the reasons for the objective function failing to reach the global minimum.

For any optimization problem, the effect of parameters governing the solution strategy, in this case MMA algorithm, such as step size, penalty parameters, and filtering of sensitivities must be studied. Such a study was carried out in this work for the case of exfoliated morphology and 10% bio-resin content. For brevity purposes detailed results of the study are not provided, but a brief summary is given in the following. It was found that a penalty parameter (p) of 5 allowed faster convergence of results. Values greater than $p=5$, led to solution convergence away from the global minima. Similarly, a step size of 0.75 led to faster convergence, but in some cases caused the solution to diverge. Overall, the default values of the MMA algorithm [9-12] with the penalty parameter value of 3 and step size value of 0.5 performed reasonably well and were thus used in this work.

As mentioned earlier, the objective of the study was not to accurately solve the material design problem but to provide an insight into the distribution of bio-resin that would allow the development of enhanced three-phase RVEs for multi-FE simulations. Considering the variations in experimental results and the assumptions involved in determining the target properties, it is difficult to make strong conclusions on the resulting material layout. Nevertheless, as expected it was observed that the weaker bio-resin gravitated to accumulate around the clay platelet. It was also noted that for 10% bio-resin content the bio-resin elements were distributed along the periphery of the clay platelet, while for 20% bio-resin layout was accumulated at the clay particle ends. The reduction in elastic properties for the 10% bio-resin content was minimal (γ=0.97) relative to 20% bio-resin content (γ=0.64). Considering the load transfer between the clay platelet and the surrounding matrix suggests that in order to reduce the stress-transfer efficiency, the weaker material should affect the interface between the stiff material and the matrix. This notion supports results obtained for models with 10% bio-resin contents. One would expect similar results for models with 20% bio-resin content. Nevertheless, it was found in these cases that the weaker material accumulated in pocket type regions around the ends of clay platelet. When stress transfer along 1-direction occurs, these bio-resin rich areas at clay-ends will provide considerable compliance and hamper the efficiency of the clay platelet.

In spite of the assumptions and shortcomings in convergence of solution, the study revealed two unique bio-resin distibutrion for 10% and 20% bio-resin contents. The resulting material layouts were simplified and idealized RVEs were proposed/developed for these two bio-resin contents. Figure 9-10a and Figure 9-10b show the simplified idealized RVEs developed from this study.

Overall, the material design based optimization approach is a very powerful technique, and holds great promise in understanding phenomena that cannot be observed or experimentally measured. Nevertheless, the accuracy of the technique is as good as the assumptions and hence care should be taken in drawing conclusions, considering the random nature of the material, the simplicity of the models (single platelet and gallery) and the lack of accurate target properties.

9.5 Multi-FE simulations: Tensile behavior using idealized RVEs

The idealized three-phase RVEs (Figure 9-10) obtained from the optimization based material layout design study were used in multi-level FE algorithms to predict the tensile behavior of bio-based nanocomposites. Details of the multi-FE approach, the material models used and comparison of the two-phase and three-phase RVEs along with random clay distribution are provided in Chapter 8. Figure 9-11a and Figure 9-11b provide the comparison of tensile response from the multi-FE simulation predictions and experiments for bio-based polymer/clay nanocomposites with 10% and 20% EML contents respectively. Overall, the enhanced three-phase RVEs obtained from the outcome of the material layout study reported here was found to capture the non-linear response better and match the average experimental data very well. For instance, the multi-FE simulated tensile response from the idealized RVE for 20% bio-resin (Figure 9-10b) agreed with average experimental response for up to 70% of average experimental ultimate strain, and the stress prediction from the simulation at average experimental ultimate strain deviated within 5% of average experimental ultimate stress. This was expected as the accuracy of the model increases when the material is modeled as realistic as possible. Detailed results of the multi-FE simulations are provided in Chapter 8.

9.6 Conclusion

Novel eco-friendly bio-based nanocomposites obtained from reinforcing layered silicates (nanoclays) in blends of petroleum and natural polymers (bio-resin) have been shown to exhibit properties that are superior or similar to the base petroleum-polymer. The addition of bio-resin reduces stiffness and barrier properties, which can b recovered by the use of nanoclay reinforcement. The distribution of nanoclay can be observed experimentally through electron micorscopy, but similar observations on the distribution of petro and bio-resin constituents is infeasible. To understand and model these materials efficiently, the distribution of bio/petro resin was sought. The material layout problem presented in this work was aimed to develop an enhanced RVE for multi-level computational simulation. The was the use of topology optimization along with experimental data. The goal was to provide to provide insight to the distribution of bio-resin in the RVE, and not necessarily to accurately solve the material design problem. As with any optimization problem, the accuracy of the material design topology optimization problem used in this work, which minimizes the error between the experimental target properties and homogenized model predictions, depends on the input parameters. Any assumptions or incorrect target properties will clearly influence the outcome of the optimization problem, and the obtained solution is specific to the problem considered and cannot be generalized to other material compositions. Solution of the material layout problem revealed affinity of the weak bio-resin material to the stiff nanoclay platelet. This was expected as bio-resin addition reduced mechanical properties, suggesting that it affected the stress-transfer between the stiff inclusion and the matrix. Additionally, polymer chemistry literature indicates that functionalization/chemical affinity of the bio-resin can have a strong influence in attracting the nanoclay [9-4], thereby supporting the results from the study. Idealized RVEs for 10% and 20% EML contents with 2.5 wt.% nanoclay, with exfoliated and intercalated morphologies, were deduced from material layout studies and used in multi-level FE predictions of the tensile behavior of bio-based nanocomposites. The tensile response predictions using the idealized RVEs developed from this study captured the non-linear response and agreed with average experimental response in initial stiffness. Also, in case of idealized RVE corresponding to 20% bio-resin content, the simulations agreed with average experimental response for up to 70% of average experimental ultimate strain, and the stress prediction from the simulation at average experimental ultimate strain deviated within 5% of average experimental ultimate stress. Overall, the material design based optimization approach is a very powerful technique and holds great promise in designing unique materials, and in understanding phenomena that cannot be observed or measured experimentally.

9.7 Acknowledgements

This work was supported by the National Science Foundation under grant CMS-0409666. The implementation of the method of moving asymptotes used here was provided by Prof. Krister Svanberg from the Department of Mathematics at KTH in Stockholm. We thank Prof. Svanberg for allowing us to use his program. Authors are thankful to Dr. Alejandro Diaz, Professor of Mechanical Engineering, Michigan State University, for his help in understanding the theory and formulation of the problem during this study. Authors are also thankful to Dr. Amar K Mohanty and Dr. Manju Misra, School of Packaging, Michigan State University, for their expertise in chemistry and processing of these materials.

9.8 Tables and Figures

Table 9-1. Model Description for the material design layouts studied in this work

#	Model Name	Nanoclay Morphology	Weight Factors		Bio-resin content Volume fraction		Initial Value of design Variable ρ_{ini}*
			WE	WA	Actual	Available for optimization	
1	Case-1	exfoliated	1	1	10	10	0.1
2	Case-2	exfoliated	1	1	20	20	0.2
3	Case-3	exfoliated	1	1	20	10	0.1
4	Case-4	exfoliated	1	1	10	10	Linear variation
5	Case-5	intercalated	1	1	10	10	0.1
6	Case-6	intercalated	1	1	20	20	0.2
7	Case-7	intercalated	1	1	20	10	0.1
8	Case-8	intercalated	1	1	10	10	Linear variation

* Uniform distribution of ρ_{ini} assumed except for case-4 and case-8 wherein Linear variation of initial value of design variable with value decreasing as the element is away from the centroid of the RVE.

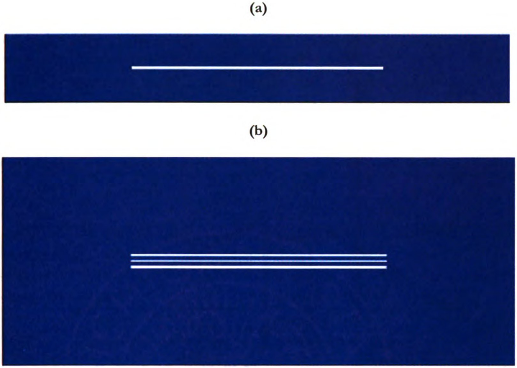

Figure 9-1. Base Cells: a) Exfoliated Morphology, b) Intercalated Morphology. The white region represents the nanoclay and the blue region represents the design domain containing blends of bio-resin and petro-resin

(a)

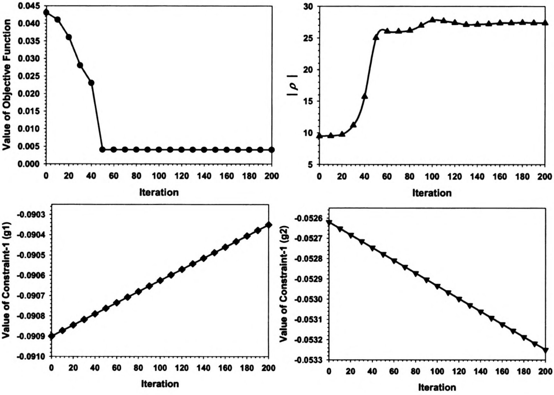

(b) Iteration # 50

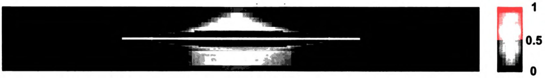

(c) Iteration # 200

Figure 9-2. Case-1, Exfoliated morphology with 10% bio-resin. a) Evolution of design, plots showing change of objective function, magnitude of design variable vector, and constraints, b) material layout at iteration step 50, and c) material layout at iteration step 200.

(a)

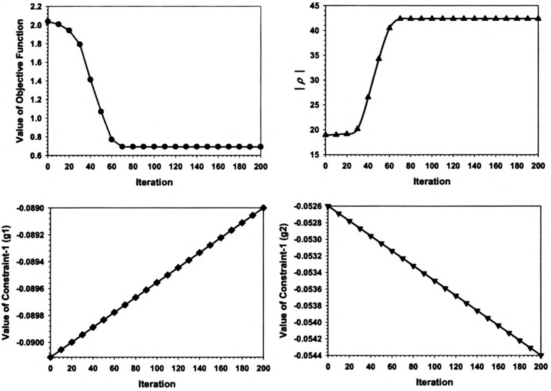

b) Iteration # 50

(c) Iteration # 200

Figure 9-3. Case-2, Exfoliated morphology with 20% bio-resin. a) Evolution of design, plots showing change of objective function, magnitude of design variable vector, and constraints, b) material layout at iteration step 50, and c) material layout at iteration step 200.

(a)

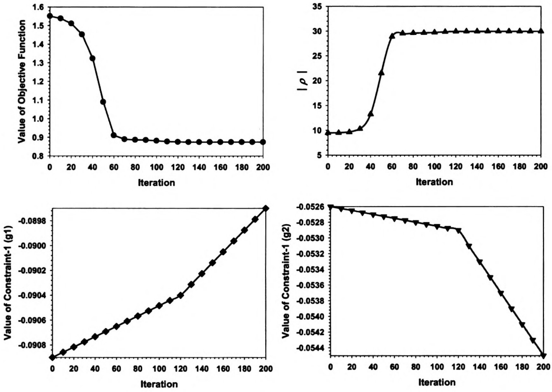

b) Iteration # 50

(c) Iteration # 200

Figure 9-4. Case-3, Exfoliated morphology with 20% bio-resin content and only 10% available for material design . a) Evolution of design, plots showing change of objective function, magnitude of design variable vector, and constraints, b) material layout at iteration step 50, and c) material layout at iteration step 200.

(a)

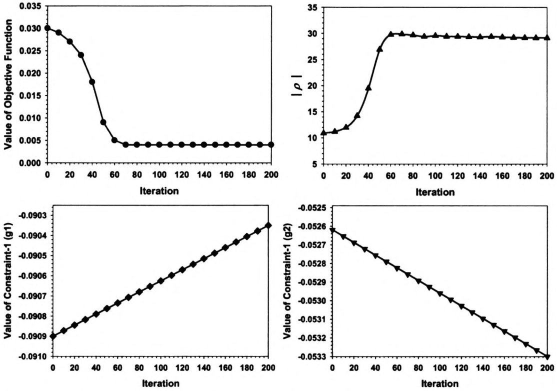

(b) Initial Value of Design Variable

(c) Iteration # 50

(c) Iteration # 200

Figure 9-5. Case-4, Exfoliated morphology with 10% bio-resin. a) Evolution of design, plots showing change of objective function, magnitude of design variable vector, and constraints, b) Distribution of initial value of the design variable, c) material layout at iteration step 50, and c) material layout at iteration step 200.

(a)

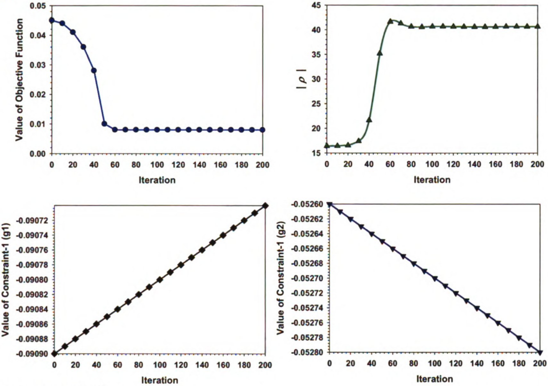

b) Iteration # 50

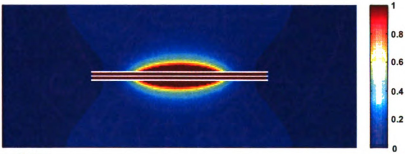

(c) Iteration # 200

Figure 9-6. Case-5, Intercalated morphology with 10% bio-resin content a) Evolution of design, plots showing change of objective function, magnitude of design variable vector, and constraints, b) material layout at iteration step 50, and c) material layout at iteration step 200.

(a)

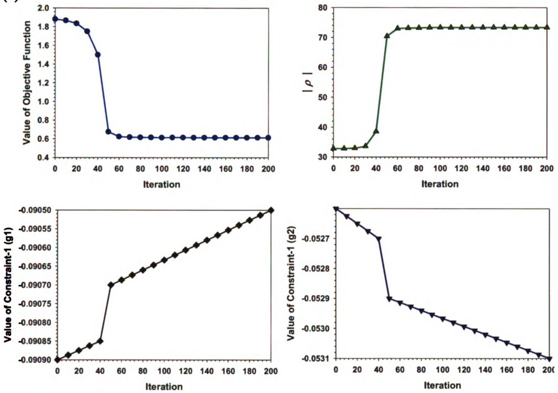

b) Iteration # 50

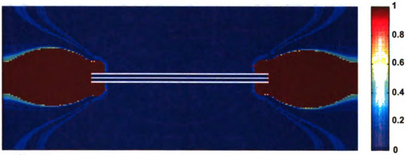

(c) Iteration # 200

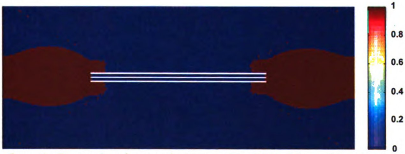

Figure 9-7. Case-6, Intercalated morphology with 20% bio-resin content and all 20% available for material design. a) Evolution of design, plots showing change of objective function, magnitude of design variable vector, and constraints, b) material layout at iteration step 50, and c) material layout at iteration step 200.

(a)

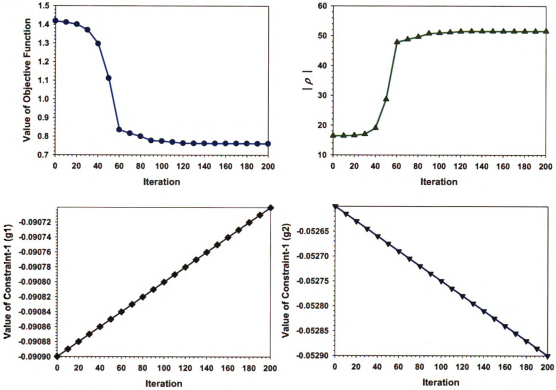

b) Iteration # 50

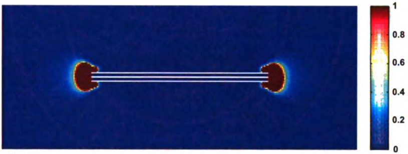

c) Iteration # 200

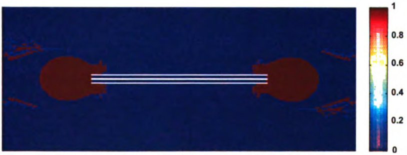

Figure 9-8. Case-7, Intercalated morphology with 20% bio-resin content and only 10% available for material design . a) Evolution of design, plots showing change of objective function, magnitude of design variable vector, and constraints, b) material layout at iteration step 50, and c) material layout at iteration step 200.

(a)

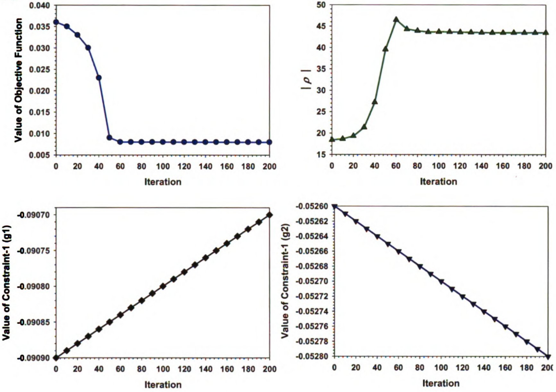

(b) Initial Value of Design Variable

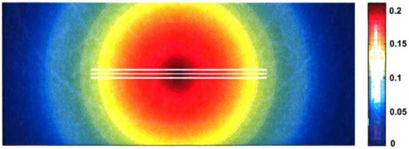

Figure 9-9. Case-8, Intercalated morphology with 10% bio-resin. a) Evolution of design, plots showing change of objective function, magnitude of design variable vector, and constraints, b) Distribution of initial value of the design variable, c) material layout at iteration step 50, and c) material layout at iteration step 200.

Figure 9-9 continued. . .

(c) Iteration # 50

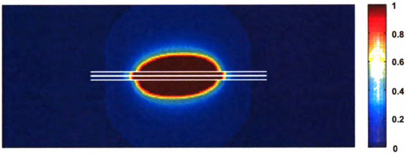

(c) Iteration # 200

Figure 9-10. Simplified, idealized RVEs. The green, red and black regions represent petro-resin (UPE), bio-resin (EML) and nanoclay respectively. a) 10% EML, b) 20% EML

(a)

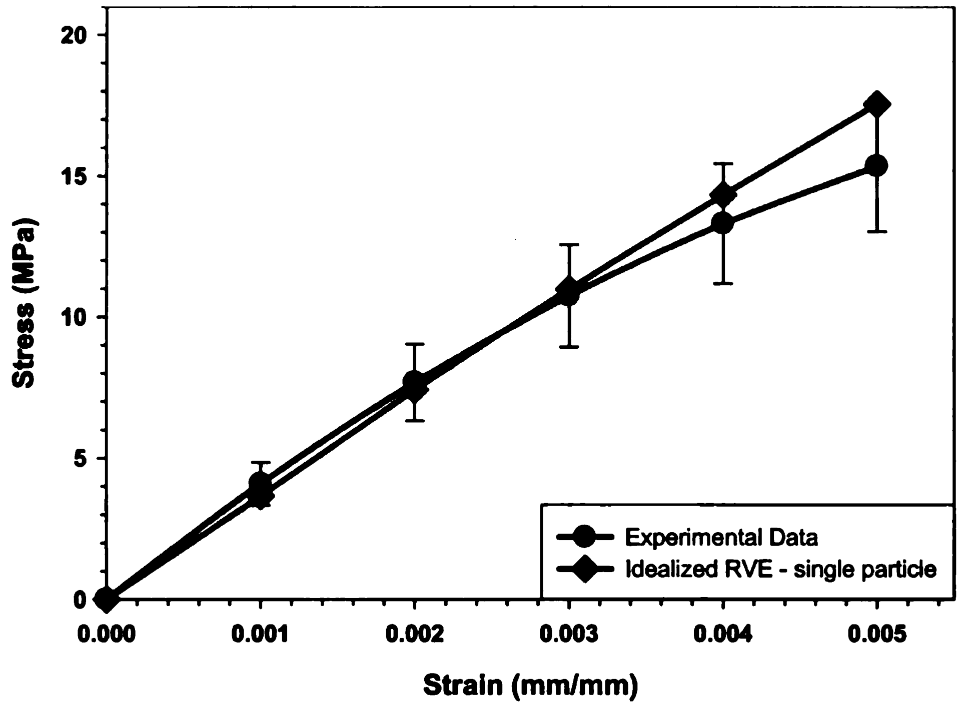

(b)

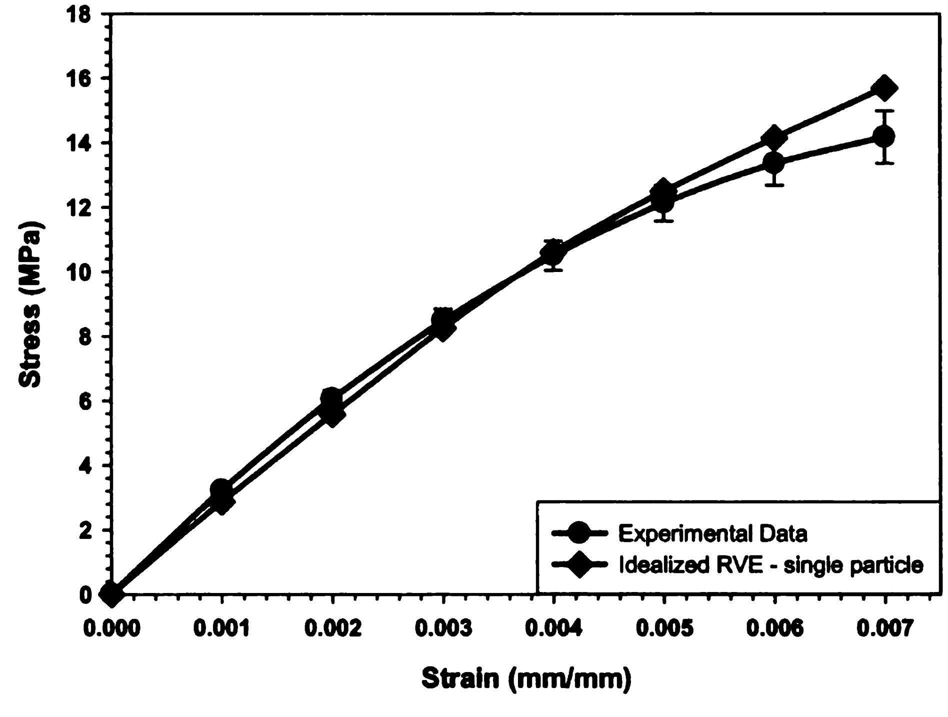

Figure 9-11. Comparison of tensile response from multi-FE simulations using idealized three-phase RVEs with experimental data, (a) 90/10/2.5, and (b) 80/20/2.5

9.9 References

[9-1]. Haq M, Burgueño R, Mohanty AK, Misra M. "Processing techniques for bio-based unsaturated-polyester/clay nanocomposites: tensile properties, efficiency and limits." Composites: A 2009; 40:394-403.

[9-2]. Haq M, Burgueño R, Mohanty AK, Misra M. "Bio-based unsaturated polyester/layered silicate nanocomposites: characterization and thermo-physical properties." Composites: A 2009; 40:540-547.

[9-3]. Haq M, Burgueño R, Mohanty AK, Misra M. "Development and Thermophysical Characterization of Clay Nanocomposites from Blends of Linseed oil and Unsaturated Polyester." Composites: A, Communicated.

[9-4]. Drown EK, Mohanty AK, Parulekar Y, Hasija D, Harte BR, Misra, M, Kurian JV. The surface characteristics of organoclays and their effect on the properties of poly(trimethylene terephtahalate) nanocomposites. Composites Science and Technology, 2007, 67:3168-3175.

[9-5]. Sigmund O., "Design of material structures using topology optimization." Ph.D. Thesis, Department of Solid Mechanics, Technical University of Denmark, 1994.

[9-6]. Sigmund O., "Materials with prescribed constitutive parameters: an inverse homogenization problem." International Journal of Solids and Structures, 1994; 31(17):2313–2339.

[9-7]. Sigmund O., "Tailoring materials with prescribed constitutive parameters." Mechanics of Materials, 1995; 20: 351–368.

[9-8]. Sigmund O. and Torquato S., "Design of Materials with Extreme Thermal Expansion using a Three-Phase Topology Optimization Method," Journal of the Mechanics and Physics of Solids, 1997; 45(6):1037-1067.

[9-9]. Diaz, A., and Benard, A., "Designing materials with prescribed elastic properties using polygonal cells," International Journal for Numerical Methods in Engineering, 2003; 57:301-314.

[9-10]. Guest, J.K. and Prevost, J, H., "Optimizing multifunctional materials: Design of microstructures for maximized stiffness and fluid permeability," International Journal of Solids and Structures, 2006; 43:7028–7047.

[9-11]. Guest, J.K. and Prevost, J, H., "Design of maximum permeability structures." Computer Methods in Applied Mechanics and Engineering, 2007; 196:1006-1017.

[9-12]. Svanberg K., "The method of moving asymptotes." International Journal for Numerical Methods in Engineering, 1987; 24:359 –373.

[9-13]. Kruijf, N., Zhoue, S., Li, Q., and Mai, Y.W., "Topological design of structures and composite materials with multiobjectives," International Journal of Solids and Structures, 2007; 44:7092–7109.

[9-14]. Zeng, Q.H.,Yua, A.B., and Lub, G.Q., "Multiscale modeling and simulation of polymer nanocomposites," Progress in Polymer Science, 2008; 33:191-269.

[9-15]. Sigmund O., "A 99 line topology optimization code written in Matlab," Structural and Multidisciplinary Optimization, 2001; 21:120-127.

[9-16]. Bendsoe MP., "Optimal shape design as a material distribution problem," Structural Optimization 1989; 1:193–202.

Chapter 10. Summary and Conclusions

10.1 Summary:

Environmental concerns related to the use of synthetic, or petroleum based, polymer matrix composites has propelled the development of composite materials based on natural or renewable sources. Biocomposites, composed of natural fibers in synthetic or natural polymer matrices have recently gained much attention due to their low cost, eco-friendliness, and their potential to compete with synthetic composites. Nonetheless, the use of bio-based composites has been limited due to their lower mechanical and thermo-physical properties compared to synthetic composites and conventional structural materials. In this work, hybrid bio-based composites consisting of multiscale reinforcements, namely natural fibers and nanoclay embedded in blends of petroleum based (unsaturated polyester) and vegetable oil based resins (derivatives of soybean and linseed oils), were developed through integrated experiments and computational simulations. Experimental studies included development of novel processing techniques for bio-based polymer nanocomposites and detailed characterization of physical, thermal, mechanical and barrier properties of both nanocomposites and biocomposites. Computational simulations that take into account the detailed morphologies at various hierarchical length scales were developed and validated/integrated with experiments. Electron microscopy aided the development of realistic computational models (RVE, representative volume elements). The distribution of bio-resin in nanocomposites could not be observed experimentally (microscopy), hence, the available experimental data was used along with topology optimization to determine the distribution of the bio-resin and develop an enhanced RVE for modeling the three-phase material. A multi-level finite element approach was implemented to link different length scales. The multi FE approach was used to evaluate the tensile response of clay+bio-based nanocomposites and micro-fiber+clay+bio-based composites. Overall, eco-friendly, tailorable, cost-effective and multiscale reinforced bio-based composites were successfully developed through the integration of experiments and computational simulations. It is believed that the approach of integrating simulations and experiments, as attempted in this work, holds great promise and similar methodology can be applied for other types of hierarchical materials, thereby providing guidance in designing those materials.

10.2 Research Findings

10.2.1 Processing of Bio-based Nanocomposites

- Processing plays a vital role in the resulting properties of both nanocomposites and biocomposites.
- In order to exploit the benefits/synergy offered by the hybrid hierarchical bio-based materials studied in this work, incorporation of large amounts of bio-resin and nanoclay is needed, but such incorporation is controlled by the processing limitations of bio-based nanocomposite resins. Also, the overall properties of the bio-based composites are highly dependable on efficient processing of bio-based nanocomposite resins.
- Solvent-based processing of nanoclay reinforced bio-based resin systems brings about new challenges, such as phase separation, thermal degradation of the resin system and limitations on the maximum feasible bio-resin and nanoclay content.

- Two novel efficient solvent based processing techniques were developed through a study that compared four different techniques. The effects of sonication energy, processing time, solvent type and the associated processing issues for each of the techniques were assessed by evaluating the nanoclay morphology and the tensile properties of the resulting polymer nanocomposites. Processes that enable incorporation of relatively large amount of bio-resin and nanoclay content with minimal processing problems, lower processing time and desirable tensile properties were considered to have good overall efficiency.
- In particular, two processes were found to have good overall efficiency. One of them (Process B) consists of using acetone as a solvent and led to the best nanoclay dispersion and exfoliation, resulting in samples with high tensile modulus. The second one (Process D) consists of direct sonication of nanoclay in the resin system diluted with styrene. This process eliminates the use of a foreign solvent, thereby reducing processing time, and the resulting nanocomposites showed a good balance of tensile properties, namely a balanced improvement of stiffness and toughness.
- Depending on desired properties and applications, either of these processes is deemed suitable for effective production of bio-based nanocomposites.

10.2.2 Study on Bio-based Polymer Nano-composites

- Bio-based resin systems from partial substitution of petroleum based resins (primary) with natural polymers (secondary) provide environmental friendliness, cost-effectiveness and improved toughness.
- Experimental characterization of thermo-physical, mechanical, barrier properties and microscopic observations were studied on bio-based nanocomposites with

unsaturated polyester (UPE, primary resin, petro-based) and two types of bio-resins, namely epoxidized methyl soyate (EMS, soybean oil derivative) and epoxidized methyl linseedate (EML, linseed oil derivative), reinforced with nanoclay.

- It was observed that the combination of nanoclays and bio-resins in UPE resin systems lead to composites with similar or better properties than the original virgin UPE resin system.
- The drawbacks from the addition of bio-resins to the base polymer were shown to be recoverable through nanoclay reinforcement and vice versa.
- The addition of bio-resin increases toughness but reduces stiffness of the resin system.
- Similarly, the addition of nanoclay increases stiffness along with brittleness of the resulting nanocomposites, i.e., a reduction in toughness and ductility.
- The studies showed that a proper stiffness- toughness balance can be obtained and can be tailored by controlling the amount of bio-resin and nanoclay contents.
- Additionally, a comparative study of neat resins (no clay), from blends of EMS and EML in UPE revealed similar tensile properties for both resin blends. Nevertheless, considering ease of processing, EML resin is recommended for use. Also, EML composites have relatively better transparency than EMS composites.
- If the transparency/translucency of resulting nanocomposites is an indication of phase-separation, EMS composites seemed to have had a higher degree of phase-separation (less transparent), also indicating that EML composites have relatively better compatibility with primary petro-resin UPE.

10.2.3 Hybrid Bio-based Composites:

- Hybrid bio-based composites that exploit the synergy between natural fibers (industrial hemp) in a nanoreinforced (nanoclay) bio-based polymer (unsaturated polyester + linseed/soybean oil based resins) can lead to improvements in multiple properties while maintaining environmental appeal and cost-effectiveness.
- The properties of the resulting biocomposites are tailorable and seem controllable by the amount and distribution of the constituents.
- Experimental characterization studies showed that the addition of bio-resin lowers mechanical parameters, such as stiffness and ultimate tensile stress, but increases toughness parameters, such as impact strengths and ductility.
- The addition of nanoclay enhances stiffness but seems to decrease toughness. Thus, the study shows that a proper stiffness/toughness balance can be obtained by controlling the amount of bio-resin and nanoclay content. The enhancement in stiffness due to nanoclay addition was found to be less pronounced in biocomposites than in nanocomposites, as the hemp fibers control the stiffness of the biocomposites
- The synergistic behavior is not limited to stiffness-toughness balance, and similar balance was observed in thermal and barrier properties, wherein the detrimental properties of bio-resin were recovered by nanoclay addition and vice versa.
- The multiphase nature of the hybrid bio-based composites revealed multi-functional attributes, such as improved barrier and thermal properties along with improvements in mechanical properties.
- The multiscale reinforcement provided enhancements at different length scales. The addition of nanoclay improved the properties of the polymer matrix, thereby

improving the barrier (thermal + moisture movement) properties, while the micro-sized hemp fibers govern most macroscopic mechanical properties of resulting biocomposites.

- Tensile fracture surfaces (scanning electron microscopy) revealed an increase in the interfacial gap (gap between the hemp fiber and the matrix), and increased amount of pulled-out fibers, with an increase in bio-resin content. This indicates an adverse effect of bio-resin on interfacial properties. Increased pull-out of fibers indicates higher dissipation of energy, thereby higher ductility and improved toughness as observed in experimental results.

10.2.4 Analytical and Computational Modeling

- The success of any modeling to predict the overall properties of a heterogeneous material depends on the representative volume element (RVE) or unit cell.
- The RVE should be selected such that it is large enough to represent the microstructure and small enough to allow efficient computations.
- Unlike most conventional nanoparticles/fillers, nanoclays pose unique modeling issues such as a) particle size, b) hierarchical/intercalated morphology and c) interface and inter-gallery properties.
- Exfoliated clays may have thicknesses in range of nanometers and highly intercalated clay agglomerations may have thicknesses in the order of micrometers. Moreover, it is commonly agreed that polymer clay nanocomposites exhibit both exfoliated hierarchical morphologies. Hence most analytical models that have assumptions of uniform properties with a constant aspect ratio for all particles fail to model nanoclay composites efficiently.

- Finite element based RVEs allow detailed/realistic modeling of the material including different particle shapes and morphologies, and non-linear material properties with complex loading, and were thus used to successfully model the hybrid material in this study.
- Finite element RVEs used in this work modeled the material as realistically as possible and took into account the random distribution (due to processing) and morphologies (exfoliated, intercalated and both) of nanoclay platelets.
- A comparison of FE based RVEs and analytical models (Mori-Tanaka estimates) with experimental data revealed better agreement of FE based RVEs with experiments than analytical models. This is attributed to the more realistic modeling of the material.

10.2.5 Material layout

- The distribution of nanoclay in the polymer matrix could be observed using electron microscopy, but the distribution of bio-resin in the primary petro-resin cannot be observed by this method. In order to model the hybrid composite in greater detail, it is essential to realistically model the three-phase material, and hence the distribution of bio-resin was sought.
- The material layout problem used in this work was aimed to develop an enhanced three-phase RVE by using experimental data along with topology optimization in an attempt to provide insight to the distribution of bio-resin in the RVE. Thus the goal was not to accurately solve the material design problem.
- As with any optimization problem, the accuracy of the material design topology optimization problem used in this work, which minimizes the error between the

experimental target properties and homogenized model predictions, depends on the input parameters. Any assumptions or incorrect target properties will influence the outcome of the optimization problem, and is specific to the problem considered and cannot be generalized to other material compositions.

- The bio-resin distribution resulting from a material layout problem with any single target parameter (e.g., modulus) may not yield the same distribution from any other parameter (e.g., thermal expansion). Nevertheless, in reality the material should have a unique distribution that matches all experimental parameters. As a result, a material distribution/design problem that uses multiple target parameters, like the one used in this work increases the confidence of the result.
- Optimization algorithms rely on many input variables, such as step size, penalty parameter, initial value of the design variable, etc. These variables are specific to any given problem and need to be changed for every problem.
- Solution of the material layout problem revealed affinity of the weak bio-resin material to the stiff nanoclay platelet. This was expected as bio-resin addition reduced mechanical properties, suggesting that it affected the stress-transfer between the stiff inclusion and the matrix. Additionally, in order to incorporate higher amounts of bio-resin and nanoclay, the knowledge from chemists reveal that the bio-resin may have functionalization/chemical affinity with nanoclay thereby supporting the results from the study.
- Idealized RVEs for 10% and 20% EML contents with 2.5 wt.% nanoclay, with exfoliated and intercalated morphologies were deduced from material layout studies and used in multi-FE prediction of tensile behavior of bio-based nanocomposites.

10.2.6 Multi-scale simulations / Multi-FEA

- Multiscale modeling is a term that covers a wide range of simulations and modeling techniques. Ideally, a multiscale modeling scheme would be the one that links all the scales from atomistic level to macro/structural level. In other words, it should connect the discrete molecular structure with the bulk continuous structure. At the same time, any modeling scheme that links any two scales is commonly considered a multiscale modeling scheme, hence making the use of this descriptive analysis term subjective.
- The most important aspect of multiscale modeling is the accurate prediction of physical/chemical properties and behavior from a lower scale (e.g., nano or micro scale) to a larger (or macro scale) without loss of intrinsic information. In other words, accurate *transfer* of effective properties from one length scale to other (also termed as hand-shaking) governs the success of the computational simulation.
- A multi-level finite element (FE) computation does not require any constitutive equations to be written at the macroscopic scale; all non-linearites are obtained from separate FE analyses at lower hierarchical (micro/nano) scale.
- In this work, a multi-level FE algorithm was implemented to model the hybrid bio-based materials. A two-level (nano-micro) multi-FE algorithm was used to predict the tensile response of two-phase (nanoclay + matrix) and three-phase (nanoclay + petro-resin + bio-resin) bio-based nanocomposites. Also, a three-level multi-FE (nano-micro-macro) algorithm was implemented to predict the tensile behavior of bicomposites (natural fiber + nanoclay + petro-resin + bio-resin).
- For bio-based nanocomposites, the multi-level FE predictions of all the models were in good agreement with the initial stiffness, obtained from average experimental data.

- The two-phase intercalated models matched the average experimental response for up to 50% of average experimental ultimate strain value, while this value was only 35% for exfoliated model. Also, the stress prediction corresponding to average experimental ultimate strain deviated from experimental stress by 45% and 35% for exfoliated and intercalated models, respectively. Overall, models with intercalated clay models showed better performance than exfoliated clay models. This was expected as the accuracy of the model increases when the material is modeled as realistic as possible.
- The three-phase idealized single-particle model had the best performance of all models with good agreement up to 70% of the ultimate strain observed from average experimental response. Also, considering the deviations in the experimental data, the stresses predicted by the single-particle idealized RVE, corresponding to the average experimental ultimate tensile strain, were within 5% of the average experimental ultimate tensile stresses. Overall, the simulated responses agreed reasonably well with experimental results and were able to capture the nonlinear response.
- The multi-FE predictions of tensile response of hybrid biocomposites matched average experimental response with respect to initial stiffness. The virgin UPE biocomposite deviated from average experimental response at strain levels of 25% of ultimate strains, while this value was 35% for hybrid biocomposite (20% EML & 2.5 wt.% nanoclay) using idealized three-phase RVE. This suggests that material non-linearity helps in capturing the non-linear behavior, but is not the only source of non-linearity.
- The deviation of the simulation from the experimental data is due to many factors, including material non-linearity, random distribution of the short hemp fibers,

interaction of the short-fibers, fiber pull-out, straightening of the curved fibers, interfacial properties, etc. Hence, relying purely on material non-linearity will still be unable to capture the non-linear response accurately, particularly near ultimate response. Nonetheless, properly designed multiscale FE simulations can shed light in understanding the aforementioned complexities and sources of non-linearity

- A simplified RVE was used in this work, with the objective of illustrating the promise of the multi-level computational scheme. A more realistic RVE with enhanced material properties and modeling of the reinforcement morphology would enable accurate modeling of such materials.
- One of the main drawbacks of multi-FE algorithm is that it is basically a more sophisticated homogenization/averaging scheme, but cannot model damage. Once the damage occurs the periodicity of the RVE ceases to exist and the assumptions of the multi-FE method are violated. Also, stress-concentrations and numerical anomalies (if any) get averaged out and hence the scheme may over-predict the actual response.
- Overall, multi-FE algorithms hold great promise in modeling different length scale within the continuum regime.

10.2.7 Closure

- In order to understand hybrid materials as the ones dealt with in this dissertation, including the interactions between the polymer blends and the effect of nano-inclusions and micro-fibers on the overall properties, a good understanding of chemistry of such materials combined with atomistic simulations and proper experiments at the respective scales (including nano/lower scale) is essential.

- The current work focused on mechanical behavior. A similar approach can be extended to thermal and diffusion reseonse. The success of this computational scheme will enable prediction of macroscopic responses for various material compositions and macroscopic shapes. A similar methodology could be applied for other types of nanoparticles and hierarchical materials thereby providing guidance in designing those materials.
- Overall, the study used an integrated experimental and simulations based approach to develop and understand hybrid, hierarchical, tailorable and eco-friendly materials. The study showed that bio-based composites with proper stiffness/toughness balance can be obtained while preserving environmental friendliness and cost effectiveness. The improved multifaceted features possible for these sustainable bio-based materials are likely to increase their appeal for use in transportation and housing structural applications.

10.3 Philosophical Conclusions

10.3.1 Sustainability

One of the most common terminologies used in the literature for eco-friendly materials is "sustainablility". The term "sustainable" is subjective and at times misleading. Oxford dictionary defines sustainable as "avoiding depletion of natural resources." Although materials with plant-based origin or eco-friendly appeal may be used to develop "green" materials, it is not necessary a sustainable alternative by itself. The amount of energy utilized to produce these materials, or the effort spent on making such materials feasible may circumvent the benefits offered by their natural origin. Ideally, whenever sustainability is defined, it should be combined with life-cycle assessment and energy efficiency of production and disposal.

10.3.2 Multi-scale Computations

The advancements in measurement sciences and availability of computational power make multiscale simulations feasible. Nevertheless, the use of these multiscale computational schemes to determine simple elastic properties might be an unnecessary effort Nevertheless, such powerful computational schemes can be used to understand complex materials, time dependent properties, non-linear behavior, modeling damage and phenomena that cannot be measured experimentally. In a similar note, most computational schemes have inherent assumptions in their theory and their numerical models, and thereby the resulting accuracy is dependent on these assumptions. For instance, multiscale schemes that rely on local periodicity cannot model material damage. Once damage occurs, the assumption of local periodicity is lost, and the scheme is invalid. Overall, the success of the computational scheme depends on how realistic/detailed the models are, the assumptions/simplifications made in the theory and the parameters under consideration.

10.3.3 Integration of Experimental results and Computational simulations

The use of experimental data to validate computational models and the use of such validated models to predict properties of complex materials for constituent concentrations to which experimental data is not available, is one of the major advantages of this approach Nevertheless, the use of average properties to validate the models is questionable, especially when there is a large deviation in the parameter studied. In such cases, a probabilistic approach needs to be taken, and a relatively larger number of simulations need to be performed.

10.3.4 Electron Microscopy / Measurements at Lower Scale

The use of electron microscopy or in general measurements at lower scale is very subjective and care should be taken in its interpretation. For instance, an electron micrograph studying nano-particle distribution in a polymer may show good dispersion in one experimental slide and completely agglomerated (i.e., bad) dispersion on another. In such cases, the overall dispersion of the particulates is a subjective call. A better understanding of the equipment, its working technique and sample preparation should be taken into consideration before conclusions from such sensitive observations are made. For instance, in transmission electron microscopy, the material that is kept under observation has a size of few microns with a thickness of approximately 100 nm. Considering the macroscopic size, the randomness in processing techniques, and varied observations in different material slides, drawing strong conclusions on the macroscopic material from observations at that scale can be tricky and subjective and should be handled with care.

10.4 Research Needs

10.4.1 Atomistic Simulations, Transient and Non-linear Properties:

Atomistic simulations (molecular dynamics) can be used to understand the phenomena for which experimental data is not available. For instance, a study on the interaction of polymer chains of petro-resin and bio-resin, bio-resin and bio-resin, and their interaction with nanoclay will shed light on the polymer blends and influence better chemistry and processing of the materials. Such knowledge will allow better design of these materials and incorporation of more bio-resin. Additionally, the use of robust multi-scale computations should be used to understand the influence of lower scale heterogeneities on macroscopic time-dependent, transient properties such as thermal and barrier properties.

Similarly it is essential to model the progression of damage of these composites. It is believed that damage initiates at the lower/atomic scales and proper use of robust multiscale computational schemes will help understand failure initiation and better design and development of complex materials.

10.4.2 Statistical Considerations in Experimental Results

As expected, the experimental data revealed scatter/variations in measured parameters. These variations were specifically larger for failure-dependent parameters, such as tensile failure strains, tensile strengths and impact strengths. In this work, only the average values were considered and hence a qualitative effect and overall trends based on average values could be obtained. Detailed statistical analyses taking into account these variations should be performed to quantitatively and precisely obtain the effects of constituents, namely bio-resin and nanoclay.

10.4.3 True Bio-degradable "Green" Materials

The work reported uses blends of petroleum resins and bio-resins along with natural fibers. The use of all bio-resins was limited due to performance concerns. Recent advancements in the areas of bio-polymers and material science have shown promise in use of 100% bio-resins that are also bio-degradable, with improved performance. Also, the natural fibers used in this work were untreated. This was done so that a lower limit on performance could be obtained. For instance, a combination of "engineered" (or treated) fibers with 100% bio-resin and use of bio-based nano-particulates (such as cellulose whiskers, clay platelets, silica) would produce efficient "green" materials. Due to the rapid advancements in material science and chemistry (functionalizations), high-performance and "green" material are becoming a reality.

10.4.4 True Integration of Experiments and Computational Simulations

The computational materials based approach of developing materials requires proper integration of experiments and computational simulations. This indicates that computational models at each scale should essentially be compared/matched with experiments at respective scale. In such a case, material properties for computational models at nano-scale or any lower scale require experiments at that scale. Bulk material properties cannot be used for local/lower scale models. For instance, macroscopic properties of a polymer nanocomposite cannot be used in a computational model that studies the effect of nanoparticle. Instead experiments such as nano-indentation or atomic force microscopy (AFM) will produce more realistic local properties. Additionally, it is believed that AFM allows observation of soft and hard regions within a polymer. Ideally, such observations could enable obtaining the actual bio-resin distribution, thereby enabling better modeling of three-phase nanocomposites. Also, such observations could be used to validate models, similar to the ones developed in this study that determine the bio-resin layout using topology optimization. Overall, true integration of experiments and simulation requires measurements and simulations at respective scales.

10.4.5 Structural Application of Biocomposites and Large-scale Testing

The bio-based materials used in this work show great promise in use for structural applications. One of the main concerns of use of these materials for structural applications has been durability. The addition of nanoclay in the resin system delays the moisture reaching the natural fibers and thereby is believed to improve the durability of resulting structural component. Also, their load-bearing efficiency can be improved if they are used in sandwich/hollow-core designs. Finally, large scale manufacturing and testing of such biocomposite materials is essential to prove their feasibility.

10.5 Research Impact

The approach attempted in this work, namely the integration of experiments and computational simulations has promise in the understanding of micro/nanoscale mechanisms governing various parameters, thereby enabling tailoring of macroscopic properties by proper synergy and distribution of materials at respective scales. This methodology is not limited to hybrid bio-based materials used in this work, but could be applied for other nanoparticle types and hierarchical materials. Ideally, computational models validated with selective experiments would allow prediction of properties for material compositions to which experimental data is not available. In the current study, experimentally validated computational models were developed at nanoscale, and were used to predict the overall macroscopic response. At the same time, in a true sense, these validated models were not implemented in determining properties for unknown material compositions. It is believed that such predictions are direct extension to the current work. Ideally, such predictions would eliminate costly trial and error experiments and enable better understanding and consequently help in design of complex materials. Overall, a successful modeling scheme, as the one used in this research could enable development of novel, efficient, cost effective multifunctional materials. This technique is powerful and can be used in diverse applications such as: a) modeling of bones and development of prosthetics, b) design of textiles, c) development of alloys and materials from a combination of heterogeneities etc. On the other hand, development of bio-based materials and their applications for structural applications would lead to sustainable, environmental friendly, bio-degradable and cost effective materials.